The role of sirtuins in epigenetic regulation

Pin Zhao

MÜNCHEN 2019

The role of sirtuins in epigenetic regulation

Pin Zhao

Dissertation
an der Fakultät für Biologie
der Ludwig-Maximilians-Universität
München

vorgelegt von
Pin Zhao
aus Henan, China

München, den 22.02.2019

Erstgutachter: Prof. Dr. Heinrich Leonhardt

Zweitgutachter: Prof. Dr. Wolfgang Enard

Tag der mündlichen Prüfung: 18.03.2019

TABLE OF CONTENTS

TABLE OF CONTENTS

Summary

Epigenetic mechanisms regulating gene expression mainly involve DNA methylation, histone modification, and non-coding RNAs. Disruption of these mechanisms may lead to cancer, complicated disorders such as behavioral disorders, amnesia, autoimmune disease, and addiction. DNA methylation is a widespread modification found in various species, which is produced by DNA methyltransferases (DNMTs), including Dnmt1, Dnmt2, Dnmt3a, Dnmt3b and Dnmt3L, and also considered as a stable gene-silencing mechanism. Specifically, the inhibition of gene transcription occurs, either by blocking the binding of transcriptional factors or through the recruitment of methylated DNA binding domain proteins. However, DNA methylation is also linked with histone modifications. Histones undergo a series of covalent modifications, like methylation, acetylation, ubiquitination, phosphorylation, and sumoylation. Furthermore, histone modifications are determined by the substrate specificity of the enzymes as well as enzymes that remove these marks. Among these modifications, histone acetylation is regarded as one of the marks for transcriptional activation and deacetylation of histone is closely associated with gene repression.

In this work, we found that the nicotine adenine dinucleotide (NAD^+)-dependent deacetylase sirtuins family is involved in epigenetic regulation, and connects histone deacetylation with DNA methylation. On the one hand, Sirt1 can interact with non-histone proteins, like Dnmt1 and Uhrf1, and influence protein stability and DNA methylation. Sirt1 mediated deacetylation stabilizes Uhrf1 in combination with the deubiquitinase Usp7. Functionally, deacetylation of Uhrf1 is a prerequisite for Uhrf1 to be phosphorylated by Cdk2 and enter into S phase of the cell cycle. The expression level of Uhrf1 fluctuates in different phases of the cell cycle and plays a crucial role in the regulation of DNA methylation. On the other hand, Sirtuins have been reported to deacetylate various substrates of histones, such as H3K9ac, H3K14ac, H4K16ac, and H1K6ac (Imai et al., 2000; Vaquero et al., 2004). Not only Sirt7 is a highly selective H3K18ac deacetylase for maintaining cellular transformation, but also Sirt1, Sirt2, and Sirt6 can deacetylate H3K18ac and regulate metabolism by downregulating some target genes. Significantly, these genes are regulated via a transcriptional factor, Hif1a, which

provides new insights into therapies and metabolic diseases. Specifically, these genes are downregulated via the increased DNA methylation because sirtuins-mediated H3K18 deacetylation promotes Uhrf1-associated ubiquitination of H3K18, which is essential for Dnmt1 binding and DNA methylation (Qin et al., 2015a). Taken together, our data suggest that H3K18 acetylation, as one of the common histone substrate of sirtuin proteins, is enriched at the transcription start site (TSS) of active and poised genes, offends DNA methylation and thereby promotes transcriptional activation of these genes.

1 Introduction

1.1 Epigenetic regulation

In eukaryotic nuclei, histones tightly compact chromosomal DNA and make the nucleosome a basic unit, in which histones are small and positively charged proteins and DNA is negatively charged from phosphate groups in its phosphate-sugar backbone (Richmond and Davey, 2003). For one nucleosome, 146 bases of DNA are packaged by the histone octamer which includes double core histones termed H2A, H2B, H3, and H4 and additional 20 bases DNA is wrapped by one H1 (Holde, 1989). A long chain of nucleosomes forms a structure called chromosome, which contains over 100 million base pairs of DNA on average. As a high-order structure, chromosomes and nucleosomes pose barriers to processes such as replication and transcription preventing the two strands of DNA to separate temporarily. In general, it is reversible as chromatin can be modified by other proteins to make it more accessible by histone acetylation, methylation or phosphorylation (Fischle et al., 2003).

‘Epigenetics’ is defined as heritable changes in gene expression (active and inactive genes) without alterations in the DNA sequence. These changes are a natural and common occurrence in the distinct cell types for the formation of multicellular organisms and tissues, but can also be influenced by aging or environment. Chromatin is the major relevant substrate for all the genetic processes in eukaryotic cells. Dynamic changes in the local or global level of chromatin influence genomic functions. So the epigenetic changes, including various post-transcriptional histone modifications, exchange of histone variants and genome-wide DNA methylation, are critical events for the organization of chromatin status and biological processes. Epigenetic regulations are crucial for development and differentiation in normal cells, as well as various cancers. In fact, epigenetic changes, especially DNA methylation, caused by a certain environment, are more susceptible to increase the risk of cancer. Collectively, the fundamental mechanisms behind epigenetic regulation contain at least five aspects: (I) DNA methylation; (II) histone modifications; (III) histone variants; (IV) chromatin remodeling; (V) non-coding RNA (ncRNA)-associated gene silencing (Akimaru et al.). In the last

decades, an increasing number of studies have uncovered considerable changes in these epigenetic mechanisms that are associated with different gene expression. The new theories explaining these epigenetic mechanisms encourage people to apply in potential epigenetic therapies or improve the treatment of various diseases.

1.1.1 DNA methylation

Currently, DNA methylation is one of the most studied epigenetic modifications. Since the methylated base 5-methylcytosine (m^5C) was discovered in 1948, Aharon Razin and Arthur D. Riggs have emphasized that DNA methylation is a key element in the control of gene function and differentiation in 1980 (Hotchkiss, 1948; Razin and Riggs, 1980). DNA methylation occurs when the methyl group is transferred from S-adenosyl methionine to a cytosine base by DNA methyltransferase enzymes. In this reaction, a cytosine base in normal B-DNA is flipped completely out of the helix into an extrahelical position so that DNA methyltransferase enzymes can access and methylate the cytosine (Roberts and Cheng, 1998). This phenomenon of base flipping was discovered with the first crystal complex structure at 2.8 Å resolution in 1994 (Klimasauskas et al., 1994) (**Figure 1**).

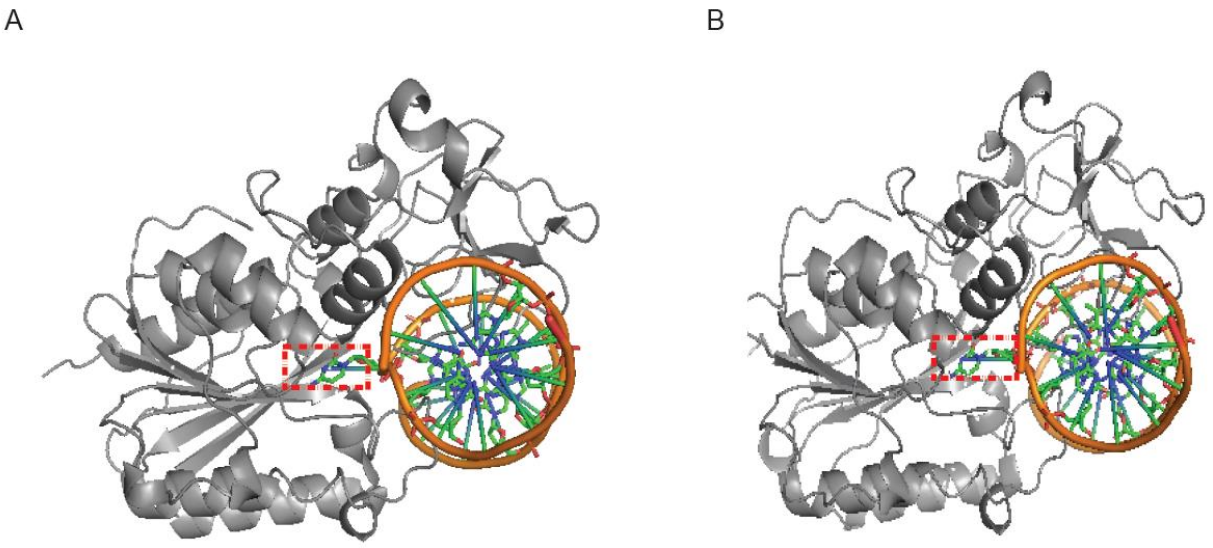

Figure 1. The crystal structures of HhaI methyltransferase with its substrate DNA. (A) HhaI can bind to unmodified DNA (PDB: 3MHT) (O'Gara et al., 1996a). (B) HhaI binds to hemimethylated DNA (PDB: 5 MHT) (O'Gara et al., 1996b). The flipped cytosine base is labeled in red dot block. And the protein HhaI is shown in grey. The sugar-phosphate backbone is in orange and the side chains of DNA are in green, the bases are in blue.

DNA methylation occurs ubiquitously in prokaryotes and eukaryotes. In bacterial genomes, DNA methylation is post-replicative and occurs at specific DNA sequences, which functions as part of an immune protector by introducing sequence-specific restriction enzymes to degrade the unmethylated foreign DNA to avoid bacteriophage infection. In plants, DNA is highly methylated with 5-methylcytosine (m^5C) and N6-methyladenine (m^6A), and m^5C is located not only in symmetrical CG and CNG sequence but also in other non-symmetrical contexts (Vanyushin, 2006). In mammals' genome, DNA methylation occurs mainly in a CpG dinucleotide context. Specifically, more than 98% of DNA is methylated in a CpG site in the somatic cells, while there is still around one-quarter of DNA methylation occurring in a non-CpG context in embryonic stem cells (ESCs) (Lister et al., 2009). In addition, non-CG methylation is mostly enriched in gene bodies and dynamically exists in protein binding sites and enhancers, which disappears in the differentiation of embryonic stem cells (Lister et al., 2009).

In eukaryotes, DNA methylation is essential in a wide range of key cellular processes including gene regulation, genome stability, imprinting and X-chromosome inactivation (Bender, 2004; Gopalakrishnan et al., 2008). Deregulation of DNA methylation can result in diseases like cancer. Global DNA hypomethylation is one of the epigenetic hallmarks of cancer (Suzuki and Bird, 2008). Mostly, DNA methylation in promoter elements can disturb the binding of transcriptional factors and repress gene transcription, which also indirectly promotes the formation of tight chromatin by recruiting the methyl DNA-associated proteins (Bird, 2002). The proteins which catalyze cytosines to methyl-cytosines are members of DNA methyltransferase (DNMT) protein family, including DNMT1, DNMT2, DNMT3A and DNMT3B (Cheng and Blumenthal, 2008; Okano et al., 1998). All the DNMTs except DNMT3L contain a highly conserved methyltransferase catalytic domain in their C-terminal regions (**Figure 2**). Mammalian Dnmt1 preferentially

methylates hemimethylated DNA and functions as the maintenance methyltransferase for the DNA methylation of daughter strand during DNA replication (Probst et al., 2009). While Dnmt3A and Dnmt3B, different from DNMT1, prefer to bind unmethylated DNA and perform *de novo* methylation during development. Although DNMT2 shares a similar sequence and structure with the other DNMTs, DNMT2 does not methylate DNA but instead a small RNA, specially methylating cytosine 38 in the anticodon loop of a tRNA (Goll et al., 2006).

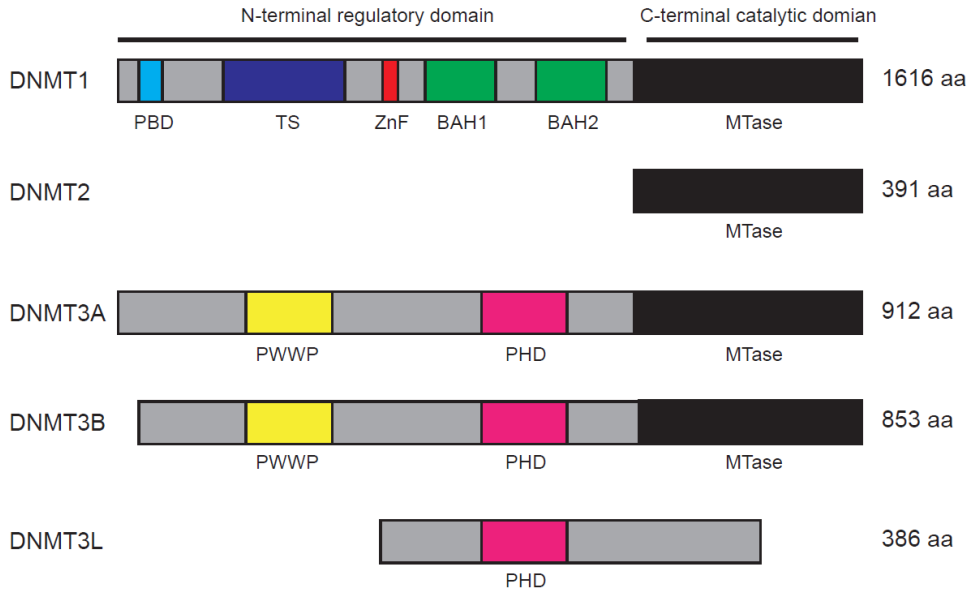

Figure 2. Domain structures of human DNMT family proteins. All DNMTs except DNMT2 and DNMT3L contain a regulatory N-terminal and a conserved C-terminal catalytic domain. DNMT2 only contains a catalytic domain. PBD: PCNA binding domain; TS: targeting sequence; ZnF: zinc finger domain; BAH: bromo-adjacent homology domain; PWWP: Pro-Trp-Trp-Pro motif containing domain; PHD: plant homeodomain; MTase: methyltransferase domain. AA: amino acid. The numbers of amino acids of DNMTs are indicated (Maresca et al., 2015).

DNA methylation is timely removed after the zygote formation and re-established after the implantation of embryonic stem cells (Lee et al., 2014). DNA methylation and demethylation determine the level and pattern of $5^{m}C$ in the different states of cells, meaning that reprogramming to reach a global hypomethylation function to erase the memory and provide a potential for diversity of transcriptional states (Lee et al., 2014).

Recently researchers have discussed that a protein family of DNA glycosylases can demethylate DNA through a base excision repair pathway (Zhu, 2009). These DNA glycosylases, such as MBD4 and TDG, repair G/T mismatches following the conversion of 5-methylcytosine to thymine that can occur spontaneously or be catalyzed by the AID/Apobec family of deaminases.

1.1.2 Histone modifications

As the major structural proteins of a chromosome, histones experience various post-translational modifications (PTMs), including phosphorylation, acetylation, methylation, ubiquitination, and sumoylation. The first histone modification was found in the early 1960s when Vincent Allfrey showed that histones can be acetylated and methylated (Allfrey et al., 1964). To explore the significant roles of histone modifications in chromatin, the high resolution of the X-ray crystal structure of the nucleosome provided a clear insight into these unknown questions (Luger et al., 1997). The structure displays that histone fold domain regulates the histone/histone and histone/DNA interactions, and histone amino-terminal tails also can be modified to connect neighboring nucleosome, influencing some key processes, including nucleosome dynamics, chromatin compaction, and transcription. Recent work has largely shown that modifications in the histone cores can directly influence replication and nucleosome stability, and even DNA damage response, stemness, leukemia and cell differentiation (Lawrence et al., 2015).

1.1.2.1 Histone acetylation

Since Vincent Allfrey has identified that histone can be acetylated, researchers have been trying to figure out the mechanism of this modification. Acetylation of histones takes place on the NH^{3+} groups of lysine residues and this reaction can be carried out by histone acetylases (HATs) and the cofactor acetyl-CoA. The acetylated lysine residues neutralize its positive charge and weaken the interaction of histones and DNA, resulting in a loose condition of chromatin, so it is thought that acetylation is closely associated with transcriptional activation. Over the past 50 years, various HATs have

been isolated from different species. In general, there are two types of HATs: Type A HATs are localized in nuclei and type B HATs are in the cytoplasm. For the type A HATs, the proteins, including Gcn5, p300/CBP, and $TAF_{II}250$, contain a conserved bromodomain for specifically binding to the acetylated lysine residues. Different from type A HATs, type B HATs without bromodomain, prefer to acetylate the newly synthesized histones or deacetylated histones. There are mainly four families of type A HATs: Gcn5-related N-acetyltransferases (GNATs); MYST HATs; global coactivators p300/CBP and CREB-binding protein, and nuclear receptor coactivators SRC-1, ACTR, and TIF2; TATA-binding protein-associated factor $TAF_{II}250$; and TFIIIC, the subunit of RNA polymerase III.

The members of the GNAT family have a conserved motif A, characterized by an Arg/Gln-X-X-Gly-X-Gly/Ala sequence that provides a base for acetyl-CoA binding (Roth et al., 2001). The GNAT family includes Gcn5, Pcna, Hat1, Elp3, Hpa2, Hpa3, ATF-2, and Nut1. Gcn5 and Pcna share a homologous sequence and contain an N-terminal domain, a highly conserved catalytic domain (HAT) and C-terminal bromodomain. Hat1 is the first identified HATs. Elp3 and Hat3 are found in yeast. ATF-2 can bind to the cAMP-responsive element (Bonapace et al.) and forms a homodimer or heterodimer with c-jun to activate CRE-dependent transcription. The GNAT HATs have been shown to acetylate lysine on histone H2B, H3, and H4. Among these, Gcn5 and Pcaf have a preference for H3K14 acetylation, but it requires other protein factors to assist Gcn5 to acetylate histones (Sterner and Berger, 2000).

The MYST family includes Moz, Ybf2 (Sas3), Sas2, Tip60, Esa1, Mof, Morf, and Hbo1, which typically contain two domains: zinc finger and chromodomain. The zinc finger is now recognized to bind DNA, RNA, protein and lipid substrates (Gamsjaeger et al., 2007; Hall, 2005; Klug, 1999; Matthews and Sunde, 2002). Chromodomain is a structural domain of about 40-50 amino acids and associated with remodeling of chromatin. The MYST family proteins mainly acetylate histone H2A, H3, and H4. Tip60, also named Kat5, is firstly found in yeast and its homolog is Mof in fruit flies. Tip60 is known for acetylating histones and non-histone proteins, involved in regulation of transcription, DNA repair, and apoptosis. Tip60 targets multiple proteins and these proteins interact as the substrates for acetylation in regulatory pathways (Lehner et al.,

2006). It has also been shown that in the late G1 phase of cell cycle, hyperacetylation of H3 and H4 occurs dependent on E2F-mediated recruitment of the Tip60 complex (Tip60, Trrap, p400, Tip48, and Tip49) (Taubert et al., 2004).

CREB-binding protein (CBP) and p300 are proposed to be the same protein family because both of them bind to E1A to co-activate CREB-mediated transcription (Akimaru et al., 1997). Both of p300 and CBP contain an N-terminal nuclear receptor-interacting domain (Fuks et al.), the CREB-binding domain (KIX), bromodomain and the three cysteine/histidine-rich regions (CH1, CH2, and CH3) (Radhakrishnan et al., 1999). It is reported that p300 and CBP not only acetylate histones but also have many non-histone substrates, including non-histone chromatin proteins HMG1, HMG14, the transcriptional factors TFIIE and TFIIF, the transcriptional activators p53 and c-Myb. But it has also been observed that p300 and CBP can be autoacetylated and regulate their own function (Kraus and Kadonaga, 1998).

1.1.2.2 Histone deacetylation

Histone acetylation is highly reversible. Histone acetylation and deacetylation are dynamic processes dependent on different states of cells. The establishment of acetylation is performed by HATs family proteins and elimination of acetylation is by histone deacetylases (HDACs). It is likely that deacetylation of histones is related to transcriptional repression and increased DNA methylation. HDACs now is also called lysine deacetylases (KDACs). In mammals, HDACs are divided into four classes based on the similarity of protein sequences: the class I Rpd3-like proteins including HDAC1, HDAC2, HDAC3, and HDAC8; class II Hda1-like proteins are HDAC4, HDAC5, HDAC6, HDAC7, HDAC9, and HDAC10; class III sirt2-like proteins containing SIRT1, SIRT2, SIRT3, SIRT4, SIRT5, SIRT6, and SIRT7; class IV protein is HDAC11. For the class I, II, IV, the proteins require a zinc ion to deacetylate acetylated lysines, but for the class III HDACs, the proteins require NAD^+ as a cofactor for the enzyme activity.

In class I HDACs, the proteins share a similar sequence with the transcription regulator reduced potassium dependency 3 (Rpd3) which is a subunit of the histone deacetylase complex in yeast. The N-terminal catalytic domain is the main part of the proteins.

HDAC1 and HDAC2 are highly similar at about 82% identity, and HDAC3 is closely related to HDAC8 with 34% identity based on their structural domain. HDAC1 and HDAC2 are only localized in nuclei with a nuclear localization signal (NLS), while HDAC3 has both nuclear localization signal (NLS) and nuclear export signal (Robertson et al.), suggesting that HDAC3 may shuttle between nucleus and cytoplasm. Till now, HDAC8 has been found in both the nucleus and cytoplasm (de Ruijter et al., 2003).

For the class II HDACs, HDAC4, HDAC5, HDAC6 have been identified from GenBank based on sequence similarity with yeast Hda1 (Grozinger et al., 1999). These three HDACs own a lower level of enzyme activity than other HDACs. In their structures, HDAC4, HDAC5, and HDAC7 have a catalytic domain in the C-terminus, followed by an NLS, while HDAC9 has the catalytic domain at the N-terminus. Both of HDAC6 and HDAC10 have two catalytic domains. It has been reported that HDAC6 is linked with the ubiquitin system through ubiquitin conjugation, suggesting that the stability of HDAC6 is regulated in the cell (Hook et al., 2002).

As the only member of class IV HDACs, HDAC11 was first described in 2002 (Gao et al., 2002). It has an N-terminal catalytic domain and localized in the nucleus. Till now, HDAC11 is not involved in any HDAC complexes, so it may have unknown physiological roles distinct from other known HDACs.

1.1.3 The correlation between DNA methylation and histone modifications

The deep insight into the role of DNA methylation and histone modifications on transcription, chromatin stability, DNA repair, cell cycle, and differentiation, reveals a complex relationship between them. For example, there is evidence that the level of DNA methylation in global or local genome affects histone states in chromatin, particularly the histone lysine methylation state, and in turn, the modifications of histone, including acetylation, methylation, phosphorylation, and ubiquitination, also influence DNA methylation in chromatin. Although histone modifications are more complex with the absence of DNA methylation in some species, it is fascinating to raise interesting

questions about the interplay between DNA methylation and histone modifications (Rose and Klose, 2014).

In mammals, the percentage of DNA methylation reach up to 80% and especially, in mouse and human, DNA methylation is essential for heterochromatin formation, transcriptional repression, and the inactive X chromosome. Like DNA methylation, H3K9me is shown to tighten heterochromatin and repress transcriptional expression. The histone methyltransferases, Suv39h1/2, which methylate H3K9, strongly associate with methylated CpG DNA binding protein MeCP2 and co-localize at pericentromeric heterochromatin (Fuks et al., 2003). However, there is no obvious lack of H3K9me3 at pericentromeric heterochromatin in the MeCP2 knockout mouse model owing that the other members of the MBD family are still essential for H3K9me3 binding to heterochromatin. For example, It has also been reported that Suv39h1 and HP1 can directly interact with MBD1 and enhance histone deacetylation and DNA methylation for transcriptional repression (Fujita et al., 2003). Another histone methyltransferase for H3K9me, SETDB1, is recruited by the methyl-CpG binding protein MBD1 to form a large complex with chromatin assembly factor CAF-1 during DNA replication. However, the absence of MBD1 leads to serious loss of H3K9 methylation, indicating that MBD1 is essential for maintenance of H3K9 methylation state in heterochromatin (Sarraf and Stancheva, 2004). Histone methylation is associated with either transcriptional repression or activation. H3K4 trimethylation is a well-known factor for gene activation. It is demonstrated that H3K4 methylation can block *de novo* DNA methylation because Dnmt3L strongly interact with unmethylated H3 and the interaction is disturbed by methylated H3K4 (Ooi et al., 2007). The interaction of Dnmt3L and unmethylated H3K4 can recruit and active Dnmt3A2 for *de novo* DNA methylation. Consistent with this discovery, DNA methylation is disrupted in Lsd2-deficient mice and Lsd2/Kdm1b is a histone demethylase for removing H3K4 methylation (Wang et al., 2008).

Besides histone lysine methylation, recent evidence has indicated that histone ubiquitination affects DNA methylation. Uhrf1 not only specifically binds to hemimethylated DNA and recruits Dnmt1 to maintain DNA methylation, but also has a role in histone ubiquitination. It has been shown that Uhrf1-dependent ubiquitylation of histone H3K 23 is markedly accumulated in the absence of Dnmt1, suggesting that

H3K23 ubiquitylation is a precondition for the maintenance DNA methylation (Nishiyama et al., 2013). Moreover, it also has been proven that H3K18 is another novel ubiquitination target of Uhrf1 and H3K18 ubiquitination binds to the newly identified ubiquitin-interacting motif (UIM) in the N-terminal regulatory domain of DNMT1, which is essential for DNA methylation (Qin et al., 2015b). It is further demonstrated with the crystal structure of the targeting sequence (TS) of Dnmt1 in complex with H3K18Ub/23Ub, which displays that the spatial rearrangement of TS binding to H3K18Ub/23Ub opens Dnmt1 active site and increases its catalytic activity for DNA methylation maintenance (Ishiyama et al., 2017).

Histone acetylation can contribute to the decondensed chromatin structure and activate gene transcription. Hyperacetylation generally represents transcriptionally active genes, where DNA methylation is low. Although histone hyperacetylation cannot dramatically reduce the level of DNA methylation, the level of histone acetylation is increased in the Dnmt1 knockout cells. Histone hypoacetylation is required for the formation and maintenance of normal heterochromatin (Casas-Delucchi et al., 2011). The acetylation of H3 at K18 and K23 is necessary for local gene activation in mammals. It is reported that a regulator of DNA demethylation, IDM1, binds to the methylated DNA without histone H3K4 methylation and further acetylates H3 for preventing DNA hypermethylation at multicopy genes and repetitive sequences in *Arabidopsis* (Qian et al., 2012). And Repressor of silencing 1 (ROS1), a DNA demethyltransferase in *Arabidopsis*, is identified to silence 35S-NPTII transgene in the RNA-directed DNA methylation (RdDM) pathway and increase H3K18 and H3K23 acetylation level (Barber et al., 2012b). Together, it is suggested that H3K18 and H3K23 acetylation probably suppress the maintenance of DNA methylation.

1.2 Maintenance DNA methylation by Dnmt1 and Uhrf1

It has been proposed that DNA methylation of the genome is inherited in somatic cells, but the enzyme for methylating half-methylated sites was not detected in eukaryotes (Riggs, 1975). Since that Dnmt1 was first discovered as a DNA methyltransferase, it has been the most widely studied. The theory that the methylated DNA sequences were

replicated in somatic cells was tested with biochemical experiments, and it has shown that methylation at modification enzyme M-Hpa II sites is replicated in the cultured cells but not with 100% fidelity (Wigler et al., 1981). Moreover, it has been demonstrated that DNA methylation is highly dynamic during mouse development (Razin and Cedar, 1993). The DNA methyltransferases, Dnmt3a and Dnmt3b, have also been identified to be indispensable for *de novo* DNA methylation that mainly occurs during the early stages of embryo development in mice (Okano et al., 1999). Furthermore, Uhrf1 has been also found and reported to recruit Dnmt1 to replication forks for the maintenance of DNA methylation (Bostick et al., 2007).

1.2.1 Dnmt1 for DNA methylation maintenance

Since that Dnmt1 has been first identified to methylate DNA, researchers have started to explore the structures and cellular functions of Dnmt1. Dnmt1 is a large protein containing around 1620 amino acids. In its structure, the N-terminal regulatory domain contains the motifs, such as PCNA binding domain (PBD), targeting sequence (TS), zinc finger domain (ZnF) and bromo-adjacent homology domain (BAH). Among these motifs, the PBD has been identified to specifically bind to PCNA and recruit Dnmt1 to DNA replication and repair sites. The CXXC motif of zinc finger domain (ZnF) has been shown to selectively bind to unmethylated DNA substrates (Frauer et al., 2011a). The TS domain mainly targets heterochromatin. The function of the BAH domain is still unclear, although it is predicted that the BAH domain forms a platform for protein-protein interaction linking DNA methylation and gene silencing (Callebaut et al., 1999). The C-terminal domain of Dnmt1 is the catalytic domain connected with the N terminus by a linker of seven glycine-lysine repeats (GK linker). However, the catalytic domain of Dnmt1 is inactive when the N-terminal part is deleted (D'Aiuto et al., 2010). The biochemical assay has also shown that the preference for hemimethylated DNA to Dnmt1 is dependent on the catalytic domain of Dnmt1, but neither the isolated catalytic domain does not methylate DNA, nor in combination with other domains, suggesting that the binding of methylated DNA stimulates the allosteric activation of the catalytic domain of Dnmt1 (Fatemi et al., 2001). In the crystal structure of the Dnmt1-DNA

complex, the CXXC motif specifically binds to unmethylated DNA, resulting in the linker between CXXC-BAH1 occupying the active site of Dnmt1 to prevent *de novo* DNA methylation (Song et al., 2011).

Although Dnmt1 is known as a DNA methyltransferase for maintenance of DNA methylation based on the biochemical data and crystal structure, it is universally expressed in proliferating and post-mitotic cells for copying the methylation pattern to the nascent strand of DNA. While the N-terminal part of Dnmt1 controls the subcellular distribution of Dnmt1 in the cell cycle, the expression level of Dnmt1 is regulated during cell differentiation and diseases. For example, Dnmt1 is downregulated in PC12 neuronal cells and upregulated in acute myeloid leukemia (AML) (Deng and Szyf, 1999; Mizuno et al., 2001). Furthermore, recent studies have also revealed that the altered expression of Dnmt1 is significantly associated with different tumors and cancers. Some types of tumors are detected with an elevated level of Dnmt1 methylation but some tumors with a low level of DNA methylation (Robert et al., 2002). And also, the importance of Dnmt1 has been deduced originally from evidence about Dnmt1 knockouts of cell lines or mice. Mouse embryonic stem cells deficient in Dnmt1 showed a three-fold reduction of global DNA methylation and increased global gene expression (Li et al., 1992). Surprisingly, the mutation of Dnmt1 is introduced into the germline of mice, causing a recessive lethal phenotype have with a reduction of the level of m^5C. In contrast, the Dnmt1 knockout murine fibroblasts undergo p53 mediated cell cycle arrest at G1 phase and apoptosis (Jackson-Grusby et al., 2001). More specifically, Dnmt1 is crucial for X-chromosome inactivation and chromatin stability. Dnmt1 has been shown to link with DNA damage and repair. Dnmt1 is rapidly recruited to the DNA double-strand breaks and interacts with the DNA damage response factors, including PCNA and the ATR effectors' kinase CHK1, for the accuracy of inherited DNA methylation (Ha et al., 2011). Furthermore, only Dnmt1, not Dnmt3a and Dnmt3b, accumulates with PCNA at DNA sites during DNA repair (Mortusewicz et al., 2005).

1.2.2 Uhrf1- a cofactor of Dnmt1

As a cofactor of Dnmt1 for maintenance of DNA methylation during DNA replication in cells, ubiquitin-like with PHD and RING Finger domains 1 (UHRF1), also known as inverted CCAAT box-binding protein of 90 kDa (ICBP90), is a nuclear factor and preferentially localized in pericentric heterochromatin but is also found in euchromatin and plays a critical role in DNA methylation and histone modifications (Bronner et al., 2010; Hopfner et al., 2000). Uhrf1 specifically binds to hemimethylated CpG dinucleotide and recruits Dnmt1 and histone deacetylase 1 (HDAC1) through distinct domains (Liu et al., 2013). Structurally, Uhrf1 contains five specific domains: Ubiquitin-like domain (UBL) at the N terminus of Uhrf1 required for its E3 ubiquitin ligase activity, tandem Tudor domain (TTD) for binding to di- or tri-methylated H3K9, plant homeodomain (PHD) interacting with G9a for H3 methylation, Set and RING Associated domain involved in maintaining DNA methylation and histone modifications by recruiting Dnmt1 and HDAC1, Really Interesting New Gene (RING) domain at the C terminal of Uhrf1 for H3 ubiquitination with its E3 ligase activity. Moreover, TTD of Uhrf1 acts to tightly contact the residues with the methylated lysine and meanwhile, it cooperates with PHD of Uhrf1 to recognize H3K9me3 and drives Uhrf1 to the pericentric heterochromatin (Cheng et al., 2013). The crystal structure of Uhrf1 and hemimethylated DNA also revealed that 5-methylcytosine flips out of the DNA helix and then gets positioned into a pocket by stacking and interacting with two conserved residues, Y478, and Y466 (Hashimoto et al., 2008). Emerging evidence indicates that the modules of UHRF1 do not act independently of each other but establish complex modes of interaction with patterns of chromatin modifications, like the cooperative interaction between TTD, PHD and SRA domain for establishment and maintenance of methylation patterns. In addition, it is also demonstrated that the SRA domain of Uhrf1 can directly bind to the replication focus targeting sequence domain of DNMT1, resulting in an almost 5-fold increase of the Dnmt1 activity (Bashtrykov et al., 2014).

The expression of Uhrf1 is tightly controlled. It is highly expressed in proliferating cells, and also peaks at late G1 and during G2/M phases in the cell cycle. There is a higher level of Uhrf1 in various cancer cell lines and the expression of Uhrf1 remains constant throughout the entire cell cycle. Aberrations in UHRF1 expression are linked with many different human diseases, especially various cancers. For example, it is easily detected

in tissue samples and urine sediments of bladder cancer patients. The detection method based on immunohistochemistry in urine sediment can be potentially applied to the current diagnosis (Unoki et al., 2009a). Knockout or downregulation of Uhrf1 in cancer cells contributes to the inhibition of cell proliferation and the increase of apoptosis (Ge et al., 2016). It is reported that the silencing of Uhrf1 in gall bladder cancer cells arrests cells at G1/S phase by increasing p21 expression in a p53-independent pathway and induces extrinsic and intrinsic apoptosis through the elevated expression level of genes, such as FasL/FADD, bax, cytosolic cytochrome c, cleaved caspase-8, -9 and -3 and cleaved PRAP (Qin et al., 2014). Besides the involvement in cancers, Uhrf1 is also reported to regulate DNA repair. Co-immunoprecipitation assay has proven the interaction between Uhrf1 and N-methylpurine DNA glycosylase (MPG), the first enzyme identified in the base excision repair pathway, that is involved in repairing single-strand DNA (Liang et al., 2013). Uhrf1 is also involved in two kinds of double-strand repair pathways, including homology-directed and nonhomologous end joining (NHEJ), with different factors. In the homologous repair pathway, Uhrf1 is phosphorylated at S674 site by the BRCT domain of BRCA1. The phosphorylated Uhrf1 then activates its E3 ubiquitin ligase activity to replication timing regulatory factor 1 (RIF1), resulting in the dissociation of RIF1 from 53BP1, initialization of homologous recombination (Zhang et al., 2016). The nonhomologous DNA repair pathway occurs when the endogenous level of the Ku heterodimer protein complex (Ku70/Ku80) is reduced by the inhibition of Uhrf1 (Yang et al., 2013).

1.3 The class III of histone deacetylases: Sirtuins

As mentioned in the part of histone deacetylation, histone deacetylases (HDACs) have four classes. Sirtuins are the class III of histone deacetylases with nicotine adenine dinucleotide (NAD+) instead of zinc as a cofactor. Sirtuins were originally identified as histone deacetylases in yeast and mouse Sirt2 mediated the deacetylation of lysine 9 and 14 of H3 and specifically lysine 16 of H4, which contributes to a tighter chromatin structure and transcriptional repression (Imai et al., 2000). Sirtuins have 7 members (Sirt1-7) in mammals and catalyze a range of post-translational modifications in histones

and nonhistone proteins, including deacetylation, desuccinylation, demalonylation and deglutarylation (Du et al., 2011; Tan et al., 2014) (**Figure 3**). The members of the sirtuin family share a conserved catalytic motif in which structurally forms a cleft for their substrates and nicotinamide.

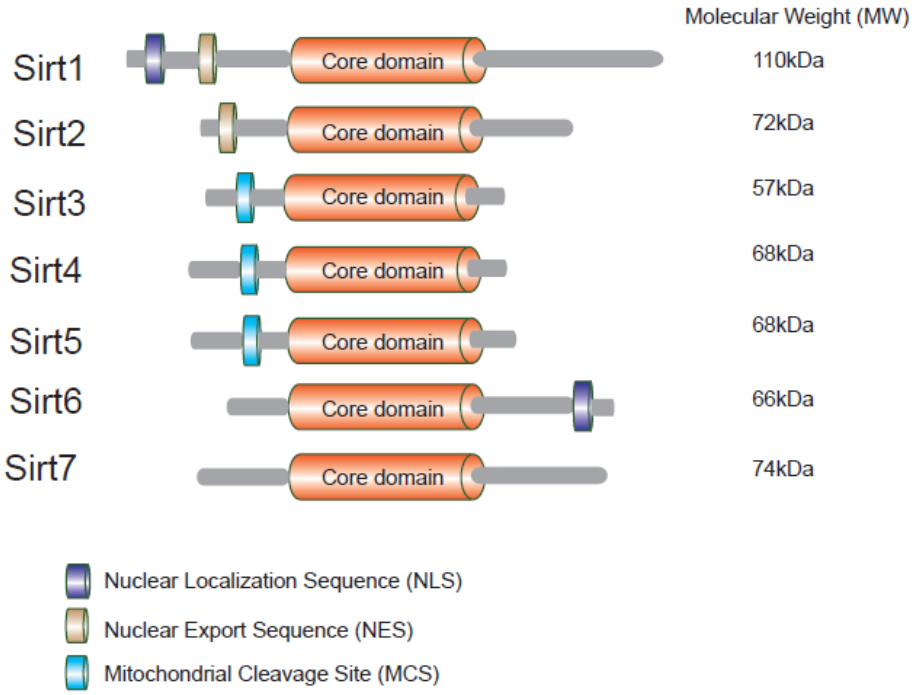

Figure 3. Schematic domains of mouse sirtuins family members, Sirt1–7, with different molecular weights. The core domain of sirtuins for enzyme activity is in orange, GFP tag is labeled in green. Nuclear localization sequence (NLS) is in purple and nuclear export sequence (NES) in light yellow. The mitochondrial cleavage site in Sirt3, Sirt4, and Sirt5 is shown in blue (Flick and Lüscher, 2012b).

Sirtuins ubiquitously distribute in tissues and the expression levels vary according to the types of tissues and cells. Generally, Sirt1 is predominately localized in the nucleus, but it also shuttles between the nucleus and the cytosol in different cell types (Tanno et al., 2007); Sirt2 is mainly expressed in the cytoplasm, but it is also involved in mitosis (Perrod et al., 2001; Vaquero et al., 2006); Sirt3, Sirt4, and Sirt5 localize in mitochondria, but Sirt3 is also present in the nucleus (Iwahara et al., 2012; Matsushita et al., 2011; Onyango et al., 2002); Sirt6 and Sirt7 are also nuclear proteins, but both of them own

distinct sub-nuclear localization patterns. In the nucleus, Sirt1 is mainly associated with euchromatin, while Sirt6 binds to heterochromatin and Sirt7 localizes in the nucleolus (Ford et al., 2006; Michishita et al., 2005). Yeast Sirt1 was originally identified to promote transcriptional silencing at many types of genomic locus, including telomeres, rDNA locus and mating type locus (Gasser and Cockell, 2001). It is reported that yeast Sirt2 functions to control longevity through suppressing extrachromosomal rDNA derived from errant intralocus recombination (Kaeberlein et al., 1999). The enzyme activity of Sirtuins requires NAD^+ as a cofactor, suggesting that the cytosolic ratio of NAD^+ and NADH connects sirtuins with the metabolic state and cellular energy state. The NAD^+ level is affected by certain conditions, including nutritional status, diet, and exercise (Opitz and Heiland, 2015). It has been reported that the decrease in the nuclear NAD^+ level is the outcome of caloric restriction (Anderson et al., 2003). Numerous evidence has demonstrated that Sirt2 in different species, including yeast, spiders, fish, and Drosophila, functions to extend the lifespan through the caloric restriction (Haigis and Guarente, 2006). However, Sirt2 can only extend life span in yeast under starvation conditions or certain exceptional mutations to extend the life span of Sirt2delta mutants (Fabrizio et al., 2005). Besides Sirt2, the traditional role of other sirtuins is also a lifespan-extending effect mediated by caloric restriction. Dysfunction of sirtuins contributes to aging and a wide range of metabolic, cardiac, and neurodegenerative diseases and cancers (Wątroba and Szukiewicz, 2016).

Despite their ability to regulate metabolism, sirtuins are ubiquitously distributed in different cells and tissues and different sirtuins are expressed distinctly dependent on tissue types and developmental stages. In the brain, each sirtuin displays a unique spatial and temporal expression pattern at different stages and the relative mRNA expression levels does not correlate with the respective protein level, which suggests that a specific sirtuin is potentially targeted or target specific substrates to display cell-type selective effects in the rat brain (Sidorova-Darmos et al., 2014).

Because of their important roles and diseases caused by sirtuins, sirtuins must be tightly controlled, including the protein level, subcellular localization and enzymatic activity (Buler et al., 2016). And they are regulated to response to intricate regulatory networks in several conditions, such as metabolic and nutritional disorder, inflammatory formation

and oxidative stress. Each sirtuin protein is uniquely regulated by a wide range of factors through the regulation of transcription. Furthermore, post-transcriptional modifications control the sirtuins' catalytic activity. Although all sirtuins share a conserved catalytic domain for binding NAD+, the enzymatic activities differ for each sirtuin family member because of its flexible N- and C- terminal extensions. To date, available evidence suggests that the N- and C- terminal extensions are the main targets of post-translational modifications that control the functions and localizations of sirtuins, thus connecting these proteins to different signaling pathways (Flick and Lüscher, 2012a).

1.3.1 Sirt1

Sirt1 is a protein of about 747 amino acids composed of a catalytic domain and has extended N- and C-terminal regions different from other members of the mammalian sirtuins family. It is mainly localized in the nucleus but is also present in the cytosol in different cell types (Tanno et al., 2007). The reason for Sirt1's different localization is that it contains two signal regions: the nuclear localization signal and a nuclear export signal. Sirt1 is distinct from other sirtuins for the extended N- and C-terminal regions. In the crystal structure of Sirt1, it has been shown that the C-terminal regulatory segment (CTR) plays a key role in its activity, especially the 25-residue C-terminal ESA sequence, which mediates the binding and inhibition of Sirt1 catalytic domain via forming a β hairpin structure to complement the β sheet of the NAD^+-binding domain (Davenport et al., 2014). It is also reported that the resveratrol and related compounds, as direct SIRT1 activators, interact with the N-terminal domain (NTD) of Sirt1 and the amino-4-methylcoumarin (AMC)-containing peptide, which provides a model for further mechanistic analysis (Cao et al., 2015).

In mammalian cells, Sirt1 deacetylates histones and many transcriptional factors, including p53, fork-head box protein O (FOXO), NF-kB, peroxisome proliferator-activated receptor g coactivator 1-a (PGC-1a) and various nuclear receptors (Poulose and Raju, 2015). Through the interaction with these numerous proteins, Sirt1 is involved in fundamental cellular processes including metabolism, glycosylation, DNA repair,

apoptosis, inflammation and mitochondrial biogenesis (Haigis and Sinclair, 2010). Consequently, dysregulation of Sirt1 in expression and function leads to several diseases, including cancers, insulin resistance and cardiac disease (Liang et al., 2009; Lin and Fang, 2013; Matsushima and Sadoshima, 2015). Sirt1 also regulates the expression of specific genes associated with cardiovascular disease, type2 diabetes (T2D) susceptibility and Parkinson's disease (Kilic et al., 2014; Rai et al., 2012; Zhang et al., 2012). Although numerous studies have shown that yeast Sirt2 extends life span via a diet of reduced calories, also known as caloric restriction (CR), there is no evidence for Sirt1 to extend life span. However, mouse models have shown a link between Sirt1 and caloric restriction. For example, caloric restriction in mice requires Sirt1 for a complex pattern of physiological and behavioral changes (Chen et al., 2005). Sirt1 transgenic mice display some metabolic phenotypes similar to CR phenotypes: more metabolically active; more glucose tolerant and reductions in blood cholesterol, adipokines, insulin and glucose (Bordone et al., 2007). Moreover, Sirt1 null mice also have shown that Sirt1 is an important regulator of energy metabolism in response to caloric restriction (Boily et al., 2008). Meanwhile, the expression level of Sirt1 is not only controlled by specific transcriptional factors but also associated with the stimuli of energy stresses, such as CR, fasting and food withdrawal. Energy deprivation promotes Sirt1 activation by increasing the ratio of NAD^+/NADH and also upregulates Sirt1 expression through the interaction between cyclic AMP response-element-binding protein (CREB) and carbohydrate response-element-binding protein (ChREBP) (Noriega et al., 2011). Sirt1 is downregulated in aging organisms. It has been demonstrated that decrease of Sirt1 in the liver of old mice is mediated by CCAAT/Enhancer Binding Protein/histone deacetylase 1 (C/EBPβ-HDAC1) complexes, which binds to Sirt1 promoter and represses its expression and consequently reduces the level of glucose and triglycerides during liver regeneration (Jin et al., 2011). Other regulators of the Sirt1 gene, such as p53, FOXO1, BMAL1, and E2F1 are deacetylated by Sirt1 and in turn, regulate Sirt1 level as to form a feedback loop. The stability of Sirt1 is also related to its post-translational modifications. Sirt1 can be stabilized by an ubiquitin-specific peptidase, USP22. USP22 interacts with Sirt1 and removes polyubiquitin chains conjugated onto Sirt1, and the USP22-mediated stabilization of Sirt1 decreases the level of acetylated

p53 and suppresses p53-dependent apoptosis (Lin et al., 2012). Previous mass spectrometry identified 13 residues of Sirt1 for phosphorylation and the mutations of T530 and S540 (threonine 530 and serine 540) that are phosphorylated by cycling/Cdk1 disturb cell cycle progression and proliferation (Sasaki et al., 2008).

1.3.2 Sirt2

Mammalian Sirt2 is homologous with yeast Sirt2 and with a smaller molecular weight of around 40 kDa. In the sirtuin family, Sirt2 is the only cytoplasmic protein. In mice, Sirt2 has two isoforms: mSIR2L2 and mSIR2L3, similar to human Sir2-like proteins SIR2L2 and SIR2L3. The two isoforms share the highly conserved core domain, however, their proteins have a different structure and intracellular localization compared to yeast Sirt2 (Yang et al., 2000). According to the crystal structure of the catalytic core of sirtuin proteins, they share a NAD-binding domain and a smaller domain composed of a helical module and a zinc-binding module, which form a conserved large groove at the interface (Yuan and Marmorstein, 2012). The pocket, composed of several hydrophobic residues in the large groove, provides the space for the binding of specific proteins. However, besides the previously established catalytic intermediates I and II, a new intermediate (III) has been reported in the crystal structures of Sirt2 in complexes with a thiomyristoyl lysine peptide-based inhibitor and NAD, which provides more mechanistic insights into sirtuin-catalytic processes (Wang et al., 2017). The distribution and abundance of Sirt2 are dependent on the cell- or tissue-type. It is reported that Sirt2 is highly expressed in the brain of mouse and rat, and human cortex, while Sirt2 is expressed at extremely low level in immortalized cultured cells, including mouse N2a, human SH-SY5Y neuroblastoma, and U87-MG glioblastoma lines (Maxwell et al., 2011).

In recent years, Sirt2 has been reported to regulate multiple cellular processes, such as cell cycle, adipogenesis, fatty acid oxidation, gluconeogenesis, insulin sensitivity, and tumorigenesis. In the cytoplasm, Sirt2 functions to deacetylate lysine-40 of alpha-tubulin, which suggests a potential role of Sirt2 in cell shape, intracellular transport, cell motility and cell division (North et al., 2003). In the cell cycle, Sirt2 shuttles to the nucleus and deacetylates H4K16Ac (acetylation of H4K16) and PR-Set7 at K90 to modulate its

chromatin localization (Serrano et al., 2013). Not only Sirt2 is involved in mitosis in the normal cell cycle, but it has also been reported that Sirt2 can block the entry to chromosome condensation in response to mitotic stress (Inoue et al., 2006). In this study, Sirt2-null mice display chromatin instability and promote tumorigenesis during mitosis. Moreover, Sirt2 also plays important roles in mammalian metabolism. For example, Sirt2 deacetylates several target proteins associated with metabolic homeostasis. Through physically interacting with insulin, Sirt2 activates Akt and targets downstream genes for insulin sensitivity. Sirt2 inhibits adipogenesis via the deacetylation of FOXO1. PGC-1α can be deacetylated by Sirt2 and involved in mitochondrial biogenesis. Sirt2 inhibits NF-κB activity by deacetylating p65 in response to inflammatory stress (Gomes et al., 2015). For some substrates, Sirt2 exhibits a catalytic activity similarity to Sirt1. Tumor suppressor p53 is a common target protein for Sirt1 and Sirt2. Both of Sirt1 and Sirt2 deacetylate and repress the transcriptional activity of p53 (Jin et al., 2008). As in the case of Sirt1, Sirt2 is also regulated by post-translational modifications (PTMs). It has been reported that the tyrosine kinase, c-Src, phosphorylates Y104 of Sirt2 and reduce the stability and catalytic activity of Sirt2 (Choi et al., 2014).

1.3.3 Sirt3

Sirt3 has been identified as a mitochondrial protein deacetylase with major roles in mitochondria, including ATP generation, metabolism and the response to oxidative stress (Zhang et al., 2013). The N-terminal 25 amino-acid residues of Sirt3 are responsible for its mitochondrial localization (Onyango et al., 2002). It also contains a highly conserved catalytic domain, which is composed of two distinct domains: a large Rossmann fold domain for NAD^+ binding and a small domain binding to a zinc atom. The cleft between the two domains provides the space for the interaction of Sirt3 with its acetylated substrates. Acetyl-CoA synthetase 2 (AceCS2) is the first reported substrate of Sirt3 and the crystal structure of the complex of Sirt3 and AceCS2 has shown that Sirt3 owns a stable interaction with AceCS2 without NAD^+ (Schwer et al., 2006). The mRNA and protein level of Sirt3 has been reported to be regulated by Peroxisome

proliferator-activated receptor c (PPARc) coactivator-1α (PGC-1α). PGC-1α stimulates Sirt3 protein expression via the recruiting an estrogen-related receptor (ERR)-binding element to the Sirt3 promoter (Kong et al., 2010). Moreover, Sirt3, in turn, stimulates PGC-1α expression through the activation of CREB phosphorylation, resulting in a positive feedback loop. In the study, overexpression of Sirt3 decreases basal ROS level by the stimulation of PGC-1α. Through regulation of ROS, Sirt3 deacetylate several metabolic enzymes and regulates crucial mitochondrial functions. For example, overexpression of Sirt3 increases the protein level of two antioxidant proteins, mitochondrial superoxide dismutase 2 (SOD2) and catalase, mediated by a transcriptional factor, FoxO3a. And the increased expression of two proteins leads to the decrease of ROS level and the maintenance of appropriate mitochondrial status (Sundaresan et al., 2009). Moreover, Sirt3 has been shown to be involved in mitochondrial metabolism by deacetylating acetyl-CoA synthetase 2 (AceCS2) and glutamate dehydrogenase (GDH), which implies that Sirt3 modulates metabolism during caloric restriction (CR) (Hallows et al., 2006). Besides the roles of Sirt3 in mitochondria, Sirt3 is also implied in tumor proliferation (Finley and Haigis, 2012). Sirt3 has been identified as a tumor suppressor linked with metabolic processes. A ROS-mediated pathway and metabolic reprogramming which are regulated by Sirt3 can stimulate carcinogenesis. Therefore, the inhibitors and activators of Sirt3 have been studied as potential drug targets (Bruzzone et al., 2013). In addition, a recent study has also shown that the defect of Sirt3 triggers the tumor phenotypes of cells in a ROS-dependent manner, which is mediated by the enhanced HIF-1α stabilization. Activation of HIF-1 and HIF-2 strongly promote the survival and proliferation of tumor cells because of their downstream genes, such as glucose transporters and glycolytic enzymes, and Vascular Endothelial Growth Factor (VEGF), is significant for the survival of tumor cells under hypoxic conditions (Schumacker, 2011). The evidence has also shown that Sirt3 function as an oncogene. To this point, it has been proved that Sirt3 may protect cancer cells from oxidative stress-mediated cell death through deacetylation of the factors responding to stress-mediated conditions. In bladder cancer, Sirt3 can deacetylate tumor suppressor p53 and rescue growth arrest and senescence (Li et al., 2010). Ku70 has also been identified as a new target of Sirt3. By binding to and deacetylating Ku70,

Sirt3 promotes the interaction of Ku70 with the proapoptotic protein Bax and thus prevents the translocation of Bax to the mitochondria, protecting HeLa cells from apoptosis under stress conditions (Sundaresan et al., 2008). The fact that Sirt3 plays a role in cancer cells may implicate Sirt3 as a potential target in cancer therapy. Although there are no studies on Sirt3 as a drug target to treat cancer, the underlying mechanisms of Sirt3 in different cancer types enhance our understanding and help us to develop a novel clinical strategy for cancer treatment.

1.3.4 Sirt4

Sirt4 is a mitochondrial matrix protein and only when it is cleaved to an active form, Sirt4 can be imported into mitochondria. Different from other sirtuin members, the enzymatic activity of Sirt4 remains unclear. Originally, Sirt4 was thought to be an ADP-ribosyltransferase (Ahuja et al., 2007). By catalyzing ADP-ribosylation of glutamate dehydrogenase (GDH), Sirt4 regulates insulin secretion. However, the ADP-ribosyltransferase activity of Sirt4 has been questioned because the weak ADP-ribosyltransferase reaction can be explained by both enzymatic and nonenzymatic reaction mechanisms (Du et al., 2009). Sirt4 has also been identified as a deacetylase, but with a limited deacetylation activity (Laurent et al., 2013). In this study, Sirt4 can deacetylate and inhibit malonyl CoA decarboxylase (MCD), an enzyme that produces acetyl CoA from malonyl CoA, to repress fatty acid oxidation and promote lipid anabolism in mice in nutrient-rich conditions. Numerous studies have shown that Sirt4 is involved in several important biological pathways. For example, Sirt4 acts on the mammalian target of rapamycin complex 1 (mTORC1) to activate glutamate dehydrogenase (GDH) for promoting glutamine anaplerosis (Csibi et al., 2013). In this process, mTORC1 destabilizes cAMP-responsive element binding 2 (CREB2) for proteasome degradation and represses the activity of Sirt4. Further, Sirt4 is also associated with cancer due to the low expression level of Sirt4 in human cancer. Overexpression of Sirt1 inhibits cell proliferation, transformation, and tumor development with high mTORC1 signaling. Dysregulation of Sirt4 has been reported to contribute to metabolic diseases including diabetes and obesity. The defect of Sirt4 in

mice activates glutamate dehydrogenase (GDH) which functions to enhance the metabolism of glutamate and glutamine by generating ATP and promoting insulin secretion (Haigis et al., 2006). Besides the role of Sirt4 in insulin secretion, Sirt4 also regulates genes related to fatty acid metabolism (Nasrin et al., 2010). Knockdown of Sirt4 results in increased fatty acid oxidation (FAO), cellular respiration, and pAMPK levels in primary myotubes. Taken together, Sirt4 plays an important role in several metabolic pathways, which might provide us with a new therapeutic strategy for some diseases associated with metabolic disorders such as type 2 diabetes.

1.3.5 Sirt5

Sirt5 has been studied because of its enzyme activity and biological functions. It is found that Sirt5 has a weak deacetylase activity compared with other sirtuins, however, it has strong desuccinylation, demalonylation, and deglutarylation activities *in vitro* and *in vivo* (Du et al., 2011; Roessler et al., 2015). In the crystal structure of Sirt5, it contains two main domains: the zinc-binding domain and Rossmann fold domain (Zhou et al., 2012). The cleft between these two domains forms the site for its catalytic activity by several loops. The change of cleft conformation switches Sirt5 from an inactive open state to an active closed state. The binding site for its desuccinylation activity is an antiparallel β-sheet with one loop from the zinc-binding domain and the other loop from the Rossmann fold domain. This β-sheet is also stabilized by the hydrogen bonds between Sirt5 and the substrate peptide. The pattern of binding succinylation site of Sirt5 is the same as the binding of acetyl peptides, and the rotation for confirmation of different states is independent of the interaction for succinylated or acylated lysine residues of substrates. Till now, many studies have reported that Sirt5 plays a crucial role in several key biological processes, including the regulation of ammonia detoxification, fatty acid oxidation, cellular respiration, ketone body formation, and reactive oxygen species (ROS) management. The dysregulation of Sirt5 is associated with some human diseases such as cancer, Alzheimer's disease, and Parkinson's disease. For example, carbamoyl phosphate synthetase 1 (CPS1), a rate-limiting enzyme in the first step of the urea cycle, has been identified as a substrate target of Sirt5. Sirt5 can deacetylate CPS1 to activate

its function in the urea cycle for generating more urea under the caloric restriction condition (Ogura et al., 2010). Sirt5 has also been found to deacetylate cytochrome c, a protein of the mitochondrial intermembrane space, to regulate oxidative metabolism and apoptosis initiation (Schlicker et al., 2008). However, there are no mitochondrial matrix proteins which can be deacetylated by Sirt5. Furthermore, the Sirt5 KO mice display reduced fatty acid oxidation and increased accumulation of acylcarnitines compared to the wild type. Currently, some clues from its biological functions and structures of Sirt5 provide a possible therapeutic treatment for diseases. Some new Sirt5 inhibitors have been designed for further studies.

1.3.6 Sirt6

Sir6, as a member of the sirtuin family, possesses histone deacetylase and mono-ribosyltransferase activity (Liszt et al., 2005). Its activity is highly selective for histone substrates. It has been confirmed that Sirt6 deacetylates histone H3K9ac, H3K18ac, H3K27, H3K56ac and a weaker activity on H3K4ac and H3K23 (Cea et al., 2016; Michishita et al., 2008; Tasselli et al., 2016; Wang et al., 2016). It exists in different species, including bacteria, archaea, and eukaryotes and is mainly expressed in skeletal muscles, brain, heart, liver, and thymus in a tissue-specific manner (Mostoslavsky et al., 2006). Sirt6 is localized in the nucleus and the C-terminus is required for proper nuclear localization. And it is mainly enriched on heterochromatin. The N-terminus of Sirt6 specifically binds to chromatin and influences its catalytic activity. In the crystal structure of the complex of SIRT6 with a H3K9 myristoyl peptide and ADP-ribose at 2.2-Angstrom resolution, Sirt6 provides a large hydrophobic pocket for accommodating long chain fatty acyl groups and removes long chain fatty acyl groups, such as K19 and K20 of tumor necrosis factor α (TNFα), for the increase of its secretion (Jiang et al., 2013). Sirt6 has been shown to play a crucial role in aging, metabolism, and diseases. For instance, SIRT6-deficient mice display metabolism disorder and shortened lifespan. Conversely, the overexpression of Sirt6 leads to a significant increase in lifespan in male mice, because transgenic males have shown decreased serum levels of insulin-like growth factor 1 (IGF1), increased levels of IGF-binding protein 1 and altered

phosphorylation levels of major components of IGF1 signaling, vital for the regulation of lifespan (Kanfi et al., 2012). Recently, genome-wide studies have suggested that aging is also associated with chromatin compaction and heterochromatin silencing at repetitive DNA elements, such as centromeres, telomeres, and retrotransposons. As one of the key elements for heterochromatin silencing, Sirt6 modulates telomeric chromatin through the deacetylation of H3K9ac, which is also required for the stable interaction with WRN, the factor that is mutated in Werner syndrome (Michishita et al., 2008). Besides the role of Sirt6 in aging, Sirt6 is also regarded as a factor for tumor suppression, may be due to the role of Sirt6 on histone deacetylation in cancers. Sirt6 also exerts its tumor suppressor activity by preventing aerobic glycolysis in cancer cells, known as the Warburg effect (Sebastián et al., 2012). Specifically, Sirt6 selectively deacetylates histone H3K9ac to alter the expression of specific genes linked to glucose homeostasis, like the transcription factor Hif1alpha (Zhong et al., 2010b).

1.3.7 Sirt7

Sirt7 is also one of the members of the sirtuin family of NAD^+-dependent protein deacetylases and highly conserved in prokaryotes and eukaryotes. Different from other sirtuin proteins (Sirt1-6), it is a nuclear protein and mainly localized in the nucleolus (Michishita et al., 2005). Similar with other sirtuin proteins, Sirt7 owns a conserved catalytic domain and a nicotinamide adenine dinucleotide (NAD^+)-binding site. However, the enzymatic activity of Sirt7 is still further studied. For example, recent research has shown that Sirt7 is also an NAD^+-dependent histone desuccinylase involved in DNA double-strand breaks (DSBs) repair through the desuccinylation of H3K122 in a PARP1-dependent manner (Li et al., 2016). For the cellular functions of Sirt7, new evidence has shown that Sirt7 is linked to cell proliferation, chromatin structure, stress response, cell cycle, energy metabolism and the maintenance of genome stability. Dysregulation of Sirt7 contributes to several diseases, including various cancers, neurodegenerative disorders and type II diabetes (Taylor et al., 2008). Previous studies have shown that Sirt7 is abundant in metabolically active mammalian cells and low in non-proliferating cells, suggesting that the expression of Sirt7 is associated with ribosome biogenesis and

cell proliferation (Ford et al., 2006). For example, Sirt7 deacetylates polymerase-associated factor 53 (Paf53) at lysine 373, a subunit of RNA polymerase I, and thereby increases rDNA occupancy of RNA polymerase I and transcription activation (Chen et al., 2013). Moreover, the subcellular distribution of Sirt7 in the nucleolus is dependent on the binding to nascent pre-rRNA. And the release of Sirt7 from the nucleolus results from hyperacetylation of Paf53, which directly leads to the downregulation of RNA polymerase I transcription and thus responses cellular stress conditions (Andersen et al., 2005). The function of Sirt7 in metabolic homeostasis is well studied. For example, the Sirt7 knockout mice display high-fat diet-induced fatty liver, obesity, and glucose intolerance. In this study, it is found that Sirt7 can positively promote the expression of TR4/TAK1, a nuclear receptor involved in lipid metabolism and consequently activate its downstream genes for increasing fatty acid uptake and triglyceride synthesis/storage. Meanwhile, Sirt7 also protects TR4 against ubiquitin-proteasome degradation by binding to the complex of DDB1-CUL4-associated factor 1 (DCAF1)/damage-specific DNA binding protein 1 (DDB1)/cullin 4B (CUL4B) E3 ubiquitin ligase (Yoshizawa et al., 2014). In support of the view that overexpression of Sirt7 enhances cell proliferation and ribosome biogenesis, Sirt7 has oncogenic potential by metabolically activating rRNA synthesis for ribosome in growing tumor cells or cancer cells, such as hepatic, ovarian, breast or lung cancers. However, Sirt7 itself cannot cause oncogenic transformation of primary fibroblasts but maintain the transformed state of cancer cells by specifically deacetylating histone H3K18Ac in the promoters of a set of gene targets linked to tumor suppression (Barber et al., 2012a). Conversely, Sirt7 knockout leads to the global hyperacetylation of H3K18ac and reduces the tumorigenicity of human cancer cell in mice. In addition, studies also suggest that microRNAs, such as miR-125a-5p, miR-125b, and miR-34a, repress Sirt7 expression and prevent the cancer cell growth (Kim Jeong et al., 2012; Zhang et al., 2015). Consistent with its role in multiple biological processes, such as transcription, ribosome biogenesis, chromatin structure, metabolism, and cell proliferation, Sirt7 is linked with several diseases and makes itself a promising target for future therapy.

1.4 The aim of this work

In mammals, the cooperation of DNA methylation and histone modifications plays a major role in the regulation of numerous key biological processes. It has been apparent that DNA methylation promotes stable transcriptional repression, whereas different kinds of histone modifications reversibly lead to diverse local formation or dissociation of heterochromatin. Furthermore, DNA methylation and histone modifications can be dependent on each other, and the crosstalk between them occurs because DNA methyltransferases interact with various enzymes for histone modifications.

The first part of the work I focused on was to explore the specific sites of Dnmt1 key for the autoinhibitory mechanism of Dnmt1 *de novo* methylation. To reach this aim, based on the crystal structure of human DNMT1 composed of CXXC, tandem bromo-adjacent homology (BAH1/2), and methyltransferase domains bound to DNA-containing unmethylated CpG sites, I analyzed the protein sequence of the linker between CXXC and BAH1 and selected the only phosphorylated site identified by quantitative mass spectrometry for further study.

The second part is about the relationship of Uhrf1 and Sirt1. Till now, little is known about the post-translational modifications of Uhrf1 and their cellular functions. To uncover the relationship between the acetylation of Uhrf1 and its interaction with Sirt1, I performed biochemical assays and found that (de)acetylation of Uhrf1 was linked to the stability of Uhrf1. It is novel to find Uhrf1 acetylation by acetylase Tip60 promoting its proteasomal degradation and only happens in the G1 phase of the cell cycle. But the acetylation-mediated degradation of Uhrf1 can be inhibited by the deubiquitinase Usp7. Furthermore, it is also found that acetylated Uhrf1 enhances its binding to Dnmt1 and heterochromatin. For Uhrf1 acetylation, we also tried to figure out acetylation sites of Uhrf1 by quantitative mass spectrometry. Because Sirt1 has been proven to inhibit the acetyltransferase activity of Tip60 via its deacetylation-driven degradation (Peng et al., 2012). After the G1 phase, Sirt1 not only interacts with Uhrf1 but also deacetylates Uhrf1, which occurs during the transition of G1 phase to S phase for stabilizing Uhrf1. Moreover, the interaction of Uhrf1 and Sirt1 structurally disturbs Cdk2 binding to Uhrf1 and thereby it happens earlier than the phosphorylation of Uhrf1 by Cdk2 in the transition of G1/S of the cell cycle.

The objective of the third part of work was to establish the connection between sirtuin proteins and the transcriptional repression of common target genes regulated by their deacetylation activity of histone H3K18ac. Specifically, sirtuin-mediated H3K18 deacetylation enhances the Uhrf1-associated ubiquitination of H3K18, which is essential for Dnmt1 binding and DNA methylation. The increased DNA methylation is a prerequisite for the transcriptional repression of these target genes. By using CRISPR-Cas9 technology to build the doxycycline-induced cell lines, I analyzed the downstream genes regulated with the different sirtuin proteins and tried to figure out the relationship between sirtuins and key cellular biological functions.

2 Methods and materials

2.1 Materials

2.1.1 Bacterial strains and cell lines

The bacterial strains, *E.coli* JM109 and BL21 (DE3) were used for all the constructs (**Table 1**). The murine C2C12 (mouse myoblasts) cell lines were used for fluorescence imaging, and mouse embryonic stem cell lines, J1 wild type and E14 wild type, were mainly used for the establishment of different gene knockin or knockout (**Table 2**). Human embryonic kidney cells were used for overexpression of proteins. A baby hamster kidney (BHK) cell line with stably integrated lac operator array was used for the detection of proteins' interactions.

Table 1. Bacterial strains

Name of the bacterial strain	Genotype	Source
E. coli JM109	*recA1, endA1, gyrA96, thi, hsdR17, supE44, relA1, Δ(lac-proAB)/F' [traD36, proAB+, lacIq, lacZΔM15]*	(Hanahan, 1983)
E. coli BL21 (DE3)	*F- ompT hsdSB (rB-mB-) gal dcm rne131 (DE3)*	(Studier and Moffatt, 1986)

Table 2. Cell lines

Name of cell line	Cell type	Antibiotic resistance	Description	Source
C2C12	Somatic cells	no	Mouse myoblast cells	(Blau et al., 1985)
HEK 293T	Somatic cells	no	Human embryonic kidney cells	(DuBridge et al., 1987)
BHK *(lacO)*	Somatic cells	no	Baby hamster kidney with stably integrated lac operator array	(Tsukamoto et al., 2000)
J1 wt	mESCs	no	Mouse wild type embryonic stem cell	(Lei et al., 1996)
E14 wt	mESCs	no	Mouse wild type embryonic stem cell	(Sharif et al., 2007)

Sirt1$^{-/-}$(KO) from J1	mESCs	G418	Mouse Sirt1 knockout cell line	this work
Sirt1$^{sirt1/sirt1}$ from J1	mESCs	G418	Mouse Sirt1 knock-in cell line	this work
Dnmt TKO from J1	mESCs	G418	Mouse Dnmt (Dnmt1, Dnmt3a, and Dnmt3b) knockout cell line	(Lei et al., 1996)
Dnmt CC from J1	mESCs	G418	Mouse Dnmt (Dnmt3a and Dnmt3b) knockout cell line	(Lei et al., 1996)
GFP-Sirt1 inducible cell from J1	mESCs	Puromycin	Mouse doxycycline-inducible GFP-Sirt1 cell line	this work
GFP-Sirt2 inducible cell from J1	mESCs	Puromycin	Mouse doxycycline-inducible GFP-Sirt2 cell line	this work
GFP-Sirt6 inducible cell from J1	mESCs	Puromycin	Mouse doxycycline-inducible GFP-Sirt6 cell line	this work
GFP-Sirt7 inducible cell from J1	mESCs	Puromycin	Mouse doxycycline-inducible GFP-Sirt7 cell line	this work

2.1.2 Plasmids and antibodies

Table 3. Plasmid constructs

Construct name	Number	Antibiotic resistance	Description	Source
pCAG-GFP-IB	PC1624	Ampicillin	CAG driven GFP expression constructed by Daniela Meilinger	(Meilinger et al., 2009)
LacI-GBP	PC1398	Kanamycin	Bacterial Lac repressor fused to GFP binding protein (GBP) and used for F3H assay constructed by Jonas Helma	(Herce et al., 2013)
pCAG-GMT1-NL-IB	PC1626	Kanamycin	CAG-driven Dnmt1 (long isoform) expression with an N-terminal GFP fusion constructed by Nan Liu	(Frauer et al., 2011b; Meilinger et al., 2009)
pCAG-Dnmt1 S717A	PC4129	Kanamycin	CAG-driven Dnmt1 mutant S717A expression with an N-terminal GFP fusion constructed by Pin Zhao	

pCAG-Dnmt1 S717E	PC4128	Kanamycin	CAG-driven Dnmt1 mutant S717AE expression with an N-terminal GFP fusion constructed by Pin Zhao	
pCAG-Ch-IB	PC1625	Ampicillin	CAG driven mCherry expression constructed by Daniela Meilinger	(Meilinger et al., 2009)
pENmRFPPCNAL2	PC1054	Ampicillin	CAG-driven PCNA expression with an N-terminal RFP fusion constructed by Ingrid Grunewald	(Sporbert et al., 2005)
pCAG-GFP-Np95-IB	PC1755	Ampicillin	CAG-driven Uhrf1 expression with an N-terminal GFP fusion constructed by Andrea Rottach	(Rottach et al., 2010)
pCAG-Uhrf1 deleted TTD -GFP	PC2984	Ampicillin	CAG-driven Uhrf1 with deleted TTD expression with a C-terminal GFP fusion constructed by Martha Smets	(Rottach et al., 2010)
pCAG-Uhrf1 deleted PHD -GFP	PC2985	Ampicillin	CAG-driven Uhrf1 with deleted PHD expression with a C-terminal GFP fusion constructed by Martha Smets	(Rottach et al., 2010)
pCAG-Uhrf1 deleted SRA -GFP	PC2986	Ampicillin	CAG-driven Uhrf1 with deleted SRA expression with a C-terminal GFP fusion constructed by Martha Smets	(Rottach et al., 2010)
pCAG-Uhrf1 deleted RING -GFP	PC2987	Ampicillin	CAG-driven Uhrf1 with deleted RING expression with a C-terminal GFP fusion constructed by Martha Smets	(Rottach et al., 2010)
pCAG-Uhrf1K644A K664A-GFP	PC4154	Ampicillin	CAG-driven Uhrf1 mutant K644A K664A expression with a C-terminal GFP fusion constructed by Pin Zhao	
pCAG-GFP-Sirt1	PC4159	Ampicillin	CAG-driven mouse Sirt1 expression with an N-terminal GFP fusion constructed by Pin Zhao	
pCAG-RFP-Sirt1	PC4148	Ampicillin	CAG-driven mouse Sirt1 expression with an N-terminal RFP fusion constructed by Pin Zhao	
pCAG-GFP-Sirt1 catalytic domain	PC4173	Ampicillin	CAG-driven mouse Sirt1 catalytic domain expression with an N-terminal GFP fusion constructed by Pin Zhao	
pCAG-GFP-Sirt1 C terminus	PC4172	Ampicillin	CAG-driven mouse Sirt1 C terminus expression with an N-terminal GFP fusion constructed by Pin Zhao	
pCAG-GFP-Sirt1 N terminus	PC4178	Ampicillin	CAG-driven mouse Sirt1 N terminus expression with an N-terminal GFP fusion constructed by Pin Zhao	
pCAG-GFP-Sirt1 N terminus and the catalytic domain	PC4177	Ampicillin	CAG-driven mouse Sirt1 N terminus and catalytic domain expression with an N-terminal GFP fusion constructed by Pin Zhao	

pCAG-GFP-Sirt1 C terminus and the catalytic domain	PC4174	Ampicillin	CAG-driven mouse Sirt1 C terminus and catalytic domain expression with an N-terminal GFP fusion constructed by Pin Zhao	
pCAG-eGFP-Chromodomain CBX1	PC4142	Ampicillin	CAG-driven CBX1 expression with an N-terminal GFP fusion constructed by Pin Zhao	
pCAG-ch-Usp7-IB	PC2612	Ampicillin	CAG-driven Usp7 expression with an N-terminal Cherry fusion constructed by Weihua Qin	(Qin et al., 2011b)
pCAG-ch-Hif1a	PC4146	Ampicillin	CAG-driven mouse Hif1a expression with an N-terminal Cherry fusion constructed by Pin Zhao	
pCAG-ch-Tip60	PC4151	Ampicillin	CAG-driven Tip60 expression with an N-terminal Cherry fusion constructed by Pin Zhao	
pCAG-GFP-Tip60	PC2058	Ampicillin	CAG-driven Tip60 expression with an N-terminal GFP fusion constructed by Nan Liu	
pCAG-ch-Cdk2	PC4145	Ampicillin	CAG-driven Cdk2 expression with an N-terminal Cherry fusion constructed by Pin Zhao	
His-Ubi	PC1632	Ampicillin	CMV driven ubiquitin expression with an N-terminal His tag constructed by Karin Fellinger	(Qin et al., 2015b)
pCAG-GFP-Sirt2	PC4179	Ampicillin	CAG-driven mouse Sirt2 expression with an N-terminal GFP fusion constructed by Pin Zhao	
pCAG-Sirt3-GFP	PC4152	Ampicillin	CAG-driven mouse Sirt3 expression with a C-terminal GFP fusion constructed by Pin Zhao	
pCAG-Sirt4-GFP	PC4153	Ampicillin	CAG-driven mouse Sirt4 expression with a C-terminal GFP fusion constructed by Pin Zhao	
pCAG-Sirt5-GFP	PC4171	Ampicillin	CAG-driven mouse Sirt5 expression with a C-terminal GFP fusion constructed by Pin Zhao	
pCAG-GFP-Sirt6	PC4181	Ampicillin	CAG-driven mouse Sirt6 expression with an N-terminal GFP fusion constructed by Pin Zhao	
pCAG-GFP-Sirt7	PC4155	Ampicillin	CAG-driven mouse Sirt7 expression with an N-terminal GFP fusion constructed by Pin Zhao	
CttP-RE-TIGHT-GFP-Sirt1	PC4162	Gentamycin	CttP-driven mouse Sirt1 expression with an N-terminal GFP fusion constructed by Pin Zhao	
CttP-RE-TIGHT-GFP-Sirt2	PC4163	Gentamycin	CttP-driven mouse Sirt2 expression with an N-terminal GFP fusion	

			constructed by Pin Zhao	
CttP-RE-TIGHT-GFP-Sirt6	PC4164	Gentamycin	CttP-driven mouse Sirt6 expression with an N-terminal GFP fusion constructed by Pin Zhao	
CttP-RE-TIGHT-GFP-Sirt7	PC4165	Gentamycin	CttP-driven mouse Sirt7 expression with an N-terminal GFP fusion constructed by Pin Zhao	

Table 4. Antibodies

Target protein	**Manufacturer**	**Species**	**Application**	**Dilution**
GFP	Roche Applied Science (11814460001)	mouse	primary antibody	1:5000
RFP or mCherry (anti-RED5F8)	Dr. Kremer, Dr. Rottach	rat	primary antibody	1:50
α-CBX1	Abcam (ab 10478)	rabbit	primary antibody	1:1000
α-CBX1-S89ph (31C11-11)	Dr. E. Kremmer	mouse	primary antibody	1:1000
acetyl lysine	Abcam (RM101)	rabbit	primary antibody	1:2500
β-actin	Sigma (A5441)	mouse	primary antibody	1:2500
Sirt1	Biolegend(690502)	rat	primary antibody	1:500
H3K9me3	Active motif (39765)	rabbit	primary antibody	1:1000
H3K18ac	Active motif (39755)	rabbit	primary antibody	1:2500
H3	Abcam (ab1791)	rabbit	primary antibody	1:1000
PCNA	Dr. Kremer, Dr. Rottach	mouse	primary antibody	1:2500
Antigen	**Manufacturer**	**Species**	**Application**	**Dilution**
HRP-conjugated antibody	Molecular Probes	rabbit	secondary antibody	1:2500
		mouse	secondary antibody	1:5000
		rat	secondary antibody	1:5000
Alexa Fluor 647N	Invitrogen	mouse	photostable dye as secondary antibody	1:2500
	Invitrogen	rabbit	photostable dye as secondary antibody	1:2500
Alexa Fluor 594	Invitrogen	mouse	photostable dye as secondary	1:2500

			antibody	
Alexa Fluor 488	Invitrogen	mouse	photostable dye as secondary antibody	1:2500

2.1.3 Primers

All primers and oligonucleotides were ordered from MWG Eurofins Operon.

Table 5. Primers

Primer name	Sequence 5'-3'	Application
F-SIRT1	AGGGCCAGAGAGGCAGTTGGAAGAT	PCR
R-SIRT1	CCGGACAGCTTCAATAGTGTTATG	
F-SIRT1-AsiS1	ACGTGCGATCGCATGGCGGACGAGGTG	
R-SIRT1-Not1	CAGCGGCCGCATTATGATTTGTCTGA	
F-SIRT1-Ca- AsiS1	ACGTGCGATCGCATGATTAACACCAT	
R-SIRT1-Ca- Not1	CAGCGGCCGCTTAGGCATATTCACCA	
F-SIRT1-C- AsiS1	ACGTGCGATCGCATGAAACTTTGTTGT	
R-SIRT1-N- Not1	CAGCGGCCGCTTAGTCTTTCCTCTTC	
F-SIRT2	GAG CAGTCGGTGACAGTC CC	
R-SIRT2	CTGTCCTGCGGGAGGTCATGGTT	
F-SIRT2-AsiS1	ACGTGCGATCGCATGGCCGAGCCGG	
R-SIRT2-Not1	CAGCGGCCGCTTACTGCTGTTCCT	
F-SIRT3	CTGCAGTAGGGTGGTGGTCATGG	
R-SIRT3	CAGGTGAAGAAGCCATAGTCTTATC	
F-SIRT3-AsiS1	ACGTGCGATCGCATGGTGGGGGCCG	
R-SIRT3-Not1	CAGCGGCCGCTTATCTGTCCTGTC	
F-SIRT4	GAATTGTGGAAGAATAAGAATGA	
R-SIRT4	GATTCAGAGTTGGAGCGGCATTG	
F-SIRT4-AsiS1	ACGTGCGATCGCATGAGCGGATTGA	
R-SIRT4-Not1	CAGCGGCCGCTTAGGGATCTTGAG	
F-SIRT5	GACTTCAACGAAAACCTGATGCG	
R-SIRT5	CATAAAAGTCAAGTCACCAACT	
F-SIRT5-AsiS1	ACGTGCGATCGCATGCGACCTCTCC	
R-SIRT5-Not1	CAGCGGCCGCTCACCAACTCTCTC	
F-SIRT6	CTTTATTGTTCCCGTGCGGCAGCGC	
R-SIRT6	GTTCCTTCAAGTTCCCCTCCCGC	
F-SIRT6-AsiS1	ACGTGCGATCGCATGTCGGTGAATTATG	
R-SIRT6-Not1	CAGCGGCCGCATCAGCTGGGGGCAGC	
F-SIRT7	AAGCGCAGTCAAAGGAGCGATGG	
R-SIRT7	TCTTTGTCAACTCCGGGCTATGCC	
F-SIRT7-AsiS1	ACGTGCGATCGCATGGCAGCCGGTGGC	
R-SIRT7-Not1	CAGCGGCCGCACTATGCCACTTTCTT	
F-Dnmt1	ACCAGTGAGAAACTGGCAATCTACGACTCCACCTC	
R-Dnmt1	CCCCATCGATGCTCACCTTCTGA	

F-Dnmt1 S717A	GATGTGTCAGAGATGCCAGCACCCAAA	
R-Dnmt1 S717A	TTTGGGTGCTGGCATCTCTGACACATC	
F-Dnmt1 S717E	GATGTGTCAGAGATGCCAGAACCCAAA	
R-Dnmt1 S717E	TTTGGGTTCTGGCATCTCTGACACATC	
F-Uhrf1- AsiS1	ACGTGCGATCGCATGTGGATCCAGG	
R-Uhrf1-R1	CCCACACATGCCATGCCTCGGCC	
F-Uhrf1-R1	CCCGGCGGGACTGGGGCCGAGGC	
R-Uhrf1- Not1	CAGCGGCCGCTTACTGCTCCAAGGC	
F-Uhrf1-R2	GAAGGGCGGGAAACACAGCCGATA	
R-Uhrf1-R2	CCCTCTGCAGGAGCGTATCGGCT	
F-Cdk2	GCCTGAGCCGCCTCACTAG	
R-Cdk2	CTTTGGGAAGGGCATCAGAG	
F-Cdk2-AsiSI	ACGTGCGATCGCATGGAGAAC	
R-Cdk2-NotI	CAGCGGCCGCTCAGAGCCGAAG	
F-Hif1a	GGCACCGATTCGCCATGGA	
R-Hif1a	CAAAAGGAATGAGATTAG	
F-Hif1a-AsiSI	ACTGGCGATCGCATGGAGGGCGCCGGC	
R-Hif1a-NotI	GAGTAGCGGCCGCCTCAGTTAACTTGATC	
F-MajorS	AAAATGAGAAACATCCACTTG	
R-MajorS	CCATGATTTTCAGTTTTCTTG	
F-CBX1 S89E-scr	GGCTCTCTTCCAAGACTAGCTC	
R-CBX1S89E-scr	GGCCAGCCTAGGCTTCTATGC	
CBX1-scr-F	GATTTCCCTGGGCTCCTCAC	
CBX1-scr-R	ATGCCCATCACAGAACTGCT	
F-GAPDH-q	GAAGGTCGGTGTGAACGG	RT-qPCR
R-GAPDH-q	TGAAGGGGTCGTTGATGG	
F-CyclinE-q	GTTATAAGGGAGACGGGGAG	
R- CyclinE -q	TGCTCTGCTTCTTACCGCTC	
F-CDK1-q	GACATCTGGAGTATAGGGACC	
R-CDK1-q	CTTCGTTGTTAGGAGTGCC	
F- E2F1-q	GCCCTTGACTATCACTTTGGTCTC	
R-E2F1-q	CCTTCCCATTTTGGTCTGCTC	
F-CDK2-q	GCTAGCAGACTTTGGACTAGCCAG	
R-CDK2-q	AGCTCGGTACCACAGGGTCA	
F-UHRF1-q	CTGGCTATGGTGTGGGTCACAG	
R-UHRF1-q	CTGGGCCTCAAACCATGCAC	
F--LDHA-q	ATCCCATTTCCACCATGATT	
R- LDHA -q	ACTGCAGCTCCTTCTGGATT	
F- PFKL -q	GAACTACGCACACTTGACCAT	
R- PFKL -q	CTCCAAAACAAAGGTCCTCTGG	
F- PLIN3 -q	TCCTGTCCAAGCTGGAGCCC	
R- PLIN3 -q	GTCGGCTGCTGGAGGATGGG	
F-Eno1-q	AGTACGGGAAGGACGCCACCA	
R-Eno1-q	GCGGCCACATCCATGCCGAT	
F- CDKN1A -q	AAGTGTGCCGTTGTCTCTTCG	
R- CDKN1A -q	AGTCAAAGTTCCACCGTTCTCG	
F -UPP1-q	TCTACCATTTCAACCTCAGCACTAGCA	
R-UPP1-q	CCATGGCTCACAGACAGCACG	

F- RAC2 -q	AAGAAGCTGGCTCCCATCACCTAC	
R- RAC2-q	AACACGGTTTTCAGGCCTCTCTG	
F -DKC1-q	TTAGGACAACGACACCACCA	
R-DKC1-q	CCCAGCTGGACATAATGCTT	
F -β-Actin-q	GACCTCTATGCCAACACAGT	
R- β-Actin -q	AGTACTTGCGCTCAGGAGGA	
F- LDHA -chip	GGGTTCTTGCGGGGGTGGGG	ChIP-qPCR
R- LDHA -chip	ATGAACCCCAAAAGGGGATG	
F- LDHA -chip	GGGTTCTTGCGGGGGTGGGG	
F- PFKL -chip	TGGGGAACCTCTGTGTTTGT	
R- PFKL -chip	TACTCAGGATTCGGTCGAAG	
F-Eno1-chip	GCTATCCGGGGAGCACTC	
R-Eno1-chip	CAACCCTGAAACTCGGTGAT	
F-MyoD-chip	GCCGGTGTGCATTCCAA	
R-MyoD-chip	TCAACCCAAGCCGTGAGAGT	

2.1.4 Kits and reagents

Table 6. Kits and reagents

Kits and chemicals	**Supplier**
4',6-Diamidino-2-phenylindol (DAPI)	Roche Diagnostics
Agar	AppliChem
Agarose	Sigma Aldrich
Ampicillin	AppliChem
Aphidicolin	Sigma Aldrich
Bromphenol blue sodium salt	AppliChem
Bovine serum albumin(BSA)	Sigma Aldrich
Carbobenzoxy-Leu-Leu-leucinal (MG132)	Sigma Aldrich
Chloroform	Roth GmbH
Cycloheximide	Sigma Aldrich
Dimethylsulfoxide (DMSO)	AppliChem
Dithiothreitol (DTT)	Carl Roth GmbH + Co. KG
Dulbecco's Modified Eagle Medium (DMEM)	PAA Laboratories GmbH
dNTPs	PeqLab
Dulbecco's PBS (1x), without Ca2+ and Mg2+	Sigma Aldrich
ECL reagent	Thermo Scientific
EDTA-dihydrate	AppliChem
Ethanol (98%)	AppliChem
Ethanol, absolute	AppliChem
Ethidium bromide	AppliChem
EZ DNA Methylation-Gold Kit™	Zymo
FastDigest® restriction enzymes + Buffer	Thermo Scientific
Fetal bovine serum (FBS)	PAA Laboratories
Formaldehyde	Sigma Aldrich

Gelatine	Sigma Aldrich
Gentamicin (50 mg/ml)	PAA Laboratories
GFP-Trap®	ChromoTek
Glycerol	Carl Roth GmbH + Co. KG
Glycin	Carl Roth GmbH + Co. KG
High Capacity cDNA Reverse Transcription Kit	Applied Biosystems
HisTrap FF	GE Healthcare
Hydrochloric acid (HCl)	Carl Roth GmbH + Co. KG
Imidazole	AppliChem
Isopropanol (2-Propanol)	Carl Roth GmbH + Co. KG
Isopropyl β-d-thiogalactopyranoside (IPTG)	AppliChem
Kanamycin	SERVA
Lysogeny broth (LB) Medium	Carl Roth GmbH + Co. KG
L-Glutamine	PAA Laboratories
LIF (ESGRO)	Millipore
Lipofectamine 3000	Invitrogen
Magnesium chloride ($MgCl_2$)	Sigma-Aldrich
MEM Non-essential amnio acid Solution	PAA Laboratories
Milk powder	Carl Roth GmbH + Co. KG
Nonyl phenoxypolyethoxylethanol (NP-40)	Sigma Aldrich
NucleoSpin Triprep Kit	Macherey Nagel
NucleoSpin® Gel and PCR Clean up	Macherey Nagel
OptiMEM	Invitrogen
PageRuler™ Prestained Protein Ladder	Fermentas
Phosphate buffer saline (PBS)	PAA Laboratories
Penicillin/Strepomycin	PAA Laboratories
Phusion® High Fidelity Polymerase + Kit	New England Biolabs
PMSF (Phenylmethylsulfonyl fluoride)	SERVA
Polyethyleneimine (PEI)	Sigma Aldrich
Potassium dihydrogen phosphate (KH_2PO_4)	Merck
Power SYBR Green PCR Master Mix	Applied Biosystems
Propidium Iodide	Sigma Aldrich
Protease Inhibitor	SERVA
Protein assay kit	Pierce
Pure Yield™ Plasmid MidiPrep System	Promega
Puromycin	Invitrogen GmbH
QIAamp DNA Mini Kit	QIAGEN
Hot Start Polymerase	QIAGEN
RNase A	AppliChem
RNase-free DNase I	Roche Diagnostics
Smart Ladder, Smart Ladder Small Fragment	Eurogentec
Sodium chloride (NaCl)	Carl Roth GmbH + Co. KG
Sodium hydroxide (NaOH)	Carl Roth GmbH + Co. KG
Sodium sulfate (Na_2SO_4)	Sigma-Aldrich
β-Mercaptoethanol	Invitrogen
StrataCloneTM PCR Cloning Kit	Agilent Technologies
Streptomycin	PAA Laboratories
Superdex 75 preparative gel filtration column	GE Healthcare

T4 DNA Ligase	New England Biolabs
TEMED	Merck
Trichloroacetic acid (TCA)	Sigma-Aldrich
Tris	Carl Roth GmbH + Co. KG
Triton X-100	Carl Roth GmbH + Co. KG
Trypsin/EDTA 1x	PAA Laboratories
Tween 20	Carl Roth GmbH + Co. KG
µ-Slide 8 well	ibidi
Vectashield Mounting Medium	Alexis
Zero Blunt® PCR Cloning Kit	Invitrogen

2.1.5 Technical devices and consumables

Table 7. Technical devices

Devices	Type	Supplier
Agarose gel imaging system	Mupid-Ex	Advance co
Small Bacterial incubator	UL 40	Memmert GmbH
Large Bacterial incubator	Certomat H+R	B.Braun
Cell microscope	EVOS xl	AMG
Laminar flow hood	Herasafe KS, Class II	Fisher Scientific GmbH
Axiophot photomicroscope	Axiophot 2	Carl Zeiss MicroImaging GmbH
Cell sorting system	FACS Aria II	Becton Dickinson
Fixed angle rotor	fixed angle 1720	Hettich Zentrifugen
Freezer (-20°C)	Comfort	neoLab Migge Laborbedarf
Freezer (-80°C)	MDF-594	SANYO GmbH
Fridge (4°C)	Premium	Liebherr
Gel documentation system	UV System	INTAS
The high content imaging system	Operetta	PerkinElmer
High-speed centrifuge	Avanti J30I	Beckman Coulter GmbH
Laser scanning confocal microscope	SP5	Leica microsystems
PCR machine	Mastercycler	Eppendorf AG
Photometer	NanoVue	GE Healthcare
Pipettor	Eppendorf Research	Eppendorf AG
Real-time PCR System	7500 Fast	Applied Biosystems
SDS PAGE system	Mini-Protean Tetra	Bio-Rad Laboratories GmbH
Shaker	DOS-10L	NeoLab Migge Laborbedarf
Sonifier	Branson Digital Sonifier 450D	G. Heinemann Ultraschall - und Labortechnick
Spinning disc confocal microscope	Ultraview VOX	PerkinElmer
Tabletop centrifuge	Mikro 22R	Hettich Zentrifugen
Table top centrifuge	Centrifuge 5454	Eppendorf AG
Microplate reader	Infinite M1000	TECAN

Vortex mixer	Neolab 7-2020	NeoLab Migge laborbedarf GmbH
Water bath	Type 1013	GFL
Waving platform shaker	Polymax 1040	Heidolph Instruments GmbH&Co
The western blot scanning system	Typhoon Trio Variable Mode Imager	GE Healthcare
RSLCnano system	UltiMate 3000	Thermo Fisher Scientific
HF Hybrid Quadrupole	Q Exactive	Thermo Fisher Scientific
Longwave Ultraviolet Crosslinker	UVP 95-0228-01	Cole-Parmer

Table 8. Consumables

Consumables	**Supplier**
Cell culture plates & flasks Falcon	Becton Dickinson
CryoTube™	Nunc GmbH & Co. KG
FACS tube	Becton Dickinson
Falcon™ Tubes (15 ml, 50 ml)	Becton Dickinson
Filter paper	Whatman
Immersol™ 518F (immersion oil)	Carl Zeiss
Laboratory bottle (100 ml, 250 ml, 500 ml, 1 L)	SCHOTT
Laboratory vacuum manifold Vac-Man®	Promega
Latex exam gloves „Satin PLUS“	Kimberly Clark
Microcentrifuge tubes (1.5 ml, 2 ml)	Eppendorf
Microscope coverslips (18 mm)	Menzel GmbH + Co KG
Nail polish	Lacura Beauty
Parafilm®M sealing film	neoLab Migge Laborbedarf-Vertriebs
Nitrocellulose Membrane (0.45 µm, 0.2 µm)	Bio-Rad
Pipette tips (10 µl / 200 µl / 1000 µl)	Brand Tech Scientific
pipettes (single channel)	Eppendorf
Pipette tips with filter (10 µl, 200 µl, 100 µl)	SLG Süd Laborbedarf
PureYield™ Binding and Clearing Columns	Promega
Serological pipettes	Carl Roth GmbH + Co. KG
Soft wipes (KIMTECH Science)	Kimberly Clark

2.2 Methods

2.2.1 Expression constructs

The plasmid pCAG-GFP-Sirt1 was derived from pCAG-GFP-IB by addition of mouse Sirt1 cDNA from E14 ESCs and unique restriction enzyme sites AsiSI and NotI (Thermo Scientific). The PCR product of the Sirt1 cDNA was obtained with primers: F-Sirt1

(forward), 5'- AGGGCCAGAGAGGCAGTTGGAAGAT -3'; and R-Sirt1 (reverse), 5'- CCGGACAGCTTCAATAGTGTTATG -3'. The primers with restriction enzyme sites AsiSI and NotI are as follows: F-Sirt1-AsiSI (forward), 5'- ACGTGCGATCGCATG GCGGACGAGGTG -3'; and R-Sirt1-NotI (reverse), 5'- CAGCGGCCGCATTATGATTTG TCTGA -3'. The construction of the plasmid pCAG-GFP-Sirt1 was shown in **Figure 2.1**. With the similar strategy for constructing other plasmids, including pCAG-GFP-Sirt2, pCAG-GFP-Sirt6, pCAG-GFP-Sirt7, pCAG-Sirt3-GFP, pCAG-Sirt4-GFP, and pCAG-Sirt5-GFP, the primers for the plasmid pCAG-GFP-Sirt2 were listed as follows: F-Sirt2 (forward), 5'- GAGCAGTCGGTGACAGTCCC -3'; R-Sirt2 (reverse), 5'- CTGTCCTGCGGGA GGTCATGGTT -3'; F-Sirt2-AsiSI (forward), 5'- ACGTGCGATCGCATGGCCGAGCCGG -3'; and R-Sirt2-NotI (reverse), 5'- CAGCGGCCGCTTACTGCTGTTCCT -3'. The primers for the plasmid pCAG-Sirt3-GFP: F-Sirt3 (forward), 5'- CTGCAGTAGGGTGGTGGTCATGG -3'; R-Sirt3 (reverse), 5'- CAGGTGAAGAAGCCATAGTCTTATC -3'; F-Sirt3-AsiSI (forward), 5'- ACGTGCGATCGCATGGTGGGGGCCG -3'; and R-Sirt3-NotI (reverse), 5'- CAGCGGCC GCTTATCTGTCCTGTC -3'. The primers for the plasmid pCAG-Sirt4-GFP: F-Sirt4 (forward), 5'- GAATTGTGGAAGAATAAGAATGA -3'; R-Sirt4 (reverse), 5'- GATTCAGAGTT GGAGCGGCATTG -3'; F-Sirt4-AsiSI (forward), 5'- ACGTGCGATCGCATGAGCGGATTGA -3'; and R-Sirt4-NotI (reverse), 5'- CAGCGGCCGCTTAGGGATCTTGAG -3'. The primers for the plasmid pCAG-Sirt5-GFP: F-Sirt5 (forward), 5'- GACTTCAACGAAAACCTGATGCG -3'; R-Sirt5 (reverse), 5'- CATAAAAGTCAAGTCACCAACT -3'; F-Sirt5-AsiSI (forward), 5'- ACGTGCGATCGCATGCGACCTCTCC -3'; and R-Sirt5-NotI (reverse), 5'- CAGCGGCCGCT CACCAACTCTCTC -3'. The primers for the plasmid pCAG-GFP-Sirt6: F-Sirt6 (forward), 5'- CTTTATTGTTCCCGTGCGGCAGCGC -3'; R-Sirt6 (reverse), 5'- GTTCCTTCAAGTTCCC CTCCCGC -3'; F-Sirt6-AsiSI (forward), 5'- ACGTGCGATCGCATGTCGGTGAATTATG -3'; and R-Sirt6-NotI (reverse), 5'- CAGCGGCCGCATCAGCTGGGGGCAGC -3'. The primers for the plasmid pCAG-GFP-Sirt7: F-Sirt7 (forward), 5'- AAGCGCAGTCAAAGGAGCGATG G -3'; R-Sirt7 (reverse), 5'- TCTTTGTCAACTCCGGGCTATGCC -3'; F-Sirt7-AsiSI (forward), 5'- ACGTGCGATCGCATGGCAGCCGGTGGC -3'; and R-Sirt7-NotI (reverse), 5'- CAGCGGCCGCACTATGCCACTTTCTT -3'.

For the construction of truncations of Sirt1, the fragments of Sirt1, including its N terminus, catalytic domain, C terminus, Sirt1 with deletion of the C terminus, and Sirt1

with deletion of its N terminus, were amplified by PCR (**Figure 2.2**). The primers for cloning the N terminus of Sirt1were shown as follows: F-SIRT1-AsiS1 (forward), 5'-ACGTGCGACGCATGGCGGACGAGGTG -3'; R-SIRT1-N-Not1 (reverse), 5'- CAGCGGCCGC TTAGTCTTTCCTCTTC -3'. The primers for the catalytic domain of Sirt1: F-SIRT1-Ca-AsiS1 (forward), 5'- ACGTGCGATCGCATGATTAACACCAT -3', and R-SIRT1-Ca-Not1 (reverse), 5'- CAGCGGCCGCTTAGGCATATTCACCA -3'. The primers for the C terminus of Sirt1: F-SIRT1-C-AsiS1 (forward), 5'- ACGTGCGATCGCATGAAACTTTGTTGT -3', and R-SIRT1-Not1 (reverse), 5'- CAGCGGCCGCATTATGATTTGTCTGA -3'. The primers of F-SIRT1-AsiS1 and R-SIRT1-Ca-Not1 were used for amplifying the N terminus and catalytic domain of Sirt1, and the primers of F-SIRT1-Ca-AsiS1 and R-SIRT1-Not1 were used for the fragment of the catalytic domain and C terminus of Sirt1.

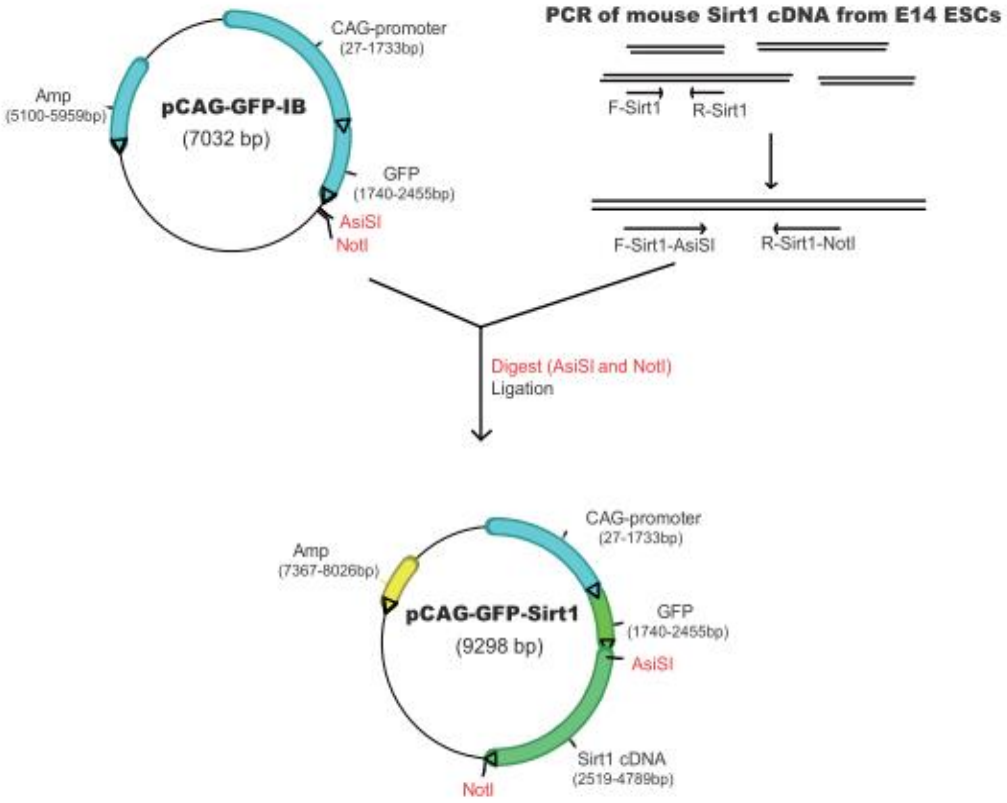

Figure 2.1. Construction of the plasmid pCAG-GFP-Sirt1. The DNA sequences coding for mouse Sirt1 were amplified from E14 ESCs by PCR using fusion high-fidelity DNA polymerase and then amplified again with AsiSI and NotI. The PCR products and the vector pCAG-GFP-IB were digested with unique restriction enzyme sites AsiSI and NotI and then ligated at 16°C

overnight. The plasmid inserted with Sirt1 cDNA was sequenced and stored. These two enzymes were labeled in red. Amp means Ampicillin.

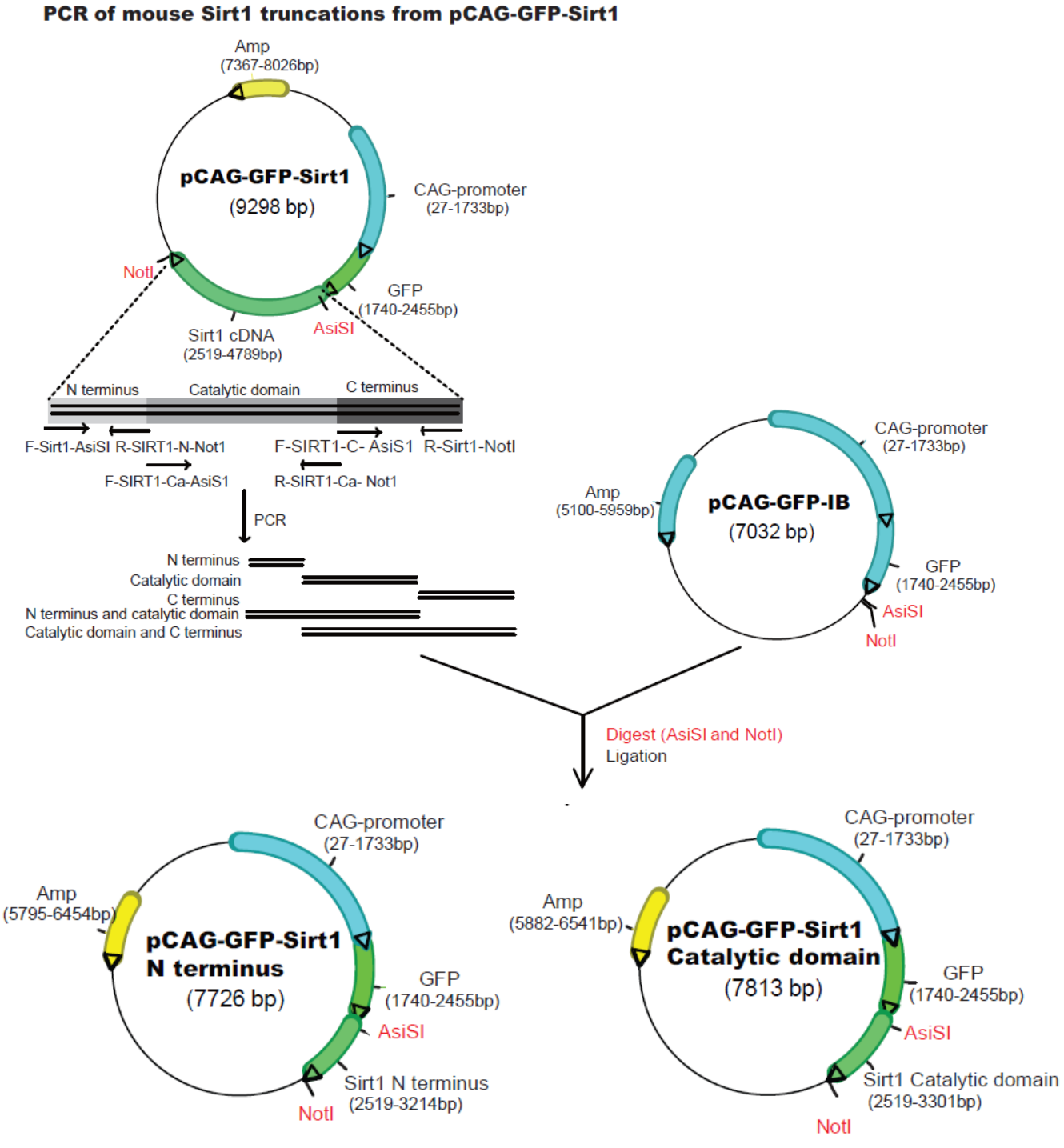

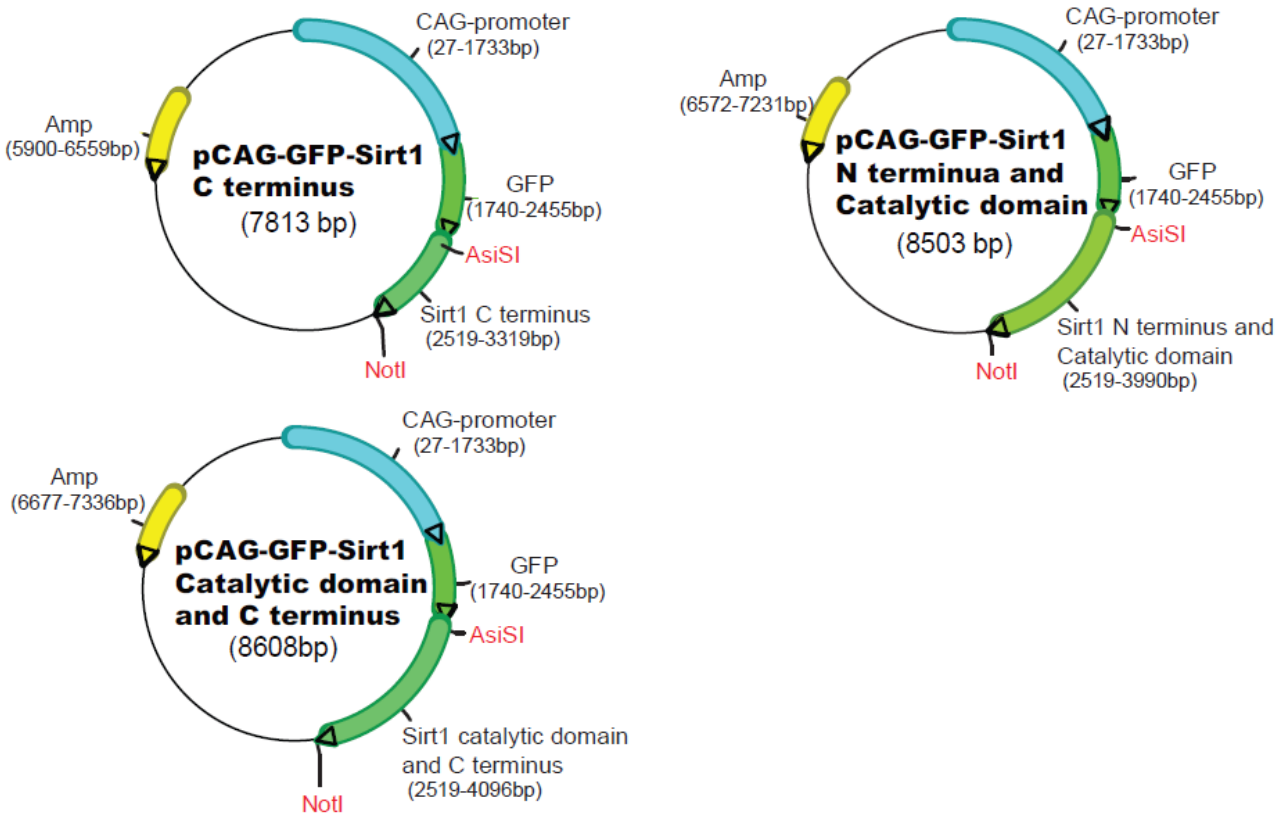

Figure 2.2 Construction of Sirt1 truncations. The different fragments of Sirt1, including its N terminus, catalytic domain, C terminus, the N terminus and catalytic domain, and catalytic domain and C terminus, were amplified by PCR with the corresponding primers (F-SIRT1-AsiS1, R-SIRT1-Not1, F-SIRT1-Ca- AsiS1, R-SIRT1-Ca- Not1, F-SIRT1-C- AsiS1, R-SIRT1-N- Not1). And the plasmid pCAG-GFP-Sirt1 was used as a template. Afterward, the PCR products and the vector pCAG-GFP-IB were digested with AsiSI and NotI. Each digested PCR product was ligated with the digested GFP vector at 16°C overnight. The plasmids inserted with various Sirt1 fragments were sequenced and stored. These two enzymes were labeled in red. Amp means Ampicillin.

The expression constructs of GFP-Dnmt1, LacI-GBP, GFP-Uhrf1, RFP-Uhrf1, and the truncation of Uhrf1, including Uhrf1 deletion of TTD, PHD, SRA, and RING domains have been generated previously (Meilinger et al., 2009; Rottach et al., 2010; Schermelleh et al., 2005). To generate GFP-Dnmt1 S717E and S717A, pCAG-GFP-IB was digested with restriction endonucleases AsiSI and NotI and ligated with the

fragments of Dnmt1 S717E and S717A constructed by overlapping PCR with wild type Dnmt1 (**Figure 2.3**). The primers for Dnmt1 S717A and S717E were listed as follows: F-Dnmt1 (forward), 5'- ACCAGTGAGAAACTGGCAATCTACGACTCCACCTC-3'; R-Dnmt1 (reverse), 5'- CCCC ATCGAT GCTCACCTTCTGA -3'; F-Dnmt1 S717A (forward), 5'- GATGTGTCAGAGATGCCAGCACCCAAA -3'; R-Dnmt1 S717A (reverse), 5'- TTTG GGTGCTGGCATCTCTGACACATC -3'; F-Dnmt1 S717E (forward), 5'- GATGTGTCAG AGATGCCAGAACCCAAA -3'; and R-Dnmt1 S717E (reverse), 5'- TTTGGGTTCTGGCA TCTCTGACACATC -3'. The double mutation of GFP-Uhrf1, K644R, and K664R, was obtained by overlapping extension PCR from wild type Uhrf1 and linked to the digested pCAG-GFP-Sirt7 (**Figure 2.4**). The overlapping extension PCR of Uhrf1 was composed of three fragments. The primers for the first fragment of PCR were F-UHRF1- AsiS1 (forward), 5'- ACGTGCGATCGCATGTGGATCCAGG -3' and R-UHRF1-R1 (reverse), 5'- CCCACACATGCCATGCCTCGGCC -3'. The second fragment was amplified with the primers, including F-UHRF1-R1 (forward), 5'- CCCGGCGGGACTGGGGCCGAGGC -3' and R-UHRF1-R2 (reverse), 5'- CCCTCTGCAGGAGCGTATCGGCT -3'. The primers for the third fragment were: F-UHRF1-R2 (forward), 5'- GAAGGGCGGGAAAC ACAGCCGATA -3' and R-UHRF1- Not1 (reverse), 5'- CAGCGGCCGCTTACTGCTCCA AGGC -3'.

GFP-Cbx1 and RFP-Usp7 have also been generated previously (Ma et al., 2014; Qin et al., 2011b). Mouse Cdk2 and Hif1a were amplified from mouse cDNA and inserted into the backbone of pCAG-Ch-IB digested with AsiSI and NotI. The primers for Cdk2: F-Cdk2 (forward), 5'- GCCTGAGCCGCCTCACTAG -3'; R-Cdk2 (reverse), 5'- CTTTGGG AAGGGCATCAGAG -3'; F-Cdk2-AsiS1 (forward), 5'- ACGTGCGATCGCATGGAGAAC -3'; and R-Cdk2-NotI (reverse), 5'- CAGCGGCCGCTCAGAGCCGAAG -3'. The primers for Hif1a were listed: F- Hif1a (forward), 5'- GGCACCGATTCGCCATGGA -3'; R-Hif1a (reverse), 5'- CAAAAGGAATGAGATTAG -3'; F-Hif1a-AsiS1 (forward), 5'- ACTGGCGA TCGCATGGAGGGCGCCGGC -3'; and R-Hif1a-NotI (reverse), 5'- GAGTAGCGGCCGC CTCAGTTAACTTGATC -3'. The plasmid pCAG-RFP-Tip60 was generated by cutting the Tip60 fragment from pCAG-GFP-Tip60 with AsiSI and NotI and linking to pCAG-RFP-IB. The four plasmids, including CttP-RE-TIGHT-GFP-Sirt1, CttP-RE-TIGHT-GFP-Sirt2, CttP-RE-TIGHT-GFP-Sirt6, CttP-RE-TIGHT-GFP-Sirt7, were derived from CttP-

RE-TIGHT-GFP. The cloned fragments of Sirt1, Sirt2, Sirt6, and Sirt7 were inserted into the vector CttP-RE-TIGHT-GFP with AsiSI and NotI. The plasmid information was shown in **Figure 2.5**. All primers were also listed in Materials and Methods (**Table 5**). And all constructs were verified by DNA sequencing (Eurofins).

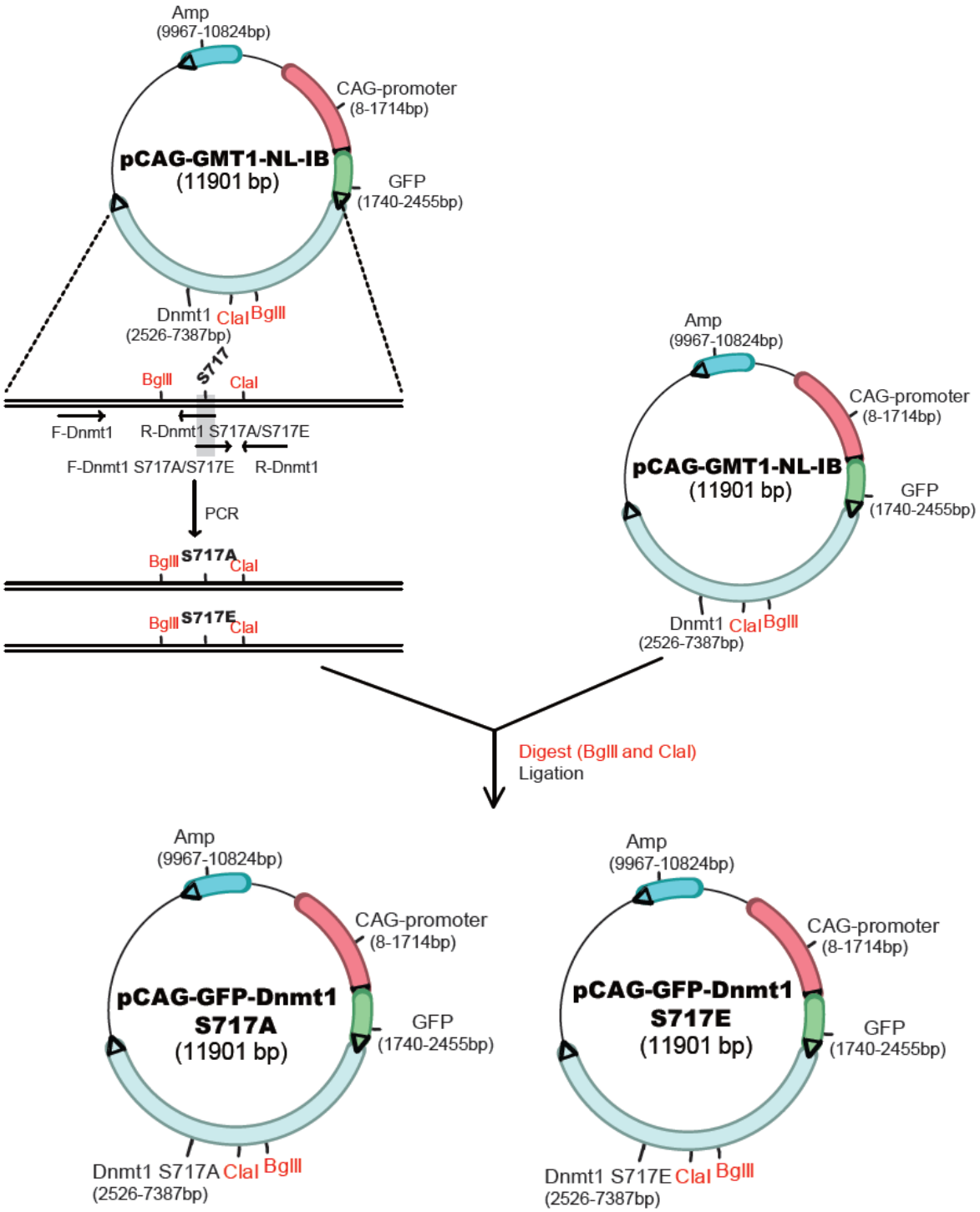

Figure 2.3 Construction of Dnmt1 mutation S717A and S717E. The fragments of two Dnmt1 mutants, S717A and S717E, were derived from wild type Dnmt1 with the designed primers. The PCR products were digested with restriction enzymes, BgIII and ClaI, and then ligated at 16°C overnight. The plasmids inserted with fragments of the Dnmt1 mutant were sequenced and stored. These two enzymes were labeled in red. Amp means Ampicillin.

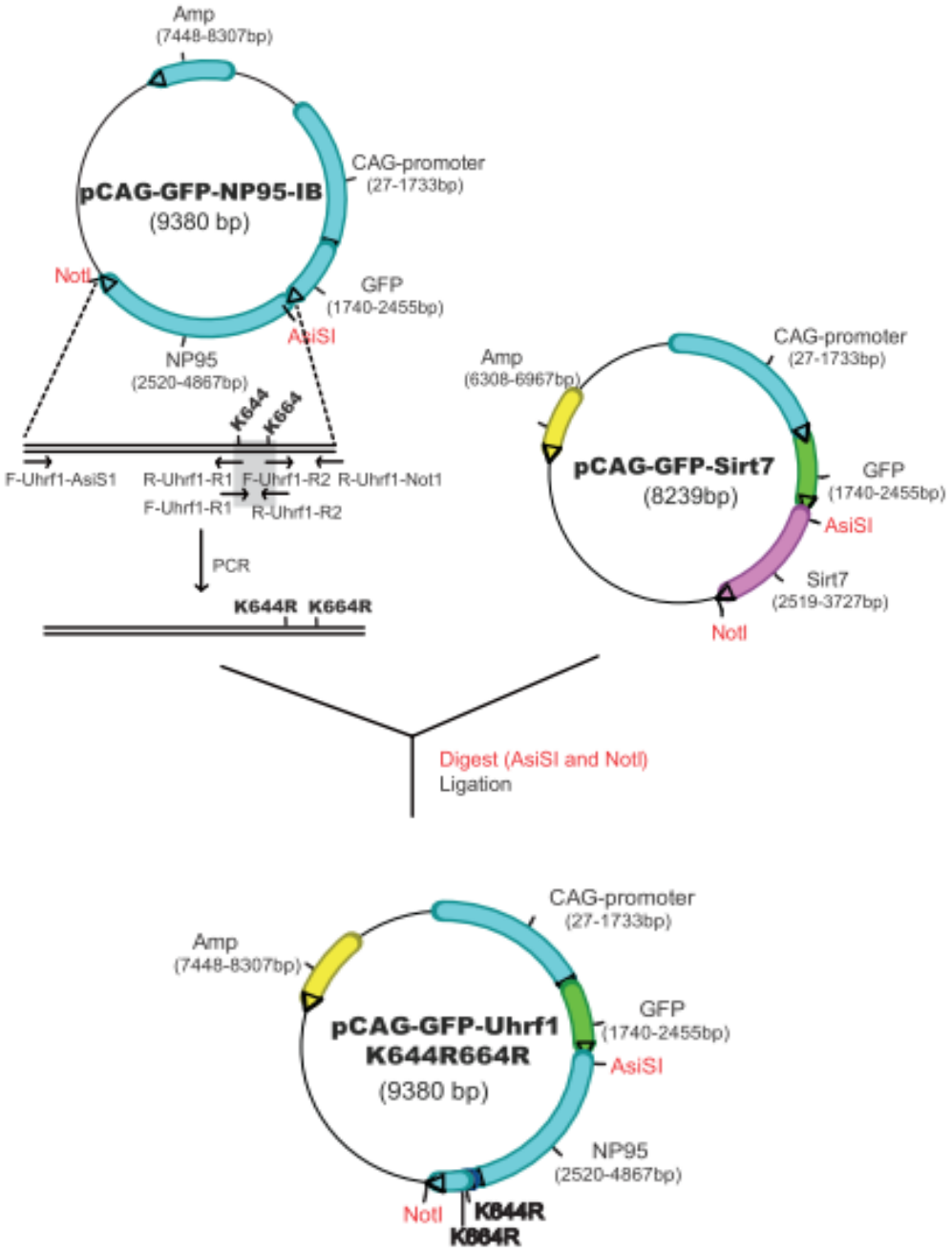

Figure 2.4 Construction of Uhrf1 double mutation K644RK664R. The three fragments of Uhrf1 mutation were derived from wild type Uhrf1 of the plasmid pCAG-GFP-Np95-IB with the designed primers. The PCR products were digested with restriction enzymes, AsiSI and NotI, and then ligated with the backbone pCAG-GFP-Sirt7 at 16°C overnight. The plasmid inserted with Uhrf1 K644RK664R was sequenced and stored. These two enzymes were labeled in red. Amp means Ampicillin.

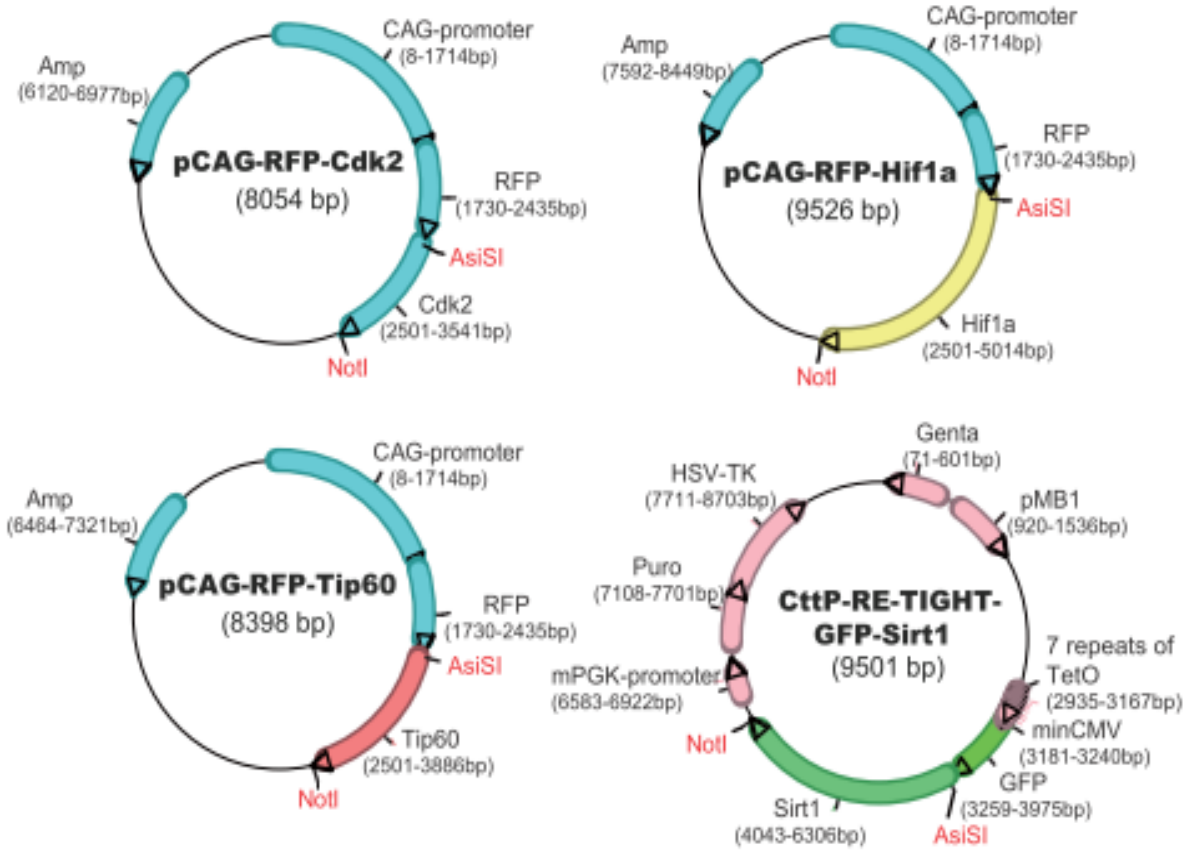

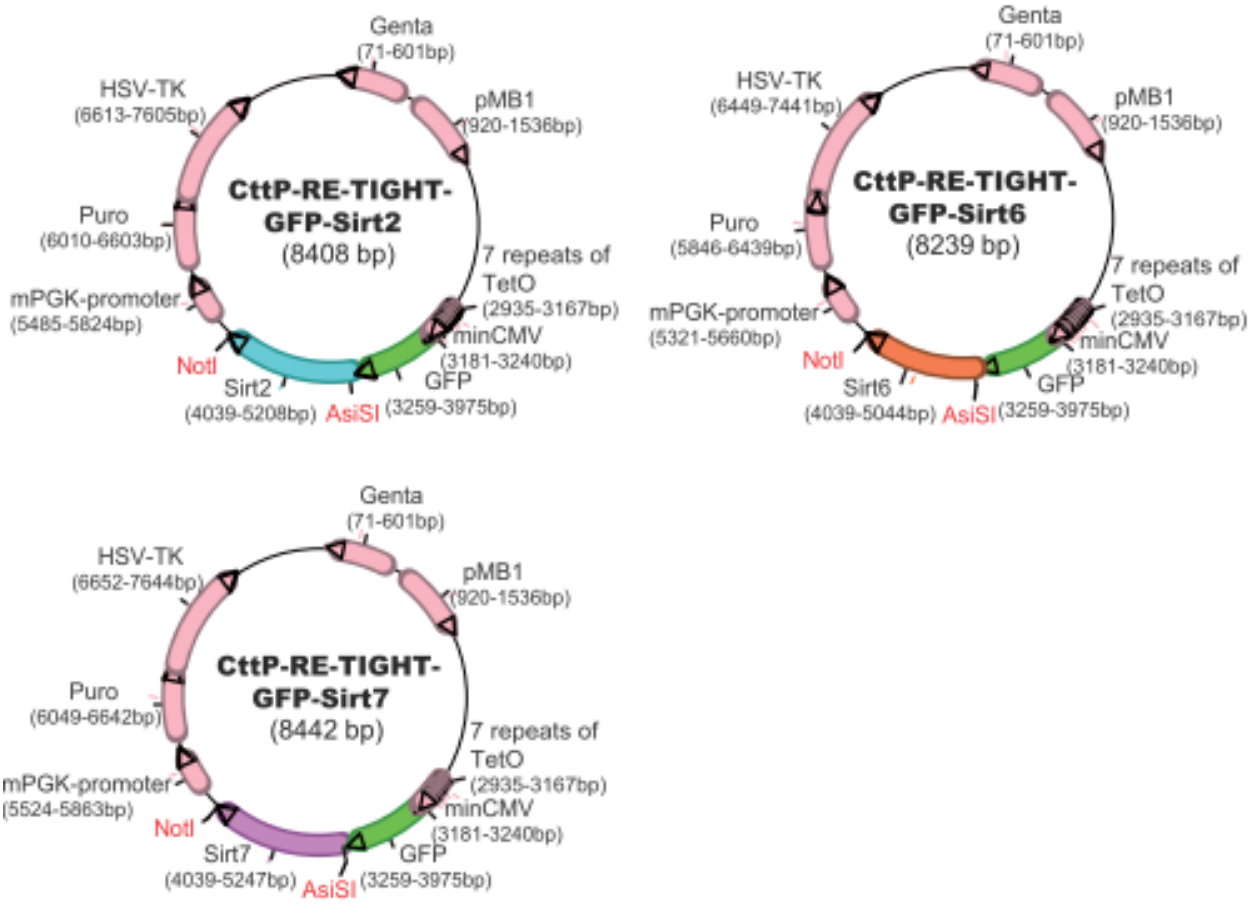

Figure 2.5 Graphic maps of seven plasmids, including pCAG-RFP-Cdk2, pCAG-RFP-Hif1a, pCAG-RFP-Tip60, CttP-RE-TIGHT-GFP-Sirt1, CttP-RE-TIGHT-GFP-Sirt2, CttP-RE-TIGHT-GFP-Sirt6, and CttP-RE-TIGHT-GFP-Sirt7. All of the plasmids were constructed with restriction enzymes, AsiSI and NotI. The two enzymes were labeled in red. Amp meaned Ampicillin; Genta meaned gentamycin; Puro was puromycin.

2.2.2 Cell culture and transfection

Human embryonic kidney (HEK) 293T cells were cultured in Dulbecco's modified Eagle's medium (DMEM) plus 10% fetal calf serum and 50 μg/ml gentamycin (PAA). C2C12 cells were maintained in DMEM supplemented with 20% fetal calf serum and 50 μg/ml gentamycin. J1 ESCs were maintained in gelatin-coated dishes in DMEM supplemented with 20% fetal bovine serum (FBS, Biochrom), 0.1 mM β-mercaptoethanol (Invitrogen), 2 mM l-glutamine, 2 mM 100 U/ml penicillin, 100 μg/ml

streptomycin (PAA Laboratories GmbH), 1 × MEM non-essential amino acids, 1000 U/ml recombinant mouse LIF (Millipore) and 2i (1 μM PD032591 and 3 μM CHIR99021) (Axon Medchem, Netherlands). Baby hamster kidney (BHK) cells were cultured in DMEM supplemented with 10% fetal calf serum and 50 μg/ml gentamycin. HEK293T cells and BHK cells were transfected with transfection reagent of polyethyleneimine (Sigma) according to the manufacturer's instructions. C2C12 cells were transfected with Lipofectamine 2000 reagent (Invitrogen) according to the manufacturer's instructions. Mouse ESCs were also transfected with Lipofectamine 2000 reagent.

2.2.3 Co-immunoprecipitation and Western blot

For the co-immunoprecipitation assay, pull down of GFP-protein with its interactors using the GFP-Trap beads (ChromoTek) were performed as described (Rothbauer et al., 2008). Briefly, the harvested cells were incubated on ice for 30 minutes in 400 μl lysis buffer (20 mM Tris-HCl, pH 7.5, 0.5 mM EDTA, 150m M NaCl, 0.5% NP-40, and 1 mM PMSF and protease inhibitor cocktail, SERVA). Cell lysates were sonicated and precleared by centrifugation at 14000 g for 10 minutes at 4°C. The supernatants were incubated with GFP-trap beads (Chromotek) for 3 hours at 4°C and then washed with wash buffer (20 mM Tris-HCl, pH 7.5, 0.5 mM EDTA, 150 mM NaCl) for three times and mixed with 30 μl Laemmli buffer and boiled for 10 minutes at 95°C.

For the detection of targeted proteins by western blot, the boiled proteins were resolved by SDS-PAGE and transferred to nitrocellulose membranes. The membranes were blocked in TBST (Tris-buffered saline, 0.075% Tween 20) with 5% fat-free milk for 1 h at room temperature and then incubated with primary antibody overnight at 4°C. After washing with TBST three times, the membranes were incubated with secondary antibody for 1 hour at room temperature. Bound secondary antibody conjugated to horseradish peroxidase (HRP) is visualized for chemiluminescent detection according to an ECL detection kit (Pierce) Amersham Imager 600's instructions (Amersham).

2.2.4 Immunofluorescence staining and microscopy

Immunostaining was performed as described previously (Dambacher et al., 2012). Briefly, cells were cultured on coverslips for 12 hours, washed with PBS, fixed with 4% paraformaldehyde for 10 min, and permeabilized with PBST (PBS and 0.02% Tween-20) plus 0.5% Triton X-100. After washing with PBST for three times, the coverslips were blocked with 3% BSA (bovine serum albumin) in PBST for one hour and incubated the cells with primary and secondary antibody in dark chambers for one hour at room temperature. For DNA staining, coverslips were incubated with 200 ng/ml DAPI in PBST buffer for 5 minutes. The coverslips were mounted in anti-fading medium (Vectashield, Vector Laboratories) and sealed with nail polish.

For the MitoTracker Orange staining, 1 mL of warm medium was placed into each well of 6-well plate and pipetted 0.5 µl of 115 µM MitoTracker Orange into each well, and then incubated the plate in 37°C for 10 minutes.

For super-resolution microscopy, cells were cultured in µ-Slide 8 well (ibidi) with the different concentration of Dox at 0 µg/ml, 0.1 µg/ml, 0.5 µg/ml, 1 µg/ml, 2 µg/ml for 24 hours and used for images. The super-resolution images were obtained with a spinning disc confocal microscope (Ultraview VOX, PerkinElmer). The images were processed and assembled by ImageJ software (NIH Image).

2.2.5 DNA methylation assay

The DNA methylation assay has been reported to be performed by the standard protocol with EZ DNA Methylation-Gold™ Kit (Zymo research). Firstly, to get purified DNA, we used the kit from QIAamp for genomic DNA purification according to the instructions. The cell pellet was lysed and then digested by proteinase K at 56°C. After the centrifugation in microcentrifuge tubes, the mixture was added into 100% ethanol to wash the DNA samples. And then the purified DNA was collected by distilled water. For the reaction with Dnmt1 protein and genomic DNA, the methylation activity of Dnmt1 on genomic DNA was activated at the buffer NEB2 (Thermo Fisher) supplemented with Bovine serum albumin (BSA) and S-Adenosyl methionine in 37°C for 1.5 hours. The theory for bisulfite treatment of the methylated DNA is that the methylated cytosine at position 5 remains intact while the unmethylated cytosines are completely converted into

uracil following bisulfite treatment and detected as thymine following PCR. Briefly, The 20 µl DNA sample was added into 130 µl of the CT Conversion Reagent and mixed for the next step: 98°C for 10 minutes, 64°C for 2.5 hours and then stored at 4°C. The Zymo-Spin™ IC Column was prewashed with M-Binding buffer and then loaded with the DNA sample. After centrifuging at a speed of 8000 x g for 30 seconds, the column was washed by M-Wash Buffer. The sample was then mixed with M-Desulphonation buffer at room temperature for 20 minutes and washed by M-wash buffer for one more time. Finally, the Elution buffer was used to elute the DNA sample. PCR was performed using the eluted DNA as a template for amplifying the products of Major satellite repeats. The PCR products were then sequenced and analyzed for the methylation level at different CpG sites.

2.2.6 F3H assay

The F3H method has been described before (Herce et al., 2013). Due to BHK cells containing a lac operator repeats array, Cells were cultured on coverslips and co-transfected with fluorescent fusion protein expression vectors and a LacI-GBP fusion construct using polyethyleneimine and fixed about 16 h after transfection with 3.7% formaldehyde in PBS for 10 min, washed with PBST (PBS with 0.02% Tween), stained with 200 ng/ml DAPI and mounted in Vectashield medium and sealed with nail polish. The F3H sample was analyzed with an SP5 confocal fluorescence microscope. DAPI, GFP, and mCherry/RFP were excited by 405 nm diode, 488 nm argon and 561 nm diode-pumped solid-state lasers, respectively. Images were recorded and further analyzed using ImageJ software (NIH Image).

2.2.7 *In vitro* deacetylation assay

Immunoprecipitated and purified Uhrf1 and Sirt1 and its mutated proteins were incubated in HDAC buffer (10 mM Tris, pH 8.0, 150 mM NaCl, and 10% glycerol) containing 5 mM $NAD^+$for 2 hours at 30°C. Reaction products were then resolved on SDS gels and visualized by immunoblotting with an anti-acetyl-lysine antibody.

2.2.8 Protein stability assay

Cells were seeded in a 6-well plate and transfected with plasmids, including GFP-Uhrf1 and GFP-Uhrf1 with deletion of SRA. After 12 hours, fresh medium with 100 μg/ml cycloheximide (CHX) (Sigma Aldrich) and 2 μg/ml Aphidicolin (Sigma Aldrich) was added to cells and incubated for 12 hours for collection. Cell pellets were lysed in 4% SDS and subjected to SDS-PAGE and western blot analysis with indicated antibodies.

2.2.9 Slot Blot

To perform this assay, genomic DNA was firstly extracted from the ESCs induced by different concentration of Dox (doxycycline) using the Blood & Cell Culture Midi Kit (Qiagen). Genomic DNA was added to Nitrocellulose membranes (Amersham) using the Bio-Rad slot blot system according to the manufacturer's instruction. Nitrocellulose membranes were plated in Longwave Ultraviolet Crosslinker (Colo-Parmer, GZ-39462-14) and crosslinked with the "Auto" selection. After crosslinking, the members were blocked with PBST supplemented with 5% milk for 1 h at room temperature. Membranes were incubated with primary antibody against mouse mC (Eurogentec, 33D3) 1 hour at room temperature or overnight at 4°C. A secondary antibody against mouse conjugated to Alexa 488 (Life Technologies, A21202) was used for fluorescence detection and visualized with Typhoon TRIO (GE Healthcare Life Sciences). Quantification was performed by ImageJ software (NIH Image).

2.2.10 Fluorescence-activated cells sorting (FACS) analysis

Cells were seeded in 6-well plates, incubated with different concentrations of Dox at 0 μg/ml, 0.1 μg/ml, 1 μg/ml, 2 μg/ml and 4 μg/ml for 24 h, washed with PBS and incubated with Trypsin-EDTA solution for 5 minutes at 37°C. Then cells were resuspended in 1 ml PBS and transferred to a conical centrifuge tube. 5×10^4 Cells were sorted and analyzed for GFP signal on a BD FACS Aria Ⅲ cell sorter. The results were analyzed by FlowJo software (BD Biosciences).

2.2.11 Mass spectrometry

GFP-Uhrf1 was overexpressed in HEK293T cells with or without 2 µg/ml Aphidicolin (Sigma Aldrich) for 24 hours and purified with GFP-Trap beads. The samples were boiled at 95°C for 5 min and analyzed by SDS-PAGE. Gel bands were manually excised and digested with trypsin as described before (Shevchenko et al., 2000; Wilm et al., 1996). First, gel slices were washed twice with 100 µl of H_2O, three times with 100 µl of 25 mM NH_4HCO_3 and dehydrated by washing them three times with 100 µl of acetonitrile. Gel slices were then incubated 1 hour with 50 µl of 10 mM DTT in 25 mM NH_4HCO_3. Afterward, slices were incubated 30 minutes in a dark place with 50 µl of 55 mM iodoacetamide in 25 mM NH_4HCO_3 to carbamidomethylate cysteines. Gel fragments were washed with 100 µl of 25 mM NH_4HCO_3 and dehydrated again with 100 µl of acetonitrile. Ten µl of 25 ng/µl trypsin (Promega) dissolved in 25 mM NH_4HCO_3 were added to each gel slice, depending on the volume of the excised spot, incubated 45 minutes at 4ºC and then the non-absorbed trypsin removed. Gel fragments were covered with 25 mM NH_4HCO_3 and digestion took place for 16 hours at 30°C. For the peptide extraction, gel slices were washed twice with 50 µl of acetonitrile/mQ H_2O 1/1 0.25% TFA and twice more with 50 µl of acetonitrile. The resulting liquid containing the digested peptides was totally evaporated, redissolved with 15 µl of 0.1% formic acid and stored at –20 ºC until further processing.

For the mass spectrometry analysis performed by Dr. Ignasi Forné, 5 µl of peptides were injected in an RSLCnano system (Thermo) and separated in a 15 cm analytical column C18 nanocolumn (75 µm ID home-packed with ReproSil-Pur C18-AQ 2.4 µm, a 50-min gradient from 5 to 60% acetonitrile in 0.1% formic acid. The effluent from the HPLC was directly electrosprayed into a Q Exactive^{TM} HF Hybrid Quadrupole (Thermo). The Q Exactive HF instrument was operated in a data-dependent mode to automatically switch between full scan MS and MS/MS acquisition. Survey full scan MS spectra (from m/z 375–1600 were acquired with resolution R= 60,000 at m/z 400 (AGC target of $3x10^6$). The ten most intense peptide ions with charge states between 3 and 5 were sequentially isolated to a target value of $1x10^5$ and fragmented at 27% normalized collision energy. Typical mass spectrometric conditions were: spray voltage, 1.5 kV; no

sheath and auxiliary gas flow; heated capillary temperature, 250°C; ion selection threshold, 33.000 counts. Each individual thermo binary raw file was searched with Mascot/Sequest against the database (UniProt-proteome-3AUP000005640, Hsapiens. fasta). Typical search parameters for peptide were as follows: mass tolerance, 10 ppm; fragment tolerance, 0.5 Da; enzyme was set to trypsin, allowing up to two missed cleavages; static modification, carbamidomethylated cysteine (+57.0215 Da); variable modifications, methionine oxidation (+15.9949 Da) and acetylation (+42.0106).

2.2.12 RNA-seq and Real-time PCR

RNA sequencing analysis was performed as described previous (Ziegenhain et al., 2017). In brief, cells were cultured with or without induction by doxycycline for 24 hours. RNA was isolated using the RNeasy kit (QIAGEN Incorporated, Germantown, MD) according to the manufacturer's protocol. Libraries prepared by Christopher B. Mulholland in Leonhardt group. Briefly, RNA was reversing transcribed using barcoded oligo-dT primers and products pooled and concentrated. Unincorporated barcode primers were digested using Exonuclease I (New England Biolabs). Pre-amplification of cDNA pools were done with the KAPA HiFi HotStart polymerase (KAPA Biosystems). Nextera XT libraries were constructed from 5 ng of pre-amplified cDNA with a custom P5 primer (Mulholland et al.). Raw data was analyzed by Dr. Sebastian Bultmann with the the SCRB-seq (zUIMs pipeline) and assessed for the statistical significance using a threshold of $p< 0.001$ and log R script.

Total RNA from cells was isolated with NucleoSpin RNA purification kit (Macherey Nagel) following its protocol. The cDNA was synthesized using 2 µg of total RNA and RT-RCR was performed with the High Capacity cDNA Reverse Transcription Kits (Thermo Fisher) according to its instruction. Quantitative real-time PCR was performed using 10 µl diluted cDNA using Absolute Blue QPCR SYBR Green Mix (Thermo) in the LightCycler (Roche Applied Science) real-time thermocycler. The values of relative expression were normalized to GAPDH in each sample. Primer sequences were presented in Material and Methods (**Table 5**). The experiments for statistical analysis were performed in triplicates as mean ± SD.

2.2.13 ChIP and ChIP-qPCR

The ChIP assay was performed following the manufacturer's instructions (Abcam). In brief, mouse embryonic stem cells were fixed with 0.75% formaldehyde directly to cell culture media at room temperature for 10 min, followed by incubating with 125 mM glycine for 5 min at room temperature. Cells were washed with cold PBS, scraped and resuspended in lysis buffer (50 mM HEPES-KOH pH7.5, 140 mM NaCl, 1 mM EDTA pH8, 1% Triton X-100, 0.1% Sodium Deoxycholate, 0.1% SDS) with protease inhibitor cocktail (SERVA). Chromatin was then sonicated to the fragments of 0.5 kb and preincubated with the Dynabead G (Merck Millipore) and anti-H3K18ac antibody overnight at 4°C. The beads without antibody were as control of IgG. The chromatin-bound to the beads was eluted in 500 µl of freshly prepared elution buffer (1% SDS, 0.1 M $NaHCO_3$). After reversing the cross-linking, the samples were deproteinized and phenol–chloroform-extracted, and DNA was ethanol-precipitated using glycogen as a carrier. Pellets were resuspended in 100 µl of H_2O for qPCR analysis.

3 Results

3.1 The autoinhibition of *de novo* methylation in Dnmt1 requires the phosphorylation of CXXC-BAH1 linker.

3.1.1 The flexible loop between CXXC and BAH1 domains of Dnmt1 prevents *de novo* methylation

Dnmt1 has long been known for the maintenance of genomic methylation. However, the mechanism for its activity is still unclear. Firstly, the eukaryotic Dnmt1 is a multidomain protein, containing a replication foci-targeting domain (RFD), a DNA-binding CXXC domain, a pair of bromo-adjacent homology (BAH) domains (BAH1 and BAH2), and a C-terminal catalytic domain (**Figure 1.1A**). By binding to DNA, the catalytic domain of Dnmt1 repositioned relative to the CXXC domain. Furthermore, the published crystal structure of DNMT1 composed of CXXC, tandem bromo-adjacent homology (BAH1/2), and methyltransferase domains bound to unmethylated DNA, has shown that the CXXC motif binds specifically to unmethylated DNA and switch the CXXC-BAH1 linker into the active catalytic sites of Dnmt1 for preventing *de novo* methylation (**Figure 1.1B**) (Song et al., 2011). This loop in this linker is about 33 amino acids and flexible to position directly between the unmethylated DNA and the active site.

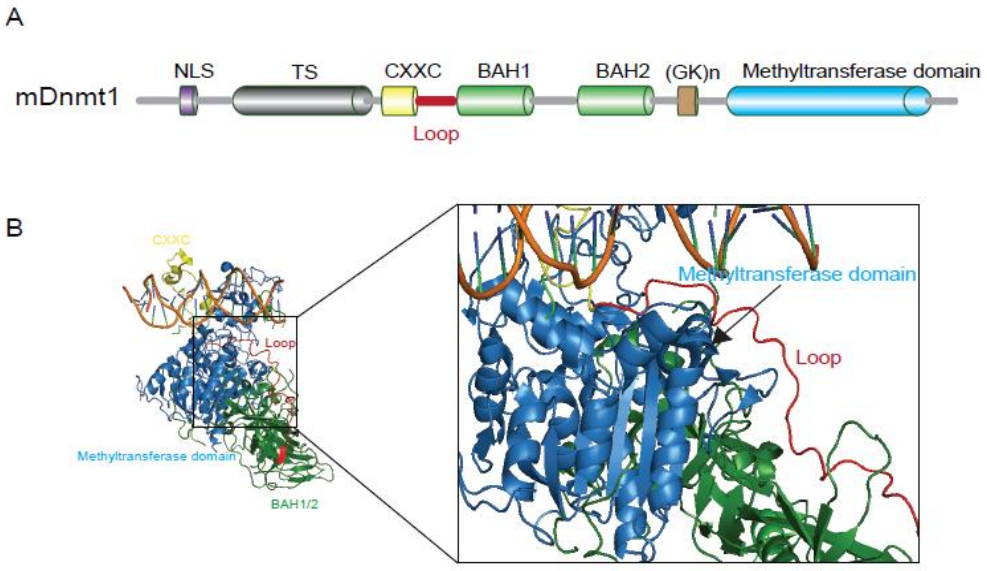

Figure 1.1 Structure of the complex of mDnmt1 composed of CXXC, tandem bromo-adjacent homology (BAH1/2), and methyltransferase domains bound to unmethylated DNA. (A) Domain structure of mDnmt1. Dnmt1 contains a methyltransferase domain at the C terminus and three main domains at the N terminus, which include a replication foci-targeting domain (RFD), a DNA-binding CXXC domain, a pair of bromo-adjacent homology (BAH) domains (BAH1 and BAH2). The RFD is represented in gray color; CXXC domain is in yellow; BAH1 and BAH2 are in green; the catalytic domain is in blue. The linker between CXXC and BAH1 is labeled in red. (B) The crystal structure of the Dnmt1 complex with 19-nucleotide oligomer (PDB: 3PT6). The different domains of Dnmt1 are in the same color above (Song et al., 2011).

3.1.2 The CXXC-BAH1 linker can be phosphorylated

It has been reported that Dnmt1 activity and stability are regulated by various post-translational modifications (Scott et al., 2014). To explore the role of the relationship between the CXXC-BAH1 linker and modifications of Dnmt1, I used GFP-Trap beads to purify Dnmt1 for mass spectrometry (**Figure 1.2A**). Analysis of the mass spectrometry of Dnmt1 has shown that there were 10 different phosphorylated sites of Dnmt1, but only one site, S717, of Dnmt1 was from the CXXC-BAH1 linker (**Figure 1.2B**). To mimic the unphosphorylated and the phosphorylated states, respectively, I mutated S717 of Dnmt1 to A717, and E717 to mimic phosphorylation on and off (phospho on and phospho off). The purified proteins, Dnmt1 S717A and S717E, were collected and tested by SDS-PAGE (**Figure 1.2C**).

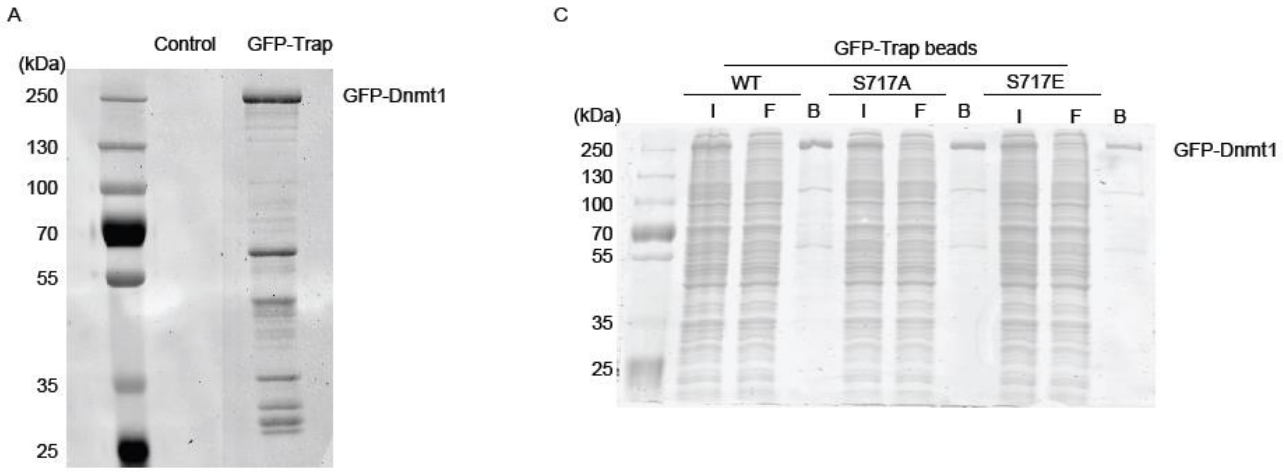

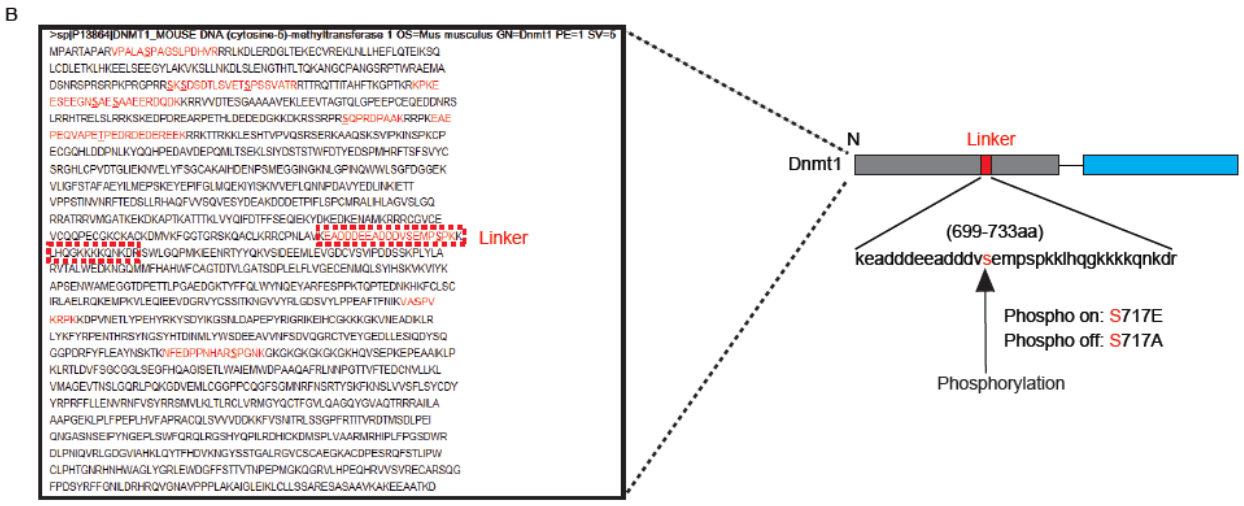

Figure 1.2 The site at the CXXC-BAH1 linker of Dnmt1 can be phosphorylated. (A) The purification and enrichment of Dnmt1. HEK293T cells were transfected with the plasmid of pCAG-GMT1-NL-IB and then GFP-Dnmt1 protein was pulled down by GFP-Trap beads. The samples were analyzed by SDS-PAGE. The untransfected cells were used as a control. This figure was from Dr. Weihua. (B) The result of the phosphorylation analysis at the CXXC-BAH1 linker by Mass Spectrometry. 10 protein sequences containing sites for phosphorylation were labeled in red. The mass spectrometry was performed by Dr. Weihua and Dr. Ignasi Forné. The mutation from serine (S) to alanine (A) prevents phosphorylation (phospho off) and serine to glutamic acid (E) can mimic the state of phosphorylation (phospho on). (C) Protein purification of Dnmt1 wild type and its mutant forms, Dnmt1 S717A and Dnmt1 S717E. The constructs of pCAG-GMT1-NL-IB, pCAG-GFP-Dnmt1 S717A, and pCAG-GFP-Dnmt1 S717E, were separately transfected and overexpressed in HEK cells. The GFP-Trap beads were used for purification of these proteins. The results were analyzed by SDS-PAGE. I was input sample; F was flowthrough sample; B was bound sample.

3.1.3 The role of phosphorylation sites of Dnmt1 in maintenance or *de novo* methylation

To test whether the phosphorylated loop of Dnmt1 influences Dnmt1 maintenance or *de novo* methylation activity *in vitro*, I designed and performed this assay according to our workflow (**Figure 1.3A**). I first prepared the plasmids, including pCAG-GMT1-NL-IB,

pCAG-GFP-Dnmt1 S717A, and pCAG-GFP-Dnmt1 S717E, and separately transfected them to HEK cells for overexpression. With GFP-Trap beads, three proteins of Dnmt1 wild type and its mutant forms, Dnmt1 S717A and Dnmt1 S717E, were purified and shown above (**Figure 1.2C**). Then two kinds of genomic DNA were extracted, one was from Dnmt1 knockout cell lines (CC cell lines), another from a triple knockout of all Dnmts (Dnmt1, Dnmt3a, and Dnmt3b) cell lines (TKO cell lines). The reason for choosing these two different cell lines is mainly because most of DNA is regarded as hemimethylated status in CC cell lines and the global DNA methylation level is very low for unmethylation in TKO cell lines. By incubating these proteins with genomic DNA, *in vitro* genomic DNA was treated with bisulfite conversion followed by EZ DNA Methylation-Gold™ Kit's instructions. The major satellite repeats were cloned from these genomic DNA after bisulfite treatment for sequencing (**Figure 1.3B**). There are at least 8 sites for methylation on the DNA sequence of the major satellite repeats (**Figure 1.3C**). By comparing with DNA sequences from CC cells without coupled with Dnmt1 protein, the percentage of DNA methylation in each CpG site of major satellite repeats was obviously increased when incubated with all of Dnmt1 wild type and mutation, but a little slightly decreased in that of Dnmt1 S717A, suggesting that Dnmt1 still owned its maintenance DNA methylation activity *in vitro* and the mutation of Dnmt1 S717A for phospho-off had little or nearly no influence on Dnmt1 maintenance DNA methylation activity (**Figure 1.3D**). For DNA methylation level in TKO cells, I also used a CpG Methyltransferase, M.Sss1, as the positive control, which is from Spiroplasma and can methylate all unmethylated or hemimethylated cytosine nucleotides at the C^5 position of double-strand DNA. Together with the control of M.Sss1 activity with 80%, it was displayed that, *In vitro*, the percentage of methylated CpG sites of Major satellite repeat reached as high as around 30% (**Figure 1.3E**). It can be concluded that Dnmt1 has a relatively weak *de novo* methylation activity *in vitro*. Notably, the methylated DNA level in Dnmt1 wild type is highest than Dnmt1 S717E, and the lowest was that of Dnmt1 S717A, suggesting that Dnmt1 phospho-off (S717A) weakened Dnmt1 *de novo* DNA methylation activity.

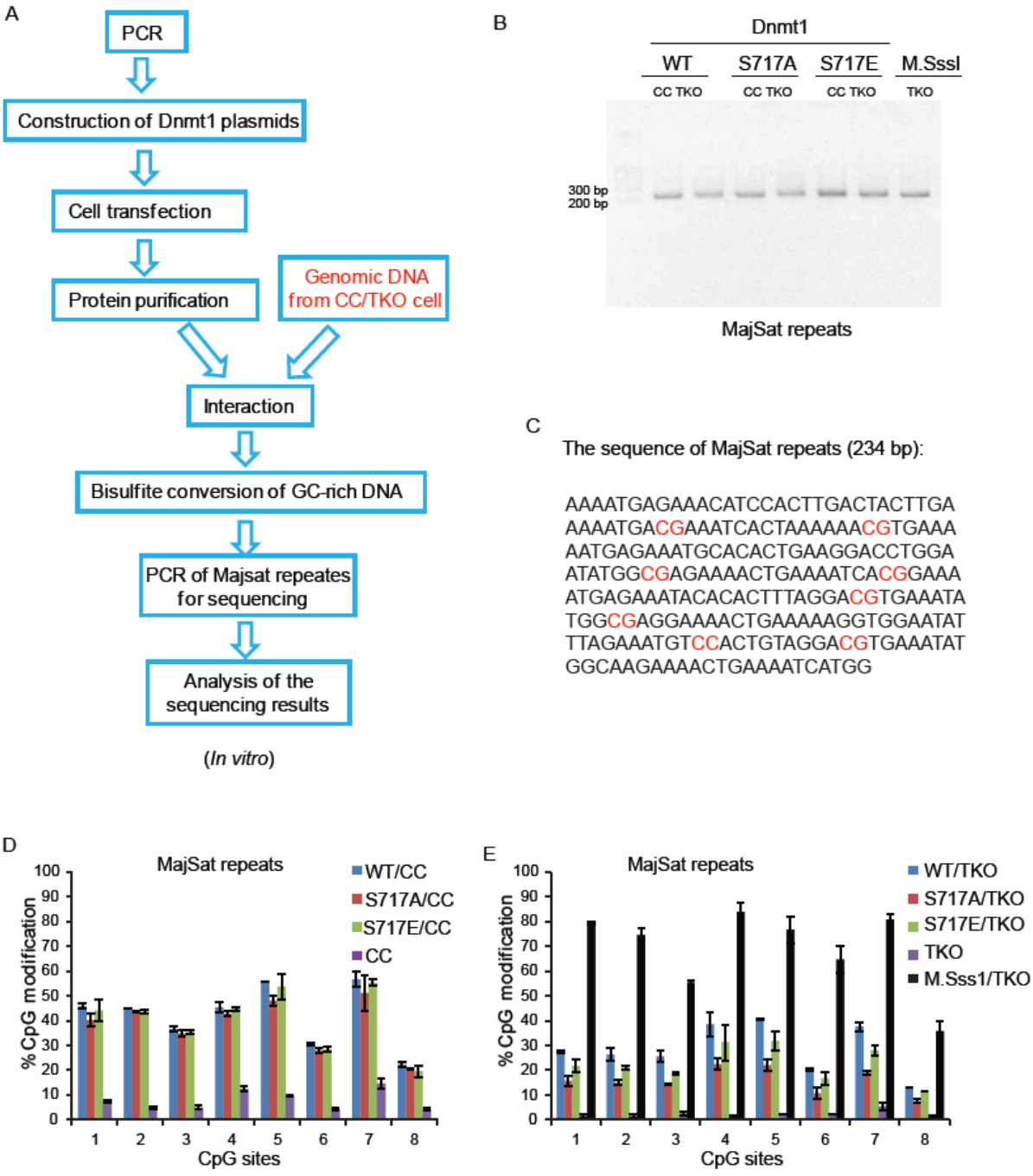

Figure 1.3 Analysis of Dnmt1 maintenance and *de novo* methylation *in vitro*. (A) The workflow of *in vitro* DNA methylation assay. The plasmids for Dnmt1 wild type and mutations, Dnmt1 S717A and S717E, were constructed and transfected in HEK cells for protein overexpression. The proteins were extracted and purified with GFP-Trap beads. Then the genomic DNA from CC cell line or TKO cell line was incubated with these proteins for *in vitro*

methylation assay. After incubation, the DNA was treated with bisulfite conversion and used for the PCR of the major satellite repeats. And the CpG sites of the DNA sequence of major satellite repeats were sequenced and the methylation level was valued by pyrosequencing (Varionostic GmbH, Ulm, Germany). This method is based on the principle of detecting the unincorporated nucleotides in the synthesis of the DNA sequence by a DNA polymerase. (B) The PCR products of major satellite repeats were amplified and run in 2% agarose gel with a DNA marker. The primers used for PCR were F-Majsat and R-Majsat. The sequence of primers was shown in Table 5. The size of the PCR band was 234 base pairs. (C) The DNA sequence of major satellite repeats was shown and the CpG sites for methylation analysis were labeled in red. (D) Comparison of the methylation level of each CpG site in the sequence of major satellite repeats from genomic DNA from the CC cell line, which was used for measuring Dnmt1 maintenance methylation activity. The PCR products were amplified from the genomic DNA of the CC cell line. The proteins of Dnmt1 wild type, S717A, and S717E, were separately incubated with the genomic DNA from the CC cell line and used as a template for PCR. The DNA untreated with Dnmt1 proteins was used as the control. The experiments were repeated two times and the values represent mean ± SD. (E) Measurement of DNA methylation level in TKO cell line for detecting Dnmt1 *de novo* methylation activity. As followed as above, Dnmt1 proteins were incubated with DNA from the TKO cell line and further used for PCR. The *Escherichia coli* CpG methyltransferase, M.SssI, was and used as positive control. The DNA untreated with Dnmt1 proteins was used as negative control. The experiments were repeated two times and the values represent mean ± SD.

Next, the effect of Dnmt1 phosphorylation on Dnmt1 maintenance or de novo methylation activity *in vivo* still needs to be further explored. The *in vivo* DNA methylation was performed differently from *in vitro* methylation assay. Briefly, the well-constructed plasmids, including pCAG-GMT1-NL-IB, pCAG-GFP-Dnmt1 S717A, and pCAG-GFP-Dnmt1 S717E, and separately transfected to CC cell lines or TKO cell lines. I sorted and collected transfected cells by FACS. Then genomic DNA was extracted from these cells and treated with bisulfite conversion for amplification of major satellite repeats. The DNA methylation level of different sites of major satellite repeats was measured similarly with the analysis of DNA methylation *in vitro* (**Figure 1.4A**). The PCR products were run and collected for further sequencing (**Figure 1.4B**). By comparing with the site-based DNA methylation level treated with different Dnmt1

proteins, there was a little influence of phosphorylation on Dnmt1 maintenance methylation activity because, for CC cell line, the total of DNA methylation of Dnmt1 S717A was as high as Dnmt1 wild type and S717E (**Figure 1.4C**). In addition, in TKO cells, DNA methylation was extremely low and even cells were transfected different Dnmt1 proteins for rescue, the level of DNA methylation was too low to calculate (**Figure 1.4D**). However, it was also suggested that Dnmt1 *de novo* methylation activity was inhibited by other mechanisms *in vivo*.

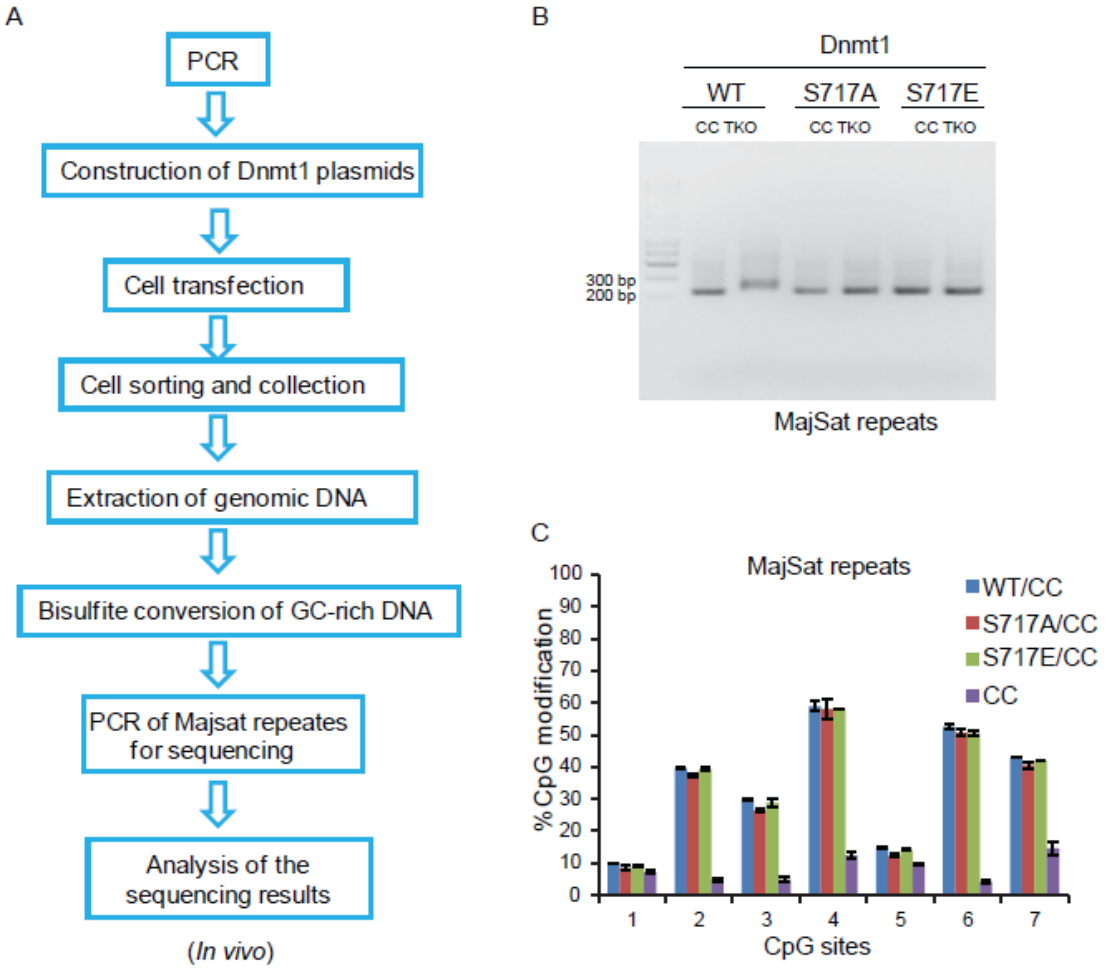

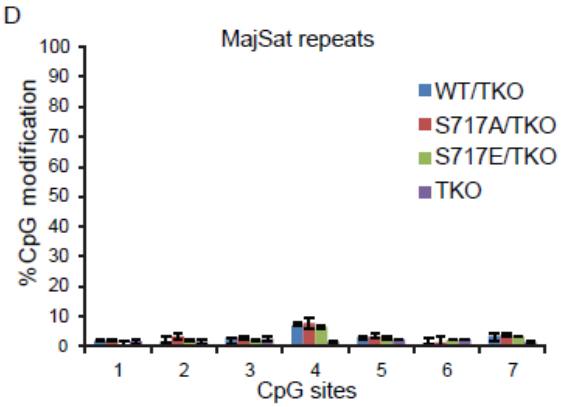

Figure 1.4 Analysis of Dnmt1 maintenance or de novo methylation *in vivo*. (A) The workflow of *in vivo* DNA methylation assay. The plasmids for Dnmt1 wild type and mutants, Dnmt1 S717A and S717E, were constructed and transfected in CC cells or TKO cells for protein overexpression. Then genomic DNA from CC cell line or TKO cell line was extracted and treated with bisulfite conversion and used for the PCR of the major satellite repeats. And the CpG sites of the DNA sequence of major satellite repeats were sequenced and the methylation level was valued by pyrosequencing. (B) The PCR products of major satellite repeats were amplified and run in 2% agarose gel with a DNA marker. The primers used for PCR were F-Majsat and R-Majsat. The sequence of primers was shown in Table 5. The size of the PCR band was 234 base pairs. (C) Comparison of the methylation level of each CpG site in the sequence of major satellite repeats from genomic DNA from the CC cell line, which was used for measuring Dnmt1 d methylation activity. The PCR products were amplified from the genomic DNA of the CC cell line. The DNA untransfected with Dnmt1 plasmids was used as the control. The experiments were repeated two times and the values represent mean ± SD. (D) Measurement of DNA methylation level in TKO cell line for detecting Dnmt1 *de novo* methylation activity. As followed as the workflow, DNA from the TKO cell line was used for PCR. The DNA untransfected with Dnmt1 plasmids was used as negative control. The experiments were repeated two times and the values represent mean ± SD.

3.2 Sirt1 mediated deacetylation controls the stability of Uhrf1 during cell cycle progression.

3.2.1 Uhrf1 interacts with Sirt1

Previous evidence has shown that Sirt1-mediated deacetylation of DNMT1 is crucial for DNMT1's multiple effects, including its methyltransferase activity, gene silencing and the capability to regulate G2/M transition of the cell cycle (Peng et al., 2011). Due to the influences of interaction with Sirt1 on Dnmt1, I tried to explore the connection of Uhrf1 and Sirt1. HEK293T cells were transfected with the plasmids of pCAG-GFP-NP95 and pCAG-RFP-Sirt1. Then GFP-Uhrf1 protein was purified with GFP-Trap beads and incubated with the cell lysate transfected with pCAG-RFP-Sirt1. The untransfected cell lysate was used as a control. The pull-down assay verified the direct interaction of Uhrf1 and Sirt1 (**Figure 2.1A**). As reported that Uhrf1 recruits and interacts with Dnmt1 (Berkyurek et al., 2013), we also observed the direct interaction of GFP-Uhrf1 and Dnmt1. Further, we identified the interaction of GFP-Uhrf1, GFP-Dnmt1, and RFP-Sirt1 by co-immunoprecipitation with GFP-Trap beads (**Figure 2.1B**). These experiments suggested that Sirt1 was associated with the Uhrf1-Dnmt1 complex. To further validate our finding, we also assessed its interaction by fluorescent three-hybrid assay (F3H) (**Figure 2.1C**) (Herce et al., 2013). GFP-labeled protein A can be specially recruited to the LacO array via GBP-LacR within the nucleus. If RFP-labeled protein B interacts with protein A, it will also display an accumulation at the LacO site. As a negative control, GFP was efficiently recruited to the LacO site, but RFP-Uhrf1 did not efficiently bind to the light dot accumulated by GFP on the LacO site. For GFP-Sirt1, RFP-Uhrf1 was recruited to the LacO site (**Figure 2.1D**) and the fluorescence signal for its interaction was detected. The 20 images for LacOp-mediated this interaction were collected and analyzed by ImageJ software. Then the relative binding intensity was calculated by measuring the relative signal intensity of each dot. The average binding intensity was valued and it was found that the intensity of RFP-Uhrf1 displayed on the LacO site of GFP-Sirt1 was as stronger as around 4-fold than that of GFP (**Figure 2.1E**).

3.2.2 SET- and-RING associated domain of Uhrf1 interacts with the catalytic domain of Sirt1

Then we tried to dissect which domain of Uhrf1 interacts with Sirt1. As it was shown, Uhrf1 has five domains: the ubiquitin-like (UBL), plant homeodomain (PHD), tandem

Tudor domain (TTD), SET- and-RING associated, and really interesting new gene (RING) domain (**Figure 2.1F**). Sirt1 contains three common domains, N-terminus, a conserved catalytic domain for deacetylation activity and C-terminus (**Figure 2.1G**). We constructed plasmids with serial truncation of Uhrf1 and subjected to the co-immunoprecipitation assay. RFP-Sirt1 interacted robustly with all of the domains of GFP-Uhrf1, but there was a weaker interaction for Uhrf1 with the deletion of the SRA domain (GFP-Uhrf1 delta SRA) (**Figure 2.1H**). And also, we specifically identified that there was nearly no interaction when Uhrf1 lost its SRA domain (**Figure 2.1I**). We as well constructed several plasmids harboring truncated mutants of Sirt1 and tested their interactions with RFP-Uhrf1 using the same assay. As shown in western blot, there was a weak binding of RFP-Uhrf1 with all truncated forms without the Sirt1 catalytic domain (**Figure 2.1J**). The results suggested that UHRF1 interacted with the catalytic domain of Sirt1. Altogether, these results established that Uhrf1 interacted with Sirt1.

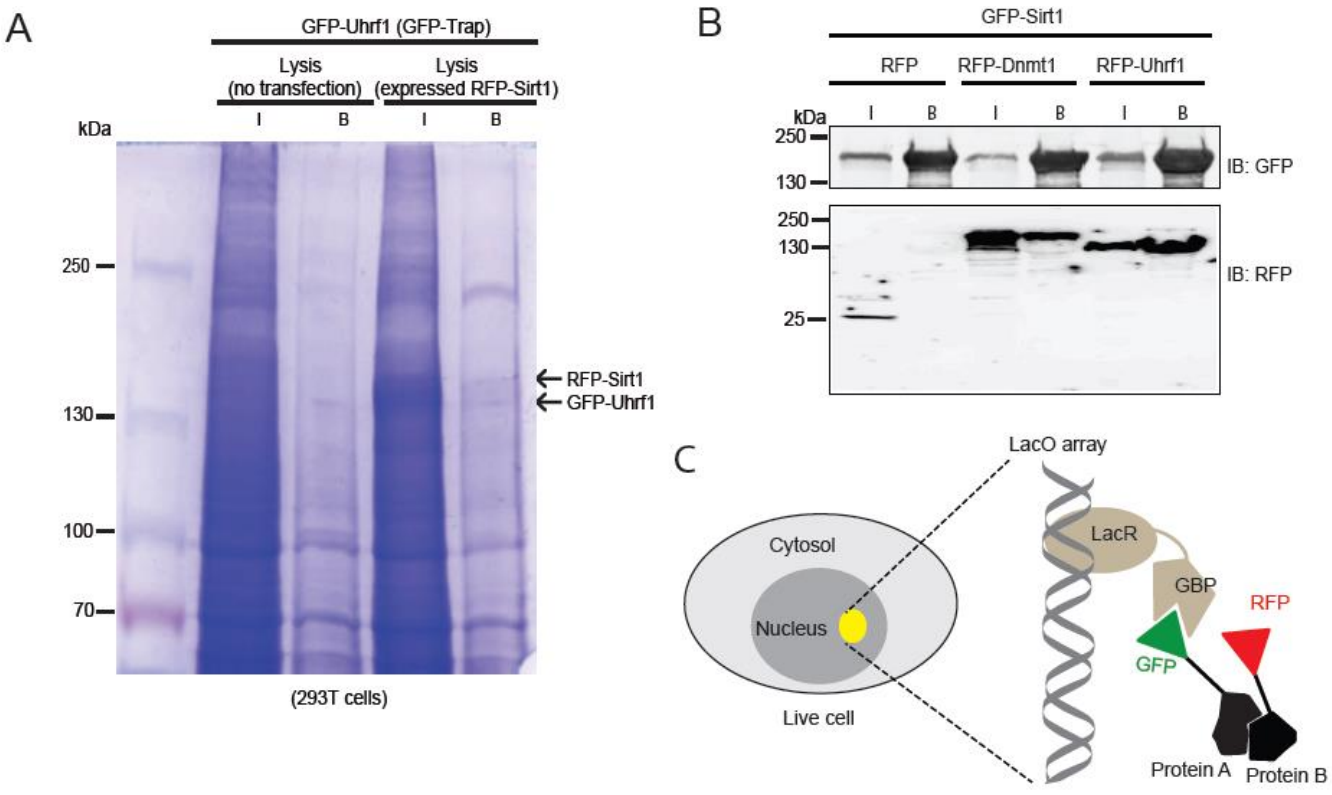

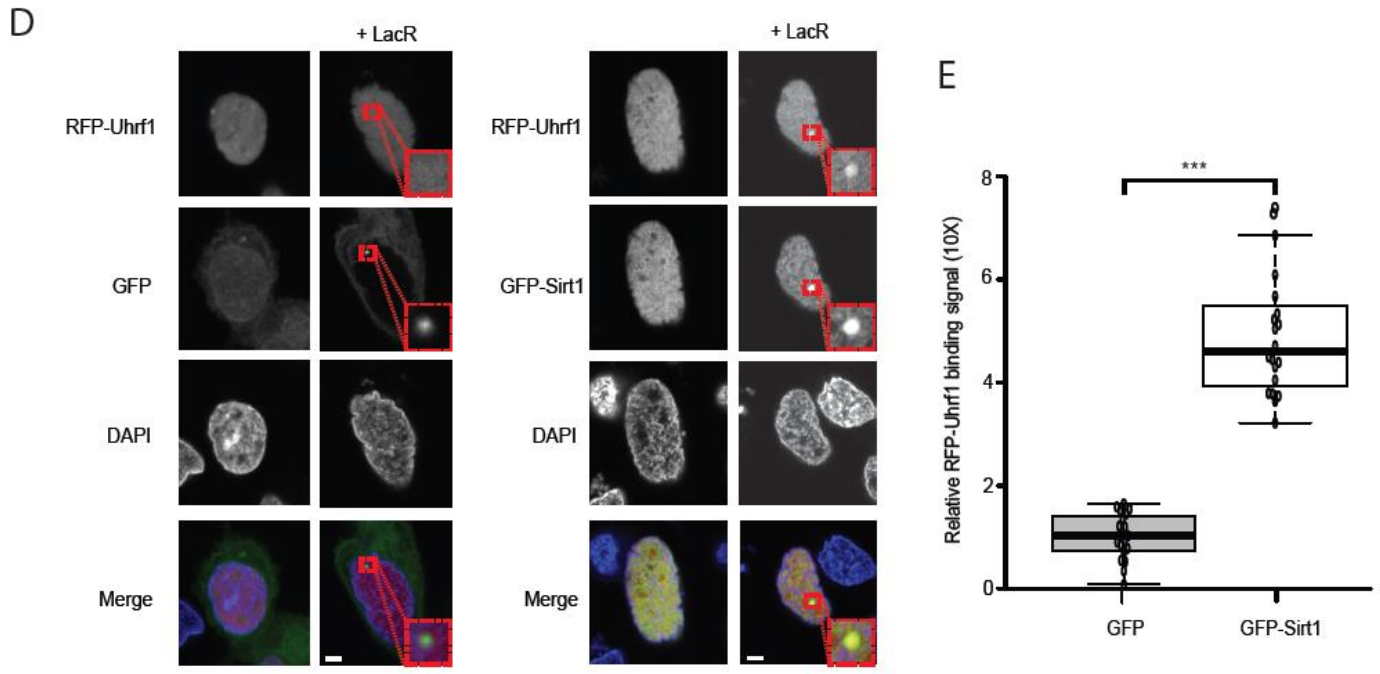
D
+ LacR
+ LacR
RFP-Uhrf1
GFP
DAPI
Merge
RFP-Uhrf1
GFP-Sirt1
DAPI
Merge
E
***
Relative RFP-Uhrf1 binding signal (10X)
8
6
4
2
0
GFP
GFP-Sirt1

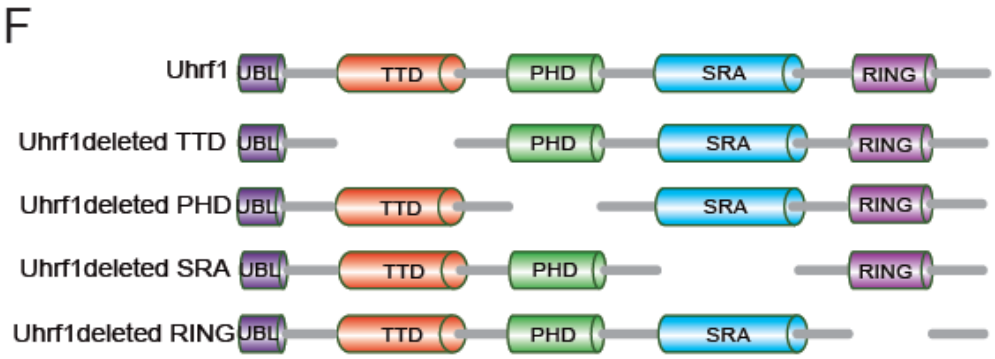
F
Uhrf1
UBL
TTD
PHD
SRA
RING
Uhrf1deleted TTD
Uhrf1deleted PHD
Uhrf1deleted SRA
Uhrf1deleted RING

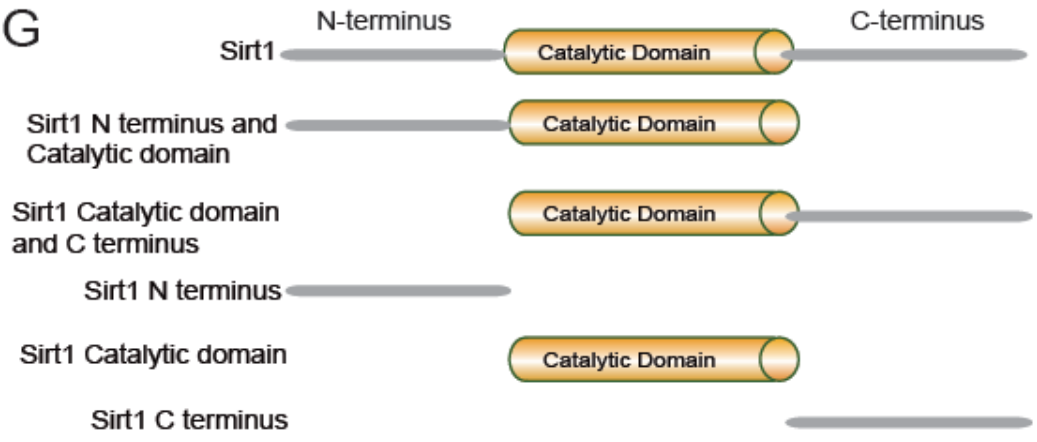
G
N-terminus
C-terminus
Sirt1
Catalytic Domain
Sirt1 N terminus and Catalytic domain
Sirt1 Catalytic domain and C terminus
Sirt1 N terminus
Sirt1 Catalytic domain
Sirt1 C terminus

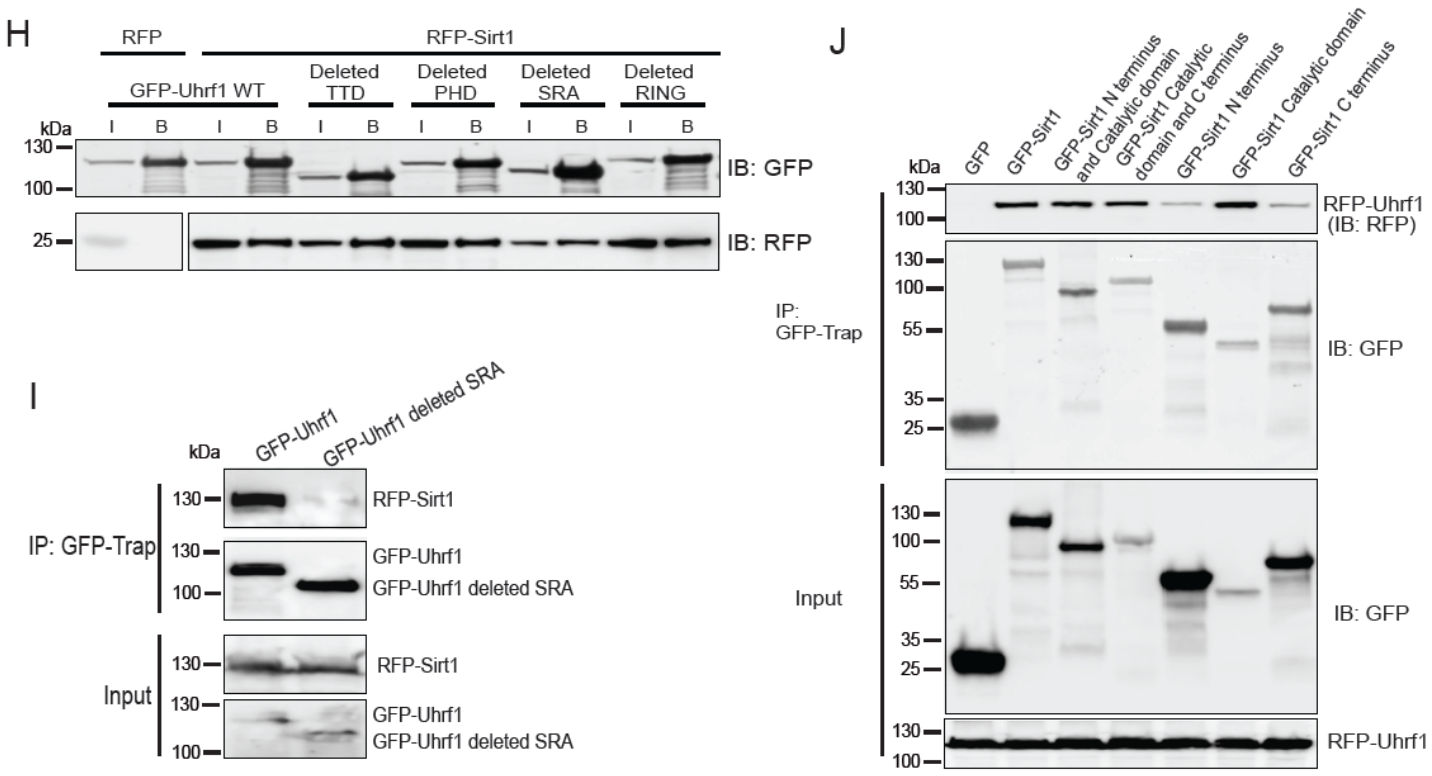

Figure 2.1 Uhrf1 interacts with Sirt1. (A) Coomassie blue stained gel showed the pull-down experiment. GFP-Uhrf1 was purified by GFP-Trap beads and incubated with the lysate of HEK cells overexpressing RFP-Sirt1. Untransfected HEK cells were used as a control. (B) Co-immunoprecipitation of GFP-Sirt1 with RFP, RFP-Dnmt1, and RFP-Uhrf1. HEK cells were co-transfected with expression constructs for GFP-Sirt1 and RFP or RFP-Dnmt1 or RFP-Uhrf1. RFP was used as the control. The complexes were immunoprecipitated (IPed) and analyzed by immunoblotting (IB). (C) The principle of the fluorescent-3-hybrid (F3H) assay. A GFP binder protein (GBP) is co-expressed with a protein (LacR) that accumulates at a well-defined location (*LacO* array) within the nucleus. The complex specifically recruits GFP-tagged protein (protein A). If RFP-labeled protein B interacts with protein A, it will also display an accumulation at the *LacO* region, which can be immediately visualized by fluorescent microscopy. (D) The interaction between Uhrf1 and Sirt1 was confirmed by the F3H assay. GFP was used as a negative control. Scale bar, 5 μm. (E) The interaction by F3H in part D was quantitated by ImageJ. By measuring the signal intensity (S) of each dot and the corresponding background (B), the relative binding intensity (V) was calculated with a formula: V= (S/B-1)*10. The average

binding intensity from 20 images was valued. The values represent mean ± SD and SEM. Data were analyzed by an unpaired Student's t-test and ANOVA test (*p<0.05, **p<0.01, ***p<0.001). (F) Schematic presentation of Uhrf1 truncations. (G) Schematic presentation of Sirt1 truncations. (H) Co-immunoprecipitation of RFP-Sirt1 with full-length Uhrf1 or various Uhrf1 truncations. GFP was used as a negative control. The complexes were IPed and analyzed by IB. (I) Co-immunoprecipitation of RFP-Sirt1 with full-length Uhrf1 or Uhrf1 lacking SRA domain (Uhrf1 deleted SRA). (J) Co-immunoprecipitation of RFP-Uhrf1 with full-length Sirt1 or various Sirt1 fragments. The complexes were IPed and analyzed by IB.

3.2.3 Uhrf1 is acetylated by Tip60 and deacetylated by Sirt1

Then we further explored the relationship between Sirt1 and Uhrf1. It has been previously proven that Uhrf1 recruits and binds the MYST domain of Tip60, while Tip60 acetylates and destabilizes Dnmt1 by triggering Uhrf1-mediated ubiquitination (Achour et al., 2009; Du et al., 2010). Consistently, our F3H assay showed that Uhrf1 interacted with Tip60 by recruiting Tip60 to the LacO site (**Figure 2.2A and 2.2B**). Tip60 protein contains several domains, including a chromodomain and MYST domain with acetylase activity (**Figure 2.2D**). Our co-immunoprecipitation assay also supported the SRA domain of Uhrf1 interacts with Tip60, suggesting that the SRA domain of Uhrf1 interacts with the MYST domain of Tip60 (**Figure 2.2C and 2.2E**). To figure out whether Tip60 interacts with Uhrf1 through acetylation, we performed *in vivo* and *in vitro* acetylation assays. We found that the acetylation of Uhrf1 was increased when Tip60 was overexpressed in cells (**Figure 2.2F**). *In vitro*, Uhrf1 was also acetylated by Tip60 in the presence of Ac-CoA (**Figure 2.2G**). Taken together, it was verified that, apart from Dnmt1, Uhrf1 was also a substrate of Tip60 in the macro-molecular complex of Uhrf1, Dnmt1, and Tip60.

As Sirt1 owns deacetylation activity, I hypothesized that Uhrf1 can be deacetylated by Sirt1. To verify it, I tried to evaluate the acetylation level of Uhrf1 in Sirt1-inhibited conditions. Nicotinamide (NAM) acts as an inhibitor of Sirtuin proteins. Treatment of HEK cells with NAM, I found that Uhrf1 acetylation level was increased in a dose-dependent manner (**Figure 2.2H**), indicating that Uhrf1 acetylation is regulated by Sirtuins. In the Sirt1 knockout embryonic stem (ES) cell lines, the acetylation level of

Uhrf1 was also increased when compared with normal E14 ES cells (**Figure 2.2I and 2.2J**). For *in vitro* deacetylation, GFP-Uhrf1, GFP-Sirt1, and its catalytic-inactive GFP-Sirt1 HA were separately overexpressed in HEK cells and purified with GFP-Trap beads. And then GFP-Uhrf1 was incubated with GFP-Sirt1 or its mutant GFP-Sirt1 HA in the presence of NAD^+. It was displayed that, GFP-Sirt1 deacetylated Uhrf1 efficiently in the presence of NAD^+. Deacetylation of Uhrf1 was inhibited by the catalytic mutation of Sirt1 (**Figure 2.2K**). Collectively, these results convincingly showed that Uhrf1 was a substrate of Sirt1. To identify the acetylation lysine of Uhrf1, we overexpressed GFP-Uhrf1 in HEK cells and treated the cells with aphidicolin. Aphidicolin (APH) is a specific inhibitor of DNA polymerase used for blocking the cell cycle at the G1 phase, but I found that Uhrf1 acetylation was increased by aphidicolin (**Figure 2.2L and 2.2M**) (Haraguchi et al., 1983). Immunopurified GFP-Uhrf1 was run by SDS-PAGE and analyzed by mass spectrometry. 6 acetylated lysine sites were detected (**Figure 2.2N**), and 5 of these lysine sites are consistent with the previously identified acetylated lysine sites. Two highly conserved acetylation sites (K644 and K664) identified in the region around the SRA domain of Uhrf1 may have a regulatory function and thus were studied further (**Figure 2.2O and 2.2P**).

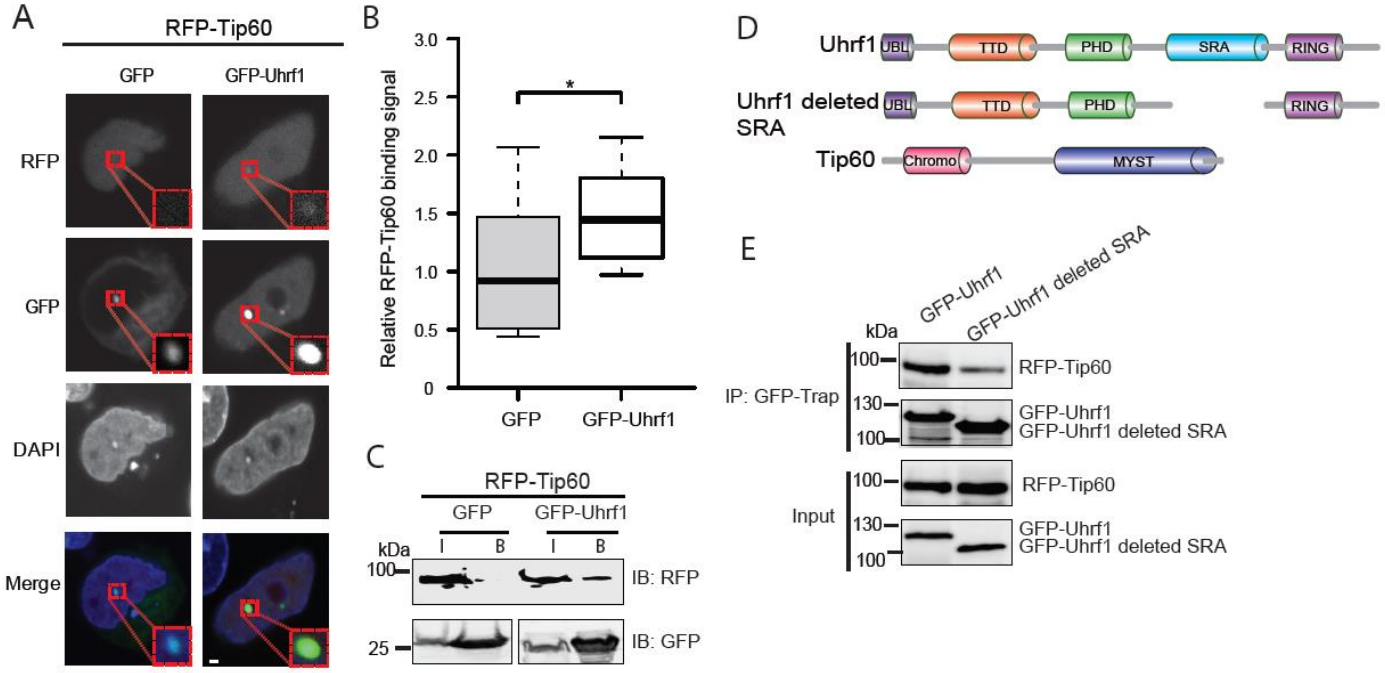

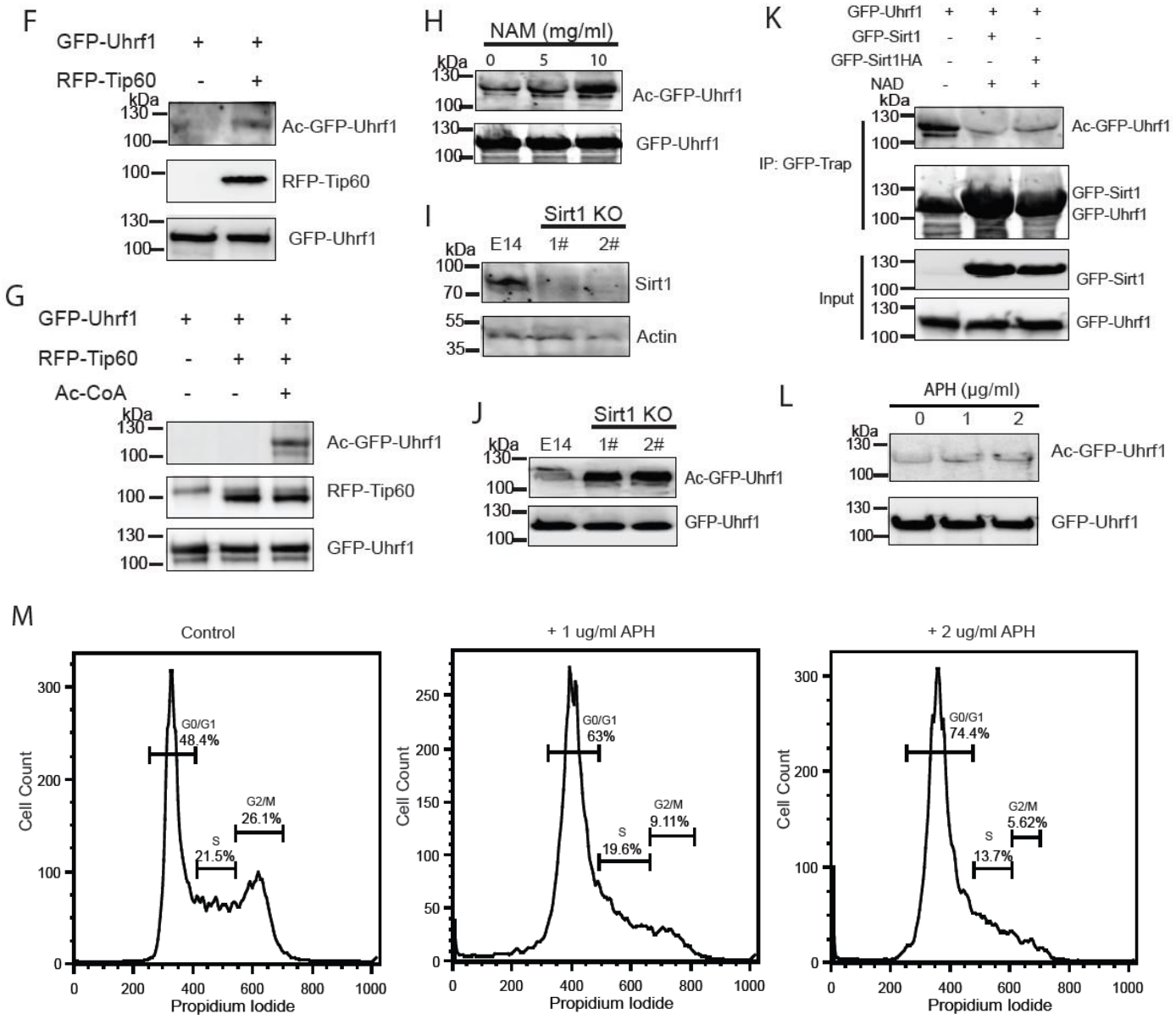
F
GFP-Uhrf1 + +
RFP-Tip60 - +
kDa
130
100
Ac-GFP-Uhrf1
100
RFP-Tip60
130
100
GFP-Uhrf1
H
NAM (mg/ml)
kDa 0 5 10
130
100
Ac-GFP-Uhrf1
130
100
GFP-Uhrf1
K
GFP-Uhrf1 + + +
GFP-Sirt1 - + -
GFP-Sirt1HA - - +
NAD - + +
kDa
130
100
Ac-GFP-Uhrf1
IP: GFP-Trap
130
100
GFP-Sirt1
GFP-Uhrf1
Input
130
100
GFP-Sirt1
130
100
GFP-Uhrf1
I
Sirt1 KO
kDa E14 1# 2#
100
70
Sirt1
55
35
Actin
G
GFP-Uhrf1 + + +
RFP-Tip60 - + +
Ac-CoA - - +
kDa
130
100
Ac-GFP-Uhrf1
100
RFP-Tip60
130
100
GFP-Uhrf1
J
Sirt1 KO
kDa E14 1# 2#
130
100
Ac-GFP-Uhrf1
130
100
GFP-Uhrf1
L
APH (μg/ml)
0 1 2
kDa
130
100
Ac-GFP-Uhrf1
130
100
GFP-Uhrf1
M
Control
+ 1 ug/ml APH
+ 2 ug/ml APH
Cell Count
Propidium Iodide
G0/G1
48.4%
S
21.5%
G2/M
26.1%
G0/G1
63%
S
19.6%
G2/M
9.11%
G0/G1
74.4%
S
13.7%
G2/M
5.62%

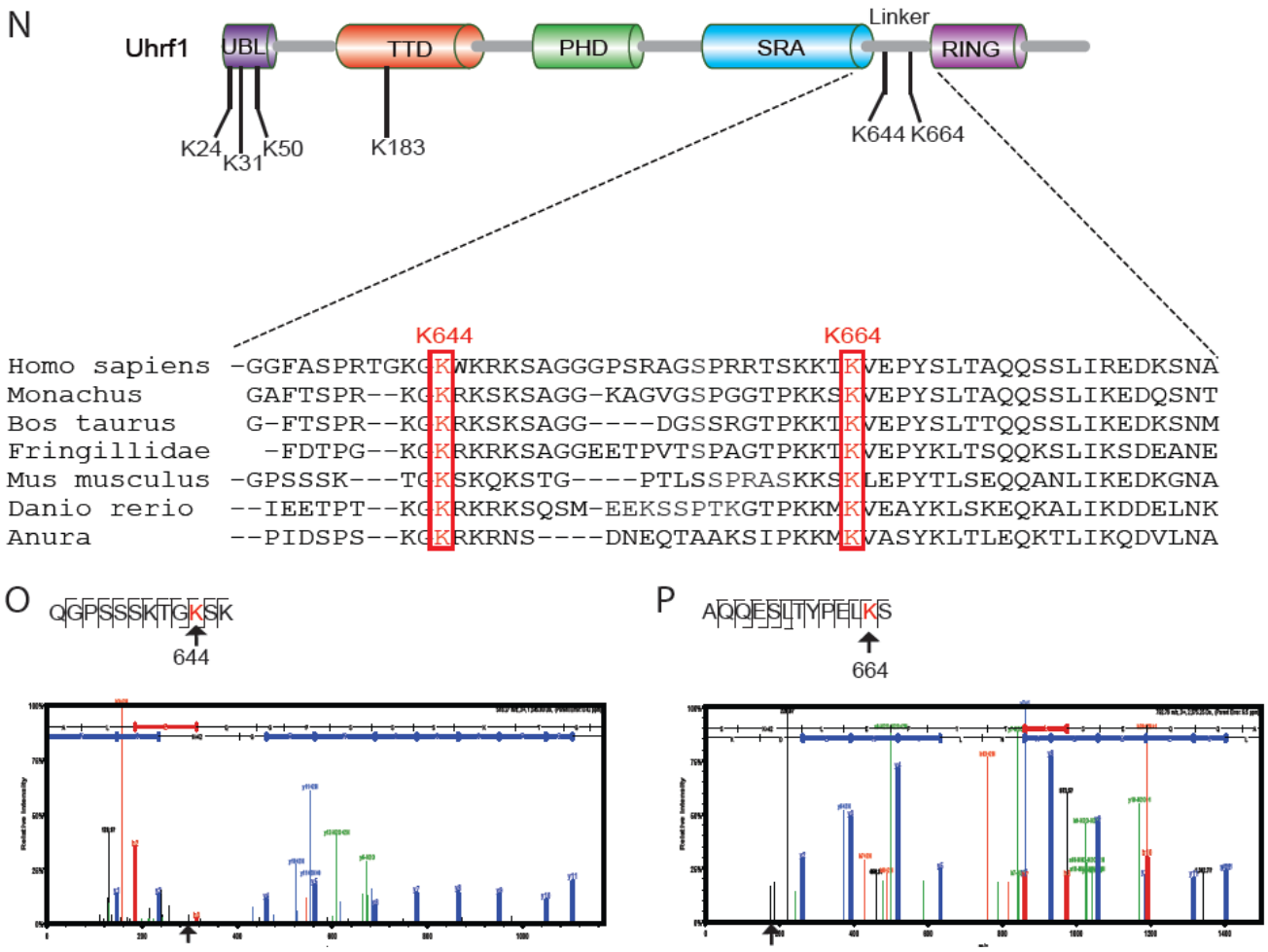

Figure 2.2 Uhrf1 was acetylated by Tip60 and deacetylated by Sirt1. (A) The interaction between Uhrf1 and Tip60 was confirmed by the F3H assay. GFP was used as a negative control for RFP-Tip60 binding. Scale bar, 5 μm. (B) The interaction of F3H in figure A was quantitated by ImageJ. The relative binding intensity was calculated with the same method as above for the interaction of GFP-Sirt1 and RFP-Uhrf1. The values represent mean ± SD and SEM (n=13). Data were analyzed by an unpaired Student's t-test and ANOVA test (*p<0.05, **p<0.01, ***p<0.001). (C) Co-immunoprecipitation of RFP-Tip60 with GFP or GFP-Uhrf1. HEK cells were co-transfected with plasmids of pCAG-RFP-Tip60 and pCAG-GFP-IB or pCAG-GFP-NP95-IB. GFP was used as the control. The complexes were immunoprecipitated (IPed) and analyzed by immunoblotting (IB). (D) Schematic presentation of Uhrf1, Uhrf1 deleted SRA domain and Tip60. (E) Co-immunoprecipitation of RFP-Tip60 with full-length Uhrf1 or Uhrf1 deleted SRA. The complexes were IPed and analyzed by IB. (F) *In vivo* acetylation assay. HEK cells were transfected with plasmids of pCAG-GFP-NP95-IB and pCAG-RFP-Tip60. The acetylation level

of Uhrf1 was measured by immunoprecipitation and immunoblotting (IB) with an anti-acetyl antibody. The cells only transfected GFP-Uhrf1 was used as a negative control. (G) In vitro acetylation assay. GFP-Uhrf1 and RFP-Tip60 were separately purified and then incubated in HAT buffer (50 mM Tris, pH 8.0, 1 mM EDTA, 1 mM dithiothreitol, and 10% glycerol) in the presence of acyl-CoA at 30°C for 2 hours. The complexes were IPed and analyzed by IB. (H) HEK cells were transfected with the plasmid of pCAG-GFP-NP95-IB and treated with 5 and 10 mg/ml nicotinamide (NAM). GFP-Uhrf1 was IPed and analyzed by IB. (I) Western blot for endogenous Sirt1 in Sirt1 knockout (Sirt1 KO) embryonic stem cell lines. (J) Acetylation level of Uhrf1in Sirt1 KO embryonic stem cell lines. GFP-Uhrf1 was overexpressed in cells and purified with GFP-Trap beads. E14 ES cells were used as negative control. The acetylation level of Uhrf1 was detected with an anti-acetyl-lysine antibody. (K) *In Vitro* deacetylation assay. HEK cells were transfected with the plasmid, pCAG-GFP-NP95-IB, and treated with 2 μg/ml APH for 12 hours. Then GFP-Uhrf1 was purified by GFP-Trap beads and incubated with GFP-Sirt1 or GFP-Sirt1 HA in addition to 10mM NAD^+. The reaction was performed and analyzed by western blot. (L) HEK cell overexpressing GFP-Uhrf1 was treated with or without 2 μg/ml aphidicolin (APH) overnight. The GFP-Uhrf1 was immunoprecipitated and acetylation level of Uhrf1 was detected with an anti-acetyl-lysine antibody. (M) Cell cycle analysis using propidium iodide (PI) staining and flow cytometry. HEK cells were transfected with the plasmid pCAG-GFP-NP95-IB for 24 hours and treated with APH for 12 hours. The percentages of different phages were analyzed by FlowJo. (N) The acetylation sites of GFP-Uhrf1 were analyzed by mass spectrometry. The acetylated GFP-Uhrf1 was enriched by overexpressing GFP-Uhrf1 in HEK cells with 2 μg/ml aphidicolin. In this part, I prepared samples and Dr. Ignasi Forné performed mass spectrometry and analyzed the results. 6 acetylated lysines were identified and labeled on the structure domain of Uhrf1. The residues K644 and K664 were shown highly conserved by protein sequence alignment in different species and labeled in red. The peptides fragments used to calculate the mass of residues 644 and 664 were highlighted by bold arrowheads (O and P).

3.2.4 Uhrf1 acetylation enhances the interaction with Dnmt1 and the binding to heterochromatin while disturbing the interaction with Usp7.

Uhrf1 has been shown to stimulate and recruit Dnmt1 by its SET and RING-associated domain to hemimethylated DNA for maintaining DNA methylation (Berkyurek et al.,

2013). To identify whether acetylation of Uhrf1 influences its interaction with Dnmt1, we used aphidicolin (APH) to determine it because aphidicolin has been shown to promote the acetylation of Uhrf1. Our results of co-immunoprecipitation showed that more Uhrf1 bound Dnmt1 when the acetylation of Uhrf1 was increased (**Figure 2.3A**). This interaction was also validated with nicotinamide (NAM), as an inhibitor of Sirtuin proteins (**Figure 2.3B**). Aphidicolin-driven acetylation and nicotinamide-inhibited deacetylation collectively explained that Uhrf1 acetylation enhanced its binding to Dnmt1. In addition, when two acetylated sites of Uhrf1, K644, and K664, were mutated to arginine (R), the binding of Dnmt1 was slightly decreased (**Figure 2.3C**).

It is clear that Uhrf1 is able to associate with pericentric heterochromatin and recruits Dnmt1 by binding either H3K9me2/3 or hemimethylated CpG sites (Liu et al., 2013). Given that H3K9me3 has been considered as the marker of heterochromatin, I tried to test the binding intensity of Uhrf1 and its mutation to heterochromatin *in vivo* and *in vitro*. *In vivo*, Uhrf1 was efficiently bound to heterochromatin and present some bright spot area, compared to those of Uhrf1 deleted SRA and K644RK664R (2KR), suggesting that the SRA domain of Uhrf1 was mainly responsible for its binding to heterochromatin, and especially, two sites for acetylation on SRA domain, K644, and K664, were crucial for its heterochromatin binding (**Figure 2.3D and 2.3E**). *In vitro*, cell nuclei were extracted and incubated with GFP-Uhrf1, or GFP-Uhrf1 deleted SRA, or GFP-Uhrf1 K644RK664R (2KR). After incubation, the level of H3K9me3 was tested by western blot. Thus, our result confirmed it again that Uhrf1 acetylation on its SRA domain influenced its binding to heterochromatin *in vitro* (**Figure 2.3F**).

To further determine the acetylation of Uhrf1 promotes its binding to heterochromatin, I used aphidicolin to test it. By treating cells with aphidicolin *in vivo*, more H3K9me3 was accumulated than that without aphidicolin, hinting that Uhrf1 acetylation promoted its binding to heterochromatin (**Figure 2.3G**). Furthermore, I also identified the binding assay *in vitro*. Briefly, I isolated nuclei and incubated with purified acetylated GFP-Uhrf1 and GFP-Uhrf1 deleted SRA. Then the reaction mixtures were assessed by western blot with an anti-H3K9me3 antibody. It was concluded that acetylation of Uhrf1 enhanced its association with heterochromatin, but deletion of the SRA domain has eliminated its binding to heterochromatin *in vitro* (**Figure 2.3H**).

While it has been clearly illustrated how the deubiquitinase Usp7 structurally interacts with Uhrf1 and regulates its chromatin association, the relationship between acetylation on the SRA domain of Uhrf1 and Usp7 is still one of the open questions. Firstly, I used the F3H method to verify the interaction of Uhrf1 and Usp7. We noted that there was not a strong interaction of Usp7 and Uhrf1 maybe because of the binding site on LacO sequence, not binding in heterochromatin (**Figure 2.3I and 2.3J**). By my co-immunoprecipitation assay, I found that, when acetylation of Uhrf1 was increased by aphidicolin, its interaction with Usp7 was weakened (**Figure 2.3K**), suggesting that Usp7 disturbed Uhrf1 acetylation. In addition, I also observed that, when the catalytic activity of Sirt1 was inhibited by nicotinamide, there were less Sirt1 proteins binding to Uhrf1 (**Figure 2.3L**). When cells were treated with aphidicolin for Uhrf1 acetylation, the interaction between Sirt1 and Uhrf1was enhanced (**Figure 2.3M**).

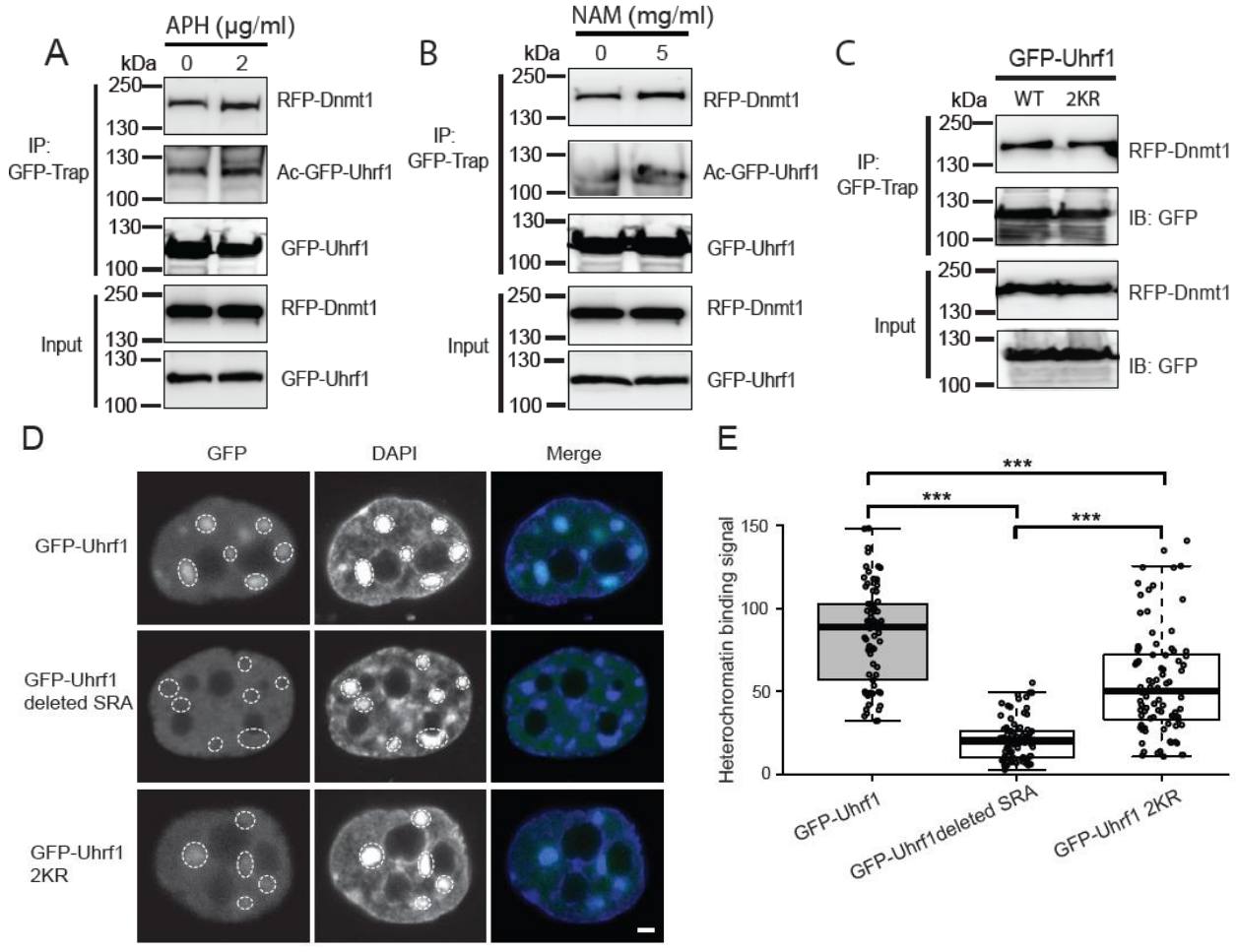

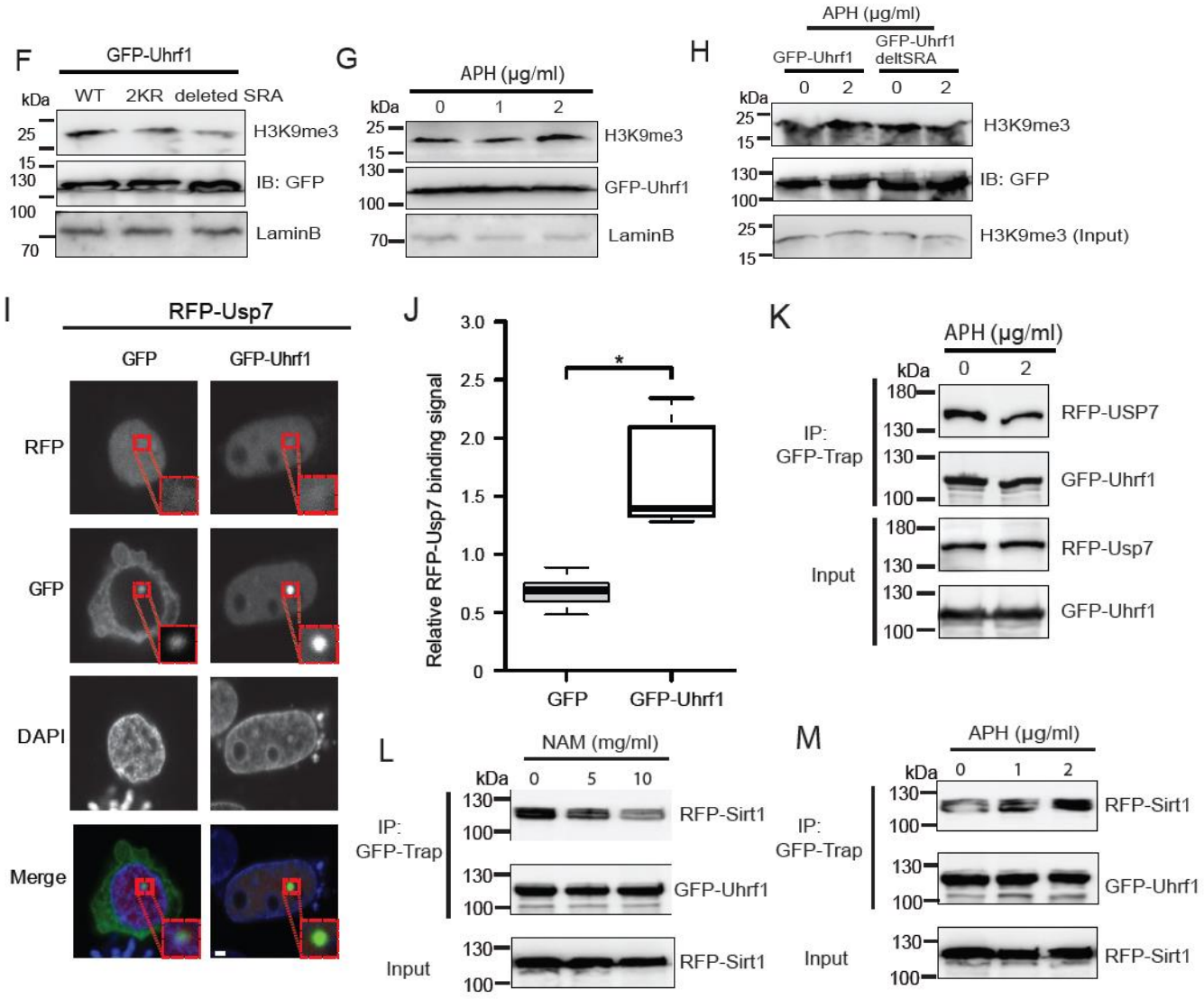

Figure 2.3. Acetylation of Uhrf1 enhances Dnmt1 and heterochromatin binding while disturbing its interaction with Usp7. (A) HEK cells were co-transfected with two plasmids of pCAG-GFP-NP95-IB (GFP-Uhrf1) and pCAG-RFP-Dnmt1 and treated with APH or NAM (B) for 12 hours. The complexes were IPed and analyzed by IB. (C) HEK cells were transfected with the plasmid pCAG-RFP-Dnmt1 with pCAG-GFP-NP95-IB or pCAG-GFP-Uhrf1 K644RK664R (2KR). The complexes were IPed and analyzed by IB. (D) The binding of GFP-Uhrf1, GFP-Uhrf1 deleted SRA, and 2KR to heterochromatin. C2C12 cells were separately transfected with plasmids of pCAG-GFP-NP95-IB, pCAG-GFP-Uhrf1 deleted SRA, and pCAG-GFP-Uhrf1 K644RK664R (2KR), and imaged by microscope. DAPI was used for staining chromatin and DAPI-dense dots were labeled to represent clusters of pericentric chromatin. Scale bar, 5 μm. (E) The heterochromatin binding signals in figure D were valued by ImageJ. By measuring the

signal intensity (S) of each dot and the corresponding background (B), the relative binding intensity (V) was calculated with a formula: V= (S/B-1)*10. the number of dots I counted for imaging was 77 in GFP-Uhrf1, 85 in GFP-Uhrf1 deleted SRA and 87 in GFP-Uhrf1 2KR. The values represent mean ± SD and SEM. Data were analyzed by an unpaired Student's t-test and ANOVA test (*p<0.05, **p<0.01, ***p<0.001). (F) HEK cells were transfected with plasmids of pCAG-GFP-NP95-IB, pCAG-GFP-Uhrf1 deleted SRA, and pCAG-GFP-Uhrf1 K644RK664R (2KR, the levels of H3K9me3 were analyzed by IB. Lamin B was used as control. (G) GFP-Uhrf1 were overexpressed in HEK cells and treated with APH for 12 hours. The equal amount of GFP-tagged proteins was analyzed and the heterochromatin marker Histone 3 lysine 9 tri-methylated (H3K9me3) was blotted and Lamin B as the control. (H) *In Vitro* heterochromatin binding assay. HEK cells were transfected with plasmids of GFP-NP95-IB and pCAG-GFP-Uhrf1 deleted SRA and treated with APH for 12 hours. The equal amount of GFP-Uhrf1 and GFP-Uhrf1 deleted SRA were incubated with the same amount of prepared chromatin extracted from HEK cells and analyzed the heterochromatin marker Histone 3 lysine 9 tri-methylated (H3K9me3). Lamin B was used as a control. (I) The interaction between Uhrf1 and Usp7 was confirmed by the F3H assay. GFP was used as a negative control for RFP-Usp7 binding. Scale bar, 5 μm. (J) The interaction of F3H assay in figure H was qualified by ImageJ. The binding signal intensity was calculated similarly to the interaction for Sirt1 and Uhrf1. The values represent mean ± SD and SEM (n=11). Data were analyzed by an unpaired Student's t-test and ANOVA test (*p<0.05, **p<0.01, ***p<0.001). (K) HEK cells were co-transfected with plasmids of pCAG-GFP-NP95-IB and pCAG- RFP-Usp7 and treated with APH for 12 hours. The complexes were IPed and analyzed by IB. (L) HEK cells were co-transfected with plasmids of pCAG-GFP-NP95-IB and pCAG-RFP-Sirt1 and treated with APH or NAM (M) for 12 hours. The complexes were IPed and analyzed by IB.

3.2.5 Uhrf1 stability is regulated by acetylation and deacetylation.

We also wanted to know whether the acetylation level of Uhrf1 could as well modulate the protein stability of Uhrf1, we measured the mRNA level of Uhrf1 in Sirt1 knockout (Sirt1 KO) embryonic cells and we found that without Sirt1, the expression level of Uhrf1 was increased (**Figure 2.4A**). To specifically figure out how acetylation regulated Uhrf1 stability, we overexpressed GFP-Uhrf1 and His-Ubi with or without aphidicolin (APH) and nicotinamide (NAM) and evaluated the ubiquitination level of GFP-Uhrf1 by western

blot. The ubiquitination level of GFP-Uhrf1 was increased after adding APH or NAM, suggesting that acetylation of Uhrf1 promotes its proteasomal degradation, while deacetylation of Uhrf1 by Sirt1 protects it from degradation (**Figure 2.4B, 2.4C, and 2.4D**). Furthermore, we confirmed that the deletion of ubiquitin-like (UBL) domain of Uhrf1 did not affect its degradation, suggesting that the specific lysine sites in UBL domain of Uhrf1, previously identified 4 sites, have nearly no effect on Uhrf1 stability (**Figure 2.4E and 2.4F**), but the deletion of the SRA domain of Uhrf1 dramatically inhibited degradation of Uhrf1 in the presence of APH or NAM (**Figure 2.4G and 2.4H**). Moreover, I found by western blot that the two acetylated sites, K644 and K664, were important for stabilizing Uhrf1 and inhibiting its degradation (**Figure 2.4I and 2.4J**). Also, APH treatment, which increased the acetylation level of Uhrf1, significantly decreased GFP-Uhrf1 half-life (**Figure 2.4K**). In contrast, the deletion of the SRA domain did not affect Uhrf1 half-life and the 2KR mutant was starkly more stable than wild-type Uhrf1 (**Figure 2.4L and 2.4M**). Moreover, when cells were treated with APH and NAM, the protein half-life of GFP-Uhrf1, deleted SRA, and 2KR was dramatically different. The protein of GFP-Uhrf1 deleted SRA was the most stable and GFP-Uhrf12KR was less stable (**Figure 2.4N and 2.4O**). Given that Usp7 stabilizes Dnmt1 and Uhrf1 at chromatin sites, we also overpressed GFP-Uhrf1, RFP-Usp7, and His-ubiquitin in HEK cells and explored the possibility that Usp7 can protect Uhrf1 from degradation (**Figure 2.4P**). Intriguingly, the acetylation of Uhrf1 promoted by APH still triggered Uhrf1 degradation in the presence of Usp7 (**Figure 2.4Q**).

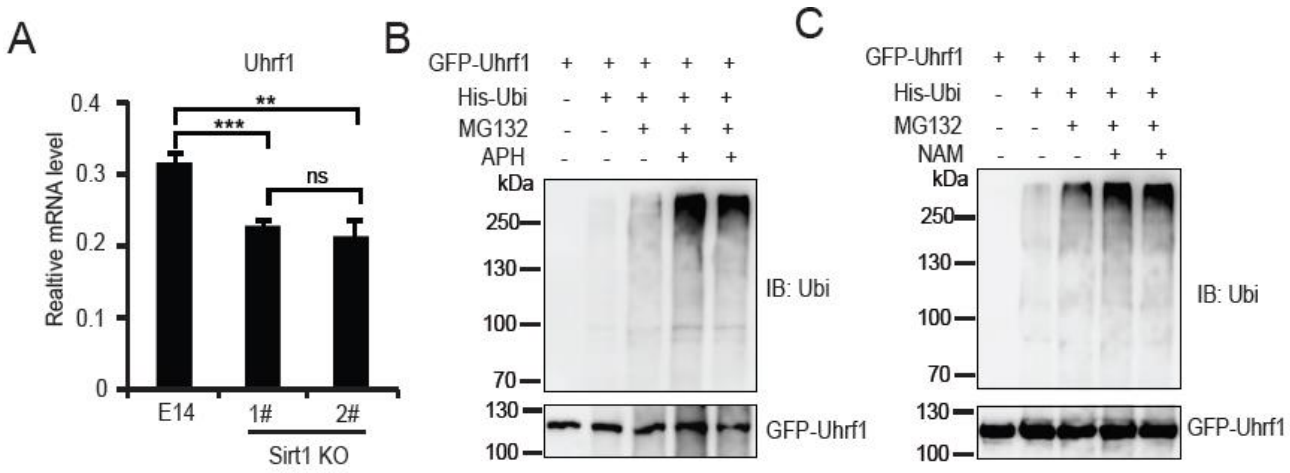

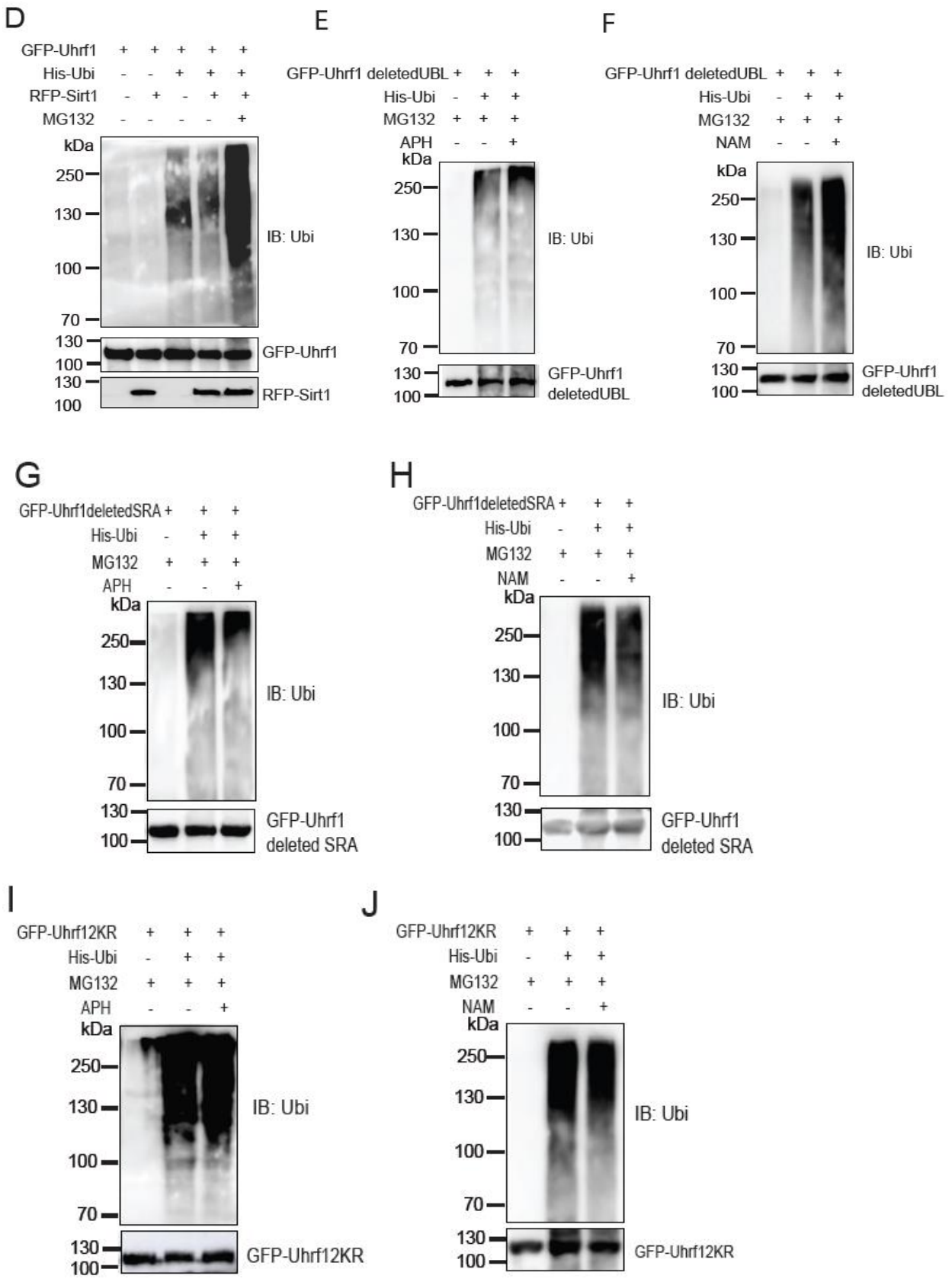
D
GFP-Uhrf1 + + + + +
His-Ubi - - + + +
RFP-Sirt1 - + - + +
MG132 - - - - +
kDa
250
130
100
70
IB: Ubi
130
100
GFP-Uhrf1
130
100
RFP-Sirt1
E
GFP-Uhrf1 deletedUBL + + +
His-Ubi - + +
MG132 + + +
APH - - +
kDa
250
130
100
70
IB: Ubi
130
100
GFP-Uhrf1
deletedUBL
F
GFP-Uhrf1 deletedUBL + + +
His-Ubi - + +
MG132 + + +
NAM - - +
kDa
250
130
100
70
IB: Ubi
130
100
GFP-Uhrf1
deletedUBL
G
GFP-Uhrf1deletedSRA + + +
His-Ubi - + +
MG132 + + +
APH - - +
kDa
250
130
100
70
IB: Ubi
130
100
GFP-Uhrf1
deleted SRA
H
GFP-Uhrf1deletedSRA + + +
His-Ubi - + +
MG132 + + +
NAM - - +
kDa
250
130
100
70
IB: Ubi
130
100
GFP-Uhrf1
deleted SRA
I
GFP-Uhrf12KR + + +
His-Ubi - + +
MG132 + + +
APH - - +
kDa
250
130
100
70
IB: Ubi
130
100
GFP-Uhrf12KR
J
GFP-Uhrf12KR + + +
His-Ubi - + +
MG132 + + +
NAM - - +
kDa
250
130
100
70
IB: Ubi
130
100
GFP-Uhrf12KR

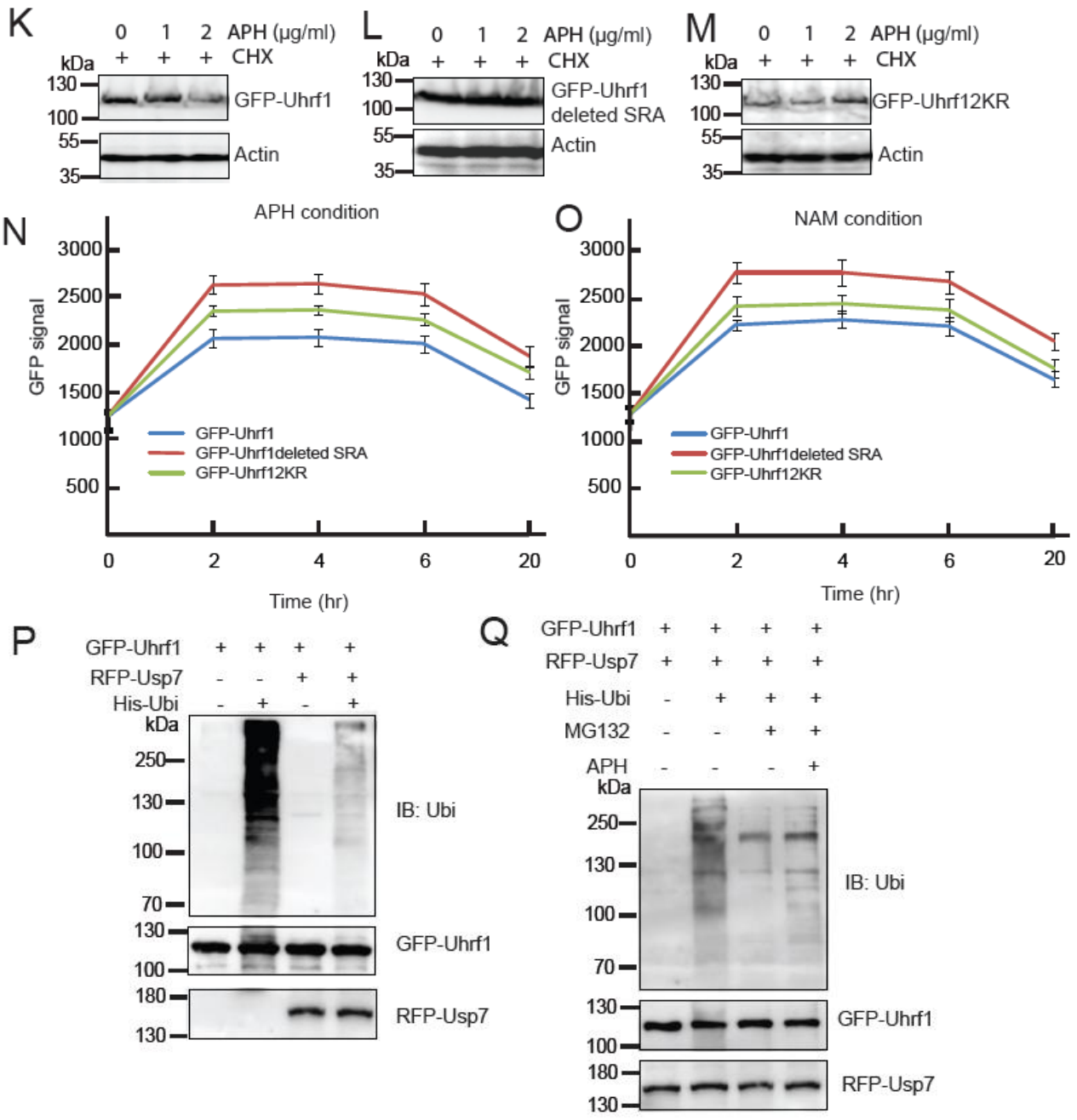

Figure 2.4. Uhrf1 stability is regulated by acetylation and deacetylation. (A) The expression level of Uhrf1 in Sirt1 knockout (KO) cell lines with RT-qPCR. The values represent mean ± SD and SEM, and data were analyzed by an unpaired Student's t-test and ANOVA test (*p<0.05, **p<0.01, ***p<0.001). (B) HEK cells were transfected with the plasmid of pCAG-GFP-NP95-IB, with or without His-Ubi for 12 hours, treated with MG132 and APH or NAM (C) for 12 hours. The cell lysates were analyzed by IB. (D) HEK cells were transfected with the plasmids of pCAG-

GFP-NP95-IB and pCAG-RFP-Sirt1, and treated with MG132 for 12 hours. The cell lysates were analyzed by IB. (E) HEK cells were transfected with the plasmid of pCAG-GFP-Uhrf1 deleted UBL, with or without His-Ubi for 12 hours, treated with MG132 and APH or NAM (F) for 12 hours. The cell lysates were analyzed by IB. (G) HEK cells were transfected with plasmids of pCAG-GFP-Uhrf1 deleted SRA (H) or pCAG-GFP-Uhrf1 K644RK664R (2KR) (I and J), treated with MG132 and NAM for 12 hours. The cell lysates were analyzed by IB. (K) HEK cells were transfected with plasmids of pCAG-GFP-NP95-IB, pCAG-GFP-Uhrf1 deleted SRA (L) or pCAG-GFP-Uhrf1 K644RK664R (2KR) (M) for 24 hours, incubated with cycloheximide (CHX) and treated with APH or NAM for 12 hours. The cell lysates were analyzed by IB. (N) HEK cells were transfected with plasmids of pCAG-GFP-NP95-IB, pCAG-GFP-Uhrf1 deleted SRA and pCAG-GFP-Uhrf1 K644RK664R (2KR), and treated with APH and CHX or NAM and CHX (O), cells were measured the GFP signal at indicated time and the signals were represented protein levels and analyzed with mean ± SD. (P) HEK cells were transfected with plasmids of pCAG-GFP-NP95-IB, His-Ubi, and pCAG-RFP-Usp7 for 12 hours, treated with or without MG132 for 12 hours. The cell lysates were analyzed by IB. (Q) HEK cells were transfected with plasmids of pCAG-GFP-NP95-IB, His-Ubi, and pCAG-RFP-Usp7 for 12 hours, treated with or without MG132 and APH for 12 hours. The cell lysates were analyzed by IB.

3.2.6 Uhrf1 acetylation in the G1 phase and deacetylation in the early S phase in the cell cycle

Although we have shown that Uhrf1 was acetylated by APH when cells were blocked at G1 phase in the cell cycle, we also used PCNA as a marker of the cell cycle to analyze Sirt1 localization in the cell cycle. Our immunofluorescence assay showed that Sirt1 interacted with Uhrf1 at the early S phase (**Figure 2.5A and 2.5B**), suggesting that deacetylation of Uhrf1 occurred in the early S phase. To analyze the distribution of acetylated Uhrf1 in the cell cycle, we used propidium iodide (PI) staining to assess DNA content of APH treated cells (**Figure S1C**), and our result indicated that acetylation of Uhrf1 by Tip60 happened at G1 phase. Furthermore, it has been reported that Sirt1 overexpression induced the cell cycle arrest at G1/S transition *in vitro*, whereas RNAi-mediated knockdown of Sirt1 resulted in the opposite effect (Li L, 2011). Here, Sirt1 inhibition by NAM, arrested cells at G1 and G2/M phases and fewer cells were at S

phase (**Figure 2.5C**). In Sirt1 knockout cells, more cells were arrested at the G2/M phase (**Figure 2.5D**). Altogether we concluded that Sirt1-mediated deacetylation regulates the stability of Uhrf1 at the early S phase.

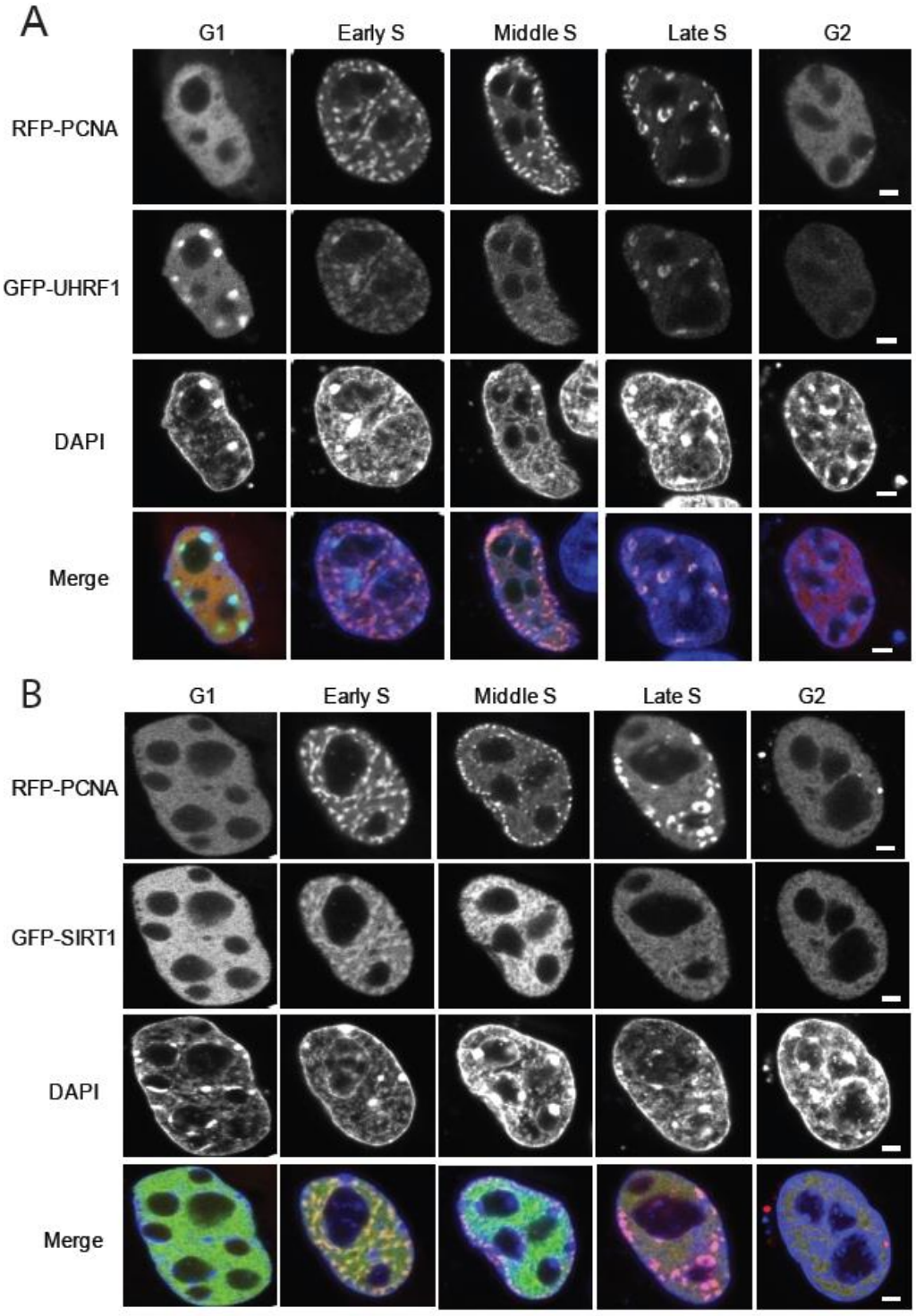

C

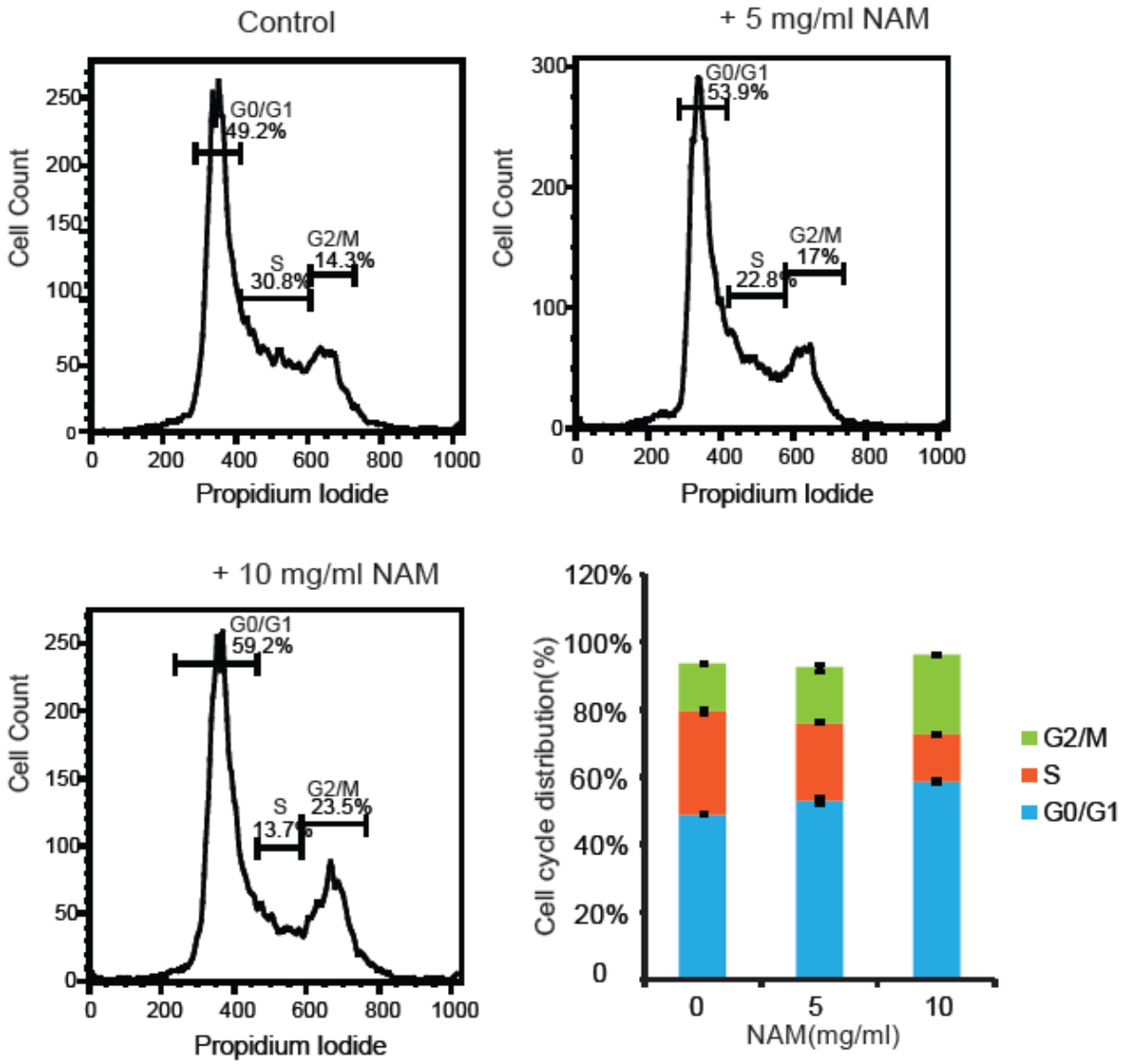
Control
+ 5 mg/ml NAM
+ 10 mg/ml NAM
Cell Count
Propidium Iodide
G0/G1
49.2%
S
30.8%
G2/M
14.3%
G0/G1
53.9%
S
22.8%
G2/M
17%
G0/G1
59.2%
S
13.7%
G2/M
23.5%
Cell cycle distribution(%)
NAM(mg/ml)
G2/M
S
G0/G1

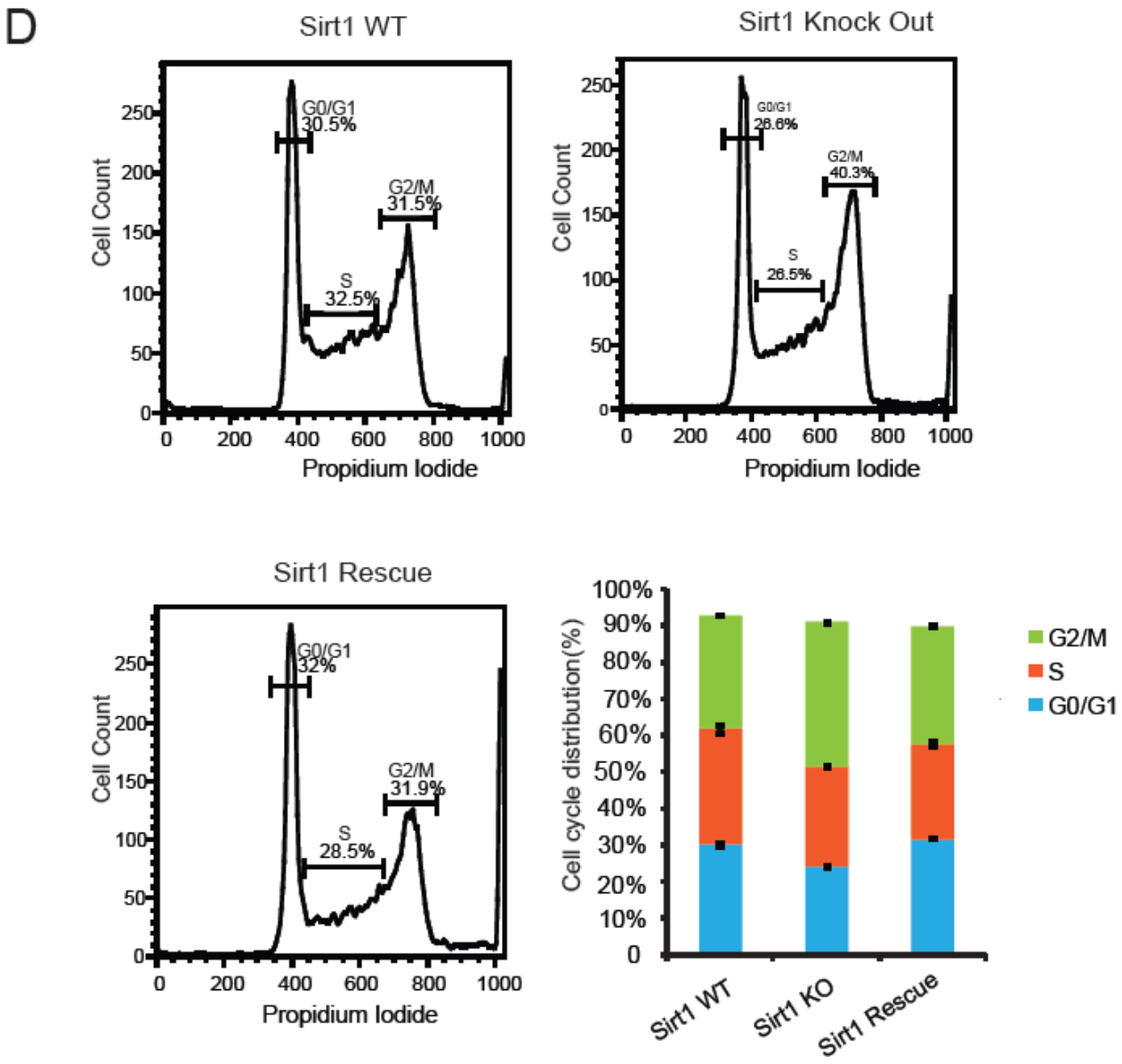

Figure 2.5. Uhrf1 acetylation in the G1 phase and deacetylation in the early S phase in the cell cycle. (A) RFP-PCNA displays cell cycle-dependent punctuate patterns in C2C12 cell lines. GFP-Uhrf1 (A) or GFP-Sirt1 (B) was co-transfected with RFP-PCNA in C2C12 cells and separately displayed their distribution in G1, early S, middle S, late S and G2 phases in cell cycle with confocal. DAPI was used for chromatin counterstaining. Scale bar, 10 μm. (C) Cell cycle analysis of HEK cells using propidium iodide (PI) staining and flow cytometry. HEK cells were treated with nicotinamide for 12 hours and stained with PI for cell cycle analysis. The percentages of different phases were measured by the software FlowJo. The values represent mean ± SD. (D) Cell cycle analysis of Sirt1 wild type, Knockout, and Rescue cell lines with PI

staining. The percentage of different phases was measured by the software FlowJo. The values represent mean ± SD.

3.2.7 Sirt1 mediated deacetylation drives Cdk2 to phosphorylate Uhrf1 in the transition from G1 to S phase of cell cycle.

To explore how Sirt1 regulated Uhrf1 in the cell cycle, we overexpressed GFP-Sirt1 and GFP-Uhrf1, and found that the cell cycle was arrested at G1 phase, which was consistent with the result for GFP-Sirt1 catalytic domain and GFP-Uhrf1 (**Figure 2.6A**). To explore how Sirt1 dynamically regulated Uhrf1 in the early S phase of the cell cycle, we further studied cell cycle related genes, such as Cdk1, E2f1, cyclin E and Cdk2. There was no dramatic change on their mRNA levels in the cell lines in different cell lines, including Sirt1 knockout, cell lines with overexpression of GFP-Uhrf1, GFP-Sirt1, and GFP-Uhrf1-SRA deletion, indicating that these cell cycle-related proteins genetically acted as upstream factors to regulate Sirt1 and Uhrf1 to some extent (**Figure 2.6B**). Meanwhile, previous reports have shown that Cdk2 and Cdk1 play a role in different checkpoints in the cell cycle by phosphorylating Uhrf1 at different serine sites. Furthermore, it has been demonstrated that Cdk2 can directly interact with PCNA and both of them were involved in the S phase (Koundrioukoff et al., 2000). More specially, I found that Cdk2 co-localized with PCNA in the early S phase (**Figure 2.7A**). And only the site S657 of Uhrf1 was reported to be phosphorylated by Cdk2, which is in the interface of Uhrf1 interacting with Sirt1 (**Figure 2.7B**). Our results showed that double mutation of lysine sites in Uhrf1 (K644R and K664R) weakened the interaction of Sirt1 and Uhrf1, which promoted the S phase to G2/M phase transition of the cell cycle with Cdk2 (**Figure 2.7C**), suggesting that overexpression of Sirt1 occupied the region of the SRA domain and the linker in Uhrf1 and blocked Cdk2 to phosphorylate Uhrf1, which resulted in G1/S arrest in the cell cycle. Taken together, it can be concluded that Sirt1-mediated deacetylation stabilizes Uhrf1 and promotes it phosphorylated by Cdk2 and then pushes cells into S phase.

A

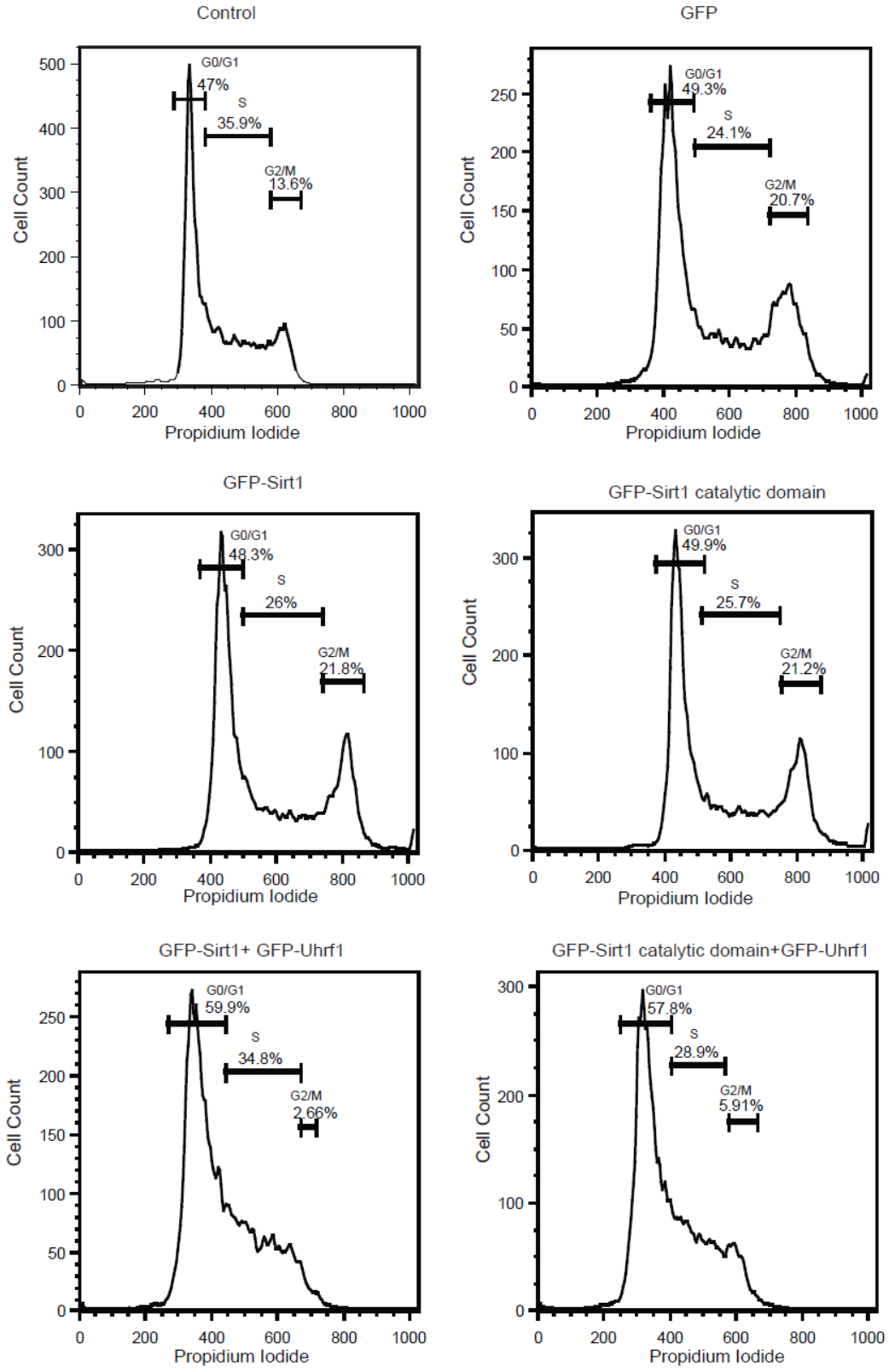
Control
G0/G1
47%
S
35.9%
G2/M
13.6%
Cell Count
Propidium Iodide
GFP
G0/G1
49.3%
S
24.1%
G2/M
20.7%
Cell Count
Propidium Iodide
GFP-Sirt1
G0/G1
48.3%
S
26%
G2/M
21.8%
Cell Count
Propidium Iodide
GFP-Sirt1 catalytic domain
G0/G1
49.9%
S
25.7%
G2/M
21.2%
Cell Count
Propidium Iodide
GFP-Sirt1+ GFP-Uhrf1
G0/G1
59.9%
S
34.8%
G2/M
2.66%
Cell Count
Propidium Iodide
GFP-Sirt1 catalytic domain+GFP-Uhrf1
G0/G1
57.8%
S
28.9%
G2/M
5.91%
Cell Count
Propidium Iodide

B

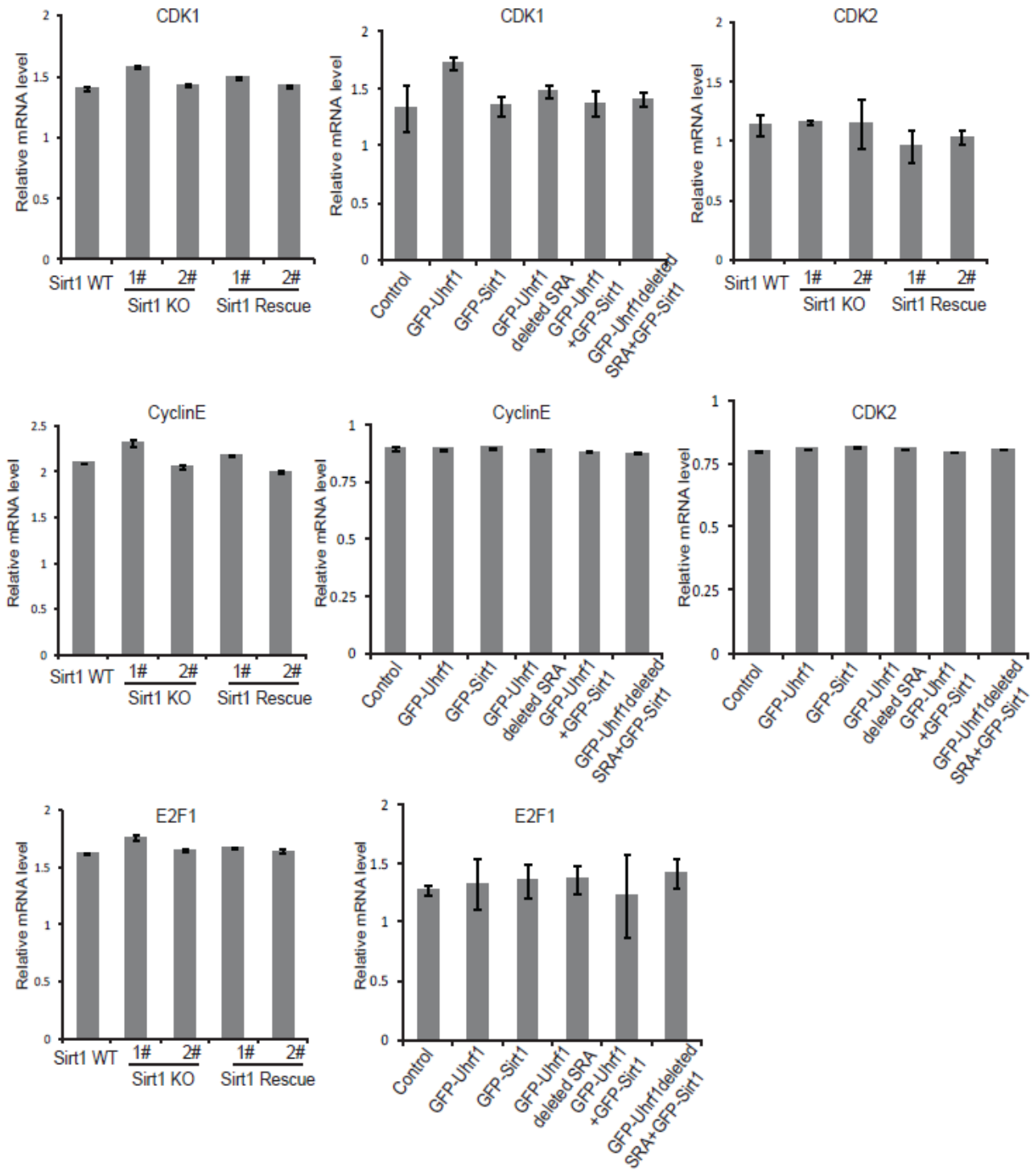
CDK1
Relative mRNA level
Sirt1 WT
1#
2#
1#
2#
Sirt1 KO
Sirt1 Rescue
CDK1
Relative mRNA level
Control
GFP-Uhrf1
GFP-Sirt1
GFP-Uhrf1 deleted SRA
GFP-Uhrf1 +GFP-Sirt1
GFP-Uhrf1deleted SRA+GFP-Sirt1
CDK2
Relative mRNA level
Sirt1 WT
1#
2#
1#
2#
Sirt1 KO
Sirt1 Rescue
CyclinE
Relative mRNA level
Sirt1 WT
1#
2#
1#
2#
Sirt1 KO
Sirt1 Rescue
CyclinE
Relative mRNA level
Control
GFP-Uhrf1
GFP-Sirt1
GFP-Uhrf1 deleted SRA
GFP-Uhrf1 +GFP-Sirt1
GFP-Uhrf1deleted SRA+GFP-Sirt1
CDK2
Relative mRNA level
Control
GFP-Uhrf1
GFP-Sirt1
GFP-Uhrf1 deleted SRA
GFP-Uhrf1 +GFP-Sirt1
GFP-Uhrf1deleted SRA+GFP-Sirt1
E2F1
Relative mRNA level
Sirt1 WT
1#
2#
1#
2#
Sirt1 KO
Sirt1 Rescue
E2F1
Relative mRNA level
Control
GFP-Uhrf1
GFP-Sirt1
GFP-Uhrf1 deleted SRA
GFP-Uhrf1 +GFP-Sirt1
GFP-Uhrf1deleted SRA+GFP-Sirt1

Figure 2.6 Sirt1 mediated deacetylation of Uhrf1 in the transition from G1 to S phase of cell cycle, which was regulated by the cell cycle-associated factors. (A) Cell cycle analysis of Uhrf1 and Sirt1 in HEK cells. HEK cells were transfected with plasmids of pCAG-GFP-NP95-IB and pCAG-GFP-Sirt1 or pCAG-GFP-Sirt1 catalytic domain for 24 hours. No transfection of HEK cells was used as the control. (B) The relative mRNA levels of CDK1, CDK2, Cyclin E and E2F1 in Sirt1 Wild type, Knockout and Rescue ES cell lines and HEK cells overexpressing GFP-Uhrf1, GFP-Sirt1, GFP-Uhrf1 deleted SRA, GFP-Uhrf1 together with GFP-Sirt1 and GFP-Uhrf1 deleted SRA together with GFP-Sirt1 cells by RT-qPCR. The values represent mean ± SD (n=3).

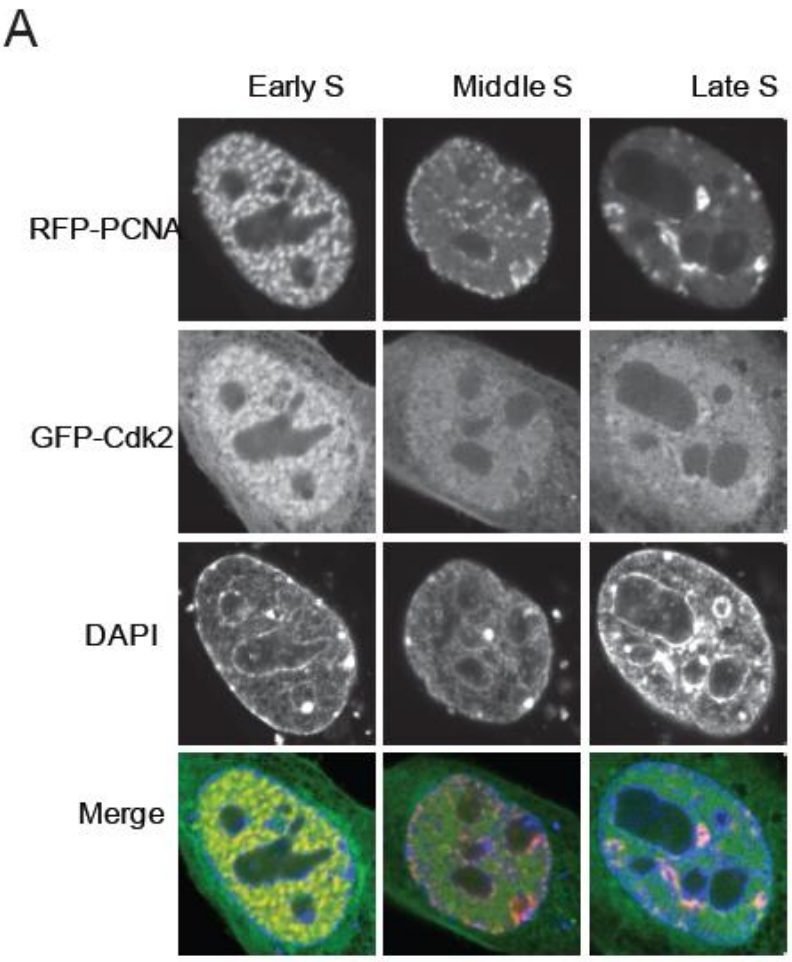

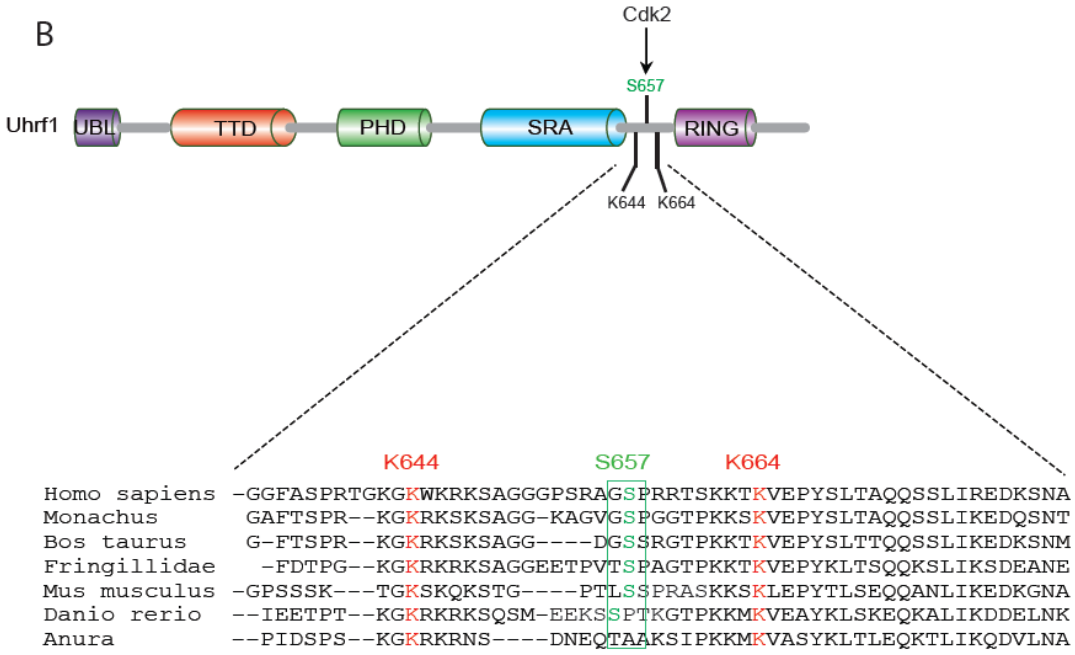
B
Cdk2
S657
Uhrf1
UBL
TTD
PHD
SRA
RING
K644
K664
K644
S657
K664
Homo sapiens -GGFASPRTGKGKWKRKSAGGGPSRAGSPRRTSKKTKVEPYSLTAQQSSLIREDKSNA
Monachus GAFTSPR--KGKRKSKSAGG-KAGVGSPGGTPKKSKVEPYSLTAQQSSLIKEDQSNT
Bos taurus G-FTSPR--KGKRKSKSAGG----DGSSRGTPKKTKVEPYSLTTQQSSLIKEDKSNM
Fringillidae -FDTPG--KGKRKRKSAGGEETPVTSPAGTPKKTKVEPYKLTSQQKSLIKSDEANE
Mus musculus -GPSSSK---TGKSKQKSTG----PTLSSPRASKKSKLEPYTLSEQQANLIKEDKGNA
Danio rerio --IEETPT--KGKRKRKSQSM-EEKSSPTKGTPKKMKVEAYKLSKEQKALIKDDELNK
Anura --PIDSPS--KGKRKRNS----DNEQTAAKSIPKKMKVASYKLTLEQKTLIKQDVLNA

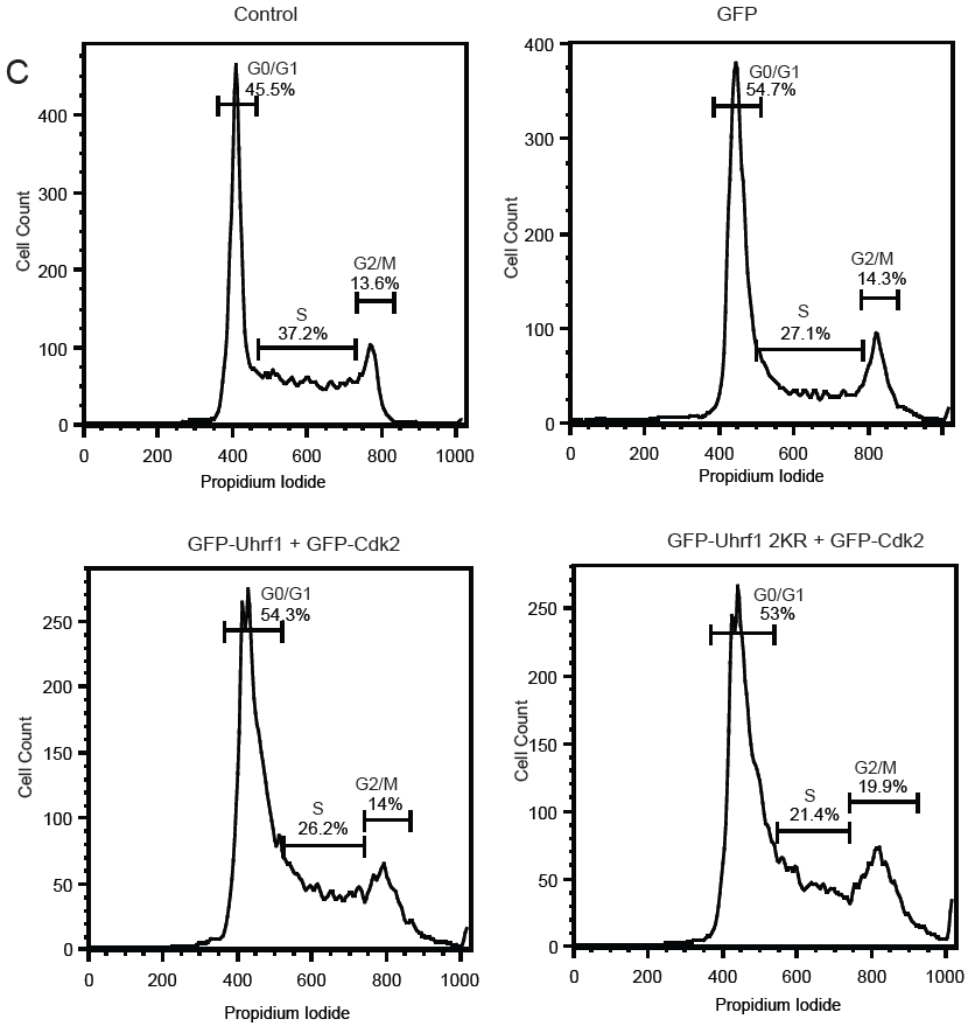
C
Control
G0/G1
45.5%
S
37.2%
G2/M
13.6%
GFP
G0/G1
54.7%
S
27.1%
G2/M
14.3%
GFP-Uhrf1 + GFP-Cdk2
G0/G1
54.3%
S
26.2%
G2/M
14%
GFP-Uhrf1 2KR + GFP-Cdk2
G0/G1
53%
S
21.4%
G2/M
19.9%
Cell Count
Propidium Iodide

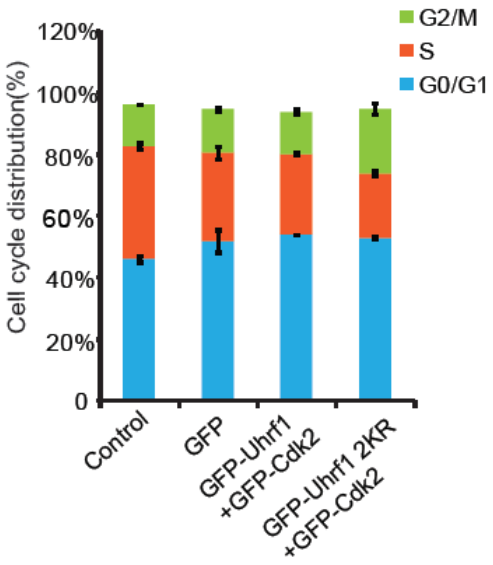

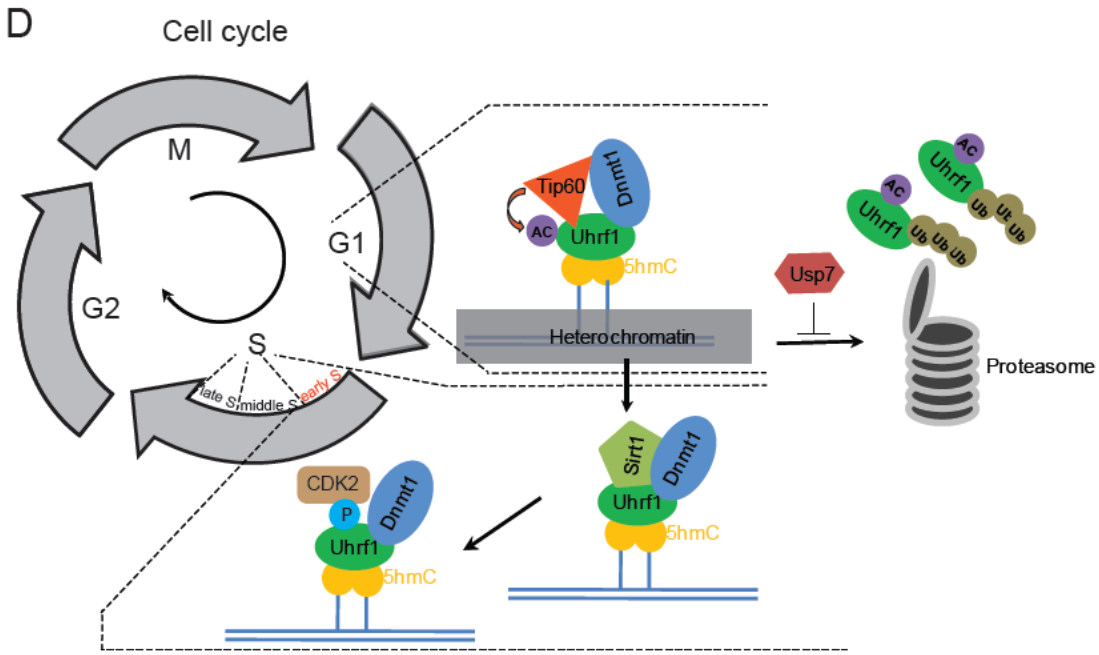

Figure 2.7 Sirt1 mediated deacetylation drives Cdk2 to phosphorylate Uhrf1 in the transition from G1 to S phase of the cell cycle. (A) GFP-Cdk2 was co-expressed with RFP-PCNA in C2C12 cells and its distribution in early S, middle S, late S phases in cell cycle was monitored with confocal. DAPI was used for chromatin counterstaining. Scale bar, 10 μm. (B) The phosphorylation site of Uhrf1 by Cdk2 was shown between the two lysine sites targeted by Sirt1. (C) Cell cycle analysis of Uhrf1 2KR and Cdk2 in HEK cells. HEK cells were transfected with plasmids of pCAG-GFP-Cdk2 and pCAG-GFP-NP95-IB or pCAG-GFP-Uhrf1 K644RK664R

(2KR) for 24 hours. The untransfected HEK cells were used as the control. The values represent mean ± SD. (D) Model of dynamic regulation of Uhrf1 stability driven by (de)acetylation in the cell cycle.

3.3 Sirtuin proteins link histone H3 lysine 18 deacetylation to metabolism via Hif1a

3.3.1 Different sirtuin proteins are expressed with distinct subcellular distribution.

Mammalian sirtuin proteins share a conserved catalytic core domain with a flanking N or C terminal sequence, which consistently decide their different molecular weights (**Figure 3.1A and 3.1B**). I constructed all of the sirtuin proteins with GFP tag and determined their localization in C2C12 cells. Previous evidence has shown, that subcellular localization of sirtuin proteins are dependent on their N- or C-terminal sequence, which is also responsible for their interactions with different partners and substrates (Haigis and Sinclair, 2010). Specifically, Sirt1, Sirt6, and Sirt7 are located in the nuclear and Sirt7 mainly in nucleolus; Sirt2 is cytoplasmic (**Figure 3.1C**); Sirt3, Sirt4, and Sirt5 are mitochondrial. When Sirt2 is overexpressed, it is shuttled to the nucleus (**Figure 3.1D**).

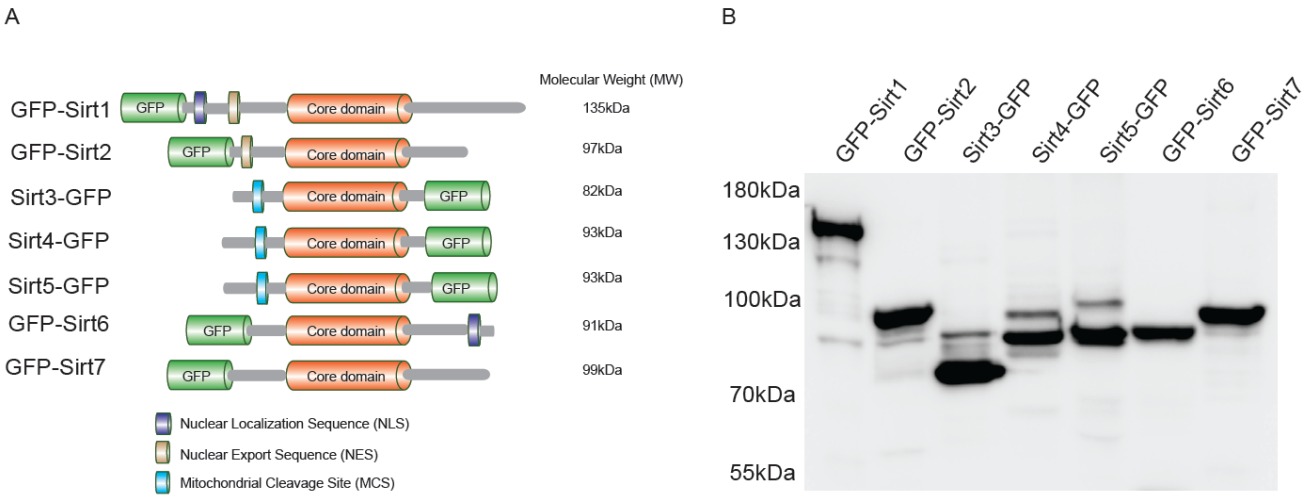

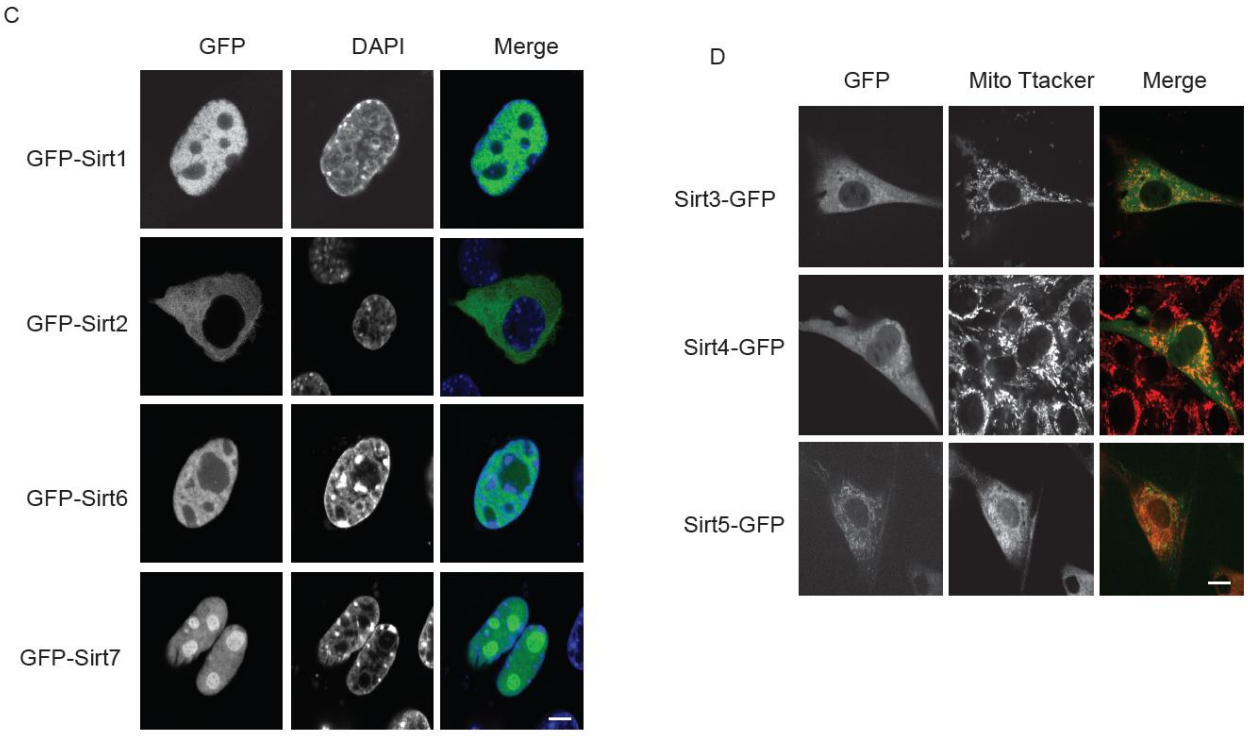

Figure 3.1 schematic structures of different sirtuin proteins with GFP tag and their subcellular distribution. (A) The domain structures of sirtuin proteins, including Sirt1, Sirt2, Sirt3, Sirt4, Sirt5, Sirt6 and Sirt7. All sirtuins shared the common core domain for catalytic activity. Sirt1, Sirt2, Sirt6, and Sirt7 were constructed with GFP tag at the N terminus, while the mitochondrial proteins, Sirt3, Sirt4, and Sirt5 only with GFP tag at the C terminus for their precise localization. NLS, nuclear localization sequence; NES, nuclear export sequence; MCS, mitochondrial cleavage site (Flick and Lüscher, 2012b). (B) The expression of all sirtuin proteins. All the constructed sirtuins with GFP tag were overexpressed in HEK cells and purified with GFP-Trap beads, and then analyzed with western blot. (C) The subcellular localization of Sirt1, Sirt2, Sirt6, and Sirt7 with a GFP tag at the N terminus. The plasmids, pCAG-GFP-Sirt1, pCAG-GFP-Sirt2, pCAG-GFP-Sirt6, and pCAG-GFP-Sirt7 were used in HEK cells and overexpressed for 12 hours. The cells were fixed and imaged by the confocal microscope. DAPI was used for chromatin counterstaining. Scale bar, 10 μm. (D) The subcellular localization of Sirt3, Sirt4, and Sirt5 with GFP tag at the C terminus. Since the mitochondrial signal was sequenced in the N terminus of Sirt3, Sirt4, and Sirt5, the GFP tag was linked to their C terminus and expressed in HEK cells for imaging. Mitochondria were labeled with a commercial and sensitive marker, the Mito tracker. Scale bar, 10 μm.

3.3.2 Effects of sirtuins overexpression on H3K18 acetylation

To explore the relationship between sirtuins protein and histone H3K18ac, I overexpressed all sirtuin proteins with GFP tag in HEK cells and investigated the histone H3K18 acetylation level *in vivo* by western blot. Although several members of the sirtuin family, including Sirt1, Sirt2, Sirt3, Sirt6, and Sirt7, are known to directly deacetylate specific acetylated histone, I overexpressed sirtuin proteins in HEK cells and discovered that only four sirtuin proteins, Sirt1, Sirt2, Sirt6, and Sirt7, can downregulate H3K18ac (**Figure 3.2A**). Sirt3, Sirt4, and Sirt5 had nearly no influence on H3K18ac level, mainly because of their mitochondrial localization (**Figure 3.2B**). Consistent with my western blot, the immunofluorescence staining for H3K18ac also showed that H3K18ac was regulated by Sirt1, Sirt6, and Sirt7 (**Figure 3.2C and 3.2D**).

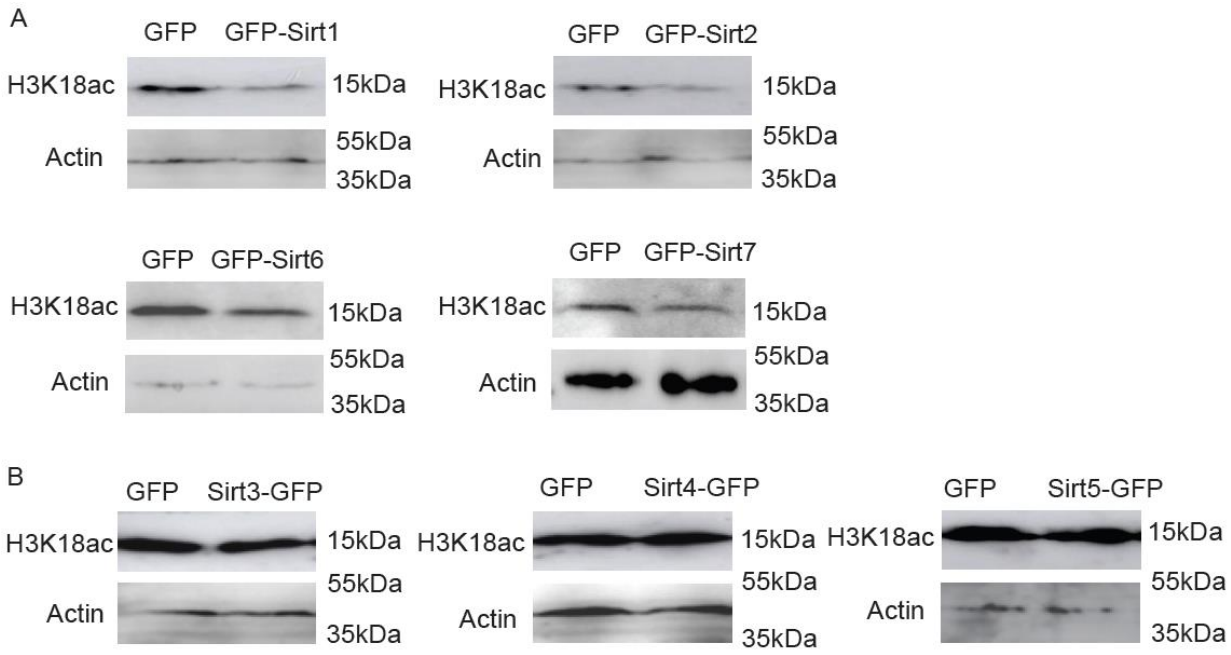

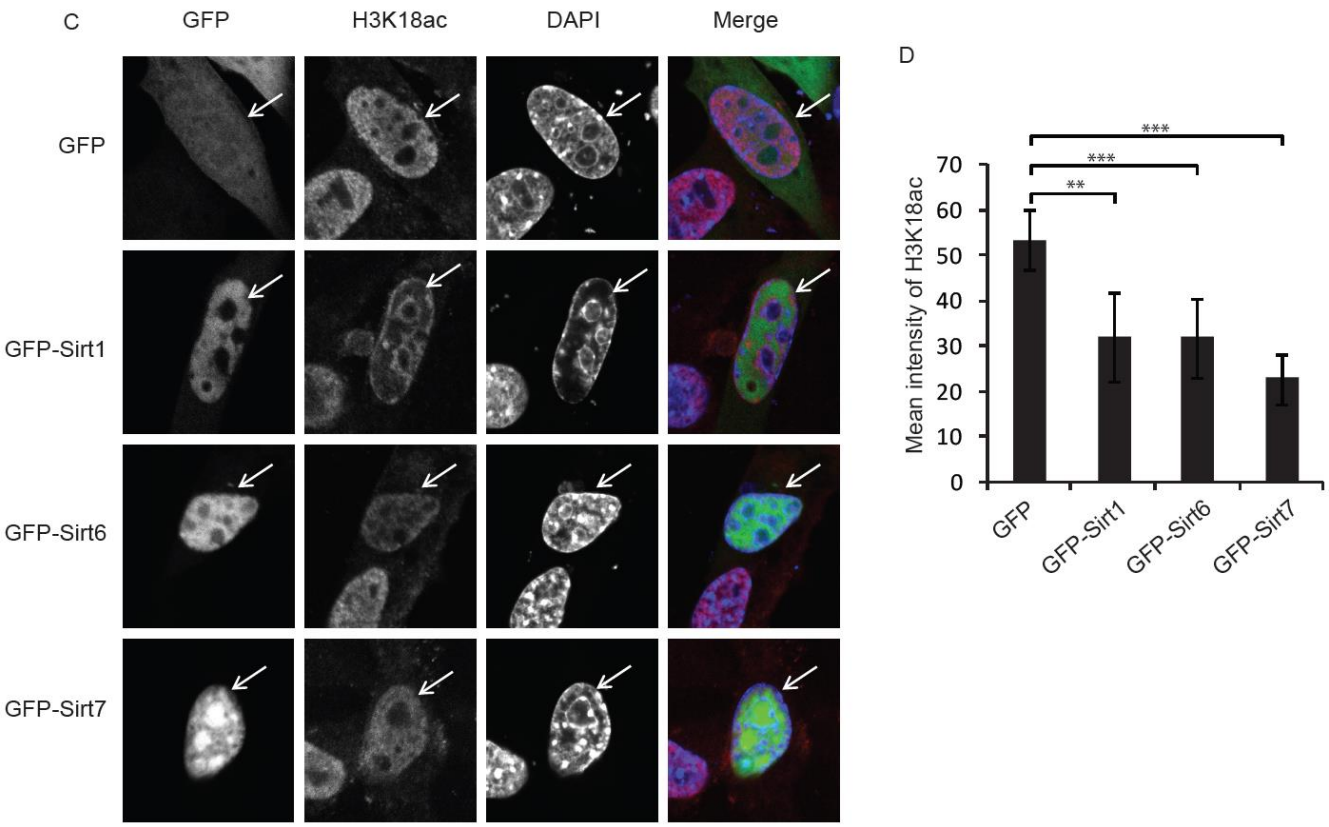

Figure 3.2 The effect of sirtuin proteins on the level of histone H3K18ac. (A) The H3K18ac level was measured in HEK cells overexpressing GFP-Sirt1, GFP-Sirt2, GFP-Sirt6, and GFP-Sirt7 by western blot. (B) The H3K18ac level in HEK cells overexpressing Sirt3-GFP, Sirt4-GFP, and Sirt5-GFP by western blot. (C) The fluorescence imaging of the H3K18ac level in HEK cells overexpressing GFP-Sirt1, GFP-Sirt6, and GFP-Sirt7. And then the mean intensity of H3K18ac was quantitated by ImageJ (D). The values represent mean ± SD and SEM (n=20). Data were analyzed by an unpaired Student's t-test and ANOVA test (*p<0.05, **p<0.01, ***p<0.001).

3.3.3 The establishment of stable cell lines for doxycycline induction with the Tet-On system

To further quantify the correlation between the protein level of sirtuins and the enzyme activity on histone H3K18 in cells, we used a Tet-on system, based on the Tet repressor protein (TetR) and Tet operator (TetO) DNA elements derived from the Tn10-encoded tetracycline resistance operon, and generated a doxycycline-dependent sirtuins

expression model in mouse embryonic stem cells. For establishing these inducible cell lines, I set up and implemented the process as follows (**Figure 3.3A**). Specifically, I used the multifunctional integrase (MIN) tag as an attachment site for the serine integrase Bxb1 to efficiently introduce two functional cassettes into the genomic locus of Rosa26. The one cassette is the tetracycline transactivator (tTA) gene and the other one is the gene of sirtuins. The novel strategy of MIN-Tagging and Bxb1-mediated recombination is based on a CRISPR/Cas assisted in-frame insertion of an *attP* site and firstly developed by our lab (Mulholland et al., 2015). After generation of these recombined cell lines, doxycycline (dox) was added in an exclusively bound rTA protein, which promotes the expression of sirtuin proteins with GFP tag by coupling on a minimal promoter of a tetracycline response element (TRE). To identify MIN-tagged cells, Rosa26$^{attp/attp}$, the DNA sequence surrounding the ATG was amplified using the screening primers and digested by the restriction enzyme HincII for that there is only restriction site (**Figure 3.3B**) (primers in **Table 5**). For Rosa26$^{attp/rtTA}$ cell lines analysis, I amplified the DNA sequence by PCR with the same primers and run it in 2% agarose gel together with PCR products from wild type, MIN-tagged cell lines. It was displayed that there were two bands for Rosa26$^{attp/rtTA}$ cell lines because MIN tag only remained at one strand of DNA (**Figure 3.3C**). To screen for Bxb1-mediated cell lines, Rosa26 ^{rtTA} $^{/GFP-Sirt}$, a three-primer PCR strategy with primers for MIN-tagged locus and the attL-specific primer was employed (**Figure 3.3D**) (primers in **Table 5**).

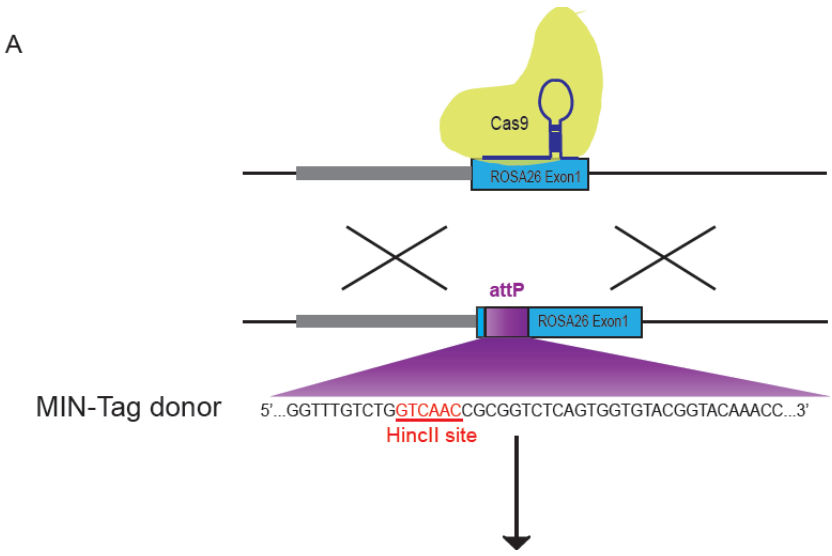

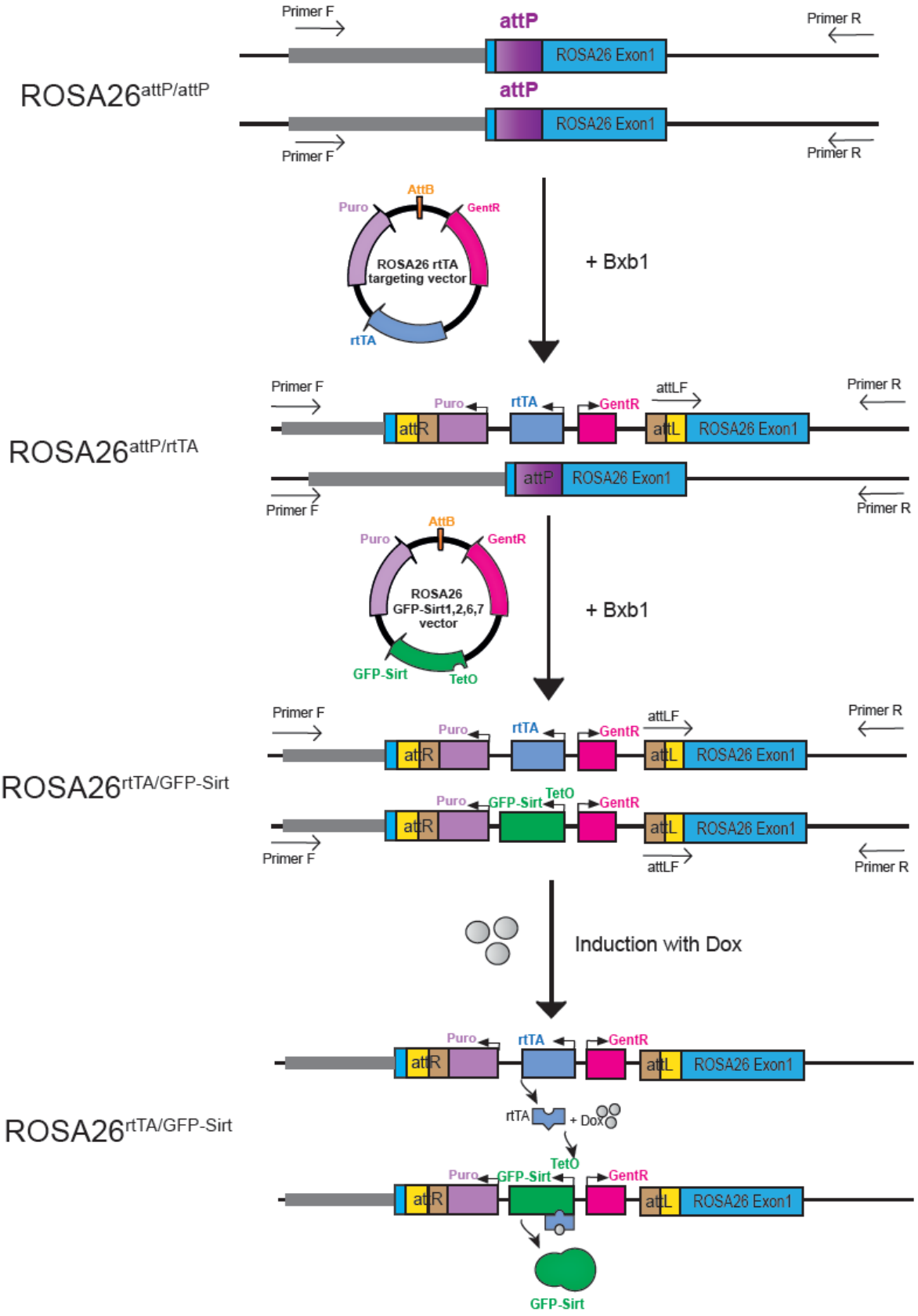
ROSA26attP/attP
Primer F
attP
Primer R
ROSA26 Exon1
attP
ROSA26 Exon1
Primer F
Primer R
AttB
Puro
GentR
ROSA26 rtTA targeting vector
rtTA
+ Bxb1
ROSA26attP/rtTA
Primer F
Puro
rtTA
GentR
attLF
Primer R
attR
attL
ROSA26 Exon1
attP
ROSA26 Exon1
Primer F
Primer R
AttB
Puro
GentR
ROSA26 GFP-Sirt1,2,6,7 vector
GFP-Sirt
TetO
+ Bxb1
ROSA26rtTA/GFP-Sirt
Primer F
Puro
rtTA
GentR
attLF
Primer R
attR
attL
ROSA26 Exon1
Puro
GFP-Sirt
TetO
GentR
attR
attL
ROSA26 Exon1
Primer F
attLF
Primer R
Induction with Dox
ROSA26rtTA/GFP-Sirt
Puro
rtTA
GentR
attR
attL
ROSA26 Exon1
rtTA
+ Dox
TetO
Puro
GFP-Sirt
GentR
attR
attL
ROSA26 Exon1
GFP-Sirt

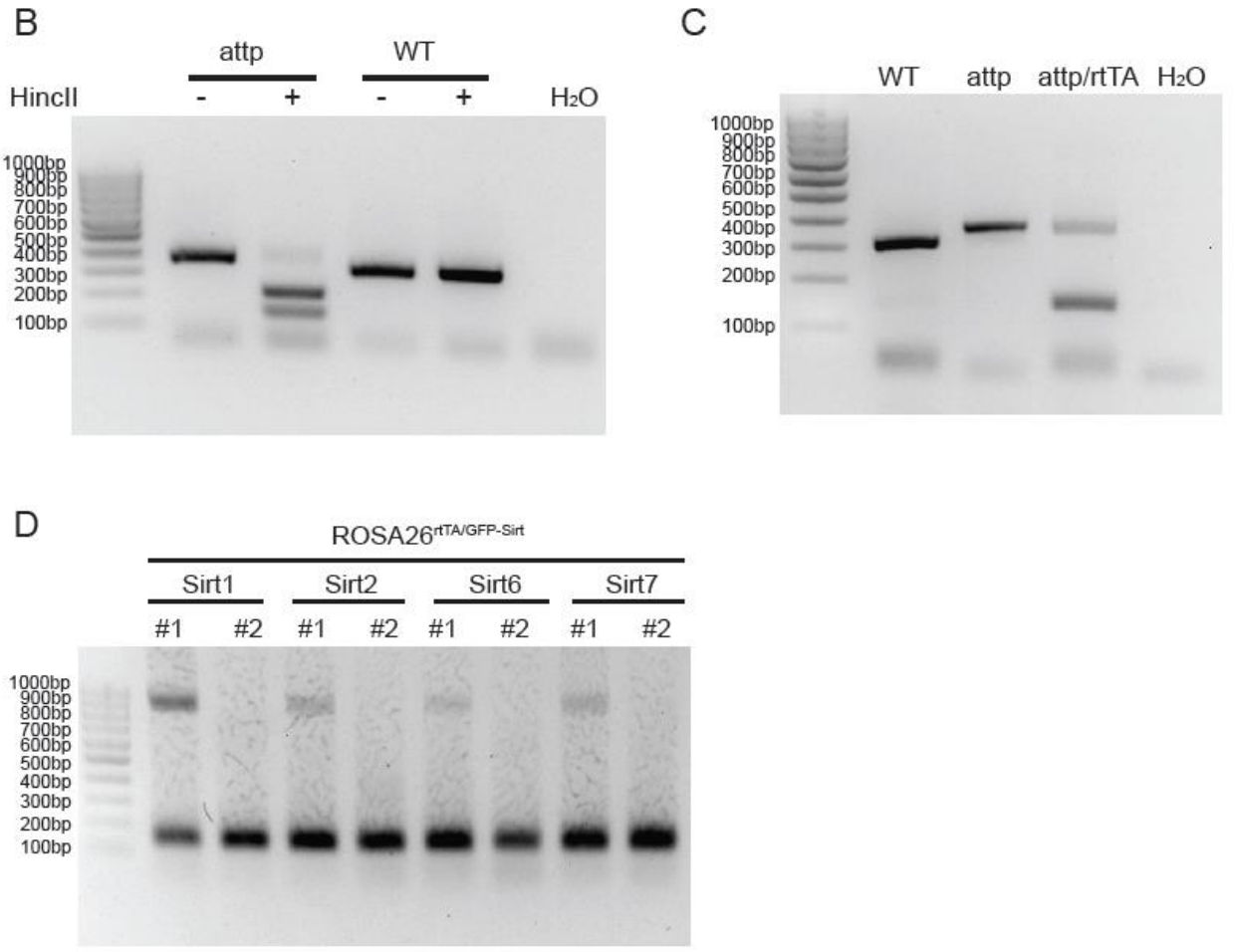

Figure 3.3 The generation of doxycycline-inducible cell lines. (A) Schematic overview of the establishment of doxycycline-inducible cell lines. The MIN-tag donor harbors the *attP* site and homology to the genomic sequence 5′ and 3′ of the start codon of Rosa26. Integration is facilitated by double-strand breaks created by Cas9 directed to the target sequence by a specific gRNA. Restriction enzyme HincII recognition site used for screening in this study are indicated with a red line above the *attP* sequence. With Bxb1-mediated recombination, the plasmid of tetracycline transactivator (tTA) gene and vectors expressing GFP-Sirt1, GFP-Sirt2, GFP-Sirt6, and GFP-Sirt7, were successfully introduced the Rosa26 genome. When doxycycline was added in, it can recruit rTA protein to bind a minimal promoter, a tetracycline response element (TRE), and promote expression of sirtuins with GFP tag. (B) The analysis of Rosa26$^{attp/attp}$ cell lines by PCR. The DNA sequence surrounding the ATG was amplified using the screening primers and digested by the restriction enzyme HincII and run in 2% agarose gel. The cells without any editing were used as a control. H2O was used as a negative PCR control. (C) The

Rosa26$^{attp/rtTA}$ cell lines analysis. DNA sequences from WT, Rosa26$^{attp/attp}$, and Rosa26$^{attp/rtTA}$ cell lines were amplified by PCR with same primers and run it in 2% agarose gel. (D) The analysis of Rosa26 $^{rtTA\ /GFP\text{-}Sirt}$ cell lines. Every sirtuin protein had two subclones. The DNA sequence was amplified by PCR with a three-primer PCR strategy. Three primers, namely primer F, primer R, and primer attLF (all primers were listed in **Table 5**).

3.3.4 The expression level of proteins is dependent on the concentration of doxycycline

To test whether doxycycline induces sirtuins expressing in the cell lines, we cultured the cells with different concentrations of doxycycline at 0.1, 0.5, 1, 2 μg/ml and tested sirtuins expressing by UltraVIEW VoX spinning disk microscope and western blot. Both of them showed that, with increasing doxycycline concentration, the expression level of sirtuins was unregulated (**Figure 3.4A and 3.4B**). In short, sirtuins expression was doxycycline-dependent in these inducible cell lines.

To determine the percentage of cells expressing sirtuin proteins with doxycycline, I used fluorescence-activated cell sorting (FACS) to sort and measure the GFP signal of each cell by treating with different concentration of doxycycline. When the concentration of doxycycline was the highest at 4 μg/ml, there were around 80% of 5 × 10^5 cells expressing GFP-Sirt1, 87% for GFP-Sirt2, 95% for GFP-Sirt6, and 63% for GFP-Sirt7 (**Figure 3.4C**).

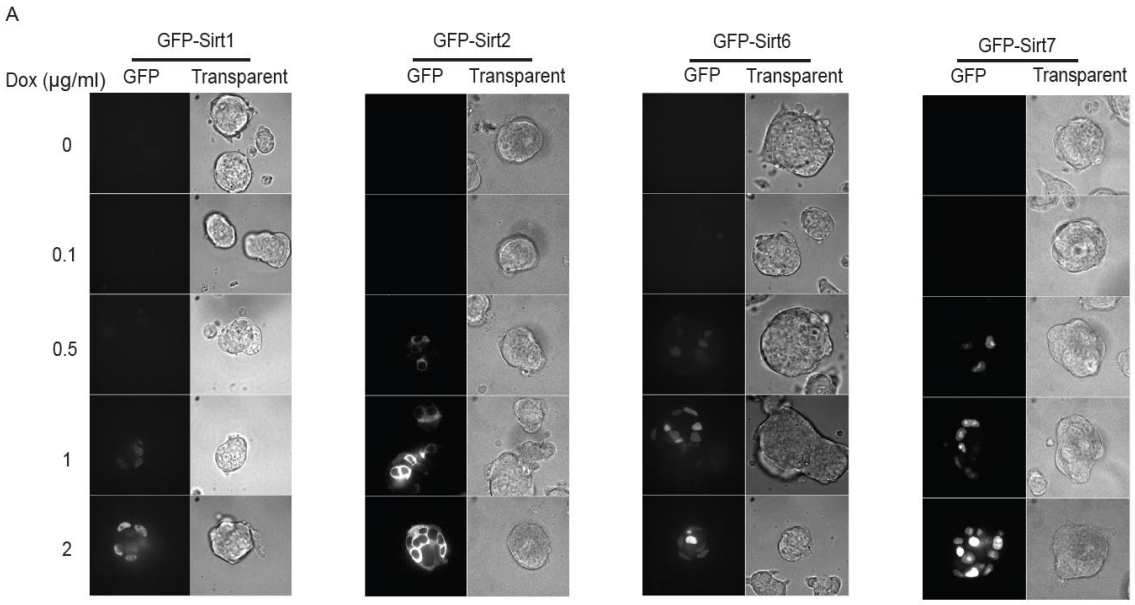

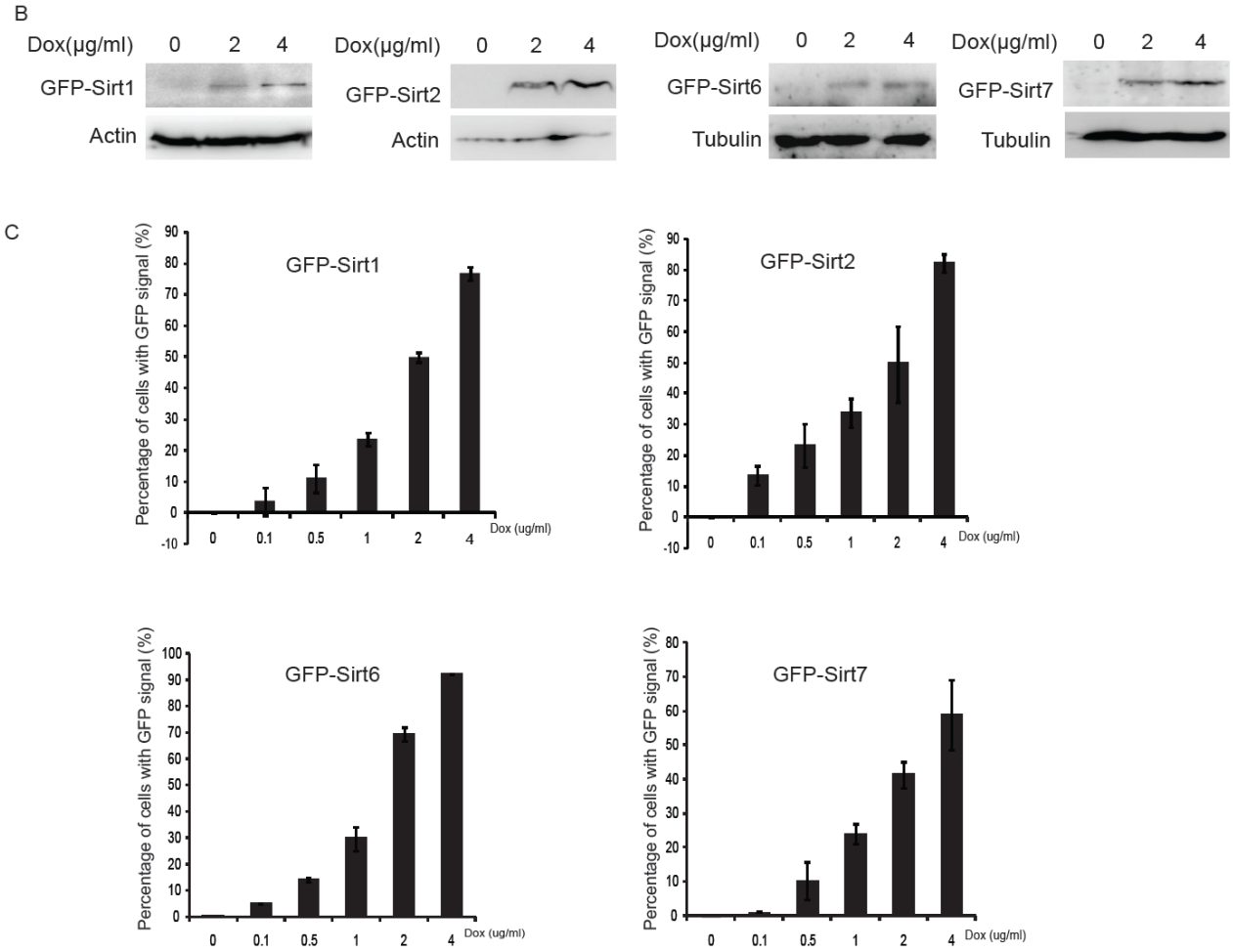

Figure 3.4 The characterization of doxycycline-induced cell lines. (A) The fluorescence imaging of doxycycline-inducible cell lines. The inducible cell lines were cultured in different concentrations of doxycycline (Dox) at 0, 0.1, 0.5, 1, 2 μg/ml for 12 hours and imaged their GFP signal by UltraVIEW VoX spinning disk microscope. (B) The protein expression levels of sirtuins were analyzed by western blot. The cell lines were cultured with different concentration of doxycycline for 12 hours and then analyzed by western blot. The antibody of GFP was used for the detection of sirtuins and antibodies of β-actin and tubulin were used as a control. (C) Analysis of the percentage of cells with GFP signals by FACS. With Dox increased, the percentage of cells expressing sirtuins was dependently raised from 5% to 80% or more.

3.3.5 H3K18 acetylation decreases with increasing sirtuins expression

After I have previously verified that overexpression of Sirt1, Sirt2, Sirt6, and Sirt7 decreased the level of H3K18ac in HEK cells, it is necessary to test H3K18ac level in these inducible cell lines. By treating cells with different concentrations of doxycycline, I found by western blot that H3K18ac was reduced with increasing sirtuins expressing, pointing out again that sirtuin proteins, including Sirt1, Sirt2, Sirt6, and Sirt7, exerted the deacetylase activity on H3K18ac (**Figure 3.5A, 3.5B, 3.5C, and 3.5D**).

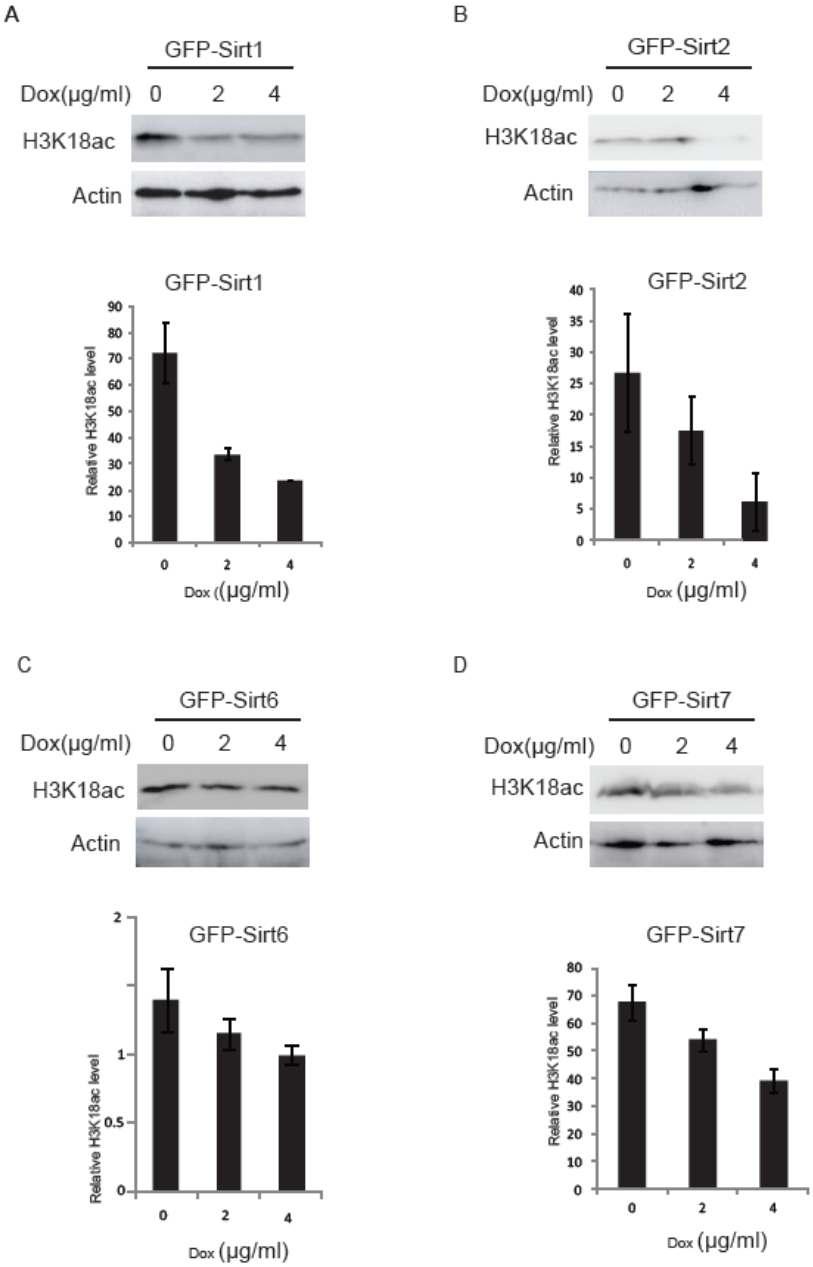

Figure 3.5 The H3K18ac levels decreases with increasing sirtuin expression. (A) The analysis of H3K18ac level in GFP-Sirt1 or GFP-Sirt2 (B) or GFP-Sirt6 (C) or GFP-Sirt7 (D) expressing cells by western blot. The inducible cell lines were cultured in different concentrations of doxycycline (Dox) at 0, 2 and 4 μg/ml for 12 hours. And the level of H3K18ac was measured with the antibodies of acH3K18 and β-actin by western blot. The column showed that western blot for H3K18ac was performed and repeated three times, and then the results were quantitated by ImageJ. The values represent mean ± SD.

3.3.6 The global DNA methylation is correlated with the H3K18ac deacetylation activity of sirtuin proteins

Extensive studies have established that histone acetylation was primarily associated with gene activation. H3K18 acetylation mainly accumulates for a robust peak at the transcription site (TSS) of active and poised genes and prevents DNA methylation for transcriptional silencing. With the induction with doxycycline in these recombined cell lines, sirtuin proteins were upregulated and dramatically deacetylate H3K18ac, leading to an increase in the level of DNA methylation. Different sirtuin proteins influenced the DNA methylation to a different extent (**Figure 3.6A, 3.6B, 3.6C, and 3.6D**). Here it can be explained that the increased global DNA methylation is mainly because sirtuins-mediated H3K18 deacetylation promotes Uhrf1-associated ubiquitination of H3K18, which is essential for Dnmt1 binding and DNA methylation.

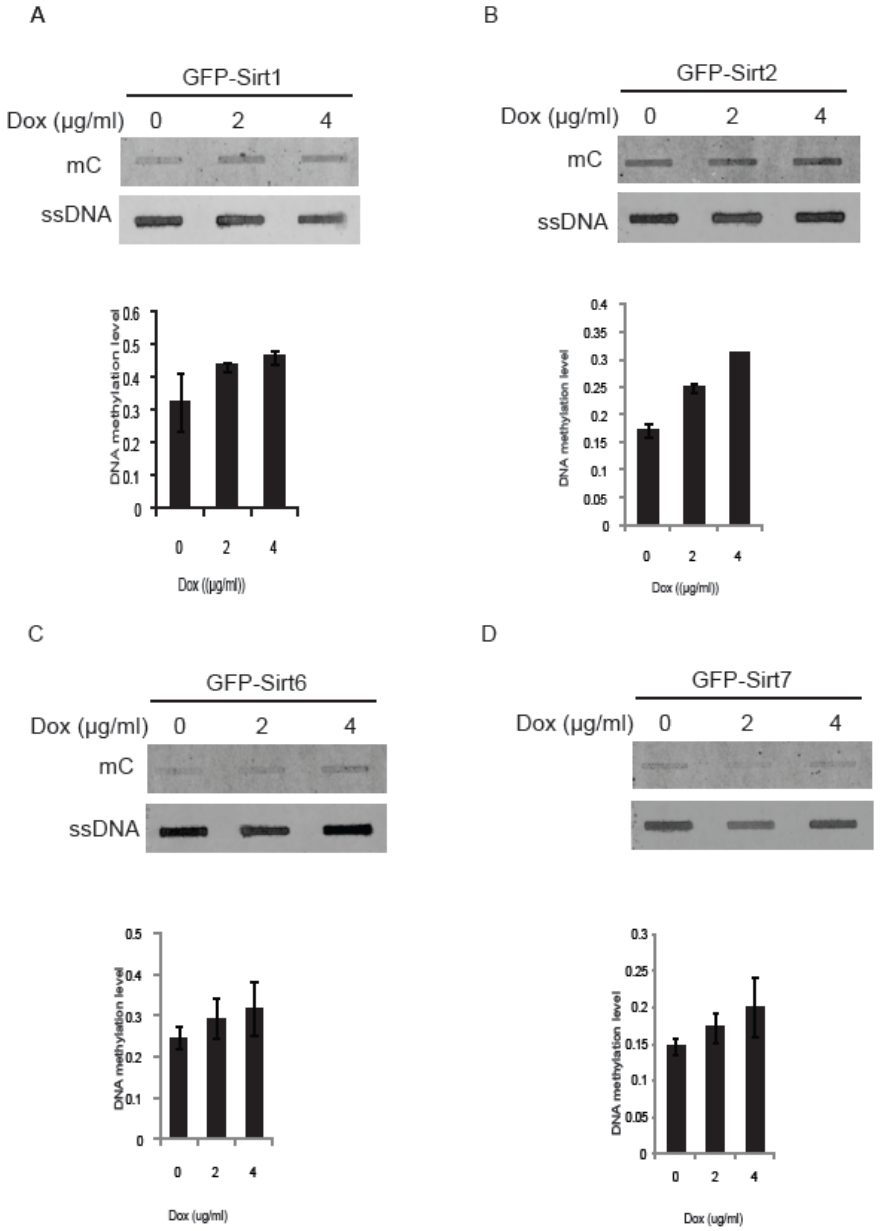

Figure 3.6 The global DNA methylation in cell lines with induced expression of sirtuins. (A) The analysis of global DNA methylation level in GFP-Sirt1 or GFP-Sirt2 (B) or GFP-Sirt6 (C) or GFP-Sirt7 (D) expressing cells by slot blot. The inducible cell lines were cultured in different concentrations of doxycycline (Dox) at 0, 2 and 4 μg/ml. After 12 hours, genomic DNA was extracted and incubated with antibodies against mC and single-stranded DNA for slot blot. ssDNA means single-strand DNA. The column shows that the slot blots for global DNA

methylation was performed and repeated three times, and then the results were quantitated by ImageJ. The values represent mean ± SD.

3.3.7 Metabolism is regulated by sirtuin proteins via the deacetylation of histone H3K18ac

To identify the specific genes regulated by sirtuin proteins, I isolated RNA from the cells with or without doxycycline induction and performed RNA-seq with the help of my colleagues. We found that overexpression of each sirtuin protein affected different genes (**Figure 3.7A**). We further identified 10 genes regulated by all of the sirtuin proteins (**Figure 3.7B**). Compared with wild type embryonic stem cell, J1 ES cells without doxycycline induction, the expression level of all of these 10 genes are decreased to a different extent (**Figure 3.7C**). By using the Ingenuity System Database (IPA) software, we analyzed signaling pathways with these downregulated genes that were altered significantly at or above $P < 0.001$ level between control and treated groups. Among these signaling pathways, three common signaling processes linked with metabolism, especially glycolysis, were further evaluated, which were tightly linked with the upstream regulator, the transcriptional factor Hif1a (**Figure 3.7D**). The targeted genes include *LDHA, PFKL, ENO1, TPI1* and *PLIN3*, and also HIF1a-associating genes, like *RAC2, CDKN1A, UPP1*and *DKC1*, were downregulated, as shown by RT-qPCR, when Sirt1, Sirt2, Sirt6, or Sirt7 expressing in cell lines (**Figure 3.7E**). In addition, to further test H3K18 acetylation is also affected in promoters of these genes, I selected three genes, *LDHA, ENO1,* and *PFKL,* and used chromatin immunoprecipitation (ChIP) to evaluate the occupancy of H3K18ac in these genes' promoters with the anti-acH3K18 antibody. The ChIP signal obtained with this antibody in J1 ES cells was as high as J1 ES cells treated with doxycycline; however, acH3K18 occupancy was evidently reduced when doxycycline-induced sirtuins were expressed in these recombined cells (**Figure 3.7F**). These results suggested that at least at these genes' promoters, doxycycline in J1 ES cells does not affect H3K18 acetylation. This result is consistent with the western blot analysis that sirtuins are inductively expressed by doxycycline and then they affect those target genes via deacetylation of H3K18ac.

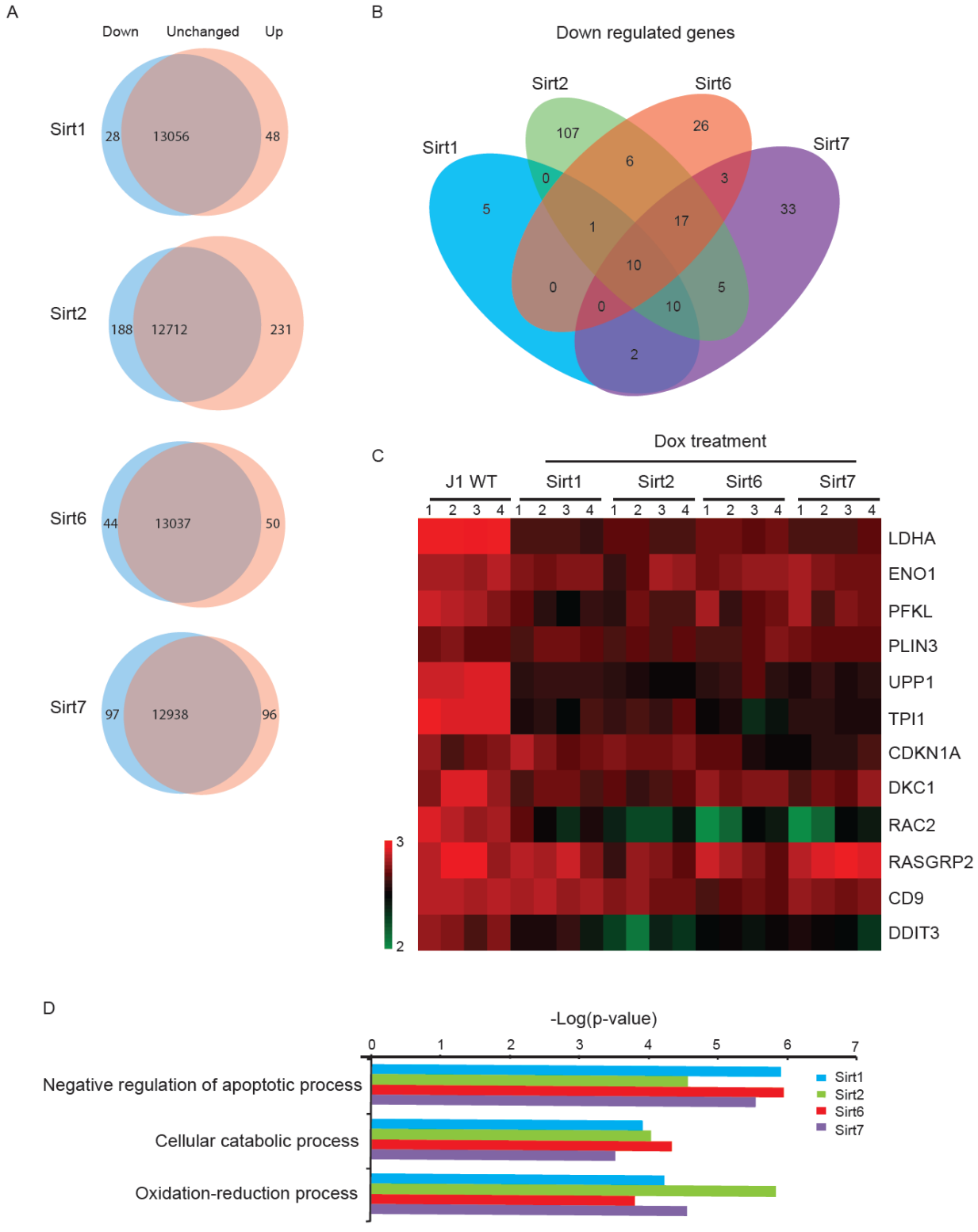
A
Down
Unchanged
Up
Sirt1
28
13056
48
Sirt2
188
12712
231
Sirt6
44
13037
50
Sirt7
97
12938
96
B
Down regulated genes
Sirt1
Sirt2
Sirt6
Sirt7
5
107
26
33
0
6
3
1
17
10
0
5
0
10
2
C
Dox treatment
J1 WT
Sirt1
Sirt2
Sirt6
Sirt7
1 2 3 4 1 2 3 4 1 2 3 4 1 2 3 4 1 2 3 4
LDHA
ENO1
PFKL
PLIN3
UPP1
TPI1
CDKN1A
DKC1
RAC2
RASGRP2
CD9
DDIT3
3
2
D
-Log(p-value)
0 1 2 3 4 5 6 7
Negative regulation of apoptotic process
Cellular catabolic process
Oxidation-reduction process
Sirt1
Sirt2
Sirt6
Sirt7

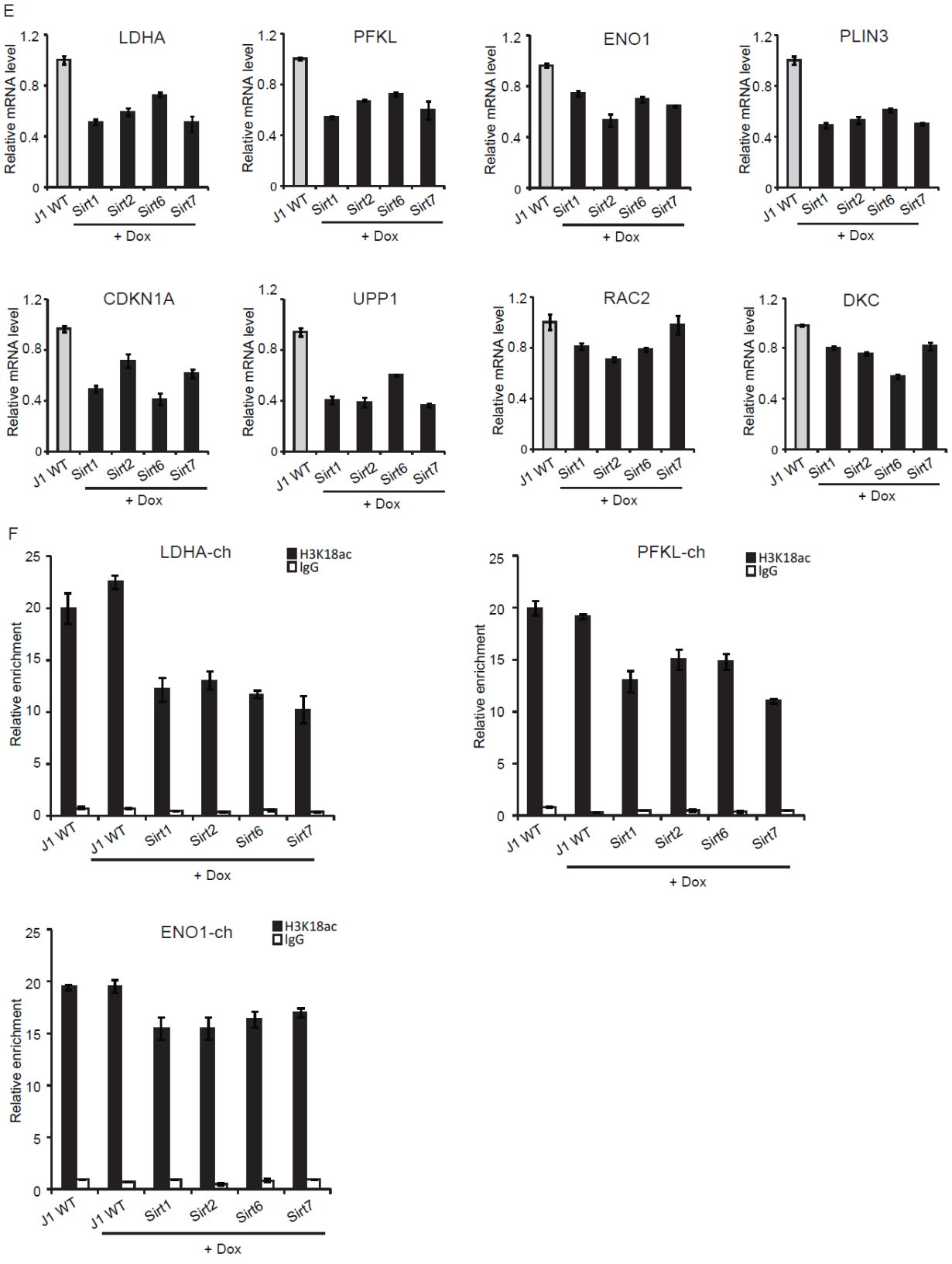
E
LDHA
PFKL
ENO1
PLIN3
CDKN1A
UPP1
RAC2
DKC
Relative mRNA level
1.2
0.8
0.4
0
J1 WT
Sirt1
Sirt2
Sirt6
Sirt7
+ Dox
F
LDHA-ch
PFKL-ch
ENO1-ch
H3K18ac
IgG
Relative enrichment
25
20
15
10
5
0
J1 WT
+ Dox

Figure 3.7 RNA-seq analysis of Dox-induced cell lines. (A) The analysis of different numbers of regulated genes in induced cell lines with the help of my colleagues, Christopher B. Mulholland, and Sebastian Bultmann. (B) The analysis of common genes downregulated in induced cell lines. (C) The hot map for the expression level of downregulated genes compared with cell lines without induction. (D) Three signaling pathways related to the downregulated genes and cooperated with the common transcriptional factor Hif1a. Four sirtuins regulated three pathways to a different extent. (E) The mRNA levels of genes, including *LDHA, PFKL, ENO1* and *PLIN3,* and even the HIF1a-associated proteins, like *RAC2, CDKN1A, UPP1*and *DKC1* were measured by RT-qPCR. The cDNA was generated from the cells with or without Dox induction, and the mRNA level of β-actin was used as the control. Error bars represent standard deviation from experimental triplicate measurements for all assays. (F) The ChIP-qPCR analysis of H3K18ac recruited to the promoters of three different targeted genes, *LDHA, PFKL, and ENO1*. Cells were treated with or without Dox for 24 hours and then extracted the genomic DNA for qPCR. ChIP with α-H3K18Ac was performed and H3K18ac occupancy was shown relative to background signals in IgG negative control ChIPs. Error bars represent SD from experimental triplicate measurements for all assays.

3.3.8 Sirtuin proteins interact with Hif1a to regulate metabolism

To specifically explore the mechanism of transcriptional repression of metabolism-associated genes, I constructed the plasmid for expressing Hif1a. Hypoxia-inducible factor 1-alpha (Hif1a) is a protein acting as the transcriptional regulator of the adaptive response to hypoxia. Under hypoxic conditions, it can activate the transcription of over 40 genes, including erythropoietin, glucose transporters, glycolytic enzymes, vascular endothelial growth factor, HILPDA, and other genes whose protein products increase oxygen delivery or facilitate metabolic adaptation to hypoxia through its heterodimer binding to the core DNA sequence 5'-TACGTG-3' within the hypoxia response element of target gene promoters (Chen et al., 2015; Kim et al., 2006; Maier et al., 2017; Mastrogiannaki et al., 2012; Mole et al., 2009; Semenza et al., 1994). It can bind to histone acetylases or deacetylases. It has been shown that p300/CBP formed a DNA binding complex with Hif1a to activate genes encoding glycolytic enzymes, erythropoietin (Epo), and vascular endothelial growth factor (Arany et al., 1996).

Therefore, we tested whether sirtuin proteins interacted with Hif1a directly or not. By the F3H assay, Hif1a showed a stronger interaction with nuclear sirtuins, including Sirt1, Sirt6, and Sirt7, than that with cytoplasmic Sirt2, and meanwhile, I found that Sirt7 had the tightest binding to Hif1a, Sirt1 was the second and Sirt6 was the last (**Figure 3.8A and 3.8B**). However, the values represent RFP-Hif1a binding intensity were not exactly consistent with the results in figure 3.8A, mainly because I did not have enough images for analysis (only 15 images for GFP, 15 images for GFP-Sirt1, 11 images for GFP-Sirt6 and 12 images for GFP-Sirt7). In addition, I performed a co-immunoprecipitation assay to evaluate their interaction level, which was consistent with the analysis of F3H assay (**Figure 3.8C**). In conclusion, I pointed out that sirtuin proteins, including Sirt1, Sirt2, Sirt6 and Sirt7, regulated metabolism, especially glycolysis, by deacetylation of H3K18ac with the transcriptional factor Hif1a.

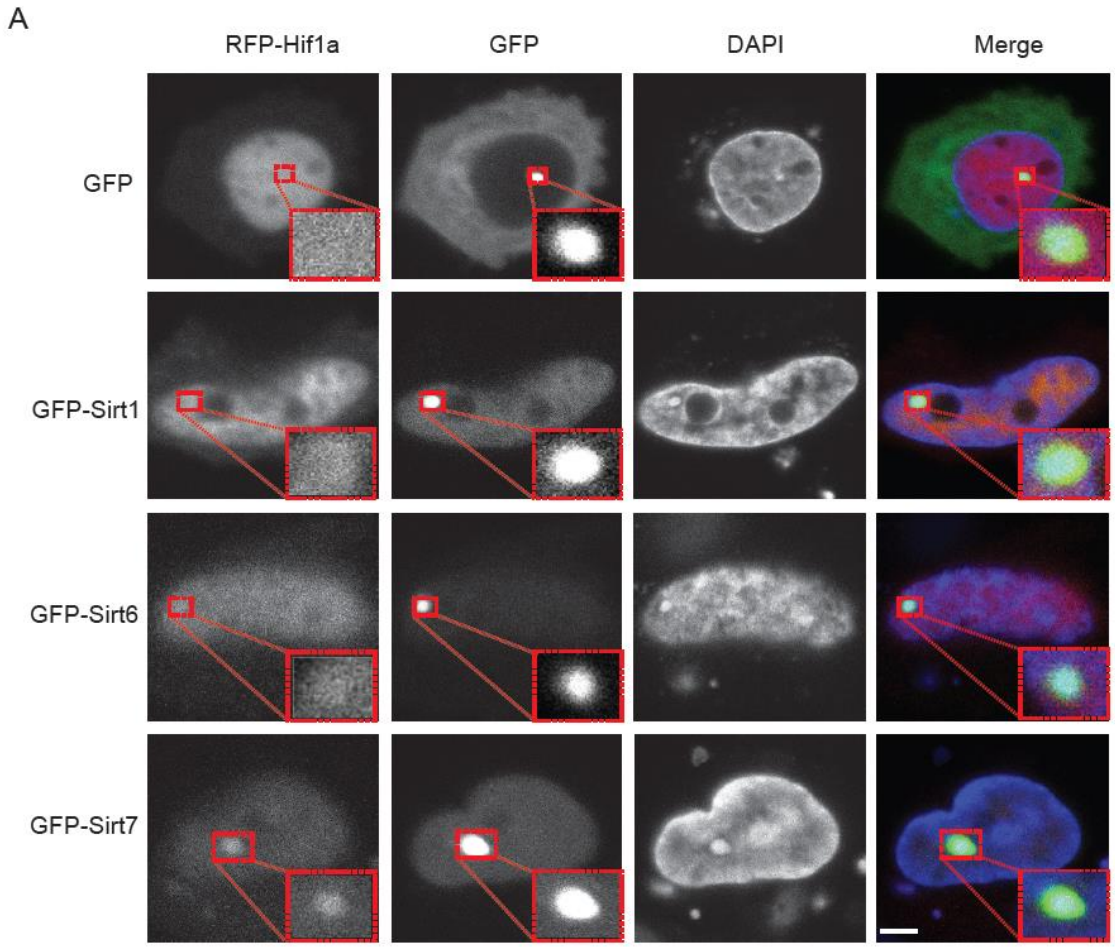

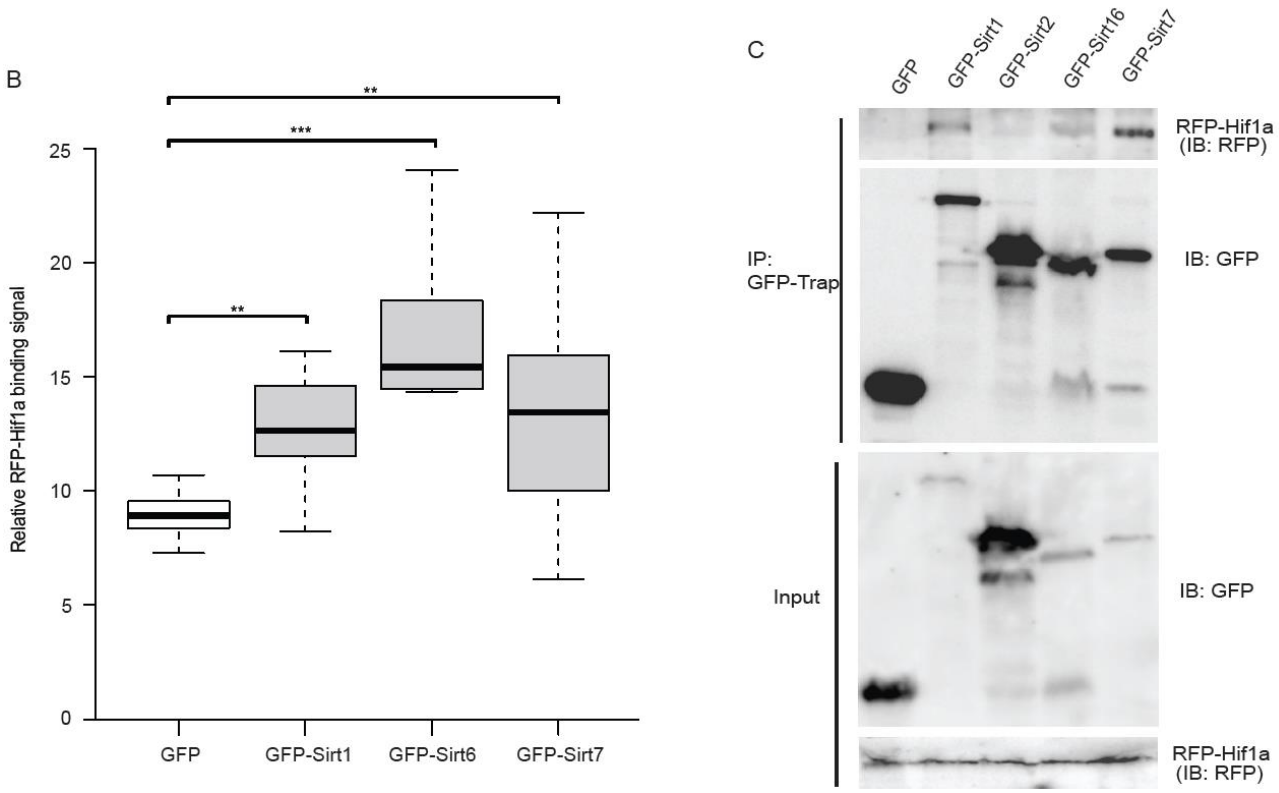

Figure 3.8 The interaction of Hif1a with sirtuin proteins. (A) The interaction between Hif1a and sirtuins was confirmed by the F3H assay. The relative RFP-Hif1a binding signal was calculated similarly to the F3H for interaction between Sirt1 and Uhrf1. GFP was used as a negative control. Scale bar, 5 μm. (B) The interaction of F3H in figure A was quantitated by ImageJ. The values represent mean ± SD and SEM (n=12). Data were analyzed by an unpaired Student's t-test and ANOVA test (*p<0.05, **p<0.01, ***p<0.001). (C) Co-immunoprecipitation of RFP-Hif1a with GFP, GFP-Sirt1, GFP-Sirt2, GFP-Sirt6, and GFP-Sirt7, separately. HEK cells were co-transfected with plasmids of pCAG-RFP- Hif1a and pCAG-GFP-IB, pCAG-GFP-Sirt1, pCAG-GFP-Sirt2, pCAG-GFP-Sirt6 or pCAG-GFP-Sirt7. GFP was used as a control. The complexes were immunoprecipitated (IPed) and analyzed by immunoblotting (IB).

4 Discussion

4.1 Various regulatory mechanisms are responsible for DNA methyltransferase 1 (Dnmt1) activity

4.1.1 Dnmt1 activity is regulated by dynamic post-translational modifications

The reversible post-modifications of Dnmt1, including methylation, acetylation, phosphorylation, sumoylation, and ubiquitination, have been reported for many years. Parts of the modifications of Dnmt1 affect its activity and stability to some extent (**Figure 1**) (Kinney and Pradhan, 2011). Previous evidence has suggested that the regulation of Dnmt1 activity is mediated by the control of the stability of Dnmt1 with various post-translational modifications. For example, Dnmt1 can be methylated by SET domain-containing lysine methyltransferase (Set7), a known histone methyltransferase, at lysine 142 (Lys142), which promotes proteasome-mediated degradation of Dnmt1 (Estève et al., 2009). Conversely, the phosphorylation of Dnmt1 at Ser143 by the serine-threonine protein kinase (Akt1) interferes with Lys142 monomethylation and prevents Dnmt1 degradation (Estève et al., 2011). Another site of human Dnmt1, Ser154, can be phosphorylated by CDKs, such as CDK1, CDK2, and CDK5, which affects the conformation structure of Dnmt1 by altering the interaction between N- and C-terminus, and thus regulates Dnmt1 activity and stability (Lavoie and St-Pierre, 2011).

I specifically analyzed phosphorylated sites of Dnmt1 by mass spectrometry and only focused on one site in CXXC-BAH linker of Dnmt1, S717, mainly because it has been shown that this linker can switch to active catalytic sites of Dnmt1 and block *de novo* methylation (Song et al., 2011). I try to figure out the relationship between the phosphorylated linker and Dnmt1 *de novo* methylation activity. By analyzing the results from *in vitro* and *in vivo* DNA methylation assay, I found that phosphorylation in CXXC-BAH linker of Dnmt1 has no influence on Dnmt1 maintenance methylation activity indeed. And also, phosphorylation of S717 of Dnmt1 does not have any effect on Dnmt1 maintenance and *de novo* methylation activity in the cell. But it is still observed a weak

impact on Dnmt1 *de novo* methylation activity *in vitro*. However, the mechanism of Dnmt1 *de novo* methylation activity is still confusing. As it has been shown that Dnmt1 activity and stability are regulated by different post-modifications, it is reasonable for us to explore the roles of various phosphorylated sites of Dnmt1 in its activity and stability. It has been reported that Dnmt1 owns a considerable *de novo* methylation activity, and I also first find that phosphorylated linker of Dnmt1 obviously affects its *de novo* methylation activity *in vitro*. Our findings provide us an insight that the deletion or mutations at the linker of Dnmt1 maybe influence Dnmt1 *de novo* methylation activity through the conformational changes of Dnmt1 structure. Moreover, it is also interesting to make clear whether phosphorylation at this linker of Dnmt1 is tightly controlled in the cell cycle and how it is regulated. Till now, it has been known that the expression and methylation activity of Dnmt1 are tightly regulated dependent on cell cycle via the modifications of Dnmt1 by other factors, suggesting that the abundance of Dnmt1 is coordinated with the need for DNA synthesis and Dnmt1 activity. Methylated DNMT1 peaks during the S and G2 phases of the cell cycle and phosphorylated DNMT1 peaks during DNA synthesis, before DNMT1 methylation, whereas, acetylated Dnmt1 occurs at either late S or G2 phases of cell cycle. Phosphorylation of Dnmt1 can weaken its interaction with PCNA and the binding of Uhrf1 at replication fork in early and mid-S phase, resulting in the prevention of erroneous methylation of DNA in late S and G2 phases (Denis et al., 2011). In addition, the interaction between Dnmt1 and Uhrf1 is enhanced during the late S phase, but this interaction is interrupted by Usp1 for the balance of Dnmt1 ubiquitination (Qin et al., 2010). So it is complex for Dnmt1 modifications in the cell cycle. But it is also meaningful to further study the functions of the linker of Dnmt1 in the cell cycle, which is likely to give us some hints on DNA *de novo* methylation activity.

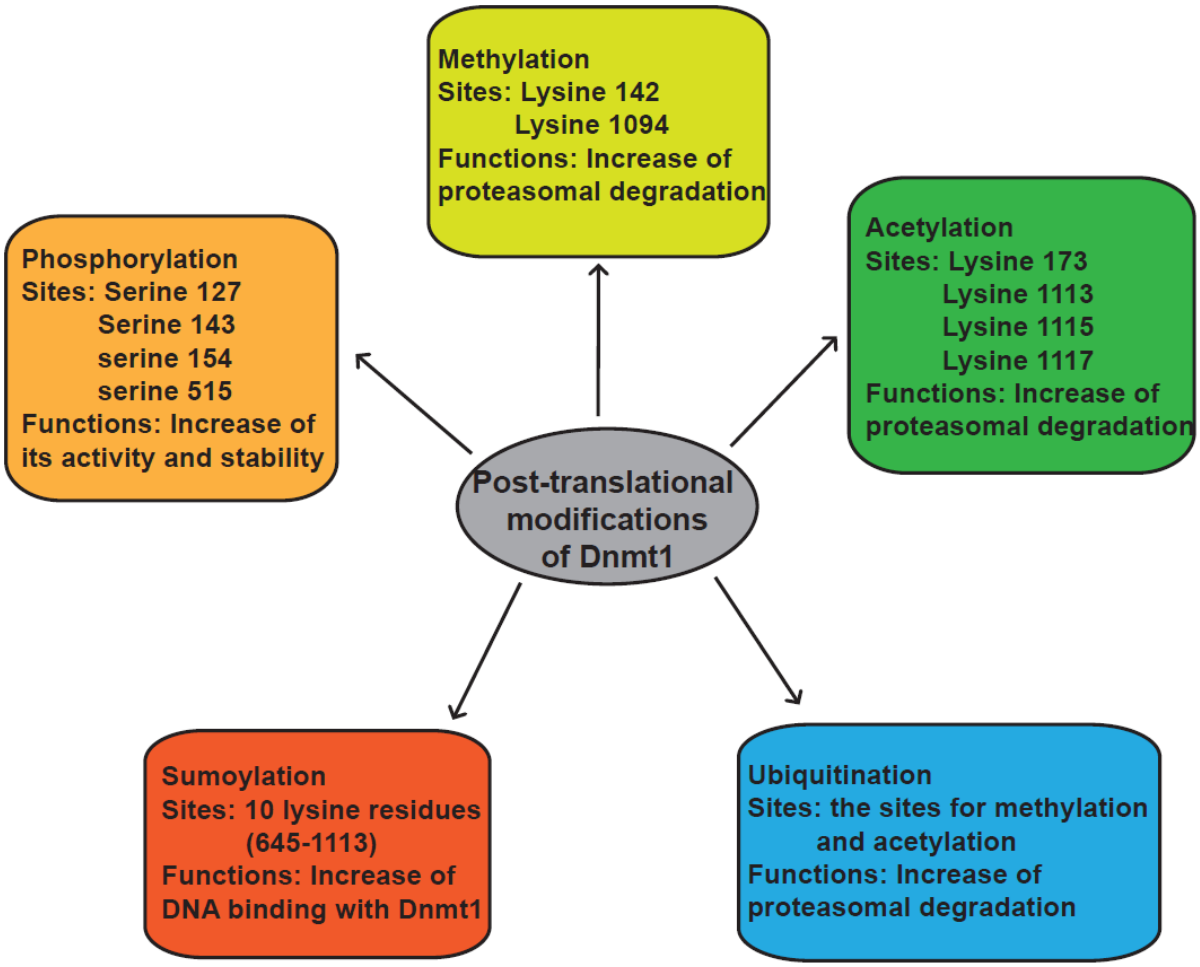

Figure 1. The summary of the five common post-translational modifications of Dnmt1 that affect its activity and stability. The main modifications include phosphorylation, methylation, acetylation, ubiquitination, and sumoylation. The different modified sites of Dnmt1 are linked to the stability and activity in a cell-cycle-dependent manner (adapted from (Kar et al., 2012)).

4.1.2 Dnmt1 activity is regulated by regulatory proteins

Recent publications have identified a number of transcriptional factors and regulators associated with Dnmt1 mediated by the interaction with Dnmt1 (**Figure 2**). However, most of the work on Dnmt1 mainly focuses on its maintenance methylation activity in cells. Here, I try to uncover the reasons why Dnmt1 *de novo* methylation activity is

blocked in cells. And even in my work, phosphorylation at the linker of Dnmt1 also has a weak influence on its *de novo* methylation activity. To analyze it, the proteins interacting with Dnmt1 are one of the important aspects. For example, by directly binding to PCNA, the methylation efficiency of Dnmt1 was increased about 2-fold, even though this interaction is not necessary for the accommodation of Dnmt1 to the DNA replicate forks (Schermelleh et al., 2007). And also the binding of Dnmt1 to *de novo* methyltransferases Dnmt3a and Dnmt3b improve the efficiency of targeted DNA methylation (Kim et al., 2002). Dnmt1 activity is activated by the interaction with HDAC1 and HDAC2, which is enhanced by the DNA binding proteins, MeCP2, MBD2 and MBD3 (Methyl-CpG-Binding Domain proteins) (Svedružić, 2011). Mechanically, the connection of MBD proteins and HDACs can enrich Dnmt1 in highly methylated regions, which is helpful for the formation of heterochromatin. It can be concluded that Dnmt1 activity, especially maintenance methylation activity, is obviously influenced by different kinds of proteins in cells. So, how about Dnmt1 *de novo* methylation activity? I try to figure out the relationship between Dnmt1 *de novo* methylation activity and its stability. I incubated the purified proteins, Usp7, His-Ubi, Dnmt1, and its mutants, Dnmt1 deletion of UBL domain, with genomic DNA from TKO cells (Dnmt1, Dnmt3a and Dnmt3b knockout cell lines) and performed *in vitro* DNA methylation assay. The results showed that Usp7-mediated stabilization of Dnmt1 enhanced its *de novo* methylation activity *in vitro* (data was not shown). But it is still interesting to know whether Usp7 promotes Dnmt1 *de novo* methylation activity *in vivo* or not.

For the establishment and maintenance of euchromatin and heterochromatin, DNA methylation is also tightly linked to Dnmt1. The activity of Dnmt1 on DNA methylation is also connected with histone modifications. The proteins involved in histone modifications also interact with Dnmt1 by binding to different domains of Dnmt1, which is also helpful to change the structural conformation of Dnmt1 for blocking its *de novo* methylation activity *in vivo.* For example, HP1β (heterochromatin binding protein 1), the histone methylation and two eukaryotic histone methyltransferases Suv39H1 (suppressor of variegation 3–9 homologs 1) and EHMT2 (euchromatic histone-lysine N-methyltransferase 2; also known as G9a), are responsible for H3K9 methylation. Dnmt1 has been reported to interact with these proteins and affects each other (Qin et al.,

2011a). In addition, the Dnmt1 activity is mechanistically linked to the PcG (Polycomb group) proteins, such as enhancer of zeste homolog 2 (EZH2) (Viré et al., 2006). EZH2 serves as a recruitment platform for Dnmt1 to methylate the promoters of EZH2-target genes. The interaction of Dnmt1 with different chromatin remodelers, including LSH (lymphoid-specific helicases) and BAZ2A (bromodomain adjacent to zinc finger domain 2A; also known as TIP5), hSNF2H (also known as SMARCA5 (SWI/SNF related, matrix associated, actin dependent regulator of chromatin, subfamily A, member 5), enhance the binding affinity of Dnmt1 to chromatin and the distribution in heterochromatic regions (Qin et al., 2011a). Dnmt1 has been proved to interact with various tumor suppressor genes, like WT1 (Wilms tumor 1), Rb and p53 (Pradhan and Kim, 2002). P53 can stimulate Dnmt1 methylation activity and thus lead to hypermethylation in tumor cells.

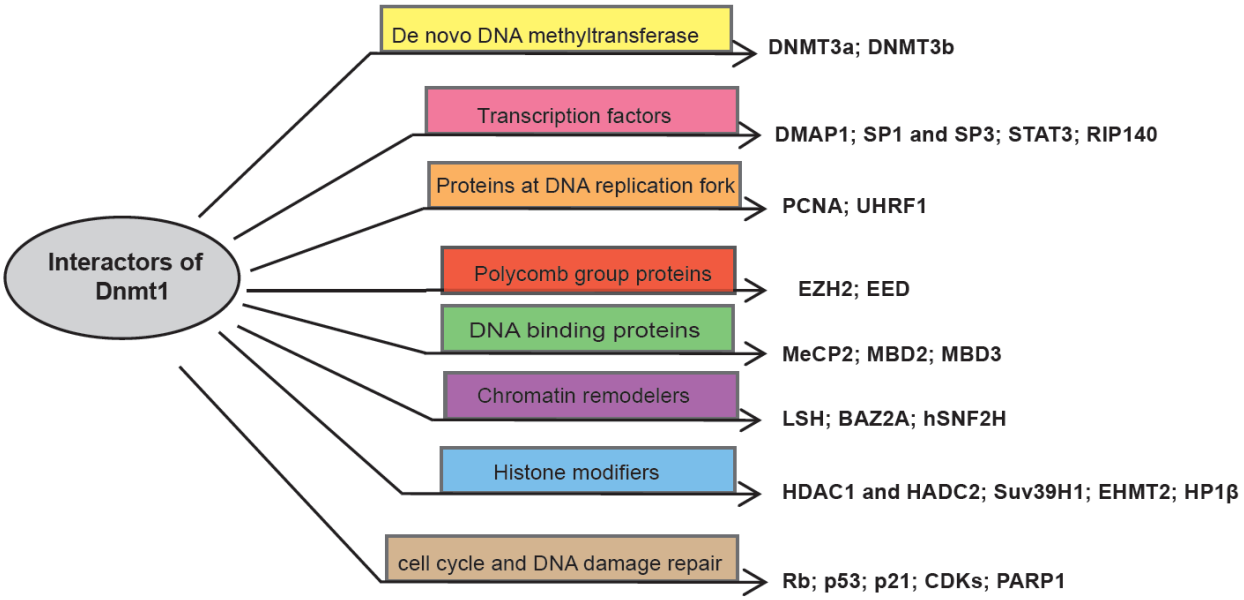

Figure 2. The various interactions of Dnmt1. Dnmt1 has been reported to bind to a number of transcription factors and simultaneously affect its activity and other related functions, including chromatin re-organization, cell cycle regulation, response to DNA damage and tumor growth (Kar et al., 2012).

4.2 The modifications of Uhrf1 play a crucial role in its stability and functions

As an important epigenetic regulator maintaining DNA methylation and histone modifications, Uhrf1 is also subjected to different post-translational modifications, including phosphorylation, ubiquitination, acetylation, and sumoylation. Our study has illuminated a previously unknown pathway that acetylation of Uhrf1 regulates its process in the cell cycle. We demonstrate that through a balance of acetylation and deacetylation at the key lysine sites, protein stability and the binding with Dnmt1 and heterochromatin of Uhrf1 are regulated by the different phases of cell cycle.

It is reported that Uhrf1 is highly expressed in proliferating cells and involved in carcinogenesis (Mousli et al., 2003; Unoki et al., 2009b; Venza et al., 2015). Uhrf1 peaks at late G1 and during G2/M phases in human lung fibroblasts and important for induction of genes at G1 to S transition (Mousli et al., 2003). Knockdown or silencing of uhrf1 in cancer cells led to decreased proliferation and increased apoptosis (Du et al., 2011; Ge et al., 2016). The mechanism behind it may have been selected for some reasons. Firstly, downregulation of Uhrf1 suppressed GC proliferation and reactivated 7 tumor suppressor genes (TSG), including CDX2, CDKN2A, RUNX3, FOXO4, PPARG, BRCA1, and PML by demethylating these promoters (Zhou et al., 2015). The second reason could be that the Uhrf1 protein level controls the process of the cell cycle. Uhrf1 downregulation arrested colorectal cancer cell at G0/G1 phase and reduced $p16^{INK4A}$-mediated apoptosis (Wang et al., 2012). Uhrf1 silencing arrested gall bladder cancer cells at G1/S phase by inducing p21 in a p53-independent manner and triggered apoptosis by upregulating the expression of FasL /FADD, Bax, cytosolic cytochrome c, cleaved caspase-8, -9 and -3 and cleaved PRAP and downregulating bcl-2 expression (Qin et al., 2014).

An immediate question arising from these findings is how Uhrf1 might regulate the maintenance of DNA methylation in the cell cycle. Our data provide a possibility that post-translational modifications of Uhrf1, especially acetylation, are crucial for its abundance and protein stability in the cell cycle. In G1 phase, Uhrf1 is acetylated by Tip60 and recruits Dnmt1, which strengthen the interaction between Tip60 and Dnmt1. The macro-complex binds to heterochromatin and ensures a condensed and transcriptional inert chromatin conformation. Previous structure and biochemical data have also provided a basis for a conformational rearrangement of Uhrf1 domains that a

polybasic region (PBR) between SRA domain and RING domain of Uhrf1 is mutated or occupied by the phosphatidylinositol phosphate PI5P, allowing the TTD domain to bind to H3K9me3 (Gelato et al., 2014). While our results suggest that acetylation in the region between SRA domain and RING domain of Uhrf1 enhances its binding with heterochromatin, suggesting that the specific interaction for SRA domain of Uhrf1 with Tip60 results in the TTD domain of Uhrf1 switch bind to H3K9me3 in heterochromatin. However, it is still not clear how Uhrf1 separates from heterochromatin and how the dynamic changes of the structural conformation for Uhrf1.

Sirt1-mediated deacetylation of Dnmt1 regulates Dnmt1 activity and its distribution in the cell cycle (Peng et al., 2011). Also, we verified that Sirt1 deacetylated Uhrf1 in early S phase of the cell cycle, which stabilizes Uhrf1 and coordinates Uhrf1 with PCNA. Other studies have identified that Sirt1 deacetylates hMOF and Tip60 and inhibits their acetyltransferase activity and promotes their ubiquitination-mediated degradation (Peng et al., 2012; Wang and Chen, 2010). It is still not clear which, Tip60 or Uhrf1, Sirt1 first deacetylates and how Sirt1 influences their stability and roles in the cell cycle. And furthermore, Sirt1 is also modified, including phosphorylation (Sasaki et al., 2008), ubiquitination (Peng et al., 2015), sumoylation (Yang et al., 2007), carbonylation (Caito et al., 2010) and methylation (Liu et al., 2011). These modifications can control Sirt1 level, activity and nuclear localization in normal or stressed cells. For example, the sites of Sirt1, T530, and S540, are targets of cyclin B/Cdk1 and their ablation inhibit the process of the cell cycle and proliferation (Sasaki et al., 2008). It is possible that Sirt1 phosphorylation is involved in the regulation of Uhrf1 and Tip60 in the cell cycle. Phosphorylation of Sirt1 might decrease its deacetylase activity independent of NAD^+ level so that Cdk2 could promote the process of the cell cycle by phosphorylating Uhrf1 at S phase in the cell cycle. Our findings provide additional implications for why the factors interacting with Uhrf1 could influence its function in cells. From a translational standpoint, the landscape of Uhrf1 PTMs has become increasingly more diverse and more evidence need to be gathered for the functions of these modifications in cancer, oxidative stress, and DNA damage.

4.3 The enzymic activity and expression level of sirtuins regulate key biological functions

4.3.1 Sirtuin proteins deacetylate different histones

Sirtuins are a conserved family of proteins and common in all different species. In mammals, the sirtuin family consists of seven sirtuins, termed Sirt1-Sirt7, all of which have a highly conserved nicotine adenine dinucleotide ($NAD^{+)}$ -dependent catalytic domain with different flanking N and C terminal sequence (RA, 2000). Sirtuins are classified as class III histone deacetylases (HDACs) and function as NAD^{+}-dependent deacetylases and or ADP-ribosylases to deacetylate histone and non-histone proteins. Although little is known about how individual epigenetic marks are set up and maintained in the process of DNA replication and cell division, sirtuin proteins undergo a variety of adaption that enables them to regulate dynamic chromatin and genome with the development of chromatin in eukaryotes. The sirtuin function associated with chromatin is mainly through direct deacetylation of specific histone acetylation marks as epigenetic modulation. Previous evidence has shown that different sirtuin proteins deacetylated special histones. In my work, I find that sirtuin proteins, including Sirt1, Sirt2, Sirt6, and Sirt7, can corporately deacetylate H3K18ac to a different extent. The targeted histone substrate H3k18ac is enriched at the transcription start site (TSS) of active and poised genes and usually considered to promote transcriptional activation of genes. So the question about how these four sirtuin proteins function through deacetylation of H3K18ac in cells even in mammals is rising. In the epigenetic level, it has been demonstrated that H3K18 acetylation prevents Dnmt1 binding and methylating DNA. In contrast, sirtuins-mediated H3K18 deacetylation promotes Uhrf1-associated ubiquitination of H3K18, which is essential for Dnmt1 binding and DNA methylation. So I have checked the unregulated global DNA methylation level with increased sirtuins expression by slot blot. My results are consistent with previous research. In addition, it is easy to test H3K18ac level with the confocal microscope in the conditions of overexpressed nuclear Sirt1, Sirt6, and Sirt7, but for cytoplasmic Sirt2, it is difficult to image it. To figure out the reason for it, it has been reported that Sirt2 deacetylases

H4K16ac during the G2/M transition of the mammalian cell cycle (Vaquero et al., 2006). And till now, it is unclear when Sirt1 deacetylate H3K18ac in the cell cycle. More work needs to be done to solve this problem.

Consistent with the localization of Sirt3 in the nucleus, Sirt3 is also capable of histone deacetylase activity for H3K9ac and H4K16ac (Iwahara et al., 2012), while Sirt4 and Sirt5 do not deacetylase histones in the mitochondria. Initially classified as a nuclear ADP-ribosyltransferase, Sirt6 is also revealed to deacetylase H3K9ac and H3K56ac to modulate telomeric chromatic, with a low deacetylase activity compared to other sirtuins (Liszt et al., 2005; Michishita et al., 2008). Sirt7 is a highly selective H3K18ac deacetylase for maintaining cellular transformation (Barber et al., 2012b). And it is also described that DNA methylation and histones modifications are mutually regulated during mammalian development (Cedar and Bergman, 2009). It seems that DNA might provide a template for some histone modification and histone modification could promote or repress DNA methylation. The modifications of histone proteins are different on chromatin, including acetylation, methylation, phosphorylation, and ubiquitination. Among these modifications, acetylation of H3K18 disturbs DNA methylation, a highly stable silencing marker, and promotes gene expression.

4.3.2 Dysregulation of sirtuin proteins leads to metabolic-associated diseases

Recent work has shown that sirtuins regulate a variety of biological processes and crucial cellular functions including aging, metabolism, neurodegeneration, cancer, transcriptional silencing, genomic stability and progression of the cell cycle (Dali‐Youcef et al., 2007; Gan and Mucke, 2008; Haigis and Sinclair, 2010; Saunders LR, 2007). It is demonstrated that Sirt1 overexpression leads to disease syndromes, including diabetes, neurodegenerative diseases and inflammation, similar with the effect of Sirt1 activators like resveratrol and newer sirtuin activating compounds (STACs) in transgenic mice (Baur et al., 2006; Bordone et al., 2007; Herranz et al., 2010; Howitz et al., 2003; Lagouge et al., 2006; Milne et al., 2007; Pfluger et al., 2008). Deletion of Sirt1 in mice also leads to metabolic dysfunction (Chalkiadaki and Guarente, 2012).

Overexpression of Sirt2 significantly affects energy metabolism via regulation of glycolytic enzymes including phosphoglycerate kinase, glyceraldehyde-3-phosphate dehydrogenase, and enolase (Cha et al., 2017). The role of Sirt6 in the regulation of cardiac metabolism is linked with the FOXO-mediated transcription of PDK4 in the heart of Sirt6 deficiency (Khan et al., 2018). It is also demonstrated that Sirt6 controls the multiple glycolytic genes as a histone H3K9 deacetylase and a co-repressor of the transcription factor Hif1 alpha (Zhong et al., 2010a). Sirt7 positively regulate fatty acid uptake and triglyceride synthesis in lipid metabolism by increasing the expression of TR4/TAK1 and binding the DCAF1/DDB1/CUL4B complex to disturb its degradation (Michan and Sinclair, 2007).

My work on sirtuins also points out that four sirtuins, Sirt1, Sirt2, Sirt6, and Sirt7, can corporately regulate metabolism, especially glycolysis, via the transcriptional factor, Hif1a. In my study, I have discovered that these four sirtuins transcriptionally repress metabolism-associated genes by deacetylating H3K18ac with the Hif1a. Specifically, sirtuins directly interact with Hif1a and deacetylate H3K18ac, which, at one hand, dissociates the complex of p300/CBP with Hif1a, and in the other hand, increases DNA methylation level on these genes' promoters (**Figure 3**). P300/CBP is a histone acetylase for H3K18 and has been reported to regulate metabolism by interacting with Hif1a.

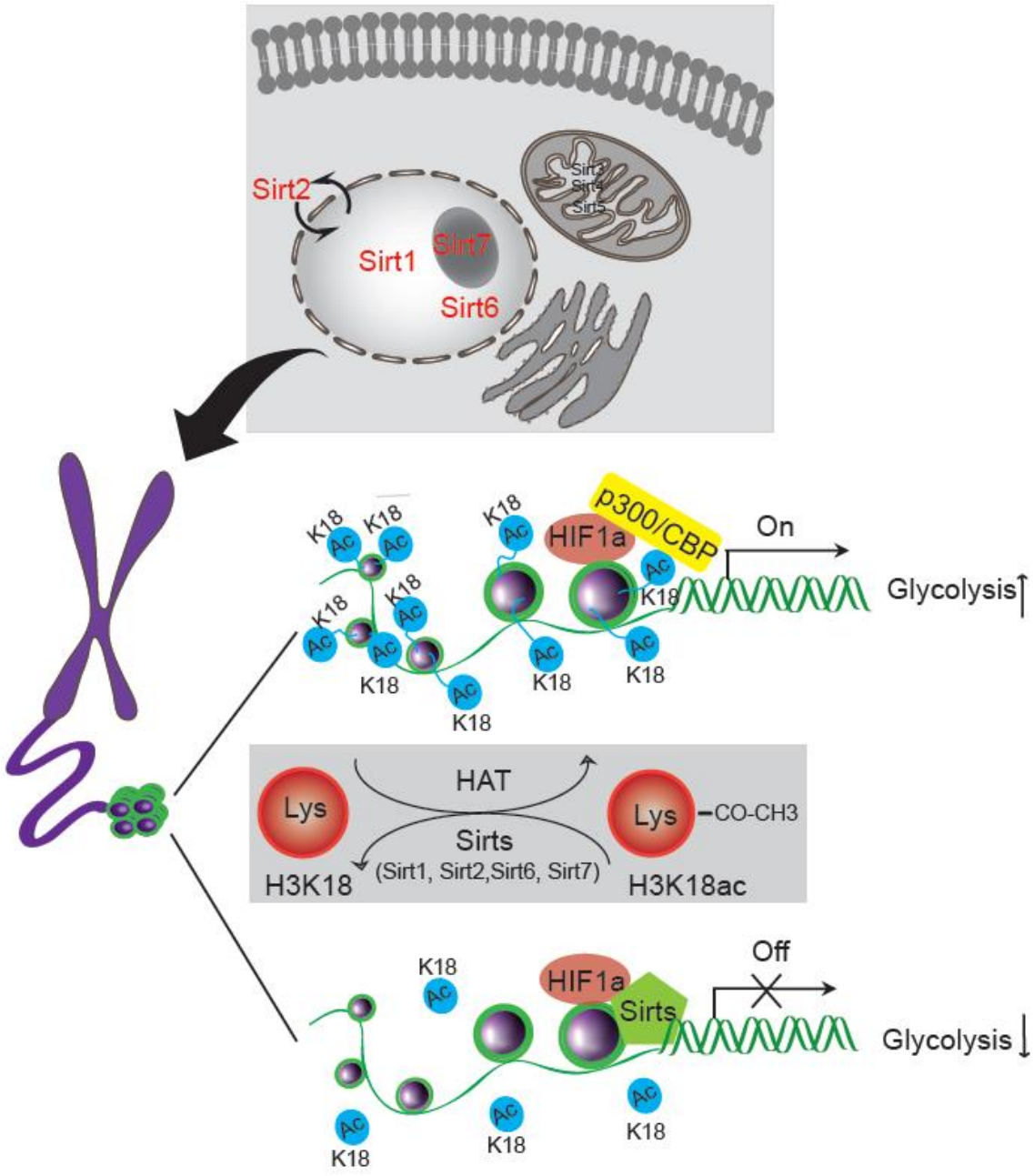

Figure 3 Model of the effect of Sirtuin proteins on metabolism. Sirt1, Sirt2, Sirt6, and Sirt7 are distributed in the nuclear and inhibit metabolism, mainly glycolysis, by deacetylating H3K18ac and interacting with Hif1a. In contrast, histone acetylase p300/CBP can acetylate H3K18ac and bind Hif1a to activate metabolism-related genes, therefore promoting glycolysis process.

For other sirtuins, I do not detect any changes of H3K18ac level in cells overexpressing the mitochondrial Sirt3, Sirt4, and Sirt5. But few publications have reported Sirt3 is also capable of histone deacetylase activity for H3K9ac and H4K16ac, while Sirt4 and Sirt5 do not deacetylase histones in the mitochondria (Iwahara et al., 2012). Moreover, Sirt3 and Sirt5 have been proved to regulate the urea cycle. Deletion of Sirt3 or Sirt5 shows a defect in the up-regulation of the urea cycle (Hallows et al., 2011; Nakagawa et al., 2009).

5 ANNEX

5.1 References

Achour, M., Fuhrmann, G., Alhosin, M., Rondé, P., Chataigneau, T., Mousli, M., Schini-Kerth, V.B., and Bronner, C. (2009). UHRF1 recruits the histone acetyltransferase Tip60 and controls its expression and activity. Biochemical and Biophysical Research Communications *390*, 523-528.

Ahuja, N., Schwer, B., Carobbio, S., Waltregny, D., North, B.J., Castronovo, V., Maechler, P., and Verdin, E. (2007). Regulation of insulin secretion by SIRT4, a mitochondrial ADP-ribosyltransferase. Journal of Biological Chemistry *282*, 33583-33592.

Akimaru, H., Chen, Y., Dai, P., Hou, D.-X., Nonaka, M., Smolik, S.M., Armstrong, S., Goodman, R.H., and Ishii, S. (1997). Drosophila CBP is a co-activator of cubitus interruptus in hedgehog signalling. Nature *386*, 735.

Allfrey, V.G., Faulkner, R., and Mirsky, A.E. (1964). Acetylation and methylation of histones and their possible role in the regulation of RNA synthesis. Proceedings of the National Academy of Sciences of the United States of America *51*, 786-794.

Andersen, J.S., Lam, Y.W., Leung, A.K.L., Ong, S.-E., Lyon, C.E., Lamond, A.I., and Mann, M. (2005). Nucleolar proteome dynamics. Nature *433*, 77-83.

Anderson, R.M., Latorre-Esteves, M., Neves, A.R., Lavu, S., Medvedik, O., Taylor, C., Howitz, K.T., Santos, H., and Sinclair, D.A. (2003). Yeast life-span extension by calorie restriction is independent of NAD fluctuation. Science *302*, 2124-2126.

Arany, Z., Huang, L.E., Eckner, R., Bhattacharya, S., Jiang, C., Goldberg, M.A., Bunn, H.F., and Livingston, D.M. (1996). An essential role for p300/CBP in the cellular response to hypoxia. Proceedings of the National Academy of Sciences *93*, 12969.

Barber, M.F., Michishita-Kioi, E., Xi, Y., Tasselli, L., Kioi, M., Moqtaderi, Z., Tennen, R.I., Paredes, S., Young, N.L., Chen, K.*, et al.* (2012a). SIRT7 links H3K18 deacetylation to maintenance of oncogenic transformation. Nature *487*, 114.

Barber, M.F., Michishita-Kioi, E., Xi, Y., Tasselli, L., Kioi, M., Moqtaderi, Z., Tennen, R.I., Paredes, S., Young, N.L., Chen, K.*, et al.* (2012b). SIRT7 links H3K18 deacetylation to maintenance of oncogenic transformation. Nature *487*, 114-118.

Bashtrykov, P., Jankevicius, G., Jurkowska, R.Z., Ragozin, S., and Jeltsch, A. (2014). The UHRF1 protein stimulates the activity and specificity of the maintenance DNA methyltransferase DNMT1 by an allosteric mechanism. The Journal of Biological Chemistry *289*, 4106-4115.

Baur, J.A., Pearson, K.J., Price, N.L., Jamieson, H.A., Lerin, C., Kalra, A., Prabhu, V.V., Allard, J.S., Lopez-Lluch, G., Lewis, K.*, et al.* (2006). Resveratrol improves health and survival of mice on a high-calorie diet. Nature *444*, 337-342.

Bender, J. (2004). DNA methylation and epigenetics. Annual Review of Plant Biology *55*, 41-68.

Berkyurek, A.C., Suetake, I., Arita, K., Takeshita, K., Nakagawa, A., Shirakawa, M., and Tajima, S. (2013). The DNA methyltransferase Dnmt1 directly interacts with the SET and RING finger associated (SRA) domain of the multifunctional protein Uhrf1 to facilitate accession of the catalytic center to hemi-methylated DNA. Journal of Biological Chemistry *289*, 379-386.

Bird, A. (2002). DNA methylation patterns and epigenetic memory. Genes & Development *16*, 6-21.

Blau, H.M., Pavlath, G.K., Hardeman, E.C., Chiu, C.P., Silberstein, L., Webster, S.G., Miller, S.C., and Webster, C. (1985). Plasticity of the differentiated state. Science *230*, 758.

Boily, G., Seifert, E.L., Bevilacqua, L., He, X.H., Sabourin, G., Estey, C., Moffat, C., Crawford, S., Saliba, S., Jardine, K.*, et al.* (2008). Sirt1 regulates energy metabolism and response to caloric restriction in mice. PLoS One *3*, e1759.

Bonapace, I.M., Latella, L., Papait, R., Nicassio, F., Sacco, A., Muto, M., Crescenzi, M., and Di Fiore, P.P. (2002). Np95 is regulated by E1A during mitotic reactivation of terminally differentiated cells and is essential for S phase entry. The Journal of Cell Biology *157*, 909-914.

Bordone, L., Cohen, D., Robinson, A., Motta Maria, C., Van Veen, E., Czopik, A., Steele Andrew, D., Crowe, H., Marmor, S., Luo, J.*, et al.* (2007). SIRT1 transgenic mice show phenotypes resembling calorie restriction. Aging Cell *6*, 759-767.

Bostick, M., Kim, J.K., Estève, P.-O., Clark, A., Pradhan, S., and Jacobsen, S.E. (2007). UHRF1 plays a role in maintaining DNA methylation in mammalian cells. Science *317*, 1760.

Bronner, C., Fuhrmann, G., Chédin, F.L., Macaluso, M., and Dhe-Paganon, S. (2010). UHRF1 links the histone code and DNA methylation to ensure faithful epigenetic memory inheritance. Genetics & epigenetics *2009*, 29-36.

Bruzzone, S., Parenti, M.D., Grozio, A., Ballestrero, A., Bauer, I., Rio, A.D., and Nencioni, A. (2013). Rejuvenating sirtuins: the rise of a new family of cancer drug targets. Current Pharmaceutical Design *19*, 614-623.

Buler, M., Andersson, U., and Hakkola, J. (2016). Who watches the watchmen? Regulation of the expression and activity of sirtuins. The FASEB Journal *30*, 3942-3960.

Caito, S., Rajendrasozhan, S., Cook, S., Chung, S., Yao, H., Friedman, A.E., Brookes, P.S., and Rahman, I. (2010). SIRT1 is a redox-sensitive deacetylase that is post-translationally modified by oxidants and carbonyl stress. The FASEB Journal *24*, 3145-3159.

Callebaut, I., Courvalin, J.-C., and Mornon, J.-P. (1999). The BAH (bromo-adjacent homology) domain: a link between DNA methylation, replication and transcriptional regulation. FEBS Letters *446*, 189-193.

Cao, D., Wang, M., Qiu, X., Liu, D., Jiang, H., Yang, N., and Xu, R.-M. (2015). Structural basis for allosteric, substrate-dependent stimulation of SIRT1 activity by resveratrol. Genes & Development *29*, 1316-1325.

Casas-Delucchi, C., Van Bemmel, J., Haase, S., Herce, H., Nowak, D., Meilinger, D., Stear, J., Leonhardt, H., and Cristina Cardoso, M. (2011). Histone hypoacetylation is required to maintain late replication timing of constitutive heterochromatin, Vol 40.

Cea, M., Cagnetta, A., Adamia, S., Acharya, C., Tai, Y.-T., Fulciniti, M., Ohguchi, H., Munshi, A., Acharya, P., Bhasin, M.K.*, et al.* (2016). Evidence for a role of the histone deacetylase SIRT6 in DNA damage response of multiple myeloma cells. Blood *127*, 1138-1150.

Cedar, H., and Bergman, Y. (2009). Linking DNA methylation and histone modification: patterns and paradigms. Nat Rev Genet *10*, 295-304.

Cha, Y., Han, M.-J., Cha, H.-J., Zoldan, J., Burkart, A., Jung, J.H., Jang, Y., Kim, C.-H., Jeong, H.-C., Kim, B.-G.*, et al.* (2017). Metabolic control of primed human pluripotent stem cell fate and function by the miR-200c–SIRT2 axis. Nature cell biology *19*, 445-456.

Chalkiadaki, A., and Guarente, L. (2012). High-fat diet triggers inflammation-induced cleavage of SIRT1 in adipose tissue to promote metabolic dysfunction. Cell metabolism *16*, 180-188.
Chen, D., Steele, A.D., Lindquist, S., and Guarente, L. (2005). Increase in activity during calorie restriction requires Sirt1. Science *310*, 1641.

Chen, S., Seiler, J., Santiago-Reichelt, M., Felbel, K., Grummt, I., and Voit, R. (2013). Repression of RNA polymerase I upon stress is caused by inhibition of RNA-dependent deacetylation of PAF53 by SIRT7. Molecular Cell *52*, 303-313.

Chen, X., Liu, J., He, B., Li, Y., Liu, S., Wu, B., Wang, S., Zhang, S., Xu, X., and Wang, J. (2015). Vascular endothelial growth factor (VEGF) regulation by hypoxia inducible factor-1 alpha (HIF1A) starts and peaks during endometrial breakdown, not repair, in a mouse menstrual-like model. Human Reproduction *30*, 2160-2170.

Cheng, J., Yang, Y., Fang, J., Xiao, J., Zhu, T., Chen, F., Wang, P., Li, Z., Yang, H., and Xu, Y. (2013). Structural insight into coordinated recognition of trimethylated histone H3 lysine 9 (H3K9me3) by the plant homeodomain (PHD) and tandem tudor domain (TTD) of UHRF1 (ubiquitin-like, containing PHD and RING finger domains, 1) protein. The Journal of Biological Chemistry *288*, 1329-1339.

Cheng, X., and Blumenthal, R.M. (2008). Mammalian DNA methyltransferases: a structural perspective. Structure *16*, 341-350.

Choi, Y.H., Kim, H., Lee, S.H., Jin, Y.-H., and Lee, K.Y. (2014). Src regulates the activity of SIRT2. Biochemical and Biophysical Research Communications *450*, 1120-1125.

Csibi, A., Fendt, S.-M., Li, C., Poulogiannis, G., Choo, A.Y., Chapski, D.J., Jeong, S.M., Dempsey, J., Parkhitko, A., Morrison, T.*, et al.* (2013). The mTORC1 pathway stimulates glutamine metabolism and cell proliferation by repressing SIRT4. Cell *153*, 840-854.

D'Aiuto, L., Marzulli, M., Mohan, K.N., Borowczyk, E., Saporiti, F., VanDemark, A., and Chaillet, J.R. (2010). Dissection of structure and function of the N-terminal domain of mouse DNMT1 using regional frame-shift mutagenesis. PLoS One *5*, e9831.

Dali-Youcef, N., Lagouge, M., Froelich, S., Koehl, C., Schoonjans, K., and Auwerx, J. (2007). Sirtuins: The 'magnificent seven', function, metabolism and longevity. Annals of Medicine *39*, 335-345.

Dambacher, S., Deng, W., Hahn, M., Sadic, D., Fröhlich, J., Nuber, A., Hoischen, C., Diekmann, S., Leonhardt, H., and Schotta, G. (2012). CENP-C facilitates the recruitment of M18BP1 to centromeric chromatin. Nucleus *3*, 101-110.

Davenport, A.M., Huber, F.M., and Hoelz, A. (2014). Structural and functional analysis of human SIRT1. Journal of molecular biology *426*, 526-541.

De Ruijter, A.J.M., van Gennip, A.H., Caron, H.N., Kemp, S., and van Kuilenburg, A.B.P. (2003). Histone deacetylases (HDACs): characterization of the classical HDAC family. Biochemical Journal *370*, 737-749.

Deng, J., and Szyf, M. (1999). Downregulation of DNA (cytosine-5-)methyltransferase is a late event in NGF-induced PC12 cell differentiation. Molecular Brain Research *71*, 23-31.

Denis, H., Ndlovu, M.N., and Fuks, F. (2011). Regulation of mammalian DNA methyltransferases: a route to new mechanisms. EMBO Reports *12*, 647-656.

Du, J., Jiang, H., and Lin, H. (2009). Investigating the ADP-ribosyltransferase activity of Sirtuins with NAD analogues and 32P-NAD. Biochemistry *48*, 2878-2890.

Du, J., Zhou, Y., Su, X., Yu, J.J., Khan, S., Jiang, H., Kim, J., Woo, J., Kim, J.H., Choi, B.H.*, et al.* (2011). Sirt5 is an NAD-dependent protein lysine demalonylase and desuccinylase. Science *334*, 806-809.

Du, Z., Song, J., Wang, Y., Zhao, Y., Guda, K., Yang, S., Kao, H.-Y., Xu, Y., Willis, J., Markowitz, S.D.*, et al.* (2010). DNMT1 stability is regulated by proteins coordinating deubiquitination and acetylation-driven ubiquitination. Science signaling *3*, ra80.

DuBridge, R.B., Tang, P., Hsia, H.C., Leong, P.M., Miller, J.H., and Calos, M.P. (1987). Analysis of mutation in human cells by using an Epstein-Barr virus shuttle system. Molecular and cellular biology *7*, 379-387.

Estève, P.-O., Chang, Y., Samaranayake, M., Upadhyay, A.K., Horton, J.R., Feehery, G.R., Cheng, X., and Pradhan, S. (2011). A methylation and phosphorylation switch between an adjacent lysine and serine determines human DNMT1 stability. Nature structural & molecular biology *18*, 42-48.

Estève, P.-O., Chin, H.G., Benner, J., Feehery, G.R., Samaranayake, M., Horwitz, G.A., Jacobsen, S.E., and Pradhan, S. (2009). Regulation of DNMT1 stability through SET7-mediated lysine methylation in mammalian cells. Proceedings of the National Academy of Sciences of the United States of America *106*, 5076-5081.

Fabrizio, P., Gattazzo, C., Battistella, L., Wei, M., Cheng, C., McGrew, K., and Longo, V.D. (2005). Sir2 blocks extreme life-span extension. Cell *123*, 655-667.

Fatemi, M., Hermann, A., Pradhan, S., and Jeltsch, A. (2001). The activity of the murine DNA methyltransferase Dnmt1 is controlled by interaction of the catalytic domain with the N-terminal part of the enzyme leading to an allosteric activation of the enzyme after binding to methylated DNA1 1Edited by J. Karn. Journal of Molecular Biology *309*, 1189-1199.

Finley, L.W.S., and Haigis, M.C. (2012). Metabolic regulation by SIRT3: implications for tumorigenesis. Trends in molecular medicine *18*, 516-523.

Fischle, W., Wang, Y., and Allis, C.D. (2003). Histone and chromatin cross-talk. Current Opinion in Cell Biology *15*, 172-183.

Flick, F., and Lüscher, B. (2012a). Regulation of sirtuin function by posttranslational modifications. Frontiers in Pharmacology *3*, 29.

Flick, F., and Lüscher, B. (2012b). Regulation of Sirtuin Function by Posttranslational Modifications, Vol 3.

Ford, E., Voit, R., Liszt, G., Magin, C., Grummt, I., and Guarente, L. (2006). Mammalian Sir2 homolog SIRT7 is an activator of RNA polymerase I transcription. Genes & Development *20*, 1075-1080.

Frauer, C., Rottach, A., Meilinger, D., Bultmann, S., Fellinger, K., Hasenöder, S., Wang, M., Qin, W., Söding, J., Spada, F.*, et al.* (2011a). Different binding properties and function of CXXC zinc finger domains in Dnmt1 and Tet1. PLoS One *6*, e16627.

Frauer, C., Rottach, A., Meilinger, D., Bultmann, S., Fellinger, K., Hasenöder, S., Wang, M., Qin, W., Söding, J., Spada, F.*, et al.* (2011b). Different binding properties and function of CXXC zinc finger domains in Dnmt1 and Tet1. PloS one *6*, 16627-16627.

Fujita, N., Watanabe, S., Ichimura, T., Tsuruzoe, S., Shinkai, Y., Tachibana, M., Chiba, T., and Nakao, M. (2003). Methyl-CpG binding domain 1 (MBD1) interacts with the Suv39h1-HP1 heterochromatic complex for DNA methylation-based transcriptional repression. Journal of Biological Chemistry *278*, 24132-24138.

Fuks, F., Hurd, P.J., Wolf, D., Nan, X., Bird, A.P., and Kouzarides, T. (2003). The methyl-CpG-binding protein MeCP2 links DNA methylation to histone methylation. Journal of Biological Chemistry *278*, 4035-4040.

Gamsjaeger, R., Liew, C.K., Loughlin, F.E., Crossley, M., and Mackay, J.P. (2007). Sticky fingers: zinc-fingers as protein-recognition motifs. Trends in Biochemical Sciences *32*, 63-70.

Gan, L., and Mucke, L. (2008). Paths of convergence: sirtuins in aging and neurodegeneration. Neuron *58*, 10-14.

Gao, L., Cueto, M.A., Asselbergs, F., and Atadja, P. (2002). Cloning and functional characterization of HDAC11, a novel member of the human histone deacetylase Family. Journal of Biological Chemistry *277*, 25748-25755.

Gasser, S.M., and Cockell, M.M. (2001). The molecular biology of the SIR proteins. Gene *279*, 1-16.

Ge, T.-T., Yang, M., Chen, Z., Lou, G., and Gu, T. (2016). UHRF1 gene silencing inhibits cell proliferation and promotes cell apoptosis in human cervical squamous cell carcinoma CaSki cells. Journal of Ovarian Research *9*, 42.

Gelato, Kathy A., Tauber, M., Ong, Michelle S., Winter, S., Hiragami-Hamada, K., Sindlinger, J., Lemak, A., Bultsma, Y., Houliston, S., Schwarzer, D.*, et al.* (2014). Accessibility of different histone H3-binding domains of UHRF1 is allosterically regulated by phosphatidylinositol 5-phosphate. Molecular Cell *54*, 905-919.

Goll, M.G., Kirpekar, F., Maggert, K.A., Yoder, J.A., Hsieh, C.-L., Zhang, X., Golic, K.G., Jacobsen, S.E., and Bestor, T.H. (2006). Methylation of $tRN^{Asp}$by the DNA Methyltransferase Homolog Dnmt2. Science *311*, 395.

Gomes, P., Fleming Outeiro, T., and Cavadas, C. (2015). Emerging role of Sirtuin 2 in the regulation of mammalian metabolism. Trends in Pharmacological Sciences *36*, 756-768.

Gopalakrishnan, S., Emburgh, B.O.V., and Robertson, K.D. (2008). DNA methylation in development and human disease. Mutation research *647*, 30-38.

Grozinger, C.M., Hassig, C.A., and Schreiber, S.L. (1999). Three proteins define a class of human histone deacetylases related to yeast Hda1p. Proceedings of the National Academy of Sciences of the United States of America *96*, 4868-4873.

Ha, K., Lee, G.E., Palii, S.S., Brown, K.D., Takeda, Y., Liu, K., Bhalla, K.N., and Robertson, K.D. (2011). Rapid and transient recruitment of DNMT1 to DNA double-strand breaks is mediated by its interaction with multiple components of the DNA damage response machinery. Human molecular genetics *20*, 126-140.

Haigis, M.C., and Guarente, L.P. (2006). Mammalian sirtuins—emerging roles in physiology, aging, and calorie restriction. Genes & Development *20*, 2913-2921.

Haigis, M.C., Mostoslavsky, R., Haigis, K.M., Fahie, K., Christodoulou, D.C., Murphy, Andrew J., Valenzuela, D.M., Yancopoulos, G.D., Karow, M., Blander, G.*, et al.* (2006). SIRT4 inhibits glutamate dehydrogenase and opposes the effects of calorie restriction in pancreatic beta cells. Cell *126*, 941-954.

Haigis, M.C., and Sinclair, D.A. (2010). Mammalian sirtuins: biological insights and disease relevance. Annual review of pathology *5*, 253-295.

Hall, T.M.T. (2005). Multiple modes of RNA recognition by zinc finger proteins. Current Opinion in Structural Biology *15*, 367-373.

Hallows, W.C., Lee, S., and Denu, J.M. (2006). Sirtuins deacetylate and activate mammalian acetyl-CoA synthetases. Proceedings of the National Academy of Sciences of the United States of America *103*, 10230-10235.

Hallows, W.C., Yu, W., Smith, B.C., Devries, M.K., Ellinger, J.J., Someya, S., Shortreed, M.R., Prolla, T., Markley, J.L., Smith, L.M.*, et al.* (2011). Sirt3 promotes the urea cycle and fatty acid oxidation during dietary restriction. Molecular cell *41*, 139-149.

Hanahan, D. (1983). Studies on transformation of Escherichia coli with plasmids. Journal of Molecular Biology *166*, 557-580.

Haraguchi, T., Oguro, M., Nagano, H., Ichihara, A., and Sakamura, S. (1983). Specific inhibitors of eukaryotic DNA synthesis and DNA polymerase alpha, 3-deoxyaphidicolin and aphidicolin-17-monoacetate. Nucleic Acids Research *11*, 1197-1209.

Hashimoto, H., Horton, J.R., Zhang, X., Bostick, M., Jacobsen, S.E., and Cheng, X. (2008). The SRA domain of UHRF1 flips 5-methylcytosine out of the DNA helix. Nature *455*, 826-829.

Herce, H.D., Deng, W., Helma, J., Leonhardt, H., and Cardoso, M.C. (2013). Visualization and targeted disruption of protein interactions in living cells. Nature Communications *4*, 2660.

Herranz, D., Cañamero, M., Mulero, F., Martinez-Pastor, B., Fernandez-Capetillo, O., and Serrano, M. (2010). Sirt1 improves healthy ageing and protects from metabolic syndrome-associated cancer syndrome. Nature communications *1*, 1-8.

Holde, K.E.v. (1989). Chromatin. Springer Series in Molecular Biology.

Hook, S.S., Orian, A., Cowley, S.M., and Eisenman, R.N. (2002). Histone deacetylase 6 binds polyubiquitin through its zinc finger (PAZ domain) and copurifies with deubiquitinating enzymes. Proceedings of the National Academy of Sciences of the United States of America *99*, 13425-13430.

Hopfner, R., Mousli, M., Jeltsch, J.-M., Voulgaris, A., Lutz, Y., Marin, C., Bellocq, J.-P., Oudet, P., and Bronner, C. (2000). ICBP90, a novel human CCAAT binding protein, involved in the regulation of topoisomerase IIα expression. Cancer Research *60*, 121-128.

Hotchkiss, R.D. (1948). The quantitative separation of purines, pyrimidines, and nucleosides by paper chromatography. Journal of Biological Chemistry *175*, 315-332.

Howitz, K.T., Bitterman, K.J., Cohen, H.Y., Lamming, D.W., Lavu, S., Wood, J.G., Zipkin, R.E., Chung, P., Kisielewski, A., Zhang, L.-L.*, et al.* (2003). Small molecule activators of sirtuins extend Saccharomyces cerevisiae lifespan. Nature *425*, 191-196.

Imai, S.-i., Armstrong, C.M., Kaeberlein, M., and Guarente, L. (2000). Transcriptional silencing and longevity protein Sir2 is an NAD-dependent histone deacetylase. Nature *403*, 795-800.

Inoue, T., Hiratsuka, M., Osaki, M., Yamada, H., Kishimoto, I., Yamaguchi, S., Nakano, S., Katoh, M., Ito, H., and Oshimura, M. (2006). SIRT2, a tubulin deacetylase, acts to block the entry to chromosome condensation in response to mitotic stress. Oncogene *26*, 945-957.

Ishiyama, S., Nishiyama, A., Saeki, Y., Moritsugu, K., Morimoto, D., Yamaguchi, L., Arai, N., Matsumura, R., Kawakami, T., Mishima, Y.*, et al.* (2017). Structure of the Dnmt1 reader module complexed with a unique two-mono-ubiquitin mark on histone H3 reveals the basis for DNA methylation maintenance. Molecular Cell *68*, 350-360.

Iwahara, T., Bonasio, R., Narendra, V., and Reinberg, D. (2012). SIRT3 functions in the nucleus in the control of stress-related gene expression. Molecular and cellular biology *32*, 5022-5034.

Jackson-Grusby, L., Beard, C., Possemato, R., Tudor, M., Fambrough, D., Csankovszki, G., Dausman, J., Lee, P., Wilson, C., Lander, E.*, et al.* (2001). Loss of genomic methylation causes p53-dependent apoptosis and epigenetic deregulation. Nature Genetics *27*, 31-39.

Jiang, H., Khan, S., Wang, Y., Charron, G., He, B., Sebastian, C., Du, J., Kim, R., Ge, E., Mostoslavsky, R.*, et al.* (2013). Sirt6 regulates TNFα secretion via hydrolysis of long chain fatty acyl lysine. Nature *496*, 110-113.

Jin, J., Iakova, P., Jiang, Y., Medrano, E.E., and Timchenko, N.A. (2011). The reduction of SIRT1 in livers of old mice leads to impaired body homeostasis and to inhibition of liver proliferation. Hepatology *54*, 989-998.

Jin, Y.-H., Kim, Y.-J., Kim, D.-W., Baek, K.-H., Kang, B.Y., Yeo, C.-Y., and Lee, K.-Y. (2008). Sirt2 interacts with 14-3-3 beta/gamma and down-regulates the activity of p53. Biochemical and biophysical research communications *368*, 690-695.

Kaeberlein, M., McVey, M., and Guarente, L. (1999). The SIR2/3/4 complex and SIR2 alone promote longevity in Saccharomyces cerevisiae by two different mechanisms. Genes & Development *13*, 2570-2580.

Kanfi, Y., Naiman, S., Amir, G., Peshti, V., Zinman, G., Nahum, L., Bar-Joseph, Z., and Cohen, H.Y. (2012). The sirtuin SIRT6 regulates lifespan in male mice. Nature *483*, 218-221.

Kar, S., Deb, M., Sengupta, D., Shilpi, A., Parbin, S., Torrisani, J., Pradhan, S., and Patra, S.K. (2012). An insight into the various regulatory mechanisms modulating human DNA methyltransferase 1 stability and function. Epigenetics *7*, 994-1007.

Khan, D., Sarikhani, M., Dasgupta, S., Maniyadath, B., Pandit, A.S., Mishra, S., Ahamed, F., Dubey, A., Fathma, N., Atreya, H.S.*, et al.* (2018). SIRT6 deacetylase transcriptionally regulates glucose metabolism in heart. Journal of Cellular Physiology *233*, 5478-5489.

Kilic, U., Gok, O., Bacaksiz, A., Izmirli, M., Elibol-Can, B., and Uysal, O. (2014). SIRT1 gene polymorphisms affect the protein expression in cardiovascular diseases. PLoS One *9*, e90428.

Kim, G.-D., Ni, J., Kelesoglu, N., Roberts, R.J., and Pradhan, S. (2002). Co-operation and communication between the human maintenance and de novo DNA (cytosine-5) methyltransferases. The EMBO Journal *21*, 4183-4195.

Kim, J.-w., Tchernyshyov, I., Semenza, G.L., and Dang, C.V. (2006). HIF-1-mediated expression of pyruvate dehydrogenase kinase: A metabolic switch required for cellular adaptation to hypoxia. Cell Metabolism *3*, 177-185.

Kim Jeong, K., Noh Ji, H., Jung Kwang, H., Eun Jung, W., Bae Hyun, J., Kim Min, G., Chang Young, G., Shen, Q., Park Won, S., Lee Jung, Y.*, et al.* (2012). Sirtuin7 oncogenic potential in human hepatocellular carcinoma and its regulation by the tumor suppressors MiR-125a-5p and MiR-125b. Hepatology *57*, 1055-1067.

Kinney, S.R.M., and Pradhan, S. (2011). Chapter 9 - Regulation of expression and activity of DNA (cytosine-5) methyltransferases in mammalian cells. In Progress in Molecular Biology and Translational Science, X. Cheng, and R.M. Blumenthal, eds. (Academic Press), pp. 311-333.

Klimasauskas, S., Kumar, S., Roberts, R.J., and Cheng, X. (1994). Hhal methyltransferase flips its target base out of the DNA helix. Cell *76*, 357-369.

Klug, A. (1999). Zinc finger peptides for the regulation of gene expression. Journal of Molecular Biology *293*, 215-218.

Kong, X., Wang, R., Xue, Y., Liu, X., Zhang, H., Chen, Y., Fang, F., and Chang, Y. (2010). Sirtuin 3, a new target of PGC-1α, plays an important role in the suppression of ROS and mitochondrial biogenesis. PLoS One *5*, e11707.

Koundrioukoff, S., Jónsson, Z.a.O., Hasan, S., de Jong, R.N., van der Vliet, P.C., Hottiger, M.O., and Hübscher, U. (2000). A direct interaction between proliferating cell nuclear antigen (PCNA) and Cdk2 targets PCNA-interacting proteins for phosphorylation. Journal of Biological Chemistry *275*, 22882-22887.

Kraus, W.L., and Kadonaga, J.T. (1998). p300 and estrogen receptor cooperatively activate transcription via differential enhancement of initiation and reinitiation. Genes & Development *12*, 331-342.

Lagouge, M., Argmann, C., Gerhart-Hines, Z., Meziane, H., Lerin, C., Daussin, F., Messadeq, N., Milne, J., Lambert, P., Elliott, P.*, et al.* (2006). Resveratrol Improves Mitochondrial Function and Protects against Metabolic Disease by Activating SIRT1 and PGC-1&#x3b1. Cell *127*, 1109-1122.

Laurent, G., German, N.J., Saha, A.K., de Boer, V.C.J., Davies, M., Koves, T.R., Dephoure, N., Fischer, F., Boanca, G., Vaitheesvaran, B.*, et al.* (2013). SIRT4 coordinates the balance between lipid synthesis and catabolism by repressing malonyl CoA decarboxylase. Molecular cell *50*, 686-698.

Lavoie, G., and St-Pierre, Y. (2011). Phosphorylation of human DNMT1: Implication of cyclin-dependent kinases. Biochemical and Biophysical Research Communications *409*, 187-192.

Lawrence, M., Daujat, S., and Schneider, R. (2015). Lateral thinking: how histone modifications regulate gene expression. Trends in Genetics *32*, 42-56.

Lee, Heather J., Hore, Timothy A., and Reik, W. (2014). Reprogramming the methylome: erasing memory and creating diversity. Cell Stem Cell *14*, 710-719.

Lehner, B., Crombie, C., Tischler, J., Fortunato, A., and Fraser, A.G. (2006). Systematic mapping of genetic interactions in Caenorhabditis elegans identifies common modifiers of diverse signaling pathways. Nature Genetics *38*, 896-903.

Lei, H., Oh, S.P., Okano, M., Juttermann, R., Goss, K.A., Jaenisch, R., and Li, E. (1996). De novo DNA cytosine methyltransferase activities in mouse embryonic stem cells. Development *122*, 3195.

Li, E., Bestor, T.H., and Jaenisch, R. (1992). Targeted mutation of the DNA methyltransferase gene results in embryonic lethality. Cell *69*, 915-926.

Li, L., Shi, L., Yang, S., Yan, R., Zhang, D., Yang, J., He, L., Li, W., Yi, X., Sun, L.*, et al.* (2016). SIRT7 is a histone desuccinylase that functionally links to chromatin compaction and genome stability. Nature Communications *7*, 12235.

Li L, Z.H., Chen HZ, Gao P, Zhu LH, Li HL, Lv X, Zhang QJ, Zhang R, Wang Z, She ZG, Zhang R, Wei YS, Du GH, Liu DP, Liang CC. (2011). SIRT1 acts as a modulator of neointima formation following vascular injury in mice. Circulation Research *108*, 1180-1189.

Li, S., Banck, M., Mujtaba, S., Zhou, M.-M., Sugrue, M.M., and Walsh, M.J. (2010). p53-induced growth arrest is regulated by the mitochondrial SirT3 deacetylase. PLoS One *5*, e10486.

Liang, C., Zhang, X., Song, S., Tian, C., Yin, Y., Xing, G., He, F., and Zhang, L. (2013). Identification of UHRF1/2 as new N-methylpurine DNA glycosylase-interacting proteins. Biochemical and Biophysical Research Communications *433*, 415-419.

Liang, F., Kume, S., and Koya, D. (2009). SIRT1 and insulin resistance. Nature Reviews Endocrinology *5*, 367-373.

Lin, Z., and Fang, D. (2013). The roles of SIRT1 in cancer. Genes & Cancer *4*, 97-104.

Lin, Z., Yang, H., Kong, Q., Li, J., Lee, S.-M., Gao, B., Dong, H., Wei, J., Song, J., Zhang, Donna D.*, et al.* (2012). USP22 antagonizes p53 transcriptional activation by deubiquitinating Sirt1 to suppress cell apoptosis and is required for mouse embryonic development. Molecular Cell *46*, 484-494.

Lister, R., Pelizzola, M., Dowen, R.H., Hawkins, R.D., Hon, G., Tonti-Filippini, J., Nery, J.R., Lee, L., Ye, Z., Ngo, Q.-M.*, et al.* (2009). Human DNA methylomes at base resolution show widespread epigenomic differences. Nature *462*, 315-322.

Liszt, G., Ford, E., Kurtev, M., and Guarente, L. (2005). Mouse Sir2 homolog SIRT6 is a nuclear ADP-ribosyltransferase. Journal of Biological Chemistry *280*, 21313-21320.

Liu, X., Gao, Q., Li, P., Zhao, Q., Zhang, J., Li, J., Koseki, H., and Wong, J. (2013). UHRF1 targets DNMT1 for DNA methylation through cooperative binding of hemi-methylated DNA and methylated H3K9. Nature Communications *4*, 1563.

Liu, X., Wang, D., Zhao, Y., Tu, B., Zheng, Z., Wang, L., Wang, H., Gu, W., Roeder, R.G., and Zhu, W.-G. (2011). Methyltransferase Set7/9 regulates p53 activity by interacting with Sirtuin 1 (SIRT1). Proceedings of the National Academy of Sciences of the United States of America *108*, 1925-1930.

Luger, K., Mäder, A.W., Richmond, R.K., Sargent, D.F., and Richmond, T.J. (1997). Crystal structure of the nucleosome core particle at 2.8 Å resolution. Nature *389*, 251.

Ma, R.-g., Zhang, Y., Sun, T.-t., and Cheng, B. (2014). Epigenetic regulation by polycomb group complexes: focus on roles of CBX proteins. Journal of Zhejiang University. Science. B *15*, 412-428.

Maier, A., Wu, H., Cordasic, N., Oefner, P., Dietel, B., Thiele, C., Weidemann, A., Eckardt, K.-U., and Warnecke, C. (2017). Hypoxia-inducible protein 2 Hig2/Hilpda mediates neutral lipid

accumulation in macrophages and contributes to atherosclerosis in apolipoprotein E–deficient mice. The FASEB Journal *31*, 4971-4984.

Maresca, A., Zaffagnini, M., Caporali, L., Carelli, V., and Zanna, C. (2015). DNA methyltransferase 1 mutations and mitochondrial pathology: is mtDNA methylated? Frontiers in Genetics *6*, 90.

Mastrogiannaki, M., Matak, P., Mathieu, J.R.R., Delga, S., Mayeux, P., Vaulont, S., and Peyssonnaux, C. (2012). Hepatic hypoxia-inducible factor-2 down-regulates hepcidin expression in mice through an erythropoietin-mediated increase in erythropoiesis. Haematologica *97*, 827-834.

Matsushima, S., and Sadoshima, J. (2015). The role of sirtuins in cardiac disease. American Journal of Physiology - Heart and Circulatory Physiology *309*, 1375-1389.

Matsushita, N., Yonashiro, R., Ogata, Y., Sugiura, A., Nagashima, S., Fukuda, T., Inatome, R., and Yanagi, S. (2011). Distinct regulation of mitochondrial localization and stability of two human Sirt5 isoforms. Genes to Cells *16*, 190-202.

Matthews, J.M., and Sunde, M. (2002). Zinc fingers--folds for many occasions. IUBMB Life *54*, 351-355.

Maxwell, M.M., Tomkinson, E.M., Nobles, J., Wizeman, J.W., Amore, A.M., Quinti, L., Chopra, V., Hersch, S.M., and Kazantsev, A.G. (2011). The Sirtuin 2 microtubule deacetylase is an abundant neuronal protein that accumulates in the aging CNS. Human Molecular Genetics *20*, 3986-3996.

Meilinger, D., Fellinger, K., Bultmann, S., Rothbauer, U., Bonapace, I.M., Klinkert, W.E.F., Spada, F., and Leonhardt, H. (2009). Np95 interacts with de novo DNA methyltransferases, Dnmt3a and Dnmt3b, and mediates epigenetic silencing of the viral CMV promoter in embryonic stem cells. EMBO reports *10*, 1259-1264.

Michan, S., and Sinclair, D. (2007). Sirtuins in mammals: insights into their biological function. The Biochemical journal *404*, 1-13.

Michishita, E., McCord, R.A., Berber, E., Kioi, M., Padilla-Nash, H., Damian, M., Cheung, P., Kusumoto, R., Kawahara, T.L.A., Barrett, J.C.*, et al.* (2008). SIRT6 is a histone H3 lysine 9 deacetylase that modulates telomeric chromatin. Nature *452*, 492-496.

Michishita, E., Park, J.Y., Burneskis, J.M., Barrett, J.C., and Horikawa, I. (2005). Evolutionarily conserved and nonconserved cellular localizations and functions of human SIRT proteins. Molecular Biology of the Cell *16*, 4623-4635.

Milne, J.C., Lambert, P.D., Schenk, S., Carney, D.P., Smith, J.J., Gagne, D.J., Jin, L., Boss, O., Perni, R.B., Vu, C.B.*, et al.* (2007). Small molecule activators of SIRT1 as therapeutics for the treatment of type 2 diabetes. Nature *450*, 712-716.

Mizuno, S.-i., Chijiwa, T., Okamura, T., Akashi, K., Fukumaki, Y., Niho, Y., and Sasaki, H. (2001). Expression of DNA methyltransferases DNMT1, 3A, and 3B in normal hematopoiesis and in acute and chronic myelogenous leukemia. Blood *97*, 1172-1179.

Mole, D.R., Blancher, C., Copley, R.R., Pollard, P.J., Gleadle, J.M., Ragoussis, J., and Ratcliffe, P.J. (2009). Genome-wide association of hypoxia-inducible factor (HIF)-1α and HIF-2α DNA binding with expression profiling of hypoxia-inducible transcripts. Journal of Biological Chemistry *284*, 16767-16775.

Mortusewicz, O., Schermelleh, L., Walter, J., Cardoso, M.C., and Leonhardt, H. (2005). Recruitment of DNA methyltransferase I to DNA repair sites. Proceedings of the National Academy of Sciences of the United States of America *102*, 8905-8909.

Mostoslavsky, R., Chua, K.F., Lombard, D.B., Pang, W.W., Fischer, M.R., Gellon, L., Liu, P., Mostoslavsky, G., Franco, S., Murphy, M.M.*, et al.* (2006). Genomic instability and aging-like phenotype in the absence of mammalian SIRT6. Cell *124*, 315-329.

Mousli, M., Hopfner, R., Abbady, A.Q., Monté, D., Jeanblanc, M., Oudet, P., Louis, B., and Bronner, C. (2003). ICBP90 belongs to a new family of proteins with an expression that is deregulated in cancer cells. British Journal of Cancer *89*, 120-127.

Mulholland, C.B., Smets, M., Schmidtmann, E., Leidescher, S., Markaki, Y., Hofweber, M., Qin, W., Manzo, M., Kremmer, E., Thanisch, K.*, et al.* (2015). A modular open platform for systematic functional studies under physiological conditions. Nucleic Acids Research *43*, e112.

Nakagawa, T., Lomb, D.J., Haigis, M.C., and Guarente, L. (2009). SIRT5 deacetylates carbamoyl phosphate synthetase 1 and regulates the urea cycle. Cell *137*, 560-570.

Nasrin, N., Wu, X., Fortier, E., Feng, Y., Bare, O.C., Chen, S., Ren, X., Wu, Z., Streeper, R.S., and Bordone, L. (2010). SIRT4 regulates fatty acid oxidation and mitochondrial gene expression in liver and muscle cells. The Journal of Biological Chemistry *285*, 31995-32002.

Nishiyama, A., Yamaguchi, L., Sharif, J., Johmura, Y., Kawamura, T., Nakanishi, K., Shimamura, S., Arita, K., Kodama, T., Ishikawa, F.*, et al.* (2013). Uhrf1-dependent H3K23 ubiquitylation couples maintenance DNA methylation and replication. Nature *502*, 249-253.

Noriega, L.G., Feige, J.N., Canto, C., Yamamoto, H., Yu, J., Herman, M.A., Mataki, C., Kahn, B.B., and Auwerx, J. (2011). CREB and ChREBP oppositely regulate SIRT1 expression in response to energy availability. EMBO reports *12*, 1069-1076.

North, B.J., Marshall, B.L., Borra, M.T., Denu, J.M., and Verdin, E. (2003). The human Sir2 ortholog, SIRT2, is an NAD^+-dependent tubulin deacetylase. Molecular Cell *11*, 437-444.

O'Gara, M., Klimaŝauskas, S., Roberts, R.J., and Cheng, X. (1996a). Enzymatic C5-cytosine methylation of DNA: mechanistic implications of new crystal structures for HhaI methyltransferase-DNA-AdoHcy complexes. Journal of Molecular Biology *261*, 634-645.

O'Gara, M., Roberts, R.J., and Cheng, X. (1996b). A structural basis for the preferential binding of hemimethylated DNA by HhaI DNA methyltransferase. Journal of Molecular Biology *263*, 597-606.

Ogura, M., Nakamura, Y., Tanaka, D., Zhuang, X., Fujita, Y., Obara, A., Hamasaki, A., Hosokawa, M., and Inagaki, N. (2010). Overexpression of SIRT5 confirms its involvement in

deacetylation and activation of carbamoyl phosphate synthetase 1. Biochemical and Biophysical Research Communications *393*, 73-78.

Okano, M., Bell, D.W., Haber, D.A., and Li, E. (1999). DNA methyltransferases Dnmt3a and Dnmt3b are essential for *de novo* methylation and mammalian development. Cell *99*, 247-257.

Okano, M., Xie, S., and Li, E. (1998). Cloning and characterization of a family of novel mammalian DNA (cytosine-5) methyltransferases. Nature Genetics *19*, 219-220.

Onyango, P., Celic, I., McCaffery, J.M., Boeke, J.D., and Feinberg, A.P. (2002). SIRT3, a human SIR2 homologue, is an NAD- dependent deacetylase localized to mitochondria. Proceedings of the National Academy of Sciences of the United States of America *99*, 13653-13658.

Ooi, S.K.T., Qiu, C., Bernstein, E., Li, K., Jia, D., Yang, Z., Erdjument-Bromage, H., Tempst, P., Lin, S.-P., Allis, C.D.*, et al.* (2007). DNMT3L connects unmethylated lysine 4 of histone H3 to de novo methylation of DNA. Nature *448*, 714-717.

Opitz, C.A., and Heiland, I. (2015). Dynamics of NAD-metabolism: everything but constant. Biochemical Society Transactions *43*, 1127.

Peng, L., Ling, H., Yuan, Z., Fang, B., Bloom, G., Fukasawa, K., Koomen, J., Chen, J., Lane, W.S., and Seto, E. (2012). SIRT1 negatively regulates the activities, functions, and protein levels of hMOF and TIP60. Molecular and Cellular Biology *32*, 2823-2836.

Peng, L., Yuan, Z., Li, Y., Ling, H., Izumi, V., Fang, B., Fukasawa, K., Koomen, J., Chen, J., and Seto, E. (2015). Ubiquitinated Sirtuin 1 (SIRT1) function is modulated during DNA damage-induced cell death and survival. The Journal of Biological Chemistry *290*, 8904-8912.

Peng, L., Yuan, Z., Ling, H., Fukasawa, K., Robertson, K., Olashaw, N., Koomen, J., Chen, J., Lane, W.S., and Seto, E. (2011). SIRT1 deacetylates the DNA methyltransferase 1 (DNMT1) protein and alters its activities. Molecular and cellular biology *31*, 4720-4734.

Perrod, S., Cockell, M.M., Laroche, T., Renauld, H., Ducrest, A.-L., Bonnard, C., and Gasser, S.M. (2001). A cytosolic NAD-dependent deacetylase, Hst2p, can modulate nucleolar and telomeric silencing in yeast. The EMBO Journal *20*, 197-209.

Pfluger, P.T., Herranz, D., Velasco-Miguel, S., Serrano, M., and Tschöp, M.H. (2008). Sirt1 protects against high-fat diet-induced metabolic damage. Proceedings of the National Academy of Sciences of the United States of America *105*, 9793-9798.

Poulose, N., and Raju, R. (2015). Sirtuin regulation in aging and injury. Biochimica et biophysica acta *1852*, 2442-2455.

Pradhan, S., and Kim, G.-D. (2002). The retinoblastoma gene product interacts with maintenance human DNA (cytosine-5) methyltransferase and modulates its activity. The EMBO Journal *21*, 779-788.

Probst, A.V., Dunleavy, E., and Almouzni, G. (2009). Epigenetic inheritance during the cell cycle. Nature Reviews Molecular Cell Biology *10*, 192-206.

Qian, W., Miki, D., Zhang, H., Liu, Y., Zhang, X., Tang, K., Kan, Y., La, H., Li, X., Li, S.*, et al.* (2012). A histone acetyltransferase regulates active DNA demethylation in *Arabidopsis*. Science (New York, N.Y.) *336*, 1445-1448.

Qin, W., Leonhardt, H., and Pichler, G. (2011a). Regulation of DNA methyltransferase 1 by interactions and modifications. Nucleus *2*, 392-402.

Qin, W., Leonhardt, H., and Spada, F. (2010). Usp7 and Uhrf1 control ubiquitination and stability of the maintenance DNA methyltransferase Dnmt1. Journal of Cellular Biochemistry *112*, 439-444.

Qin, W., Wolf, P., Liu, N., Link, S., Smets, M., Mastra, F.L., Forné, I., Pichler, G., Hörl, D., Fellinger, K.*, et al.* (2015a). DNA methylation requires a DNMT1 ubiquitin interacting motif (UIM) and histone ubiquitination. Cell Research *25*, 911-929.

Qin, W., Wolf, P., Liu, N., Link, S., Smets, M., Mastra, F.L., Forné, I., Pichler, G., Hörl, D., Fellinger, K.*, et al.* (2015b). DNA methylation requires a DNMT1 ubiquitin interacting motif (UIM) and histone ubiquitination. Cell Research *25*, 911-929.

Qin, Y., Wang, J., Gong, W., Zhang, M., Tang, Z., Zhang, J., and Quan, Z. (2014). UHRF1 depletion suppresses growth of gallbladder cancer cells through induction of apoptosis and cell cycle arrest. Oncol Rep *31*, 2635-2643.

RA, F. (2000). Phylogenetic classification of prokaryotic and eukaryotic Sir2-like proteins. Biochem Biophys Res Commun *273*, 793-798.

Radhakrishnan, I., Pérez-Alvarado, G.C., Parker, D., Dyson, H.J., Montminy, M.R., and Wright, P.E. (1999). Structural analyses of CREB-CBP transcriptional activator-coactivator complexes by NMR spectroscopy: implications for mapping the boundaries of structural domains11Edited by F. E. Cohen. Journal of Molecular Biology *287*, 859-865.

Rai, E., Sharma, S., Kaul, S., Jain, K., Matharoo, K., Bhanwer, A.S., and Bamezai, R.N.K. (2012). The interactive effect of SIRT1 promoter region polymorphism on type 2 diabetes susceptibility in the north Indian population. PLoS One *7*, e48621.

Razin, A., and Cedar, H. (1993). DNA methylation and embryogenesis. In DNA Methylation: Molecular Biology and Biological Significance, J.-P. Jost, and H.-P. Saluz, eds. (Basel: Birkhäuser Basel), pp. 343-357.

Razin, A., and Riggs, A.D. (1980). DNA methylation and gene function. Science *210*, 604.
Richmond, T.J., and Davey, C.A. (2003). The structure of DNA in the nucleosome core. Nature *423*, 145-150.

Riggs, A.D. (1975). X inactivation, differentiation, and DNA methylation. Cytogenetics and cell genetics *14*, 9-25.

Robert, M.-F., Morin, S., Beaulieu, N., Gauthier, F., Chute, I.C., Barsalou, A., and MacLeod, A.R. (2002). DNMT1 is required to maintain CpG methylation and aberrant gene silencing in human cancer cells. Nature Genetics *33*, 61-65.

Roberts, R.J., and Cheng, X. (1998). Base Flipping. Annual Review of Biochemistry *67*, 181-198.

Robertson, K.D., Keyomarsi, K., Gonzales, F.A., Velicescu, M., and Jones, P.A. (2000). Differential mRNA expression of the human DNA methyltransferases (DNMTs) 1, 3a and 3b during the G(0)/G(1) to S phase transition in normal and tumor cells. Nucleic Acids Research *28*, 2108-2113.

Roessler, C., Tüting, C., Meleshin, M., Steegborn, C., and Schutkowski, M. (2015). A novel continuous assay for the deacylase Sirtuin 5 and other deacetylases. Journal of Medicinal Chemistry *58*, 7217-7223.

Rose, N.R., and Klose, R.J. (2014). Understanding the relationship between DNA methylation and histone lysine methylation. Biochimica et Biophysica Acta (BBA) - Gene Regulatory Mechanisms *1839*, 1362-1372.

Roth, S.Y., Denu, J.M., and Allis, C.D. (2001). Histone acetyltransferases. Annual Review of Biochemistry *70*, 81-120.

Rothbauer, U., Zolghadr, K., Muyldermans, S., Schepers, A., Cardoso, M.C., and Leonhardt, H. (2008). A versatile nanotrap for biochemical and functional studies with fluorescent fusion proteins. Molecular & Cellular Proteomics *7*, 282-289.

Rottach, A., Frauer, C., Pichler, G., Bonapace, I.M., Spada, F., and Leonhardt, H. (2010). The multi-domain protein Np95 connects DNA methylation and histone modification. Nucleic acids research *38*, 1796-1804.

Sarraf, S.A., and Stancheva, I. (2004). Methyl-CpG binding protein MBD1 couples histone H3 methylation at lysine 9 by SETDB1 to DNA replication and chromatin assembly. Molecular Cell *15*, 595-605.

Sasaki, T., Maier, B., Koclega, K.D., Chruszcz, M., Gluba, W., Stukenberg, P.T., Minor, W., and Scrable, H. (2008). Phosphorylation regulates SIRT1 function. PLoS One *3*, e4020.

Saunders LR, V.E. (2007). Sirtuins: critical regulators at the crossroads between cancer and aging. Oncogene *26*, 5489-5504.

Schermelleh, L., Haemmer, A., Spada, F., Rösing, N., Meilinger, D., Rothbauer, U., Cardoso, M.C., and Leonhardt, H. (2007). Dynamics of Dnmt1 interaction with the replication machinery and its role in postreplicative maintenance of DNA methylation. Nucleic Acids Research *35*, 4301-4312.

Schermelleh, L., Spada, F., Easwaran, H.P., Zolghadr, K., Margot, J.B., Cardoso, M.C., and Leonhardt, H. (2005). Trapped in action: direct visualization of DNA methyltransferase activity in living cells. Nature Methods *2*, 751-756.

Schlicker, C., Gertz, M., Papatheodorou, P., Kachholz, B., Becker, C.F.W., and Steegborn, C. (2008). Substrates and regulation mechanisms for the human mitochondrial sirtuins Sirt3 and Sirt5. Journal of Molecular Biology *382*, 790-801.

Schumacker, P.T. (2011). SIRT3 controls cancer metabolic reprogramming by regulating ROS and HIF. Cancer cell *19*, 299-300.

Schwer, B., Bunkenborg, J., Verdin, R.O., Andersen, J.S., and Verdin, E. (2006). Reversible lysine acetylation controls the activity of the mitochondrial enzyme acetyl-CoA synthetase 2. Proceedings of the National Academy of Sciences of the United States of America *103*, 10224-10229.

Scott, A., Song, J., Ewing, R., and Wang, Z. (2014). Regulation of protein stability of DNA methyltransferase 1 by post-translational modifications. Acta Biochimica et Biophysica Sinica *46*, 199-203.

Sebastián, C., Zwaans, B.M.M., Silberman, D.M., Gymrek, M., Goren, A., Zhong, L., Ram, O., Truelove, J., Guimaraes, A.R., Toiber, D*., et al.* (2012). The histone deacetylase Sirt6 is a novel tumor suppressor that controls cancer metabolism. Cell *151*, 1185-1199.

Semenza, G.L., Roth, P.H., Fang, H.M., and Wang, G.L. (1994). Transcriptional regulation of genes encoding glycolytic enzymes by hypoxia-inducible factor 1. Journal of Biological Chemistry *269*, 23757-23763.

Serrano, L., Martínez-Redondo, P., Marazuela-Duque, A., Vazquez, B.N., Dooley, S.J., Voigt, P., Beck, D.B., Kane-Goldsmith, N., Tong, Q., Rabanal, R.M*., et al.* (2013). The tumor suppressor SirT2 regulates cell cycle progression and genome stability by modulating the mitotic deposition of H4K20 methylation. Genes & Development *27*, 639-653.

Sharif, J., Muto, M., Takebayashi, S.-i., Suetake, I., Iwamatsu, A., Endo, T.A., Shinga, J., Mizutani-Koseki, Y., Toyoda, T., Okamura, K*., et al.* (2007). The SRA protein Np95 mediates epigenetic inheritance by recruiting Dnmt1 to methylated DNA. Nature *450*, 908-912.

Shevchenko, A., Chernushevich, I., Wilm, M., and Mann, M. (2000). De Novo Peptide Sequencing by Nanoelectrospray Tandem Mass Spectrometry Using Triple Quadrupole and Quadrupole/Time-of-Flight Instruments. In Mass spectrometry of proteins and peptides: mass spectrometry of proteins and peptides, J.R. Chapman, ed. (Totowa, NJ: Humana Press), pp. 1-16.

Sidorova-Darmos, E., Wither, R.G., Shulyakova, N., Fisher, C., Ratnam, M., Aarts, M., Lilge, L., Monnier, P.P., and Eubanks, J.H. (2014). Differential expression of sirtuin family members in the developing, adult, and aged rat brain. Frontiers in Aging Neuroscience *6*, 333.

Song, J., Rechkoblit, O., Bestor, T.H., and Patel, D.J. (2011). Structure of DNMT1-DNA complex reveals a role for autoinhibition in maintenance DNA methylation. Science *331*, 1036-1040.

Sporbert, A., Domaing, P., Leonhardt, H., and Cardoso, M.C. (2005). PCNA acts as a stationary loading platform for transiently interacting Okazaki fragment maturation proteins. Nucleic acids research *33*, 3521-3528.

Sterner, D.E., and Berger, S.L. (2000). Acetylation of histones and transcription-related factors. Microbiology and Molecular Biology Reviews *64*, 435-459.

Studier, F.W., and Moffatt, B.A. (1986). Use of bacteriophage T7 RNA polymerase to direct selective high-level expression of cloned genes. Journal of Molecular Biology *189*, 113-130.

Sundaresan, N.R., Gupta, M., Kim, G., Rajamohan, S.B., Isbatan, A., and Gupta, M.P. (2009). Sirt3 blocks the cardiac hypertrophic response by augmenting Foxo3a-dependent antioxidant defense mechanisms in mice. The Journal of Clinical Investigation *119*, 2758-2771.

Sundaresan, N.R., Samant, S.A., Pillai, V.B., Rajamohan, S.B., and Gupta, M.P. (2008). SIRT3 Is a stress-responsive deacetylase in cardiomyocytes that protects cells from stress-mediated cell death by deacetylation of Ku70. Molecular and Cellular Biology *28*, 6384-6401.

Suzuki, M.M., and Bird, A. (2008). DNA methylation landscapes: provocative insights from epigenomics. Nature Reviews Genetics *9*, 465-476.

Svedružić, Ž.M. (2011). Chapter 6 - Dnmt1: structure and function. In Progress in Molecular Biology and Translational Science, X. Cheng, and R.M. Blumenthal, eds. (Academic Press), pp. 221-254.

Tan, M., Peng, C., Anderson, Kristin A., Chhoy, P., Xie, Z., Dai, L., Park, J., Chen, Y., Huang, H., Zhang, Y.*, et al.* (2014). Lysine glutarylation is a protein posttranslational modification regulated by SIRT5. Cell Metabolism *19*, 605-617.

Tanno, M., Sakamoto, J., Miura, T., Shimamoto, K., and Horio, Y. (2007). Nucleocytoplasmic shuttling of the NAD+-dependent histone deacetylase SIRT1. Journal of Biological Chemistry *282*, 6823-6832.

Tasselli, L., Xi, Y., Zheng, W., Tennen, R.I., Odrowaz, Z., Simeoni, F., Li, W., and Chua, K.F. (2016). SIRT6 deacetylates H3K18ac at pericentric chromatin to prevent mitotic errors and cellular senescence. Nature Structural &Amp; Molecular Biology *23*, 434-440.

Taubert, S., Gorrini, C., Frank, S.R., Parisi, T., Fuchs, M., Chan, H.-M., Livingston, D.M., and Amati, B. (2004). E2F-dependent histone acetylation and recruitment of the Tip60 acetyltransferase complex to chromatin in late G(1). Molecular and Cellular Biology *24*, 4546-4556.

Taylor, D.M., Maxwell, M.M., Luthi-Carter, R., and Kazantsev, A.G. (2008). Biological and potential therapeutic roles of Sirtuin deacetylases. Cellular and Molecular Life Sciences *65*, 4000-4018.

Tsukamoto, T., Hashiguchi, N., Janicki, S.M., Tumbar, T., Belmont, A.S., and Spector, D.L. (2000). Visualization of gene activity in living cells. Nature Cell Biology *2*, 871-878.

Unoki, M., Kelly, J.D., Neal, D.E., Ponder, B.A.J., Nakamura, Y., and Hamamoto, R. (2009a). UHRF1 is a novel molecular marker for diagnosis and the prognosis of bladder cancer. British Journal of Cancer *101*, 98-105.

Unoki, M., Kelly, J.D., Neal, D.E., Ponder, B.A.J., Nakamura, Y., and Hamamoto, R. (2009b). UHRF1 is a novel molecular marker for diagnosis and the prognosis of bladder cancer. British Journal Of Cancer *101*, 98.

Vanyushin, B.F. (2006). DNA methylation in plants. Curr. Top. Microbiol. Immunol *301*, 67-122.

Vaquero, A., Scher, M., Lee, D., Erdjument-Bromage, H., Tempst, P., and Reinberg, D. (2004). Human Sirt1 interacts with histone H1 and promotes formation of facultative heterochromatin. Molecular Cell *16*, 93-105.

Vaquero, A., Scher, M.B., Lee, D.H., Sutton, A., Cheng, H.-L., Alt, F.W., Serrano, L., Sternglanz, R., and Reinberg, D. (2006). SirT2 is a histone deacetylase with preference for histone H4 Lys 16 during mitosis. Genes & Development *20*, 1256-1261.

Venza, M., Visalli, M., Biondo, C., Oteri, R., Agliano, F., Morabito, S., Teti, D., and Venza, I. (2015). Epigenetic marks responsible for cadmium-induced melanoma cell overgrowth. Toxicology in Vitro *29*, 242-250.

Viré, E., Brenner, C., Deplus, R., Blanchon, L., Fraga, M., Didelot, C., Morey, L., Van Eynde, A., Bernard, D., Vanderwinden, J.-M*., et al.* (2006). The Polycomb group protein EZH2 directly controls DNA methylation. Nature *439*, 871-874.

Wang, F., Yang, Y.-Z., Shi, C.-Z., Zhang, P., Moyer, M.P., Zhang, H.-Z., Zou, Y., and Qin, H.-L. (2012). UHRF1 promotes cell growth and metastasis through repression of p16ink4a in colorectal cancer. Annals of Surgical Oncology *19*, 2753-2762.

Wang, J., and Chen, J. (2010). SIRT1 regulates autoacetylation and histone acetyltransferase activity of TIP60. The Journal of Biological Chemistry *285*, 11458-11464.

Wang, J., Hevi, S., Kurash, J.K., Lei, H., Gay, F., Bajko, J., Su, H., Sun, W., Chang, H., Xu, G*., et al.* (2008). The lysine demethylase LSD1 (KDM1) is required for maintenance of global DNA methylation. Nature Genetics *41*, 125-129.

Wang, W.W., Zeng, Y., Wu, B., Deiters, A., and Liu, W.R. (2016). A chemical biology approach to reveal Sirt6-targeted histone H3 sites in nucleosomes. ACS chemical biology *11*, 1973-1981.

Wang, Y., Fung, Y.M.E., Zhang, W., He, B., Chung, M.W.H., Jin, J., Hu, J., Lin, H., and Hao, Q. (2017). Deacylation mechanism by SIRT2 revealed in the 1'-SH-2'-O-Myristoyl intermediate structure. Cell Chemical Biology *24*, 339-345.

Wątroba, M., and Szukiewicz, D. (2016). The role of sirtuins in aging and age-related diseases. Advances in Medical Sciences *61*, 52-62.

Wigler, M., Levy, D., and Perucho, M. (1981). The somatic replication of DNA methylation. Cell *24*, 33-40.

Wilm, M., Shevchenko, A., Houthaeve, T., Breit, S., Schweigerer, L., Fotsis, T., and Mann, M. (1996). Femtomole sequencing of proteins from polyacrylamide gels by nano-electrospray mass spectrometry. Nature *379*, 466-469.

Yang, C., Wang, Y., Zhang, F., Sun, G., Li, C., Jing, S., Liu, Q., and Cheng, Y. (2013). Inhibiting UHRF1 expression enhances radiosensitivity in human esophageal squamous cell carcinoma. Molecular Biology Reports *40*, 5225-5235.

Yang, Y., Fu, W., Chen, J., Olashaw, N., Zhang, X., Nicosia, S.V., Bhalla, K., and Bai, W. (2007). SIRT1 sumoylation regulates its deacetylase activity and cellular response to genotoxic stress. Nature cell biology *9*, 1253-1262.

Yang, Y.H., Chen, Y.H., Zhang, C.Y., Nimmakayalu, M.A., Ward, D.C., and Weissman, S. (2000). Cloning and characterization of two mouse genes with homology to the yeast Sir2 gene. Genomics *69*, 355-369.

Yoshizawa, T., Karim, M.F., Sato, Y., Senokuchi, T., Miyata, K., Fukuda, T., Go, C., Tasaki, M., Uchimura, K., Kadomatsu, T.*, et al.* (2014). SIRT7 controls hepatic lipid metabolism by regulating the ubiquitin-proteasome pathway. Cell Metabolism *19*, 712-721.

Yuan, H., and Marmorstein, R. (2012). Structural basis for sirtuin activity and inhibition. The Journal of biological chemistry *287*, 42428-42435.

Zhang, A., Wang, H., Qin, X., Pang, S., and Yan, B. (2012). Genetic analysis of SIRT1 gene promoter in sporadic Parkinson's disease. Biochemical and Biophysical Research Communications *422*, 693-696.

Zhang, H., Liu, H., Chen, Y., Yang, X., Wang, P., Liu, T., Deng, M., Qin, B., Correia, C., Lee, S.*, et al.* (2016). A cell cycle-dependent BRCA1–UHRF1 cascade regulates DNA double-strand break repair pathway choice. Nature Communications *7*, 10201.

Zhang, L., Ren, X., Cheng, Y., Huber-Keener, K., Liu, X., Zhang, Y., Yuan, Y.-S., Yang, J.W., Liu, C.-G., and Yang, J.-M. (2013). Identification of Sirtuin 3, a mitochondrial protein deacetylase, as a new contributor to tamoxifen resistance in breast cancer cells. Biochemical Pharmacology *86*, 726-733.

Zhang, S., Chen, P., Huang, Z., Hu, X., Chen, M., Hu, S., Hu, Y., and Cai, T. (2015). Sirt7 promotes gastric cancer growth and inhibits apoptosis by epigenetically inhibiting miR-34a. Scientific Reports *5*, 9787.

Zhong, L., D'Urso, A., Toiber, D., Sebastian, C., Henry, R.E., Vadysirisack, D.D., Guimaraes, A., Marinelli, B., Wikstrom, J.D., Nir, T.*, et al.* (2010a). The histone deacetylase Sirt6 regulates glucose homeostasis via Hif1alpha. Cell *140*, 280-293.

Zhong, L., D'Urso, A., Toiber, D., Sebastian, C., Henry, R.E., Vadysirisack, D.D., Guimaraes, A., Marinelli, B., Wikstrom, J.D., Nir, T.*, et al.* (2010b). The Histone deacetylase SIRT6 regulates glucose homeostasis via Hif1α. Cell *140*, 280-293.

Zhou, L., Shang, Y., Jin, Z.a., Zhang, W., Lv, C., Zhao, X., Liu, Y., Li, N., and Liang, J. (2015). UHRF1 promotes proliferation of gastric cancer via mediating tumor suppressor gene hypermethylation. Cancer Biology & Therapy *16*, 1241-1251.

Zhou, Y., Zhang, H., He, B., Du, J., Lin, H., Cerione, R.A., and Hao, Q. (2012). The bicyclic intermediate structure provides insights into the desuccinylation mechanism of human Sirtuin 5 (SIRT5). The Journal of Biological Chemistry *287*, 28307-28314.

Zhu, J.-K. (2009). Active DNA demethylation mediated by DNA glycosylases. Annual review of genetics *43*, 143-166.

Ziegenhain, C., Vieth, B., Parekh, S., Reinius, B., Guillaumet-Adkins, A., Smets, M., Leonhardt, H., Heyn, H., Hellmann, I., and Enard, W. (2017). Comparative Analysis of Single-Cell RNA Sequencing Methods. Molecular Cell *65*, 631-643.

5.2 Abbreviations

2iLIF	Leukemia inhibitory factor containing a selective GSK3β & Mek 1/2 inhibitors
5mC	5-methylcytosine
AA	Amino acid
AceCS2	Acetyl-CoA synthetase 2
ACTR	Nuclear receptor coactivator
AKT1	Serine-threonine protein kinase
AMC	7-amino-4-methylcoumarin
APH	Aphidicolin
ATF-2	Activating transcription factor 2
BAH	Bromo-adjacent homology domain
BAZ2A	Bromodomain adjacent to zinc finger domain 2A
BRCA1	Breast cancer susceptibility gene 1
BSA	Bovine serum albumin
CBP	CREB-binding protein
CC cells	Dnmt1 knockout cell line
CD	Chromodomain
CDK2	Cyclin-dependent kinase 2
CHK1	Checkpoint kinase 1
ChREBP	Carbohydrate response-element-binding protein
CHX	Cycloheximide
CK2	Casein kinase 2
c-Myb	Avian myeloblastosis virus oncogene cellular homolog
CpG	5'- C-phosphate-G -3'
CPS1	Carbamoyl phosphate synthetase 1

CR	Calorie restriction
CSD	Chromoshadow-domain
CTR	The C-terminal regulatory segment
DAPI	4', 6-diamidino-2-phenylindole
DNA	Deoxyribonucleic acid
DNMTs	DNA methyltransferases
DNMT1	DNA methyltransferase 1
DNMT2	DNA methyltransferase 2
DNMT3A	DNA methyltransferase 3A
DNMT3B	DNA methyltransferase 3B
DNMT3L	DNA methyltransferase 3-like
Dox	Doxycycline
DSBH	Double-stranded β-helix domain
DSBs	DNA double-strand breaks
E1A	Adenovirus early region 1A
E2F1	Transcription factor family including E2F-like subunit 1
EHMT2	Euchromatic histone-lysine N-methyltransferase 2
ELP3	Elongator complex protein 3
ESA1	Essential sas2-related acetyltransferase 1
ESCs	Embryonic stem cells
EZH2	Enhancer of zeste homolog 2
FAO	Fatty acid oxidation
FADD	*Fas*-associated protein with death domain
FOXO	Fork-head box protein
FACS	Fluorescence-activated cell sorting
GDH	Glutamate dehydrogenase

GK linker	Glycine-lysine repeats
GNATs	Gcn5-related N-acetyltransferases
Gsk3β	Glycogen synthase kinase 3β
H3K9 me3	Trimethylated histone 3 lysine 9
H3K18ac	Histone 3 lysine 18 acetylation
H3K18Ub/23Ub	Histone 3 lysine 18/23 ubiquitination
HATs	Histone acetylases
HBO1	HAT bound to ORC1
HDACs	Histone deacetylases
HMG1/ HMG14	High mobility group *protein 1/14*
HP1	Heterochromatin protein 1
ICBP90	Inverted CCAAT box-binding protein of 90 kDa
IGF1	Insulin-like growth factor 1
iPSCs	Induced pluripotent stem cells
KDACs	Lysine deacetylases
KRAB	Encoding Krüppel-associated box domain
LIF	Leukemia inhibitory factor
LSH	Lymphoid specific helicases
LSD1	Histone demethylase 1
m^5C	5-methylcytosine
m^6A	N^6-methyladenine
MTase	Methyltransferase domain
MBD	Methyl-CpG binding domain
MCD	Malonyl CoA decarboxylase
MeCP2	Methyl CpG binding protein 2
MGMT	O^6-methylguanine DNA methyltransferase

MOF	Males absent on the first
MoRF	Molecular recognition feature
MOZ	Monocytic leukemia zinc finger protein
MPG	N-methylpurine DNA glycosylase
mTORC1	Rapamycin complex 1
NAM	Nicotinamide
NEL	Nuclear export sequence
NF-kB	Nuclear factor kappa-light-chain-enhancer of activated B cells
NHEJ	Nonhomologous end joining
NLS	Nuclear localization sequence
NTD	N-terminal domain
P300	Histone acetyltransferase protein 300
PBD	PCNA binding domain
PBR	Polybasic region
PBS	Phosphate-buffered saline
PBST	PBS and 0.02% Tween-20
PCAF	P300/CBP-associated factor
PCNA	Proliferating cell nuclear antigen
PDB	Protein Data Bank
PGC-1a	Peroxisome proliferator-activated receptor g coactivator 1-a
PHD	Plant homeodomain
RIF1	Replication timing regulatory factor 1
PRAP	Receptor-associated *protein*
PTMs	Post-translational modifications
PWWP	Pro-Trp-Trp-Pro motif containing domain
RdDM	RNA-directed DNA methylation

RFTS	Replication foci targeting sequence
RING domain	Really interesting new gene domain
RNA	Ribonucleic acid
ROS1	Repressor of silencing 1
Rpd3	Reduced potassium dependency 3
SETDB1	ERG-associated *protein* with SET domain
SRA domain	SET and RING finger-associated domain
SRC-1	Steroid receptor coactivator-1
SUV39h1/2	Suppressor of variegation 3–9 homologs 1/2
$TAF_{II}250$	Transcription initiation factor TFIID 250 kDa subunit
TetO	Tet operator
TFII	Transcription factor II
Tip60	Tat interactive *protein* 60kDa
TKO cell	Triple of Dnmts knockout cell line
TNFα	Tumor necrosis factor α
TRE	Tetracycline response element
TRIM28	Tripartite motif protein 28
TRRAP	Transformation/transcription domain-associated protein
TS	Targeting sequence
TSG	Tumor suppressor gene
tTA	Tetracycline transactivator
TTD	Tandem Tudor domain
UBL	Ubiquitin-like domain
Uhrf1	Ubiquitin-like with PHD and ring finger domains 1
UIM	Ubiquitin interacting motif
ZnF	Zinc finger

5.3 Declaration

Statutory declaration

Eidesstattliche Erklärung

1. Hiermit erkläre ich, dass die vorgelegte Arbeit an der LMU von Herrn Prof. Dr. Heinrich Leonhardt betreut wurde.

2. Hiermit versichere ich an Eides statt, dass die vorgelegte Dissertation von mir selbstständig undohne unerlaubte Hilfe angefertigt wurde.

3. Hiermit erkläre ich, dass die Dissertation weder als ganzes noch in Teilen an einem anderen Ort einer Prüfungskommission vorgelegt wurde. Weiterhin habe ich weder an einem anderen Ort eine Promotion angestrebt noch angemeldet noch versucht eine Doktorprüfung abzulegen.

München, den

Pin Zhao

21.03.2019

5.4 Acknowledgments

Firstly, I am grateful to my supervisor Prof. Dr. Heinrich Leonhardt for the support and guidance during these years. Thank you for providing such a platform or environment to work, which has provided me with a rare opportunity for my personal development with good training of scientific thinking.

Secondly, I also express my big thanks to all my adorable Chinese colleagues, including Congdi Song, Nan Liu, Wen Deng, Weihua and Ningjun, with whom I have spent most of my lab life and taught me too much. Most of the time, I feel proud of them and take them as good examples. As well, I would like to thank other people in Leonhardt lab, like Susanne, Hartmann, Sebastian, Chris, Michi, Joel, Jeannet and so on. They are so intelligent and warmhearted that the atmosphere of the lab is pleasant. If the lab is like a garden, every one of us represents a flower. With the sunshine from Professor Heinrich, the flowers are in full bloom. As for fruits, we know that hard work can produce a good one. There are also some energetic students who only have studied here for a short time, but they have left me a good impression and memory.

Moreover, I would like to thank the Chinese Scholarship Council for my four years' financial support of Ph.D. study. I also appreciated my supervisor for financial support in a short time. In a word, they have given me an opportunity to widen my horizon in the epigenetic field.

Last but not least, I deeply thank my family, my Mom, Dad and two sisters, who always take care of my personal life. They respect my every decision and teach me to be independent and strong in my inner mind. Thank them for everything.